IMPACTS OF UPSTREAM DAM DEVELOPMENT ON FLOW, SEDIMENT AND MORPHOLOGICAL CHANGES IN VIETNAMESE MEKONG DELTA

by

DOAN VAN BINH

2019

IMPACTS OF UPSTREAM DAM DEVELOPMENT ON FLOW, SEDIMENT AND MORPHOLOGICAL CHANGES IN VIETNAMESE MEKONG DELTA

by

DOAN VAN BINH

A Dissertation

Submitted in Partial Fulfillment of the Requirements for the Degree of

Doctor of Philosophy (PhD)

Department of Urban Management

Graduate School of Engineering

Kyoto University

2019

Acknowledgements

I would like to express my deeply sincere thanks to Prof. Dr. Tetsuya Sumi, professor of Socio and Eco Environment Risk Management laboratory, Water Resources Research Center, Disaster Prevention Research Institute, Kyoto University for offering me an opportunity to become a PhD student in his laboratory under Human Security Engineering Program. His suggestions and corrections through guidance and discussions gained me invaluable knowledge and substantially improved my research. He offered me opportunities to attend internal and international conferences that helped my way of thinking become more interdisciplinary and internationally. I learned a lot about Japanese river systems during field surveys.

I would like to express my highest gratitude to Assoc. Prof. Dr. Sameh Ahmed Kantoush, my direct supervisor, in Socio and Eco Environment Risk Management laboratory, Kyoto University for all of his support, encouragement, advice, instruction, forgiveness, and kindness. His endless knowledge with careful instruction and patient discussions improved substantially the research results and gained my knowledge. He always forgives my mistakes, and guided and supported me with his highest enthusiasm not only in my study but also in my daily life in Japan. His wide international network with famous scientists helped me overcome the difficulty in numerical simulation and scientific writing. He offered me an opportunity to attend international conferences from that I learned a variety way of thinking in solving scientific issues and expanded my career network. He is a good model of an international scientist that I would like to become in the future.

I would like to thanks to Assoc. Prof. Dr. Yasuhiro Takemon, Assis. Prof. Dr. Daisuke Nohara, and Assis. Prof. Dr. Sohei Kobayashi for their valuable suggestion and instruction during seminars and discussions. I had good experience in sampling for ecological analysis during field surveys with Assoc. Prof. Dr. Yasuhiro Takemon. Going with Assis. Prof. Dr. Sohei Kobayashi in field surveys provided me good experience on using technologic instruments such as drone measurement and imaging analysis. Discussions with Assis. Prof. Dr. Daisuke Nohara encouraged me in learning programming.

I would like to acknowledge Mrs. Obara and Ibaraki, secretary of Sumi laboratory, for their supports regarding my research, my traveling, my daughter study, and my daily life during my PhD. My thanks are to all other members of Sumi laboratory, Mrs. Morimoto, Dr. Mohammed Abdel-Fattah, Mr. Koshiba, Mr. Ogiso, Mr. Terada, Mr. Kano, Mr. Tazumi, Mr. Takata, Mr.

Ishizuka, Mss. Yamasaki, Mss. Iwamoto, Mr. Mahmood, Mrs. Tahani, Mrs. Dina, Mr. Xiao for their supports during my research.

I would like to thanks to the Rector and Director Boards of Thuyloi University for allowing me to conduct my PhD study abroad.

Special thanks are to Dr. La Vinh Trung from Vietnamese-German University and Mrs. Nguyen Thi Phuong Mai from Thuyloi University for their kind supports during field surveys and in maintaining monitoring stations. My research was significantly improved thanks to their recommendations and discussions. Their supports in collecting monitored data are much appreciated.

My sincere thanks are also extended to Assoc. Prof. Dr. Le Trung Thanh from Thuyloi University for collecting and sharing me the research data. Mr. Duong Gia Diep from the Southern Institute of Water Resources Research is appreciated for sharing data.

My PhD research is financially supported by the Ministry of Education, Culture, Sports, Science, and Technology (MEXT). The funding of my research was partly supported by Japan-ASEAN Science, Technology and Innovation Platform (JASTIP) and the Supporting Program for Interaction-Based Initiative Team Studies SPIRITS 2016 of Kyoto University.

Lastly, I would like to express my special gratitude to my father, Doan Van Hoa, my mother, Nguyen Thi Be Bay, my darling, Nguyen Thi Thu Huong, and my daughter, Doan Kim Anh for their unreasonable support, sympathy, sacrifice, and encouragement to complete my study.

I would like to dedicate this thesis to

my grandfather

Doan Van Viet

my father

Doan Van Hoa

my mother

Nguyen Thi Be Bay

my wife

Nguyen Thi Thu Huong

and my daughter

Doan Kim Anh

Table of contents

List of figures

List of tables

List of symbols

a, b: dimensionless coefficients

a, z_{ref}: reference level from riverbed (m)

C: suspended sediment concentration (kg/m^3)

C_{eq}: equilibrium near-bed concentration (kg/m^3)

C_j: mass concentration per layer (kg/m^3)

C_k: depth-averaged concentration of the kth size class (kg/m^3)

C_{zref}: near-bed concentration (kg/m^3)

C_α: confidence interval in Sen's slope method

d: sediment grain diameter (m)

D: deposition flux (m^2/s)

d_{50}: median sediment diameter (μm)

D^1, D^2: deposition fluxes of sand and mud fractions, respectively (m^2/s)

E: erosion flux (m^2/s)

$\overline{E}_j$: mean erosion rate per layer (m^2/s)

E^k, D^k: erosion and deposition rates of the kth size class (m^2/s)

E^1, E^2: erosion fluxes of sand and mud fractions, respectively (m^2/s)

E_{sj}^1, E_{sj}^2 : bed layer thickness of the sand and mud, respectively (m)

f_i, i=1, 2, …n: the estimated data which are associated with y_i

f_{1j}, f_{2j}: mass percentage of the sand and mud fractions, respectively (%)

g: gravity acceleration (m/s^2)

h: water depth (m)

H: water level (m)

i, j, k, n, N, t, T: indexes

K_t, $U_{t,T}$: Pettitt statistic parameter

k_s: skin roughness (m)

m: rank of data in flood-frequency analysis

M: Krone-Partheniades erosion constant (kg/m^2/s)

M_{sj}^1, M_{sj}^2 : mass of the sand and mud, respectively (kg)

n: number of years in the data set in flood-frequency analysis and Manning coefficient

P: plotting position in flood-frequency analysis

Q: discharge (m^3/s)

Q_b: bedload transport rate per unit width (m^2/s)

Q_{med}: Sen's slope estimator

$R = \omega_s/(\kappa u_*)$: Rouse number

R^2: coefficient of determination

$s = \rho_s/\rho$: relative density

S: Mann-Kendall statistic number parameter

S_h: source or sink of fluid (m/s)

S_T: source or sink of tracer (g/l/s)

S_x, S_y: source or sink terms in dynamic equations (m/s^2)

t: time (s)

T: passive tracer (g/l or °C)

$T_1 = \sqrt{\tau_b / \rho}$

T_2: ratio between the near-bed concentration and the mean concentration

u, v: velocities in x and y directions (m/s)

U, V: depth-averaged velocities in x and y directions (m/s)

u_*: friction velocity corresponding to the total bed shear stress

u_*^{cr} : critical shear velocity for mud deposition (m/s)

x: data values

x, y: longitudinal and transversal directions

X, Y, Z: coordinates of mesh nodes (m)

$\bar{y}$: mean of observed values

y_i, i=1, 2, …n: observed data

z: vertical distance from riverbed (m)

Z: free surface elevation (cm or m) or Mann-Kendall standard normal statistic parameter

z_b: bed level (m)

α: significance level (%)

Δt: time step (s)

ε_s: turbulent diffusivity of the sediment

θ: Shields parameter

κ: Karman constant

λ : bed porosity (%)

μ: correction factor for skin friction

ν: viscosity (m^2/s)

ν_t, ν_T: momentum and tracer diffusion coefficients (m^2/s)

ρ_s, ρ: density of the sediment and water (kg/m^3)

σ: Dispersion coefficient

σ_c: Schmidt number

τ_b: bed shear stress (N/m^2)

τ_{ce}: critical bed shear stress (N/m^2)

τ_{ce}^1 : τ_{cej}^2 : critical shear stress of sand and mud, respectively (N/m^2)

Φ_b: dimensionless current-induced bedload transport rate

ω_s: settling velocity (m/s)

Abbreviations

ADCP: acoustic Doppler current profiler

CAP: reservoir's total capacity

CI: confidence interval

CMD: Cambodian Mekong Delta

CS: cross section

DEM: digital elevation map

EDF: National Hydraulics and Environment Laboratory of Electricité de France

ENSO: El Niño Southern Oscillation

FQ: alteration index of the hydrological regime

FSC: free surface compatibility

FTU: Formazin Turbidity Units

GPS: global positioning system

HR: Hau River

IHA: indicator of hydrologic alteration

IMD: implicitation for depth

IMV: implicitation for velocity

IPCC: intergovernmental panel on climate change

JASTIP: Japan-ASEAN Science, Technology and Innovation Platform

LMB: lower Mekong River Basin

MAR: mean annual runoff

MAS: mean annual sediment load

MR: Mekong River

MRB: Mekong River Basin

MRC: Mekong River Commission

NQ: number of days

NSE: Nash-Sutcliffe number

ppm: parts per million

RMSE: root mean square error

RVA: range of variability

S_c: simulation scenario

SLR: sea level rise

SSCs: suspended sediment concentrations

SSLs: suspended sediment loads

TA: type of advection

TR: Tien River

TSL: Tonle Sap Lake

UMB: upper Mekong River Basin

Var: variance

VMD: Vietnamese Mekong Delta

VN: Vam Nao channel

1D: 1-dimensional

2D: 2-dimensional

2S: Sesan and Srepok Rivers

3S: Sekong, Sesan, and Srepok Rivers

Abstract

Natural flow and suspended sediment regimes are of crucial importance in structuring river basin morphology, hydrology, and ecosystems of the lower Mekong River (MR), particularly the Tonle Sap Lake and the Vietnamese Mekong Delta (VMD). Similar to the world's large river basins, the flow and sediment budgets of the MR have been significantly altered due to natural processes and anthropogenic activities, including river damming. The aim of this research is to examine the impacts of hydropower dams in the Mekong River Basin (MRB) on the alterations of the flow and sediment dynamics and budgets in the VMD. To that end, long-term discharge and suspended sediment budgets along the entire lower MR from Chiang Saen to the VMD were analyzed intra and interannually in daily, monthly, and annual quantities using various statistical methods (Mann-Kendall, Pettitt, and Sen's slope tests, frequency analysis, indicator of hydrologic alteration (IHA), range of variability (RVA) and alteration index of the hydrological regime (FQ)) and numerical simulations (Mike 11 and Telemac-2D), and associated driving factors were linked to flow and sediment alterations. Long-term precipitation in the MRB, and water levels and salinity concentrations in the VMD were also analyzed. Five additional turbidity and salinity monitoring stations were installed and two field surveys were conducted to overcome data limitation. To address one of the consequences of the altered flow and sediment budgets from the MR, the past changes of the river bathymetric data as well as the projected morphological changes in the VMD's rivers were quantified by using a coupled hydrodynamics (Telemac-2D) and suspended sediment transport (Sisyphe) model. As a consequence of morphological changes, low-flow water level alterations in the VMD were simulated.

Climate conditions controlled the flow regimes in the low-dam development period (1993-2008) while hydropower dams in the Mekong River basin intensified the impacts. Operations of hydropower dams in the MRB were the main driver of flow regime alterations in the high-dam development period (2009-2015), and dam impacts are expected to dominate through the 2040s. Mainstream dams manipulated the maximum and high-flow discharges while tributary dams controlled the minimum and low-flow discharges in the lower MR.

Impacts of the Lancang cascade dams up to the year 2011 (4 dams completed) on river flows in the VMD are not obvious. However, such impacts are significantly when all six dams in the Lancang cascade were in operation. Impacted by all six Lancang cascade dams, minimum discharges in the VMD increased and duration of the low-flow reduced. However, low-flow water

levels generally reduce under dam' impacts because of riverbed incision as a result of the reduction in the sediment supply, leading to an increase in tidal influence into the VMD. Additionally, six dams in the Lancang cascade have caused a reduction in both discharges and water levels in high-flow years in the VMD. Flood peak in the VMD has shifted to happen more lately due to the upstream hydropower dams.

The situation of the 2016-like drought event will become more serious if eleven proposed mainstream dams in Thailand, Lao PDR, and Cambodia are constructed. It was found that the inflow discharge in the VMD may decrease up to 14.9% while the water level near the estuary may increase more than 220% under the combined effect of 47 cm sea level rise and 11 proposed mainstream dams. These allow saltwater significantly intruding into the upper parts of the VMD, even in areas having not been affected before, with higher salinity concentrations.

The upper MRB was the main contributor to the sediment budget of the MR during the predam period (pre-1992). However, the contribution during the postdam periods became minor due to the completion of six mainstream dams in the Lancang cascade; instead, the Nong Khai-Pakse section became the largest sediment source.

Climate conditions controlled the flow and sediment regime of the MR during the predam period. The climate conditions, which mainly shifted the timing and intensities of tropical cyclones, still considerably contributed to the discharge variations and sediment reductions in the lower MR during 1993-2001. However, the 64 hydropower dams that were completed by 2015 were the main driver of sediment reductions in the entire MR during 2012-2015. Six mainstream dams in the Lancang cascade were the main cause of sediment reductions upstream of Nong Khai, whereas tributary dams additionally controlled sediment reductions in areas downstream of Nong Khai to the East Sea. Dams and reservoirs impacted the annual and high sediment transport months more than low sediment transport months in the VMD.

Under operations of all 64 dams in the MRB, the suspended sediment budgets at Chiang Saen, Luang Prabang, Nong Khai, and the VMD decreased by 89.5%, 77%, 80.5%, and 74.1%, respectively. Among the 74.1% sediment reduction in the VMD, from 166.7±33.3 Mt/yr during the predam period to 43.1 Mt/yr during 2012-2015, 40.2% was caused by the six mainstream dams in the Lancang cascade, and the Manwan and Dachaosan dams alone were the direct drivers of 32% of the reduction. Similarly, the annual sediment discharge to the East Sea of Vietnam from the MR has reduced by 74%, from 144 Mt/yr during the predam period to 37.7 Mt/yr during 2012-2015.

Due to river damming, the river morphology of the VMD has already and will significantly change in the future. If the flow and sediment budgets of 2017 remain unchanged during 2017-2026, the riverbed of the upper VMD might be, on average, incised by -1.27 m by the end of 2026. The values may reach -1.48 m, and -2.04 m under reductions of 17.5% and 84.8% of the sediment supply, respectively. Accordingly, the resulted water levels may decrease by a maximum of 0.7 m in the Tien River and 0.5 m in the Hau River by April 2026 under 84.8% sediment supply reduction.

Hydropower dams cause large-scale riverbed incision while sand mining is responsible for small-scale local scouring in the VMD. It is estimated that hydropower dams are responsible for more than 90% while sand mining is responsible for less than 10% of the riverbed incision in the VMD. Climate change may have long-term effects on morphological changes, and hydropower dams and sand mining have short to intermediate-term influences.

The findings of this study serve as a basic reference for the sound management of water conservancy, flood control, sediment management, river navigation, salinity control, and agricultural development in the VMD. The research calls collaborative watershed water and sediment management among six riparian countries in the MRB.

Keywords: hydropower dams, Mekong River (MR), Vietnamese Mekong Delta (VMD), flow regimes, discharge, sediment budget, numerical simulation, Telemac-2D, Sisyphe, morphological change, riverbed incision.

Chapter 1 Introduction and research methodology

1.1 Flow and sediment alterations due to natural and human impacts

Natural river flow regimes produce spatial and temporal variations in the environmental conditions which are critical to supporting the native biodiversity and integrity of riverine ecosystems. Important river flow characteristics, including seasonal patterns of flow; frequency, predictability, timing, and duration of extreme flows (floods and droughts) and intermittent flows; daily, seasonal, and annual flow variability are crucial controllers of key habitat parameters, for example, flow depth, velocity, and habitat volume. In rivers, the suspended sediment has an important role in structuring the morphology, hydrology, and ecosystem as well as in fisheries, agriculture, and human exploitation of a river system.

Demands for freshwater resources and energy supply globally have been increasing due to population booming, rapid socioeconomic development and urbanization, which have led to the construction of hydropower dams and diversions for electricity generation, weirs and reservoirs for multi purposes, water diversions for irrigation and navigation, and sluice gates for flow and salinity control. As estimated, the global freshwater yield is approximately 43,750 km^3/year (Minh et al., 2010) of which 8,000-10,800 km^3 is stored in artificial reservoirs (Chao et al., 2008), representing an approximately 700% increase in the standing water of rivers (Kummu and Sarkkula, 2008).

As the largest environmentally friendly energy source with little, if not without, greenhouse gas emissions, hydropower dams have been increasingly built to replace the fossil coal industry. By 2007, hydropower dams provided approximately 2.2% of the electricity demand worldwide (Kummu and Varis, 2007), but that number increased to approximately 3.8% by 2012 (REN21, 2014), which is the second largest renewable energy sector, behind the heat energy (4.2%) and followed by powers from wind, solar, geothermal, biomass, and biofuels (2%). The fastest development of hydropower dams in the world is in the 20th century. During the second half of the 20th century, the number of large dams, higher than 15m, has increased from 5,000 to 45,000 (WCD, 2000) and projected to be about 50,000 recently (Gupta et al., 2012; Kummu et al., 2010) of which about half were built in China (Wu et al., 2018). Among large dams in China, about 115 are mega dams (> 100m high and/or > 1 km^3 storage capacity). According to (REN21, 2014), by 2013, the total global hydropower capacity increased by 4% to approximately 1,000 GW in which about 40 GW was commissioned in 2013. The annual production of hydropower generation was around 3,750 TWh in 2013 (Fan et al., 2015).

Apart from positively supplying renewable energy, hydropower dams, especially mega dams, could alter the flow regimes and permanently store virtually the entire sediment load transported from the upper basin. Hydropower dams have been reported to significantly alter flow regimes in many rivers globally by affecting the quality, quantity, intra-and-inter-annual variations of the flows, and resulting in degradation of aquatic and terrestrial ecosystems. Moreover, hydropower dams could disrupt the sediment transport downstream and block fish migration path. Therefore, hydropower dams have been ranked as one of the main factors for a decreasing trend of the world sediment flux. On a global scale, as high as 53% of the world sediment flux has been trapped by reservoirs (Tena and Batalla, 2013). The sediment load in the Nile River has reduced from about 100 Mt/yr to almost zero due to the construction of Aswan High Dam (Milliman and Syvitski, 1992). In São Francisco River in Brazil, the Sobradinho dam completed in 1978 has trapped approximately 80% of the sediment generated in the basin (Walling, 2006). The completion of the Glen Canyon dam has reduced by 99.5% of the fine sediment reaching to Grand Canyon in Colorado River, USA (Tena and Batalla, 2013). The sediment budget of Yangtze river in China has reduced by approximately 63% from 490 Mt/yr during 1950-1968 to 180 Mt/yr during 2003-2004 due to the construction and completion of numerous dams in the basin (Wu et al., 2018). The closure of the Three Gorges dam in 2003 led to a 95% reduction of the sediment budget of the Yangtze river from 164 Mt/yr to 9 Mt/yr (Tena and Batalla, 2013). Similarly, the sediment flux of the Red river in Vietnam has reduced by about 70% after the completion of Hoa Binh and Thac Ba reservoirs (Lu et al., 2015).

Similar to the world's river basins, hydropower dams have been increasing planned and built in the Mekong River Basin (MRB) under a fast population boom in riparian countries. Those dams already had and will cause critical flow alteration, sediment reduction, fish blockage, environment, and ecosystem degradation. Figure 1.1 collectively shows prior researches investigating the impacts of built and planned dams on each regional part of the MRB. It can be seen that most of the prior researches focusing on the middle MRB while few studies have paid attention to the Cambodian Mekong Delta (CMD) and Vietnamese Mekong Delta (VMD). Especially, no study investigates impacts of hydropower dams in the MRB on historical (long-term) flow, sediment, and morphological alterations in the VMD due to data constraints. Therefore, the main aim of this research is to examine impacts of built and planned dams in the MRB on historical and future alterations of flow, sediment, and morphology of the VMD to bridge such knowledge gaps.

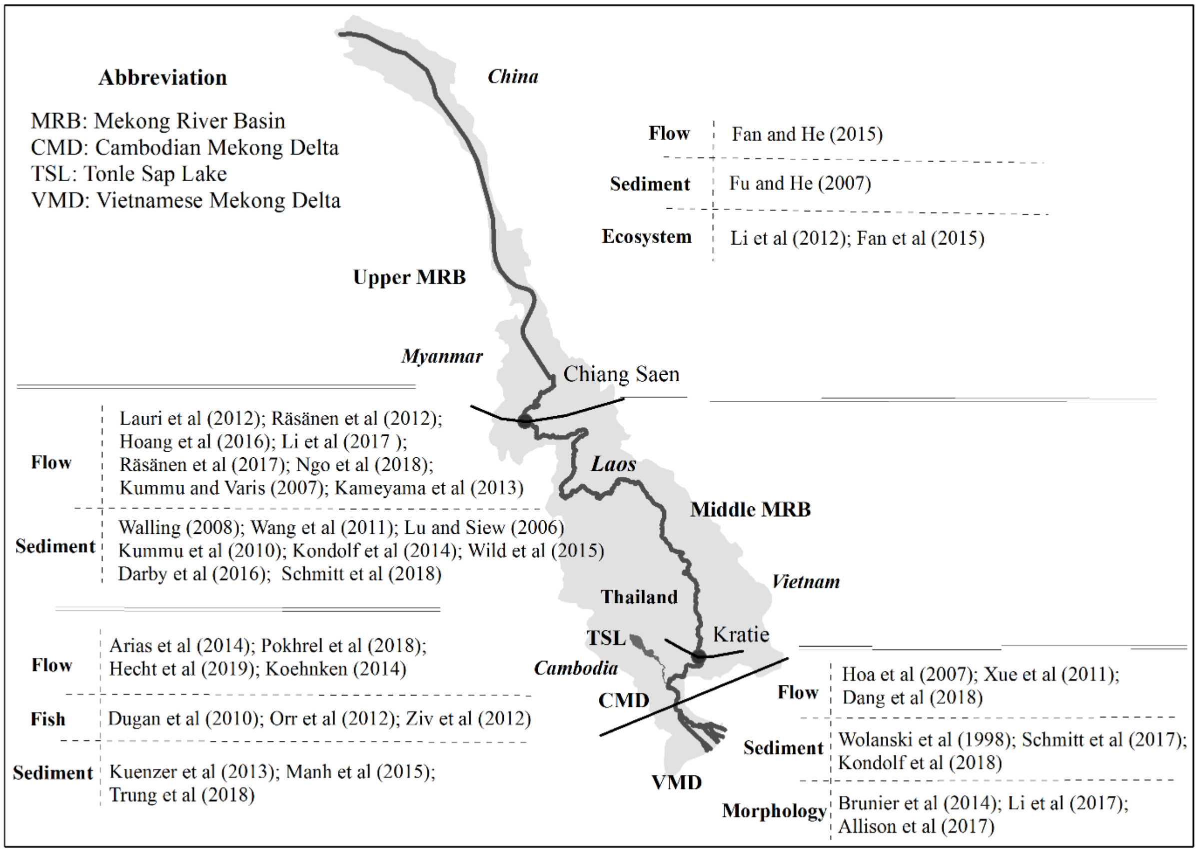

Figure 1.1 Spatial distribution of prior researches investigating dam impacts in the MRB.

1.2 Research objectives

Consideration of the research was stemmed from a series of scientific questions regarding impacts of hydropower dams in the MRB on the lower Mekong River (MR) to the VMD:

Regarding impacts on flow regime

1. In what extent, existing and planned hydropower dams alter flow regime?

2. How and how much individual and group of dams alter the flow regime?

3. Are hydropower dams the only driver of flow regime alteration downstream? If no, what are other drivers?

4. What is the role of Tonle Sap Lake (TSL) on attenuating the negative impacts of upstream hydropower dams on the VMD?

Regarding impacts on the sediment budget

1. Have existing hydropower dams reduced the sediment flux of the MR?

2. What is the main driver causing sediment reduction: hydropower dams, climate change, land use change or delta development?

3. In what extent, individual and group of dams in the MRB reduce the sediment flux of the MR?

4. What will be the future sediment budget of the MR if more planned dams are finished?

Regarding impacts on river morphology and irrigation water intake

1. Does reduction of sediment budget of the MR degrade the morphology of the VMD' rivers?

2. What is the main controller of morphological changes in the VMD?

3. How will the VMD's river morphology response to future reduced sediment budget from the MR if more planned dams are finished?

4. Does the riverbed degradation affect the possibility in obtaining intake water for irrigation in the low-flow season?

1.3 Outline of the thesis

This thesis consists of nine chapters which can be divided into six main components: (1) Introduction and research methodology (chapter 1) and literature review (chapter 2), (2) theoretical background and methods (chapter 3), (3) monitoring network and field surveys (chapter 4), (4) long-term impacts of hydropower dams on flow and sediment budgets of the lower MR (chapter 5 and 6), (5) numerical simulation (chapter 7 and 8), and (6) conclusions and recommendations (chapter 9).

Chapter 1 provides a brief introduction about the importance of natural flow and fine suspended sediment to the riverine ecosystem and environment. Why have hydropower dams been widely built in the globe? Then, the chapter addresses the necessity of this research and research objectives. An overall research methodology is provided at the end of the chapter.

Chapter 2 summarizes the basic background of the research areas, the MRB and VMD, and systematic challenges that the VMD is facing due to hydropower dams, climate change, land use change, and delta development. Prior researches on the flow and sediment alterations in the lower MR to the VMD due to various factors are reviewed in detail.

Chapter 3 analyzes long-term alterations of the flow regimes of the lower MR to the VMD under the impacts of hydropower dams and other factors by using various statistical methods. Detailed analyses on extreme (maximum and minimum), daily, monthly, seasonal, and annual discharges and water levels along the entire lower MR to the VMD are conducted. The influence of planned hydropower dams in the MRB on the flow regime of the VMD by using 1D numerical model (Mike 11) is also analyzed. In the end, strategic adaptation policies to duel with altered flow regimes are proposed to stakeholders in the VMD.

Chapter 4 analyzes long-term alterations of the suspended sediment flux of the MR and the sediment budget of the VMD under impacts of hydropower dams, climate change, land use change, and sand mining. Analyses are done in the basis of hourly, daily, monthly, seasonal, and annual suspended sediment data with the support of various statistical methods. It also provides associated consequences of reduced sediment supply from the MR to the VMD. Therefore, recommendations to stakeholders regarding the implementation of comprehensively adaptive strategies to duel with reduced sediment supply and to dams' owners regarding strategic reservoir sediment management for current and planned dams in the MRB.

Chapter 5 introduces the necessity of installing additional stations to monitor SSCs and conducting field investigations. It introduces all instrument used for the monitoring and surveys and data processing procedure. After that, acquired data are analyzed to draw holistic understandings of the flow, sediment, and morphology of the VMD's rivers. Long-term changes in VMD' morphology are also analyzed.

Chapter 6 describes governing equations and the establishment of a single Telemac-2D and a coupled TELEMAC-2D and SISYPHE models for the VMD. The chapter addresses the importance and results of sensitivity analysis. The influence of various physical and numerical parameters that involve the sensitivity analysis processes are quantified. The results of the sensitivity analysis are a set the best model's parameters that are capable of simulating to predict the riverbed evolution and low-flow water level alteration in the VMD.

Chapter 7 predicts future flow, sediment and morphological changes of the VMD under impacts of existing and planned hydropower dams in the MRB through consideration of various scenarios of sediment supply from the MR by using the established models which are calibrated in Chapter 6. The resulted river morphology is used to predict the low-flow water level alterations so that the possibility of obtaining intake water for irrigation under degraded riverbed is evaluated.

Chapter 8 summarizes new findings of the research and propose some directions for compromise future studies. It also draws some recommendations to improve the VMD in terms of sustainable water resources management and development.

1.4 Research methodology

Figure 1.2 depicts an overview of the thesis's methodology. It comprises of literature review to find knowledge gaps in order to collect the required data. The collected data are then analyzed to understand the impacts of existing hydropower dams on historical flow and sediment budgets. Through data analysis, it is realized that additional flow, sediment, and river bathymetric data are needed, thus additional monitoring stations were installed and field surveys were conducted. Data acquired from field works are analyzed to provide comprehensive understanding of hydro-sediment-morphodynamics and long-term morphological changes in the VMD. Understandings stemmed from data analysis and field surveys urge the use of numerical simulation (i.e., coupled Telemac-2D and Sisyphe) to long-term predict morphological responses of the VMD under reduced sediment supply. The altered morphology is then used to predict dry-season water levels, that is necessary to understand whether will irrigation systems get difficulty under incised river morphology caused by hydropower dams so that countermeasures can be investigated and implemented.

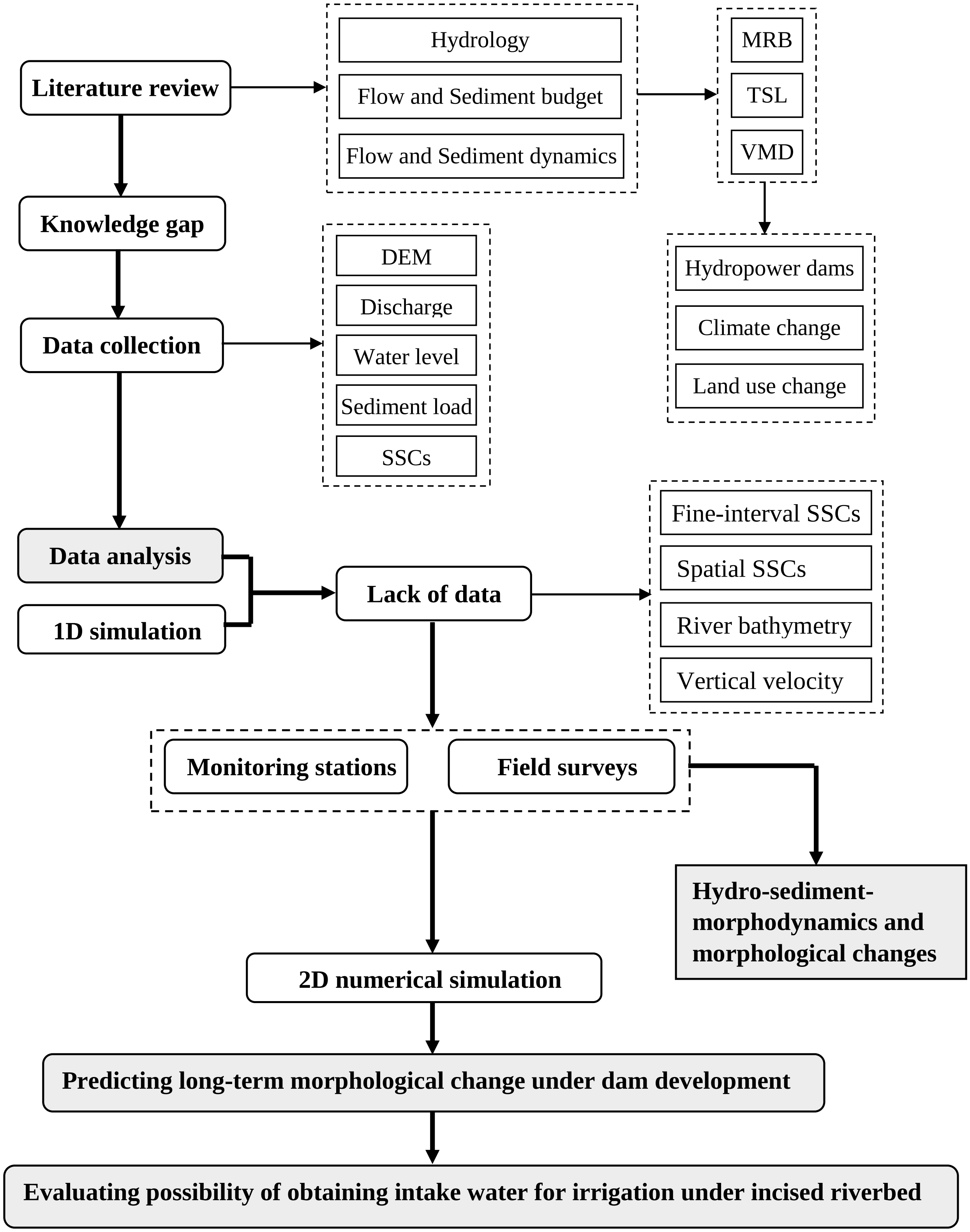

Figure 1.2 Overview of the research methodology and overall objectives.

Chapter 2 Comprehensive state-of-the-art of the Mekong River Basin and Vietnamese Mekong Delta

2.1 River hydrology and flood pulse concept

A river catchment receives water from the precipitation (i.e., rainfall or ice and snowfall, depending on weather zones). Such water becomes the river runoff after infiltration into the groundwater and evapotranspiration into the atmosphere. River flow regimes in the tropical region are normally characterized by two distinct seasons: high-flow during the wet season and low-flow during the dry season. River flow regimes with seasonal variations are essential for river ecosystem, habitat, and riverine communities. Sediment transported in rivers provides nutrients to agriculture and structures the physical habitats. It also forms the river morphology which is the base for resulting in the development of the societies.

The flood pulse, the pulsing of the river discharge, exchanges water and nutrient laterally between rivers and adjacent floodplains which are important for biota and floodplain production (Junk et al., 1989). The annual flood pulse characterized by distinct low-flow and high-flow seasons is the primary driving force for the productivity of ecosystems (Räsänen et al., 2017).

2.2 Regional settings

2.2.1 Mekong River Basin

The transboundary MR originates from the Tibetan Plateau and runs through China, Myanmar, Lao PDR, Thailand, and Cambodia before emptying into the East Sea of Vietnam through extensive alluvial floodplains in Cambodia and Vietnam (Fig. 2.1). It has a length of 4,880 km and is the 12th longest river in the world and is the largest river in Southeast Asia. It is the 10th and 8th largest river in the world in terms of water discharge and sediment budget, respectively (Meade, 1996). The MRB has a catchment area of 795 000 km^2.

In a view of bed condition, the MR can be divided into bedrock and alluvial alternately. The MR runs through upper bedrock ravines in Chinese parts to about 5 km upstream of Vientiane (near Nong Khai) (Fig. 2.1). At downstream, it runs through Laos, Thailand, Cambodia, and Vietnam. The middle alluvial reach extends downstream from Vientiane to Savannakhet, continuing by the middle bedrock until reaching Kratie in Cambodia. Downstream of Kratie, the MR is characterized by an alluvial bed with a very mild slope of river networks and known as

Mekong Delta. The Mekong Delta has two parts: the CMD extends from Kratie to the border with Vietnam, and the VMD is the remaining region from the Vietnam-Cambodia border to the East Sea. In total, the river flows over bedrocks for approximately 4,000 km (Gupta and Liew, 2007) and the remaining 880 km is the alluvial beds. The alluvial bed in Cambodia is thinner than that in Vietnam.

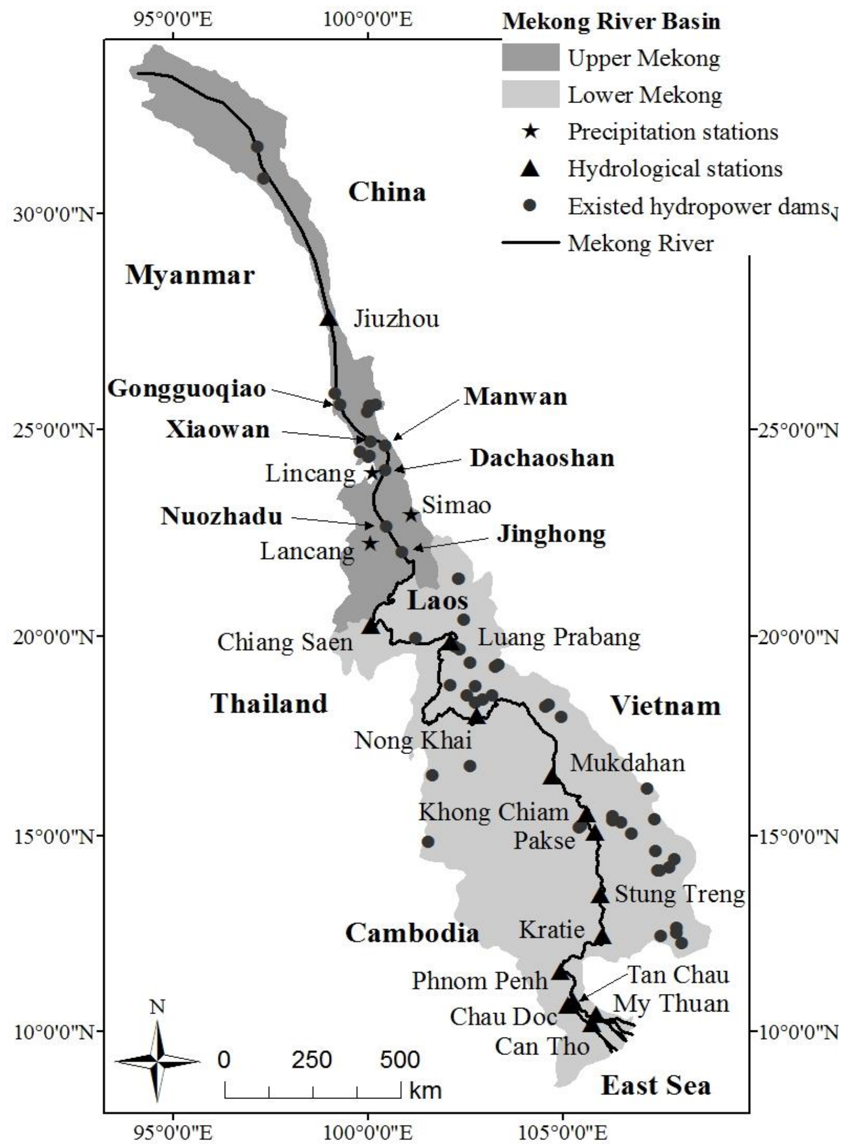

Figure 2.1 Location map of hydropower dams in the MRB, hydrological stations and available rain gauges.

At the Chatomuk conjunction near Phnom Penh (Fig. 2.1), the MR bifurcates into three branches: (1) the Tonle Sap River connects the main MR to the TSL, (2) the Mekong River, and (3) the Bassac River. The Mekong and Bassac Rivers discharge into the East Sea of Vietnam by eight distributaries through the VMD. In the territory of Vietnam, the Mekong and Bassac Rivers are named as Tien and Hau Rivers, respectively.

The MRB can be divided into two geographic parts: the upper and lower MRB. The division point of these two parts is at Chiang Saen, Thailand (Lauri et al., 2012). The upper part makes up 24% of the total basin area (189,000 km^2), running from its origin to Chiang Saen, characterized by mountainous areas with a low population density (Lu et al., 2014a). The elevation of approximately 2,000 km long falls from 4,500 m to about 500 m above the mean sea water level with an average slope of 2 m/km (Lauri et al., 2012). The lower part occupies 76% of the total basin area (606,000 km^2), within Thailand, Lao PDR, Cambodia and Vietnam (Lu and Siew, 2006), characterized by low flat topography with a high population density (Iida et al., 2011; Lu et al., 2014a). The elevation drops from 500 m to several meters above the mean sea water level, having an average slope of 0.25 m/km for the distance from Chiang Saen to Kratie, and that of 0.03 m/km from Kratie to the East Sea (Lauri et al., 2012). There are about 70 million people living in the basin with 10 million in the upper part and approximately 60 million in the downstream areas, mostly in Cambodia and Vietnam (Grumbine et al., 2012; Kummu and Varis, 2007).

2.2.2 Vietnamese Mekong Delta

The Mekong Delta which is considered as one of the most pristine and productive agro-aquaculture deltas in the world extends from Kratie in Cambodia to the East Sea of Vietnam. The total area is approximately 63,000 km^2, of which approximately 24,000 km^2 belongs to Cambodia (Manh et al., 2014). Located in the lowermost of the MR, the VMD (Fig. 2.2) is home to around 17 million people whose livelihoods are dependent on agriculture and aquaculture. It has been formed through the abundant suspended sediment discharged from the upstream since the last 6,000 years in the last 200 km stretch of the MR (Ta et al., 2002). The total area of the VMD is approximately 39,000 km^2, stretching from the Vietnam-Cambodia border, several kilometers upstream of the Tan Chau and Chau Doc gauging stations, to the East and West Seas of Vietnam (Fig. 2.2). The Tien and Hau Rivers have a length of approximately 250 and 220 km, respectively (Kantoush et al., 2017). The VMD is a low-lying area, having an average ground elevation from

0.7-1.2 m, sloping seaward (3-4 m near the border to 1-2 in the middle delta and 0.3-0.5 m near the coast).

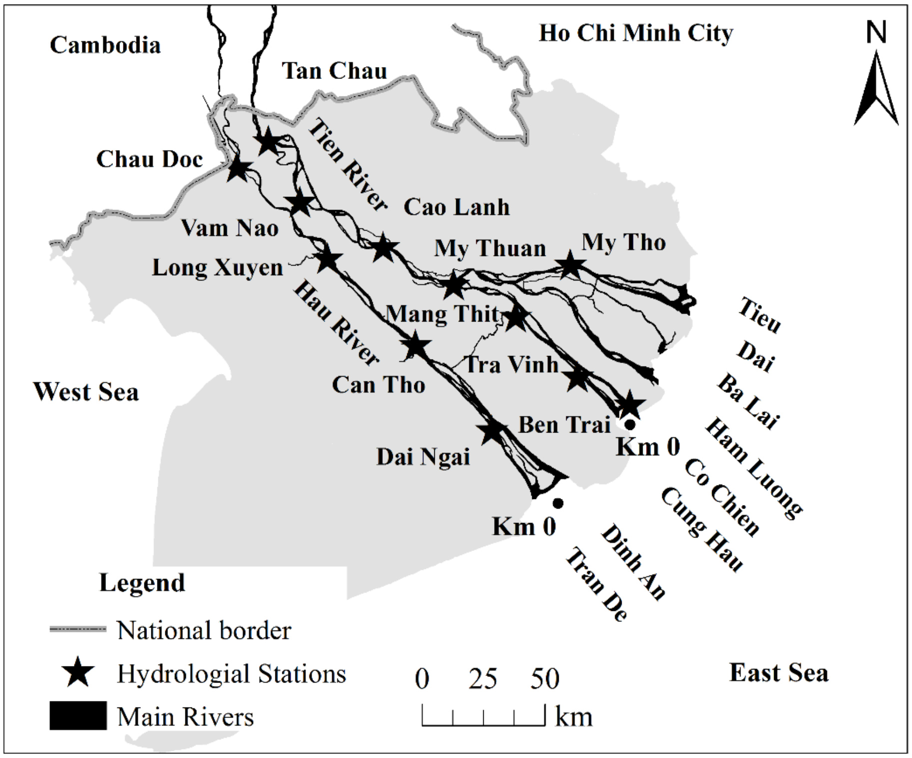

Figure 2.2 Spatial map of the VMD and distribution of hydrological stations.

The VMD consists of four main regions: (1) the Plains of Reeds, northern part of VMD on the left bank of the Tien River with an area of approximately 8,000 km^2, (2) the Long Xuyen Quadrangle, northern part of VMD on the right bank of the Hau River with an area of approximately 5,000 km^2, (3) the areas between the Tien and Hau Rivers, and (4) the coastal areas (Hung, 2011).

As the third largest delta in the world, the VMD is one of the world' most important delta in terms of food security, and known as the "rice bowl" of Vietnam. It provides 50% of Vietnam's food and 90% of Vietnam's rice production, making the country become the world's second largest rice exporter (Anthony et al., 2015). The agricultural production of the VMD largely depends on the variations of the natural flow regimes and fine sediment flux from the MR. The MR provides approximately 50% of natural fertilizer applied to the VMD annually attached in the suspended sediment (Manh et al., 2014).

2.3 Hydrological characteristics of the MRB

2.3.1 Hydrology of the main MR

The climate throughout the MRB fluctuates from cool temperature in the upper MBR to tropical monsoon in the lower MRB. Snow melting in the uppermost mountainous area controls the flow of downstream regions during the low-flow season (Wang et al., 2011). Contributing approximately 18% of the total runoff, the upper MRB is very important for the lower MRB flow regimes, especially in the low-flow season (Kummu and Varis, 2007). The mean annual rainfalls along the upper and lower MRB are 1,000 and 1,670 mm respectively. The total runoff volumes of MR derived from monsoons (130 days) are 65 and 350 km^3 in the China-Lao border and Cambodia floodplain, respectively (Bravard et al., 2013). The upper MRB contributes up to 75% of the low-flow (i.e. April-May) and over 50% of the peak flow at Vientiane and over 40% of the flow during April (the lowest month) at Kratie (Adamson et al., 2009). The hydrology of the lower MRB is divided into the wet season (May-October) and the dry season (November-April). Approximately 85-90% of the river flow is generated during the wet season with an average discharge of 45,000 m^3/s (Lu and Siew, 2006). The remaining 10-15% of the river flow takes place during the dry season with an average discharge of 15,000 m^3/s, controlled by the flow from snow melting in the upper MRB. The wet season climate is affected by monsoon, partly from the southwest and partly from the southeast. Tropical cyclones from the east are also influencing the climate in the wet season. The monsoon usually occurs within August-October with substantially high precipitation (Lauri et al., 2012).

2.3.2 Hydrology of the VMD

Approximately 80% of the flow is conveyed by the Tien River while the Hau River transports the remaining 20% (based on our data from 1980 to 2015). The hydrographs of the VMD are characterized by two distinct seasons: high-flow and low-flow. The high-flow season usually starts from June/July and ends in November/December while the low-flow season lasts for around half a year from November/December to May/June. Mean discharges (based on 1980-2015 data used in this research) at the Tan Chau and Chau Doc stations are 9,940 and 2,490 m^3/s, respectively. These mean discharges divide the hydrographs into two distinguished stages: the rising stage (April-September) and falling stage (October-March) (Fig. 2.3). In the rising stage, the flood pulse of the VMD is influenced by the inflow into the TSL which then releases the reverse flow onto the

MR when the flood is at its peak and recession stage. In months of peak flow (August-October), the tide no longer, or very little, influences the flood regimes. In the falling stage, the flood gradually reduces and the influence of the tide gets stronger again, and at its maximum influence during normally April.

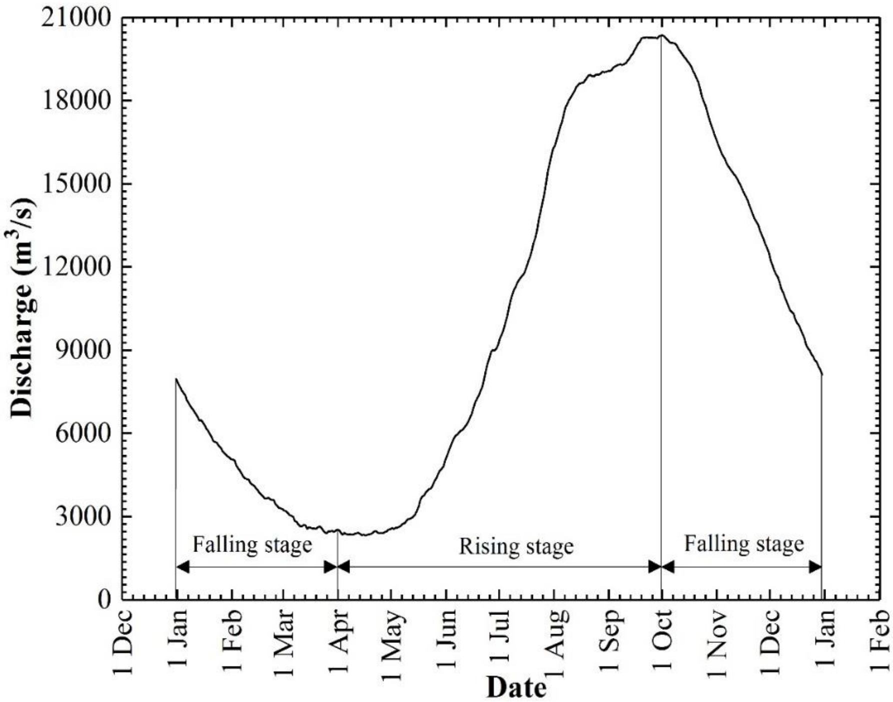

Figure 2.3 Flow hydrograph (1996-2015) at the Tan Chau station.

2.3.3 Sediment budget of the MR

Annually, the MR provides extensive suspended sediment resources to large-scale floodplains in the VMD through a dense river and channel network. Such suspended sediment load (SSL) is crucial for the development of the delta. It may help the delta sustain from adverse effects of the sea level rise (Chapman and Darby, 2016), land subsidence (Manh et al., 2014), riverbank erosion and bed incision (Kondolf et al., 2014), and coastline retreat (Anthony et al., 2015) as well as provide plentiful natural fertilizer application to the agricultural lands (Manh et al., 2014).

The understanding of the amount of bedload and its changes in the MR is limited (Kummu and Varis, 2007) due to a lack of systematic monitoring. Sporadic measured data showed that the bedload in the lower MR constituted approximately 3-15% of SSLs (Fu et al., 2008; Koehnken, 2014).

Various values of the annual suspended sediment budget of the MR have been reported in the literature, depending on the location, data sources, computation methods, and years of consideration. The estimates ranged from 50 to 170 Mt/yr based on different studies (Koehnken, 2014; Kummu et al., 2010; Lu et al., 2014a; Lu and Siew, 2006; Walling, 2008; Wang et al., 2011; Xue et al., 2011). Based on the suspended sediment data during 1962-2003 at the Khong Chiam station (Fig. 2.1), Wang et al., (2011) estimated the annual suspended sediment budget of the MR ranged from 119 to 162 Mt/yr, with an average value of 145 Mt/yr, which is similar to the annual suspended sediment budget at the Pakse station (Fig. 2.1) of 147 Mt/yr (Walling, 2005). In natural conditions (pre-1992), the annual SSL at the Mukdahan station was estimated to be 170 Mt/yr. However, the historical annual SSLs of Mukdahan and Khong Chiam were not reliable because they were overestimated due to issues related to the measurement conditions (Koehnken, 2014). The annual SSL of 160 Mt/yr at Kratie (the most downstream station before the Mekong Delta) (Fig. 2.1) has been widely quoted as the annual suspended sediment flux of the MR to the sea in pre-1992 period (Bravard et al., 2013; Kondolf et al., 2014; Meade, 1996; Milliman and Syvitski, 1992; Rubin et al., 2015). In postdam periods (post-1992), the suspended sediment budget of the MR was estimated as 50-91 Mt/yr at Phnom Penh in 2008-2010 (Lu et al., 2014a) and 44-98 Mt/yr at Kratie in 2009-2013 (Koehnken, 2014).

2.3.4 Sediment flux in the VMD

Sediment data in the VMD are not publicly available, with no accurate annual SSL entering the VMD has been reported. Based on the sediment-volume analysis of six sediment samples near the coast, (Ta et al., 2002) estimated the annual suspended sediment discharge into the East Sea was stable at 144 Mt/yr over the last 3,000 years. If 13.6% of the suspended sediment in the Vietnam-Cambodia border deposited along the Tien and Hau Rivers before reaching to the sea (Manh et al., 2014), the annual SSL entering the VMD in predam period would be 166.7 Mt/yr. Recently, (Nowacki et al., 2015) reported the annual suspended sediment flux to the sea as 40 Mt/yr based on field investigations in 2012 and 2013. Using numerical simulations from 2009-2011, (Manh et al., 2014) predicted the annual SSL reaching the East Sea of Vietnam ranging from 25.9 Mt/yr to 50.5 Mt/yr.

The suspended sediment of the Mekong Delta is mostly of silt and clay. They constituted up to 80% and 98% of the suspended sediment budget at the Kratie and Tan Chau stations respectively

(Fig. 2.1) (Bravard et al., 2013). The bed material of the main rivers in the VMD consists of mainly fine sand with a small portion of mud (Gugliotta et al., 2017). The annual sand load in suspension is 6.5±1.6 Mt/yr through eight river distributaries, of which 32% from the Dinh An distributary and 9% from the Tran De distributary of the Hau River (Stephens et al., 2017).

2.4 Challenges of the VMD

2.4.1 2015-2016 drought event

River-damming along with the effect of El Niño, have induced the most severe drought over 90 years in 2015-2016. All provinces in the VMD have been impacted by this drought event. The measured water levels were at their lowest values since 1926, even much lower than those measured in the drought year of 1998 (Fig. 2.4a). The figure shows a reduction of 3 m by comparing the water level on September 22, 2000 and 2015. Correspondingly, the SSCs in 2015 were lower compared to precedent years (one-fourth of 2011) (Fig. 2.4b). For these considerations, in the framework of JASTIP project (Japan-ASEAN Science, Technology and Innovation Platform) we established a project to study the impact of hydropower development in the upper MRB on hydrology, sediment, and salinity changes in the lower MRB with special focus on the VMD. Under this project, suspended sediment and salinity concentrations are continuously measured at six locations in the Tien and Hau Rivers, namely Tan Chau, Vam Nao, Thot Not, An Lac Tay, Bac Trang, and Dinh An, since February 2016.

The drought event in 2015-2016 was accompanied by severe saltwater intrusion in the VMD. Saltwater has intruded 45-65 km in the Tien River and 55-60 km in the Hau River, which is 20-25 km further than seasonal average values. Salinity concentrations at An Lac Tay (located 50 km from the river mouth) in 2015 and 2016 were much higher than recorded values in previous years (Fig. 2.4c). The figure shows that the salinity concentration of 2016 was 6 g/l higher than that of 2005 and 2007. Also, salinity intrusion began approximately two months earlier than average that caused serious damages to agriculture and livelihoods of people in the VMD. By the end of 2015, about 159,000 hectares (ha) paddy fields were damaged; around 195,217 households with approximately 976,000 people lacked fresh water for daily consumption.

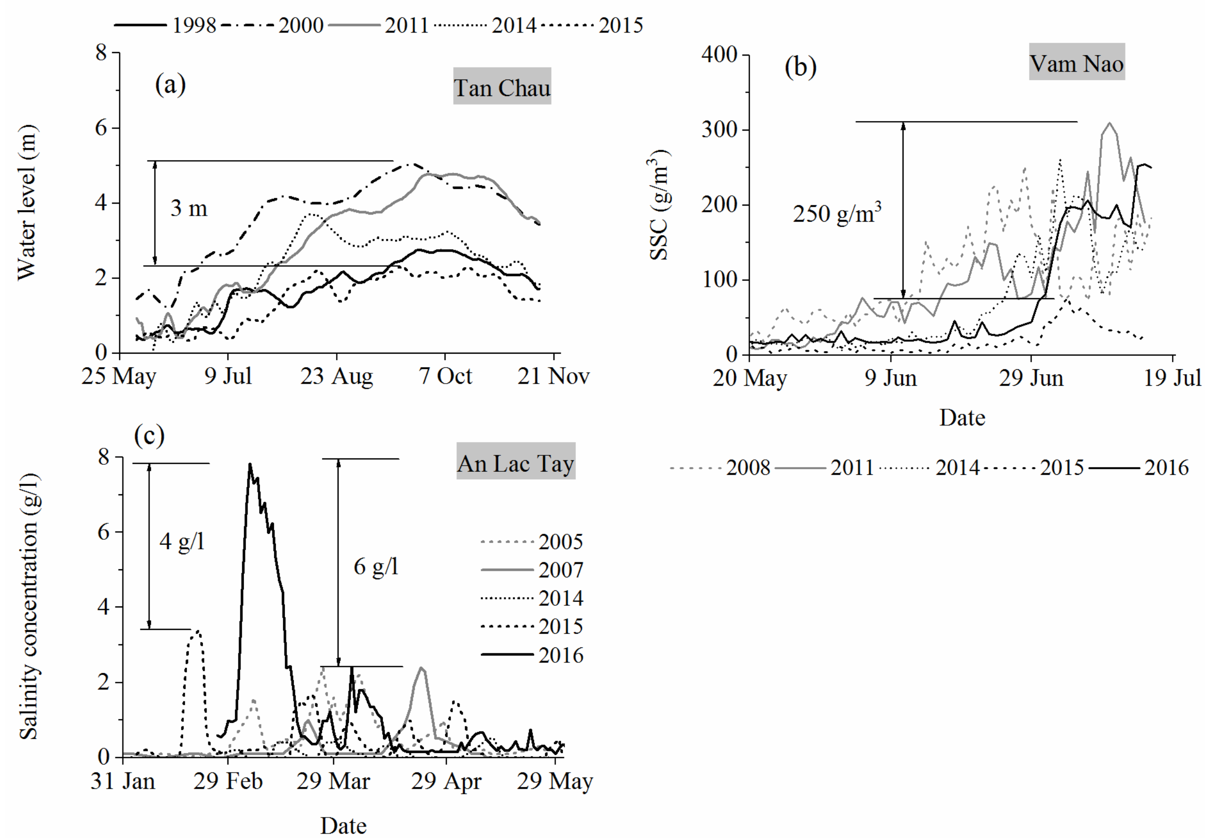

Figure 2.4 Water level, suspended sediment concentration and salinity concentration in different years at various stations.

2.4.2 Dam development in the MRB

Dams and reservoirs have been increasingly planned and built in the MRB since the 1950s under the pressure of the population boom in riparian countries. The completion of the first mega dam in the MR's mainstream, Manwan, in 1993 (Table 2.1) has triggered the construction of other five mainstream dams, namely Dachaoshan, Xiaowan, Jinghong, Gongguoqiao, and Nuozhadu in the upper MR, known as Lancang cascade and numerous smaller dams in tributaries. Sixty-four large hydropower dams (> 15 m high) (Kondolf et al., 2014) have been built in the MRB by 2015 (Fig. 2.1) with a total storage capacity of over 80.2 km^3, accounting for 96.8% and 20.1% of the annual discharges at Chiang Saen and Kratie stations, respectively (Fig. 2.1). Of total storage capacity of 80.2 km^3, over 51% (41.2 km^3) was constituted by six Lancang cascade dams in China (Table 2.1). The total capacity of these mainstream dams is over tenfold larger than the total capacity of 160 large dams in Switzerland which is 4 km^3 (Loizeau et al., 2010).

Four out of the six existing mainstream dams in the Lancang cascade were classified as black hole reservoirs (Table 2.1) which could almost trap all the sediment flowing in and provide enough flood control storage (Binh et al., 2018b). Nuozhadu and Xiaowan are the two largest dams, having a total storage capacity of 10 times more than the rest (Table 2.1). Moreover, these two dams have very large reservoir live storages, *CAP/MAS* (reservoir's total capacity (CAP)/mean annual sediment load (MAS)), and retention times, *CAP/MAR* (reservoir's total capacity/mean annual runoff (MAR)) (Table 2.1). These storages enable them to significantly trap most of the sediment and store flow generated upstream. They are, therefore, expected to have the strongest impacts on the sediment budgets of the lower MR. Mean annual sediment loads of the existing mainstream dams were not available. They were therefore estimated in this study using a linear relation in Eq. 2.1

$$MAS_i = \frac{A_i}{A_{Ch}} \times MAS_{Ch} \tag{2.1}$$

where MAS_i and MAS_{Ch}: mean annual sediment loads at dam i^{th} and at Chiang Saen (90.4 Mt yr^{-1} as predam (1961-1992) mean annual sediment load (Wang et al., 2011)), respectively; A_i and A_{Ch}: catchment areas at dam i^{th} and at Chiang Saen (189 000 km^2), respectively. Table 2.1 also shows that the retention times of the existing mainstream dams are much higher than that of a group of existing and planned dams in tributaries which were all referred to as run-of-the-river dams.

Additional eleven mainstream hydropower dams have been planned in the lower MR in Thailand, Laos PDR, and Cambodia, of which Xayaburi is under construction in Lao PDR despite the reservations of the downstream communities regarding its adverse impacts on the environment, fisheries and other aquatic resources (Pokhrel et al., 2018). Also, there are a number of small hydropower dams and diversions for irrigated agriculture throughout the MRB which may also contribute to the flow alterations downstream but at local scales (Kondolf et al., 2018). However, the understanding of the impacts of large hydropower dams in the MRB is the main focus of this research.

Table 2.1 Characteristics of dams and reservoirs of the mainstream and tributaries in the MRB. (Sources: [a]Fan et al. (2015); [b]Kummu et al. (2010); [c]Binh et al. (2018)).

Reservoir	[a]Reservoir filling year	[a]Catchment area km^2	[b]Mean annual runoff (MAR) km^3	Mean annual sediment (MAS) km^3	[a]Total capacity (CAP) km^3	CAP/MAS	CAP/MAR	[c]Reservoir classification
Mainstream dams								
Nuozhadu	Nov. 2011	144,700	55.2	0.0379	22.37	589.9	0.4053	Black hole
Xiaowan	Dec. 2008	113,300	38.5	0.0297	15.13	509.5	0.3930	Black hole
Jinghong	Apr. 2008	149,100	58.0	0.0391	1.23	31.5	0.0212	Black hole
Manwan	Mar. 1993	114,500	38.8	0.03	1.06	35.3	0.0273	Black hole
Dachaoshan	Nov. 2001	121,000	42.3	0.0317	0.88	27.7	0.0208	Sorting
Gongguoqiao	Sep. 2011	97,300	31.1	0.0255	0.51	20.0	0.0164	Sorting
Grouped dams in tributaries								
Nam Phuong	NA	3,420	5.4	0.1499	0.08	523.2	0.015	Sorting
Nam Ma	NA	1,128	1.0	0.1483	0.00	0.0	0.000	Transparent
Huai Bang Lieng	NA	657	1.7	0.0720	0.07	953.2	0.040	Sorting
Nam Beng	NA	2,193	0.9	0.2764	0.19	695.3	0.214	Sorting
Nam Kam	NA	3,506	4.7	0.0672	0.00	0.0	0.000	Transparent
Nam Chi	NA	49,067	29.5	0.4839	0.004	8.1	0.000	Transparent

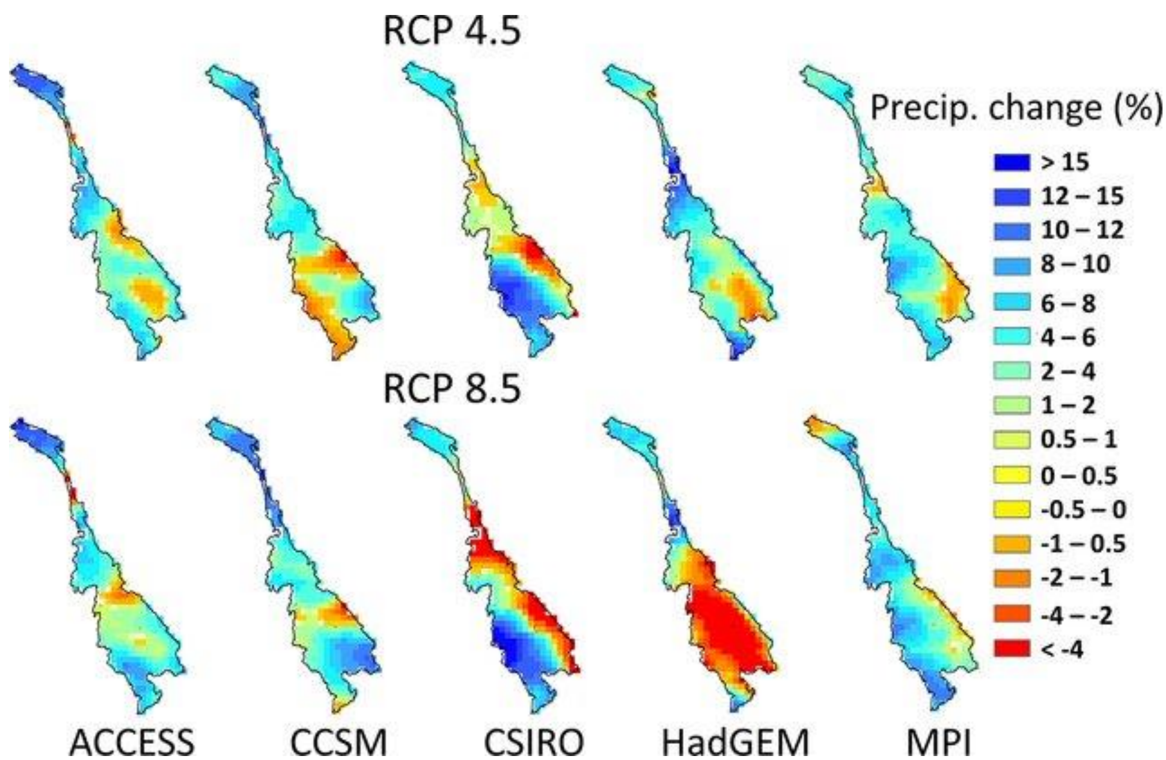

Figure 2.5 Projected change in the total annual precipitation (%) of the MRB during 2035-2065 compared to the baseline during 1971-2000. Source: (Hoang et al., 2016).

2.4.3 Climate change and sea level rise

(Hoanh et al., 2010) modified the PRECIS climate data for the observed data during 1985-2000, and applied to the future up to the year 2050. They found that the precipitation in the MRB will be increased by 2050 under climate change, with a mean value of 1.2-1.5 mm/yr, except for Cambodia and Vietnam. The future dry season will have more precipitation than the past, with an increase of 0.9 mm/yr in the upper MRB. Temperature is also projected to increase by approximately 0.23°C/yr (Hoanh et al., 2010). Based on the Vietnamese national climate change scenarios, the main temperature might increase by 3°C and rainfall may increase by 5-10% by 2100 (Toan, 2014). Comparing the projected precipitation (2036-2065) to the baseline (1971-2000), (Hoang et al., 2016) found that the precipitation in the upstream of Chiang Saen will substantially increase while the precipitation in the lower MRB may increase or decrease, depending on the location (Fig. 2.5).

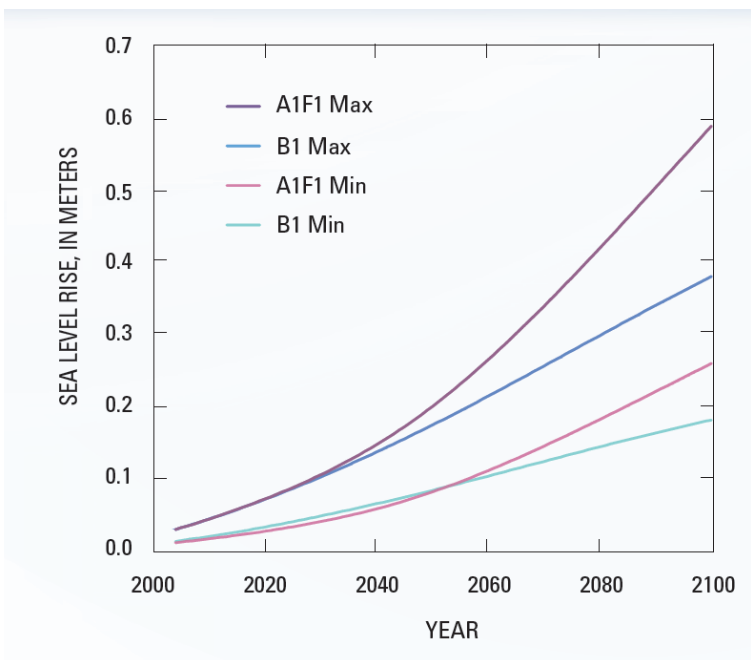

Figure 2.6 Sea level rise in the VMD by 2100 based on IPCC projections. Source: (Doyle et al., 2010)

The hourly water levels at the Hon Dau station (Hai Phong province) during 1960-2000 were observed to rise with a rate of 1.9 mm/yr, which is in the range of 1.75-2.56 mm/yr at four stations along the coast of Vietnam (Doyle et al., 2010). They also reported that water levels at Vung Tau (close to the VMD) during 1979-2001 increased with a rate of 6 mm/yr. Climate change, ice melting in the polar ice caps and glaciers, and thermal expansion of oceans were predicted to accelerate the global sea level rise (Schmitt et al., 2017). Depending on emission scenarios of the IPCC, the minimum, mean, and maximum sea level rise by 2100 were 0.28 m, 0.56 m, and 0.98 m, respectively. These values corresponded to rising rates of 3, 7, and 12 mm/yr, considering equal increases during 2016-2100 (Schmitt et al., 2017). By considering land subsidence and sea level rise, (Doyle et al., 2010) predicted the maximum relative sea level (scenario A1F1) in the VMD will rise with a rate of 5.5 mm/yr while the increased sea levels for different scenarios are shown in Fig. 2.6. Maximum sea level rises under high emission scenario (A1F1) by 2100 using Vietnamese national climate change scenarios can reach 79-99 cm, equivalent to 7.9-9.9 mm/yr (Toan, 2014).

2.4.4 Delta development and land use change

During the last decades, the Vietnamese Government has constructed numerous canals and dyke systems as well as other control structures (pumps, sluice gates, ship blocks etc.) to protect the agricultural lands from flooding for increasing the rice crops and productivity (Hung et al., 2013a). These anthropogenic interferences have separated the initial floodplains into thousands of compartments which are connected to the channels mainly by sluice gates. In addition, to protect rice crops from flooding, thirty-nine ring dikes (low and high ring dikes) have been constructed in various areas. Low ring dikes with the surface elevation of 2-2.5 m were built to mainly protect agricultural areas from the August flood for paddy field harvesting and can be overflowed during the flood peak (in September or October) so as to catch suspended sediment into compartments. High ring dikes with the surface elevation of 4-4.5 m are used to totally prevent the flooding from the triple-crops areas. In the Plains of Reeds, high ring dikes are about 33% while low ring dikes make up 67% (Hung, 2011).

According to (Hung et al., 2013b), the whole VMD has about 45,000 segments of channel network with a total length of approximately 87,500 km. The total lengths of low and high ring dikes are approximately 13,300 km and 1,300 km, respectively. There are 980 sluice gates, having the width of 3-100 m and 20,500 smaller sluice gates, having the width of less than 3 m. Currently, these structures are very important for the development of the VMD but need to be reappraised in terms of environmental sustainability, biodiversity, soil degradation, and agriculture productivity.

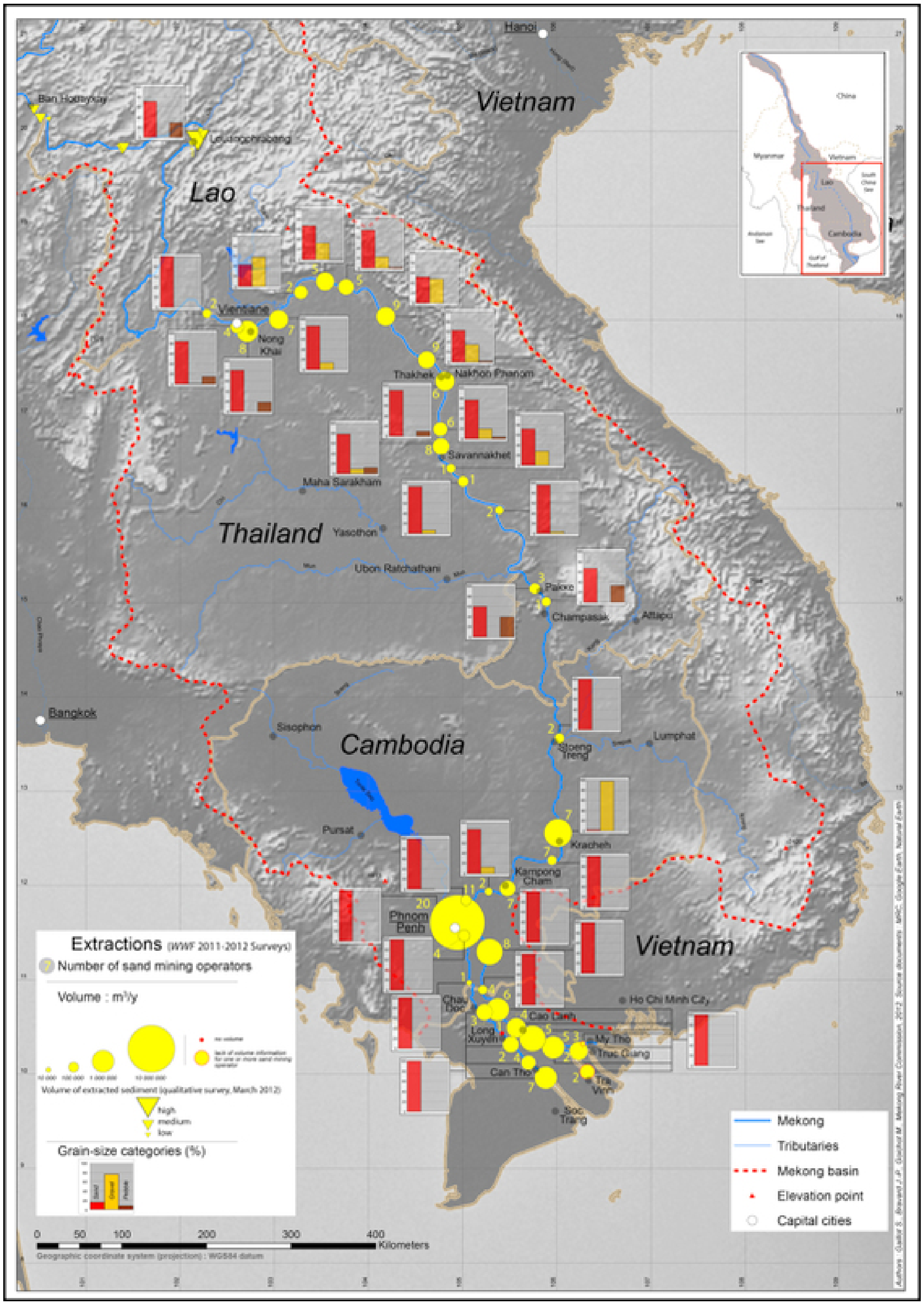

Figure 2.7 Locations and volume of sand mining along the MR. Source: (Bravard et al., 2013).

2.4.5 Sand mining, groundwater extraction, and land subsidence

Sand is an important source for construction, delta formation, coastal landforms, channel shaping, land reclamation, and export (mainly Cambodia and Vietnam export to Singapore). Sand transports in the suspended mode in the upper part of the MR during floods and in bedload mode in the VMD. To support economic development, sand has been increasingly mined in Thailand, Laos, Cambodia, and Vietnam. A field survey in 2011-2012 by (Bravard et al., 2013) was a rare document quantifying sand mining in the lower MR. They reported that approximately 31 Mm^3 of sand is annually mined from the riverbed, equivalent to 49.6 Mt/yr by considering a bulk density of 1.6 t/m^3), of which 18.7 Mm^3 in Cambodia (60%, the largest extractor), 7.8 Mm^3 in Vietnam (22%), 3.7 Mm^3 in Thailand (13%), and 1 Mm^3 in Laos (4%). Detail of locations and volumes of sand mining along the MR are shown in Fig. 2.7. Fig. 2.8 shows the mining machine and ship used to transport the mined sand in the Tien River that was taken during the field trip in August 2017. Realizing the importance of sand and negative impacts from sand mining, Vietnam has banned sand mining since 2000. Nine years later, in 2009, Cambodia also banned sand mining activities (Bravard et al., 2013). However, mining activities are still continuing along the MR in Cambodia and Vietnam at smaller scales, depending on locations.

Figure 2.8 Machine used to extract and transport mined sand in the VMD. Photos were taken by Binh, D.V. during the field trip in April 2018.

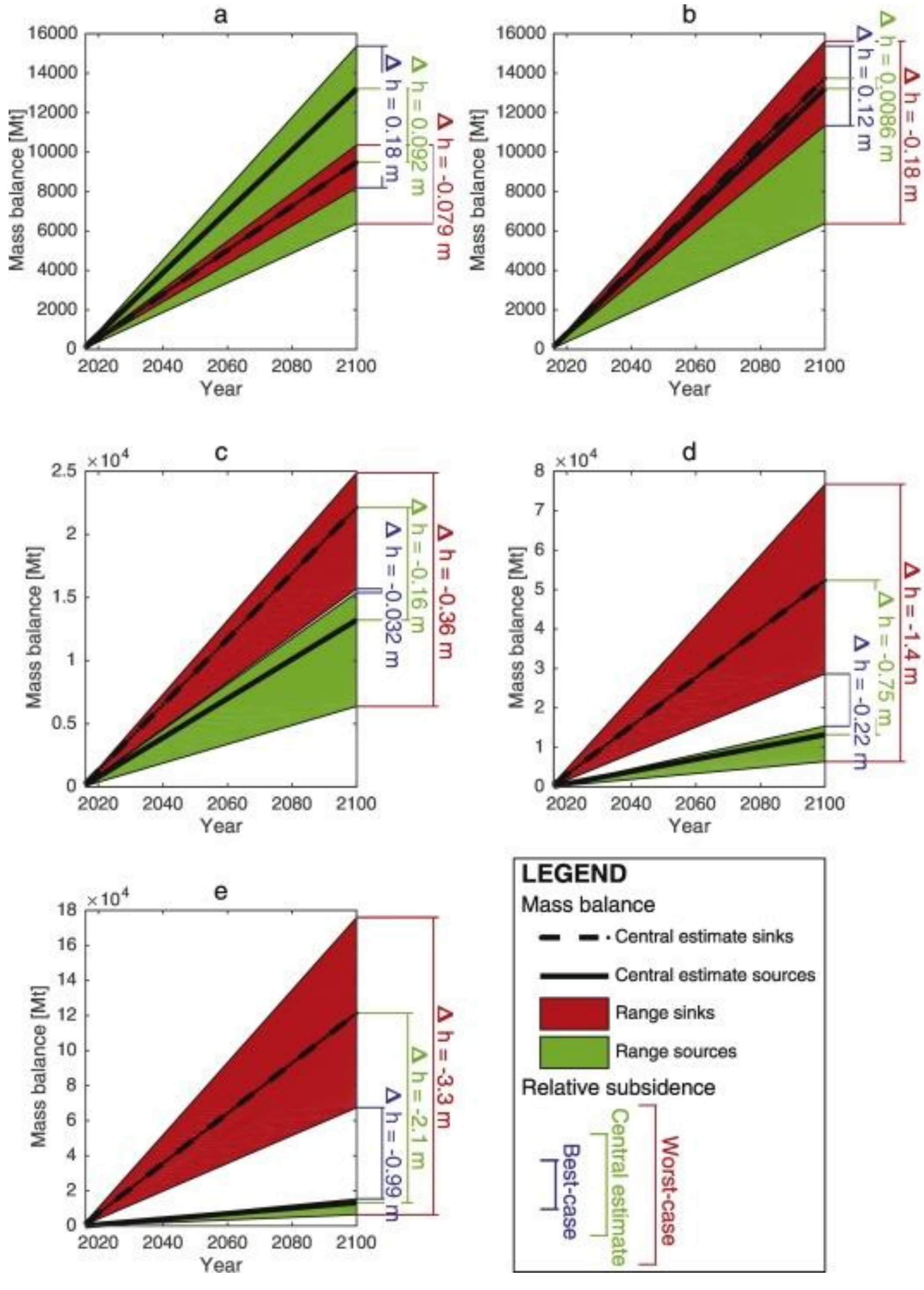

Figure 2.9 Subsidence and aggradation of the VMD under different conditions: (a) natural condition, (b) sand mining, (c) sand mining and reservoir trapping, (d) sea level rise, and (e) groundwater pumping. Source: (Schmitt et al., 2017).

Due to fast population growths in big cities in the VMD, such as Can Tho city, and lack of freshwater due to geographic remote locations, such as Ca Mau province, groundwater abstraction has been increasing to support domestic and agricultural demands. (Minderhoud et al., 2017) summarized land subsidence in the VMD that the subsiding rates were 6 mm/yr during 1987-2006 by using surface water level trend analysis, 17.1 mm/yr during 1993-2013 in Can Tho city, and 16 mm/yr during 2006-2010 at 15 monitoring stations. They then applied a process-based 3D model to estimate a mean subsiding rate of the VMD of 1.1 cm/yr, with the maximum value over 2.5 cm/yr in places. The mean subsiding rate was predicted at 1.6 cm/yr, with exceptionally high at Ca Mau (3 cm/yr) and Can Tho (2.5 cm/yr) (Kondolf et al., 2018). The total mean land subsidence of the VMD over the past 25 years was approximately 18 cm, and up to 30 cm in places by (Minderhoud et al., 2017) who argued that such critical land subsidence is mainly caused groundwater abstraction, with a rate of 2.5 Mm^3/day or 900 Mm^3/yr. (Schmitt et al., 2017) found that the VMD is largely in balance in the natural conditions with relative a subsidence of -0.08 m to an aggradation of 0.18 m during 2016-2100. However, the VMD will be subsided by -3.3 m that almost disappears by 2100 if considering the combined effects of reduced sediment supply from the MR, hydropower dam trapping (only 4% of the MR sediment is delivered to the VMD if 133 dams are built (Kondolf et al., 2014)), sand mining, groundwater pumping, sea level rise, natural compaction, and organic production (Fig. 2.9).

2.5 Prior researches regarding flow and sediment alterations, and associated consequences in the MRB under various drivers

Figure 2.10 shows a flowchart of reviewing prior studies in the MRB associated with water resources. Those prior studies were reviewed based on the study areas along the MR with different field of studies. Those prior studies were also grouped into different controlling factors such as hydropower dams, climate change or sand mining. At the lowest grouping level, tools and methods used in each research were classified. Based on the reviewing method in Figure 2.10, Table 2.2 summarized key studies in the MRB regarding flow and sediment alterations and morphological changes under impacts of various drivers such as hydropower dams, climate change, land use change, and sand mining, and fundamental understanding of the flow and sediment dynamics of the MR. Figure 1.1 and Table 2.2 show that most of the prior studies that attempted to examine the impacts of hydropower dams on alterations of the flow and sediment regimes and budgets of the MR were conducted in the middle MRB. Some studies paid attention to the VMD but no studies evaluated dam impacts on historical alterations of flow and sediment budgets of the VMD and associated consequences such as morphological change, and saltwater intrusion.

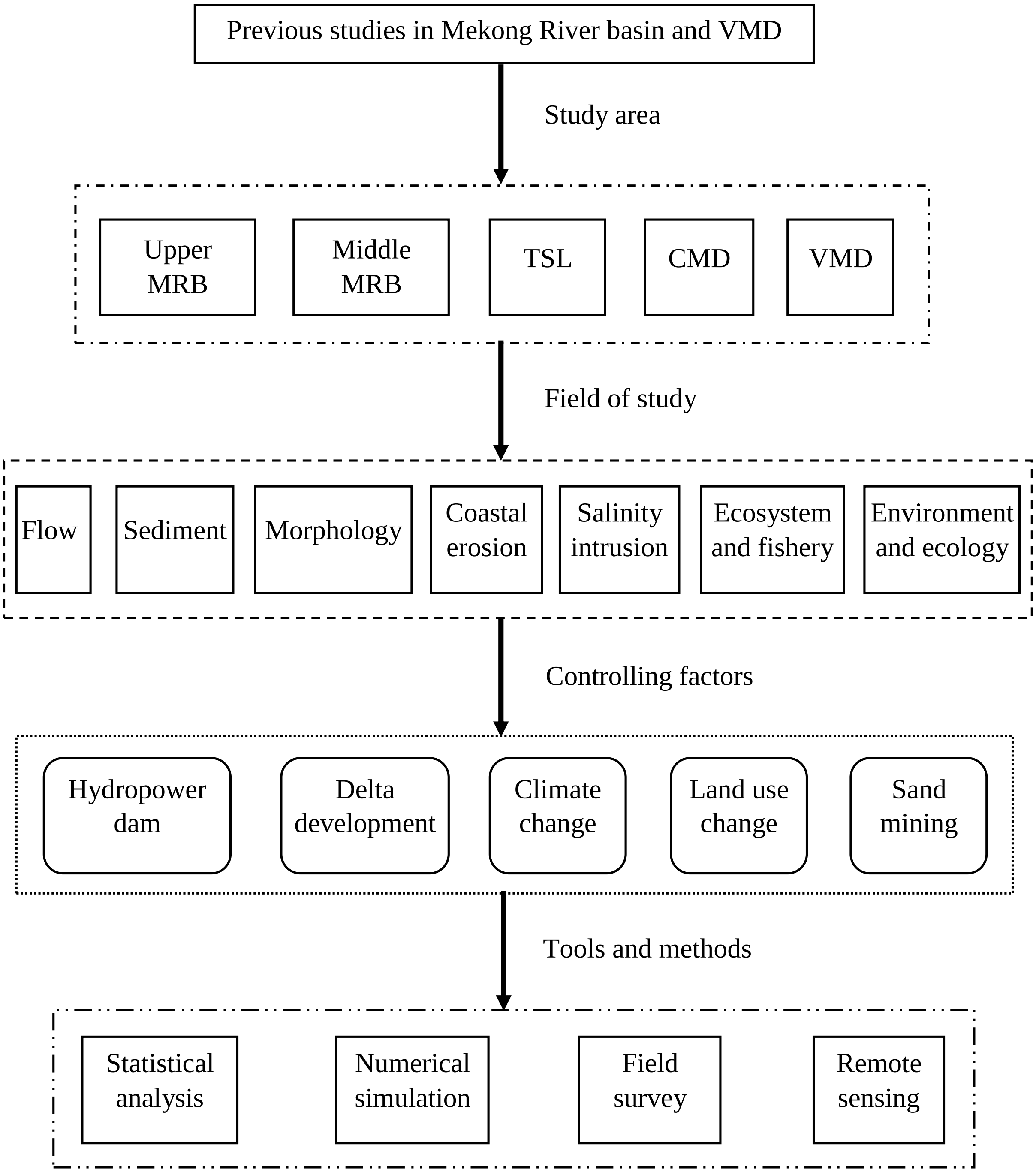

Figure 2.10 Flowchart of reviewing method of prior studies in the MRB associated with water resources.

Table 2.2 Summarized prior studies in the MRB regarding flow and sediment alterations, and morphological changes under various drivers.

Objective	Study area	Method	Main finding	Authors
Hydrological roles of Cambodia floodplain in inundation reduction	CMD and VMD	Field survey, Remote sensing, and numerical model	Floodplains reduce significantly flood peak in mainstream channels by 9,000-17,000 m^3/s. ~30% of flood discharge at Kongpong Cham is diverted to the floodplains between Kongpong Cham and Phnom Penh	(Fujii et al., 2003)
Impacts of dams, tides, storm surges, engineering structures, SLR and estuarine siltation	CMD, TSL, and VMD	Numerical model, remote sensing, and statistical analysis	Engineering structure in VMD increase the flow velocities in river and canals, leading to increasing bank erosion and bed incision SLR enhances flooding in VMD' coastal areas	(Hoa et al., 2007)
Cumulative impact of dams and climate change on the hydrology of MR within the next 20-30 years	MRB	Numerical model	Dams have larger impacts on river hydrology than climate change. Cumulative impacts of dams and climate change follow rather closely the reservoir operation impacts	(Lauri et al., 2012)
Impacts of Lancang cascade on MR's hydrology	Upper and middle MRB	Numerical model	The MR's hydrology has been significantly changed due to Lancang cascade Lancang dams increased December-May discharge (34-155%) and decreased July-September discharge (29-36%) at Chiang Saen	(Räsänen et al., 2012)
Impacts of dams and climate change on flow and aquatic net primary production	TSL	Numerical model	Hydropower dams would cause the most distinct changes of flow: increase low flow and reduce the high flow Annual net sedimentation in TSL decreases by 56±3%	(Arias et al., 2014)
Effect of temperature and precipitation on the flow	Upper MRB	Statistical analysis	Flow increases due to climate warming, with the abrupt changes in the lower MRB occurring in the mid-1960s and late 1990s	(Fan and He, 2015)
Impacts of climate change on MR's hydrology	MRB	Numerical model	Extreme high flows increase in both magnitude and frequency Extreme low flows occur less often	(Hoang et al., 2016)
Impacts of Lancang dams and climate change on flow	Middle MRB	Statistical analysis	Dams altered flow in postdam Climate change affects flow in the transition period	(Li et al., 2017)
Impacts of dams on flow alteration	MRB	Data analysis and numerical model	Hydropower operations have largely modified flow discharge downstream since 2011, and the largest changes were observed in 2014	(Räsänen et al., 2017)
Impacts of climate change and land use change on flow and nutrient yield	Middle MRB: 3S river basin	Numerical model	3S basin is sensitive to climate and land use changes Discharge and nutrient yields increase throughout the 21st century	(Trang et al., 2017)
Dam impacts on the hydrologic regime	Middle MRB: 2S river basin	Numerical model	Effects induced by climate change is smaller than by dams Dams increase dry season flow and reduce wet season flow	(Ngo et al., 2018)

Objective	Study area	Method	Main finding	Authors
			Flow change induced by climate change in seasonal and annual is small	
Potential effects of planned dams on flood pulse dynamics	Lower MRB to VMD	Numerical model	TSL can reduce flood peak from MR to vicinity areas, its role becomes less effective when more dams are built in the upstream	(Pokhrel et al., 2018)
Effects of water infrastructures, land subsidence, and SLR on flow regimes	CMD, TSL, and VMD	Numerical model	Dam operations increase and decrease by 20-70% and 0.8-5.9% of floodplain's water level in the wet and dry seasons, respectively, in river-dominated areas Land subsidence combined with SLR has great impacts on future VMD's inundation	(Dang et al., 2018)
Impacts of dams, climate change, land use change and water demand on the flow	MRB	Review	Dam impact studies should be integrated with fish passage barriers, geomorphic changes, and other contemporaneous stressors.	(Hecht et al., 2019)
Understanding fine sediment dynamics in low-flow	VMD: Dinh An branch	Field survey	Flocs occur in the saltwater region. Saltwater is more turbid than freshwater. Turbidity maximum varies with tides.	(Wolanski et al., 1998)
Sediment trapping efficiency of Lancang cascade dams	Upper MRB	Theoretical models	TE of Manwan is ~60%. TEs of Gongguoqiao, Dachaoshan, Jinghong are ~30%, 66%, and 63%.	(Fu and He, 2007)
Impacts of dams on sediment load	Middle MRB	Statistical analysis	As of 2002, dams have little impacts of sediment load but expected to reduce if more dams are built.	(Walling, 2008)
Impacts of dams on sediment trapping efficiency	Upper and middle MRB	Theoretical analysis	Upper MRB contributes 60% of MR's sediment load. Eight Lancang dams trap >50% of MR's sediment (70-73 Mt).	(Kummu et al., 2010)
Method estimating SSLs for years without good quality data	Middle MRB	Theoretical analysis	Sediment load at Chiang Saen increased during the period of Manwan construction (1986-1002) but reduce in postdam (1992-2003). Upper MRB was the largest source of sediment of the MR in predam.	(Wang et al., 2011)
Better understanding sediment transport of the VMD's shelf and roles of current, waves, and tides on along-shore sediment transport	VMD's shelf	Numerical model	In high flow, fluvial sediment deposited near river mouths which is re-suspended and transported southwestward in low flow due to wave and coastal current	(Xue et al., 2012)
Characterize and quantify suspended sediment dynamics in VMD's floodplain	VMD	Field survey	Flood wave and tidal influences control the suspended sediment dynamics in VMD. Not all suspended sediment entering the paddy fields is deposited in floodplains because the particle is very fine.	(Hung et al., 2013b)
Investigate erosion and deposition of suspended sediment in floodplains	VMD	Field survey	Mean deposition rate is 6.86 kg/m^2 (6 mm/yr). Key parameters of erosion and deposition: critical bed shear stresses. Bulk floodplain sedimentation occurs in the initial stage of floodplain inundation.	(Hung et al., 2013a)
Estimate sediment yield	Middle MRB	Statistical analysis	Applicable model to estimate sediment yield.	(Heng and Suetsugi, 2014)

Objective	Study area	Method	Main finding	Authors
Quantify suspended sediment transport and deposition	CMD, TSL, and VMD	Numerical model	River flow, tide, channel system, dikes, and sluice gate operations are the main factors controlling the spatial sediment dynamics Deposited sediment in CMD and VMD are 19-23% and 1-6% of Kratie's sediment, respectively	(Manh et al., 2014)
Understanding sediment dynamics of Mekong-Tonle Sap river confluence	Chaktomuk confluence in Phnom Penh	Field survey	Inflow sediment load towards the TSL was lower than that of the outflow (84%). Annual sediment load from TSL contribute to VMD is <15%, but its share is considerable during February-April.	(Lu et al., 2014a)
Estimate sediment yields and cumulative sediment trapping efficiency	MRB	Numerical model	"Definite future" scenario (38 dams) reduces 51% of sediment reaching to VMD "Full build-out" scenario (133 dams) will trap 96% of sediment reaching to VMD	(G.M. Kondolf et al., 2014)
Role of tropical cyclones in transmitting suspended sediment	MRB	Numerical model	32% of SSL reaching to the delta is delivered by runoff generated by rainfall associated with tropical cyclones Dams are a dominant factor in explaining past and anticipating future, declines in SSLs reaching to VMD	(Darby et al., 2016)
Suspended sediment dynamics and controlling factors in subaqueous delta	VMD	Numerical model, field survey, and remote sensing	Fluvial sediment is the major sources of sediment supplying to the VMD. SSL of VMD in 2014-2015 was 41.5 Mt. Waves have a key role in sediment re-suspension.	(Thanh et al., 2017)
Sand dynamics and export to coastal ocean	VMD: Dinh An branch	Field survey	Sand in suspension is primarily derived locally from bed material sand. Bedload sand transport is <10% of net suspended sand flux. Annual sand export of all branches is 6.5±1.6 Mt/yr.	(Stephens et al., 2017)
Derive spatial maps of SSC in VMD and historical change of SSC	VMD	Remote sensing and field survey	SSC decreased by 1% from 1987 to 2016, starting from 2001. During high flow, SSCs in Hau river estuaries increased	(Wackerman et al., 2017)
Key drivers affecting the sediment budget of VMD	VMD	Numerical model	VMD will almost completely disappear by the end of this century due to increased rates of delta subsidence and SLR if 96% sediment reduction by dams combined with the current rate of sand mining Recommendation for reducing groundwater pumping and maintaining sediment connectivity between MRB and VMD	(Schmitt et al., 2017)
Key drivers of MR' sediment budget	MRB	Review	The ecology is likely to collapse as dams prevent fish migration, living and spawning habitats.	(Kondolf et al., 2018)
Dam impacts on transport and budget of sand bed material	Middle MRB: 3S basin	Numerical model	All existing and planned dams will trap 60-96% of MR' natural sediment load 3S basin contributes 10% of total drainage area but up to 25% of MR's sediment (25 Mt out of 100-160 Mt) Current and planned dams in 3S basin trap 91% and 97% of the sand load	(Schmitt et al., 2018)
Assess bank erosion problems in the Vientiane-Nong Khai section	Middle MRB	Remote sensing and hydrographic atlases	Erosion is higher in islands than in river banks. Bank erosion was slow during 1961-1992 (0.8 m/yr) and 1992-2005 (1 m/yr) periods.	(Kummu et al., 2008)
Impacts of snowmelt, tropical storms, and monsoon precipitation on bank erosion	Middle MRB	Process-based and numerical models	Melt and tropical cyclones have a significant influence on bank erosion. Indian Ocean Dipole has a greater influence on bank erosion than El Niño Southern Oscillation.	(Darby et al., 2013)

Objective	Study area	Method	Main finding	Authors
Morphological changes of Tien and Hau Rivers and controlling factors	VMD	Data analysis	Mean river depths increased >1.3 m Sand mining is the main cause Hydrology is not the reason for the loss	(Brunier et al., 2014)
Understanding currents, salinity, and suspended sediment dynamics in the estuary in high-flow	VMD: Dinh An branch	Field survey	SSC: mostly fine silt and clay (15%) and no sand. Sand dominates in the bottom. 95% of annual sediment flux exports to sea and deposits in shallow coastal water (<20 km from river mouths), of which 5% will transport back to rivers.	(Wolanski et al., 1996)
Impacts of Lancang cascade on alteration of flow and sediment fluxes	Middle MRB	Data analysis	Manwan caused alterations of low, reductions of suspended sediment flux	(Lu and Siew, 2006)
Dam impacts on hydrology, sediment, and geomorphology	Middle MRB	Data analysis Theoretical model	Manwan caused >50% reduction of sediment at Chiang Saen. Lancang and tributary dams reduce SSL at downstream stations. Eight dams of Lancang cascade has a total trapping efficiency of 94%.	(Kummu and Varis, 2007)
Impacts of dams and climate variability on precipitation, flow, and sediment	Middle MRB to VMD	Statistical analysis	No significant change in rainfall and runoff over the past 50 years The runoff will be more sensitive to ENSO if more dams are built	(Xue et al., 2011)
Impacts of Manwan dam and watershed development on seasonal discharge and suspended sediment transport	Middle MRB	Numerical model	Manwan dam causes a moderate decrease in peak discharge during August-September and corresponding in subsequent months. Accordingly, SSL increases in months after the rainy season	(Kameyama et al., 2013)
Quantify the magnitude, timing, and sediment grain size	Middle MRB to VMD	Field survey and data analysis	Upper MRB contributes 10-15 Mt/yr of sediment in postdam while it contributed ~60 Mt/yr in predam 20% of MR's sediment transports into TSL and 80% of MR's sediment in low flow is from TSL. Sediment reduction causes channel incision and bank erosion. Dams reduce sediment grain size.	(Koehnken, 2014)
Impacts of climate change and SLR on the flood, tidal inundation, salinity intrusion, and irrigation adaptation	VMD	Numerical model	If sea level rises 1 m, saline intrusion will be 20 and 27 km further in Tien and Hau River, respectively, compared to average values. Double dikes (inner low dike and outer high dike) are recommended.	(Toan, 2014)
Assess response of floodplain hydrology and sediment dynamics to dams, climate change, and SLR	CMD, TSL, and VMD	Numerical model	Hydropower dams dominate changes in floodplain sediment dynamics of VMD while SLR has the smallest effect. Dams, climate change, and SLR slightly increase inundation in the VMD but decrease floodplain sedimentation by ~40%. The maximum change caused by all these drivers is to reduce 90% of delta sedimentation and 95% of sediment reaching to the sea.	(Manh et al., 2015)
Quantify changes in hydrodynamics and sediment transport and drivers of sediment transport processes	VMD: Dinh An branch	Field survey	Salt wedge in high-flow and partially mixed estuary in low-flow. Annual sediment discharge is 40 Mt. Fluvial flow control sediment export in high flow while the interaction between fluvial flow and tides control sediment in low flow.	(Nowacki et al., 2015)
Identify effective adaptation strategies of the VMD	VMD	Numerical model, interview, field survey	The sediment reduction rate of 55-100% (of 160-200 Mt/yr) will cause substantial economic losses and reduction of 20-65% nutrient load.	(Smajgl et al., 2015)

Objective	Study area	Method	Main finding	Authors
			Hydropower dams could delay the onset of the flood pulse in the VMD by up to two weeks, leading to a lack of water for April rice crop and an increase in salinity intrusion.	
How channel morphology and sediment distribution vary spatially	VMD	Field survey	Two main tracts of Tien and Hau Rivers: (1) upper tract is fluvial-dominated and (2) lower tract is tide-dominated. Tide-induced water level change affects entire VMD to Cambodia	(Gugliotta et al., 2017)
Examine channel bottom morphology, linked with sediment transport	VMD	Field survey	Mud layer of the riverbed is a source of re-suspended sediment. Sand mining has little impact on bed incision in the Hau River.	(Allison et al., 2017a)
Sediment transport in VMD and its influence on river morphology	VMD	Field survey	Fine-grain particles aggregated in freshwater, settled in tidal river-estuary interface zone, and re-suspended in the estuary.	(Mclachlan et al., 2017)
Impacts of dams, land use change, sand mining, population increase and SLR on flow, sediment, and morphology	VMD	Review	Less sediment arriving VMD from MR is balanced by sediment from the inner shelf. Dams cause channel-bed incision downstream that partly compensates trapped sediment by dams. Sand mining may be reduced due to dams trapping sediment; therefore, sand transporting to the sea may be reduced accordingly.	(Allison et al., 2017b)
Inflow and outflow and sediment budgets of Tien and Hau Rivers	VMD	Data analysis	La Niña increased Q by 30% and SSL by 55% El Niño decreased Q by 20% and SSL by 50%	(Ha et al., 2018)
Understanding evolutionary changes, delta progradation, and sediment discharge of VMD during late Holocene	VMD	Field survey	The last 3 kyrs were characterized by delta progradation. Estimated sediment discharge of MR for the last 3 kyr was 144±36 Mt/yr.	(Ta et al., 2002)
Clarify the Holocene sedimentary evolution in relation with relative SLR	CMD and VMD	Field survey	The shoreline retreated 20-50 km Southeast of Phnom Penh by 8 ka due to SLR. Sea level stillstand caused shoreline progradation. From 6.3 ka to present, a fluvial system has characterized the delta plain, and the delta has prograded > 200 km seaward.	(Tamura et al., 2009)
Understanding sediment distribution, accumulation rates, and modern sediment dynamics in the coast	VMD	Field survey	Sedimentation rate 1-10 cm/yr for the last century. Most of the sediment discharged from MR is trapped in subaerial and subaqueous VMD instead of exporting to the shelf.	(Unverricht et al., 2013)
Evaluate shoreline erosion and land loss between 2002 and 2012	VMD	Remote sensing	The coastline is eroded even no identified change in river discharge and wave and wind conditions. It relates to reduced SSL from MR due to dams, sand mining, and groundwater extraction. More than 50% of >600 km shoreline of the VMD is under erosion during 2003-2012. Erosion rate commonly exceeds 50 m/yr in places.	(Anthony et al., 2015)
The recent evolution of VMD and potential impacts of dams and other factors	VMD	Remote sensing	66% of the entire VMD's shoreline is under erosion. VMD shifted from growing to shrinking at around 2005 with dam construction. Dams, sand mining, groundwater extraction, irrigation, delta subsidence, and SLR will accelerate the ongoing erosion processes	(Li et al., 2017a)
Effect of low and high dikes and effectiveness of alternative rice production policies	VMD: An Gian province	System dynamic model	Current triple rice crop is only optimal for healthier groups over a short-term (about 10 years).	(Chapman and Darby, 2016)

Objective	Study area	Method	Main finding	Authors
			Small-scale farmers are the most vulnerable to high dike with triple crop policies.	
Impacts of Lancang cascade on environment and ecology	Upper MRB	Data analysis	Dams produce enormous negative effects on the environment and ecosystems.	(Fan et al., 2015)
Dam impacts on fish migration and population	MRB	Review	Dam strongly affect MR' fisheries and fisherman. Dams reduce the fish population and degrade the feeding and breeding habitats.	(Dugan et al., 2010)
Dam impact on lost fish protein and required land and water for replacing	Middle MRB and CMD	Numerical model	11 proposed mainstream dams will increase 4-7% overall water use for food production. 11 proposed mainstream and 77 tributary dams increase 6-17% required water and 19-63% required land uses.	(Orr et al., 2012)
Dam impacts on fish biomass and biodiversity	MRB	Numerical model and data analysis	Dams block critical fish migration routes between river' floodplains and upstream tributaries. Dams critically impact fish productivity and biodiversity.	(Ziv et al., 2012)
Dam impact on structure and distribution of riparian and upland vegetation	Upper MRB	Field survey and data analysis	Cascade dams enhance habitat fragmentation, reduce distribution ranges of primary vegetation and reduce the complexity of vegetation types.	(Li et al., 2012)

2.5.1 Flow regime alterations

The flow regimes of the MR have been significantly altered by hydropower dams in the MRB (Manh et al., 2015). Although climate change is known to be one of the drivers of the flow alterations, its impacts on the alterations of the flow regimes in the MR is considered to be much smaller than those caused by hydropower dams (Arias et al., 2014; Lauri et al., 2012). In general, dams have decreased high-flows while increased low-flows (Lauri et al., 2012), as observed in many rivers worldwide. For the period 2000-2010, only about 0.57% of the area experienced a change in land use, leading Li et al., (2017) to conclude that hydropower dams contributed to 62% of the flow regime changes from 1952-1991 to 2010-2014. Low-flows (evaluated by 1-, 3-, and 7-day minimum values) decreased in the postdam period (1992-2010) from the predam period (1960-1991), high-flows (evaluated by 1-, 3-, and 7-day maximum values) decreased, mean July discharge increased by 15% while mean August discharge decreased by 9% (Lu et al., 2014b). Recently, Räsänen et al., (2017) reported that discharges in March-May 2014 increased by 121-187% while those in July-August 2014 reduced by 32-46% at Chiang Saen (Fig. 2.1) compared to average discharges. At Kratie (Fig. 2.1), the degree of the flow alterations is smaller with an increase of 41-74% in March-May and a reduction of 0-6% in July-August (Räsänen et al., 2017).

Future impacts of planned dams in the MRB were assessed by Räsänen et al., (2012) using a combined hydrological model and dynamic optimization model to predict impacts of hydropower dams in the Lancang cascade, and found that at Chiang Saen, December-May discharges increased 34-155% while July-September discharges decreased 29-36%. Lauri et al., (2012) predicted that planned mainstream and tributary dams would increase low-flows 25-160% and reduce flood peaks 5-24% at Kratie (Fig. 2.1).

2.5.2 Sediment budget reductions

Various drivers have been causing changes in sediment budgets of many major rivers worldwide, including natural processes (i.e., climate change) and human activities (i.e., constructions of dams and reservoirs). Deforestation for the expansion of the cultivated fields has known to increase the sediment supply to rivers. Little evidence of the impacts of land use change on the hydrology of the MR has been reported (Adamson et al., 2009). Besides other contributing factors, dams and reservoirs and climate change are expected to cause the highest impacts on the hydrology (flow and sediment) of the MR (Lauri et al., 2012).

Dams and reservoirs may have had more impacts on the sediment budget of a river than climate change. They have been proven to be the most predominant driver leading to a reduction in the sediment budget downstream of a river (Walling, 2006). For instance, the sediment load in the River Nile has been reduced from approximately 100 Mt/yr to nearly zero due to the construction of the Aswan High Dam (Milliman and Syvitski, 1992). In San Francisco, the Sobradinho Dam completed in 1978 has trapped approximately 80% of the sediment generated in the basin (Walling, 2006). Prior studies showed that the flow and sediment regimes in the MR had been the most impacted by the development of the dams and reservoirs in the basin. Lauri et al., (2012) reported that reservoir operations have had more impacts on hydrological regimes of the lower MR than climate change. In an attempt to predict the impacts of climate projections and planned hydropower dams on the flow and sediment in the MR, Arias et al., (2014) found that the impacts of hydropower dams were significantly higher. They also revealed that the TSL has been under immediate threat as 50% of the net sedimentation in the lake was reduced due to the construction of hydropower dams rather than climate change. In a recent study, Manh et al., (2015) concluded that the hydropower dams in the MRB were the largest contributors to the changes in sediment dynamics in the Mekong Delta. On the other hand, studies related to assessments of impacts of climate change on the flow and sediment regimes of the MR were limited and highly inconclusive (Kingston et al., 2011; Lauri et al., 2012) due to the uncertainties associated with different climate models in different research studies (Manh et al., 2015).

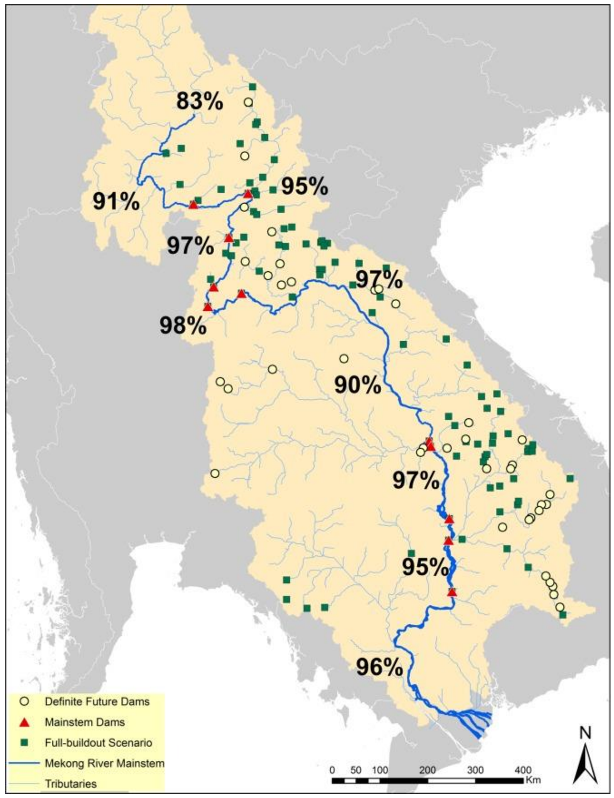

Figure 2.11 Spatial sediment reduction along the MR due to the completion of 133 dams in the MRB. Source (Kondolf et al., 2014).

As the largest driver of the MR hydrology and sediment dynamics beyond the others (Manh et al., 2015; Walling, 2006; Walling 2009), dams and reservoirs in the MRB, especially the mainstream dams, may have more impacts on the sediment budget than on the flow regime. In the predam period, the UMB contributed approximately 50-65% to the annual sediment budget of the MR (Gupta and Liew, 2007; Kondolf et al., 2014; Kummu et al., 2010). However, the annual sediment load at the Chiang Saen station (just downstream of the Lancang cascade) (Fig. 2.1), has been reduced by over 50% due to the completion of only the Manwan dam (Lu and Siew, 2006). Manwan dam has also led to a reduction of more than 60% of sediment load at the Gajiu station which is 2 km downstream of the dam (Fu et al., 2008). It is worth noting that Manwan is the fourth largest dam among the six existing mainstream dams in the UMB. These all dams were therefore expected to cause tremendous reductions in the sediment budget of the lower MR.

Dams and reservoirs impacting the sediment budget have been widely judged through sediment trapping efficiency of reservoirs. Mainstream dams in the UMB were predicted to trap approximately 83% of sediment generated in the UMB, equivalent to 40% of the sediment budget of the MR (Kondolf et al., 2014). The number can reach 94% according to predictions of (Kummu and Varis, 2007). Individually, both Nuozhadu and Xiaowan (two biggest dams) were predicted having trapping efficiencies of 92% while the values of Manwan and Dachaoshan were 68% and 66% respectively (Kummu and Varis, 2007). In the same order, Kummu et al., (2010) predicted trapping efficiencies of Nuozhadu and Xiaowan exceeding 89%. Seriously, (Kondolf et al., 2014) predicted that only 4% of the MR sediment could reach the Mekong Delta annually if 133 planned dams are constructed in the future (Fig. 2.11).

2.5.3 Morphological changes and coastline retreat

Sediment reduction is likely to cause riverbed incision and riverbank erosion (Fig. 12) along downstream reaches at different rates and time scales (reaches closer to the dams are suffering sooner with faster rates). Kummu et al., (2008), using remote sensing, estimated riverbank erosions of the MR from Vientiane to Nong Khai region were 0.8 and 1.0 m/yr (for the main channel) and 2.4 and 4.8 m/yr (for islands) in the 1961-1992 and 1992-2005 periods, respectively. Darby et al. (2013) reported mean annual rates of riverbank erosion at Ang Nyay (near Nong Khai) over the 1913-2010 period and at Pakse over the 1923-2010 period as 0.68±0.11 m/yr and 0.64±0.16 m/yr, respectively. Brunier et al., (2014) evaluated morphological change of the Tien and Hau Rivers by comparing the river depths for 1998 and 2008. They found that the thalweg incision of the Hau River is more pronounced than the Tien River (Fig. 2.13). The riverbed incision appeared in 59% of the investigated Tien River compared to 70% of the investigated Hau River. The accretion in the investigated Tien and Hau Rivers were 16% and 12%, respectively. Both Tien and Hau Rivers had a similar mean riverbed incision that -1.4 m for the Tien River and -1.34 m in the Hau River although the riverbed incision was irregular in both rivers. The largest incision in both rivers was in riffle sections. In the Tien River, the deepest incision from -5 m to -15 m was in the Ham Luong distributary while the deepest incision up to -10m to -15 m was found near the channel bar near Can Tho city (Fig. 2.13). In Cu Lao Tay island, the island near the Vam Nao station (Fig. 2.2), the mean riverbed incision was -2.47 m. In the last 50 km of the Hau River from the river mouth, the mean riverbed incision was -1.46 m. They concluded that sand mining is the main controlling factor of the morphological change in the Tien and Hau Rivers while impacts of hydropower dams were not clear because the sediment data in the VMD were not reliable.

Figure 2.12 Typical river bank erosion in the Tien River. Photos were taken by Binh, D.V. during the field trip in August 2017.

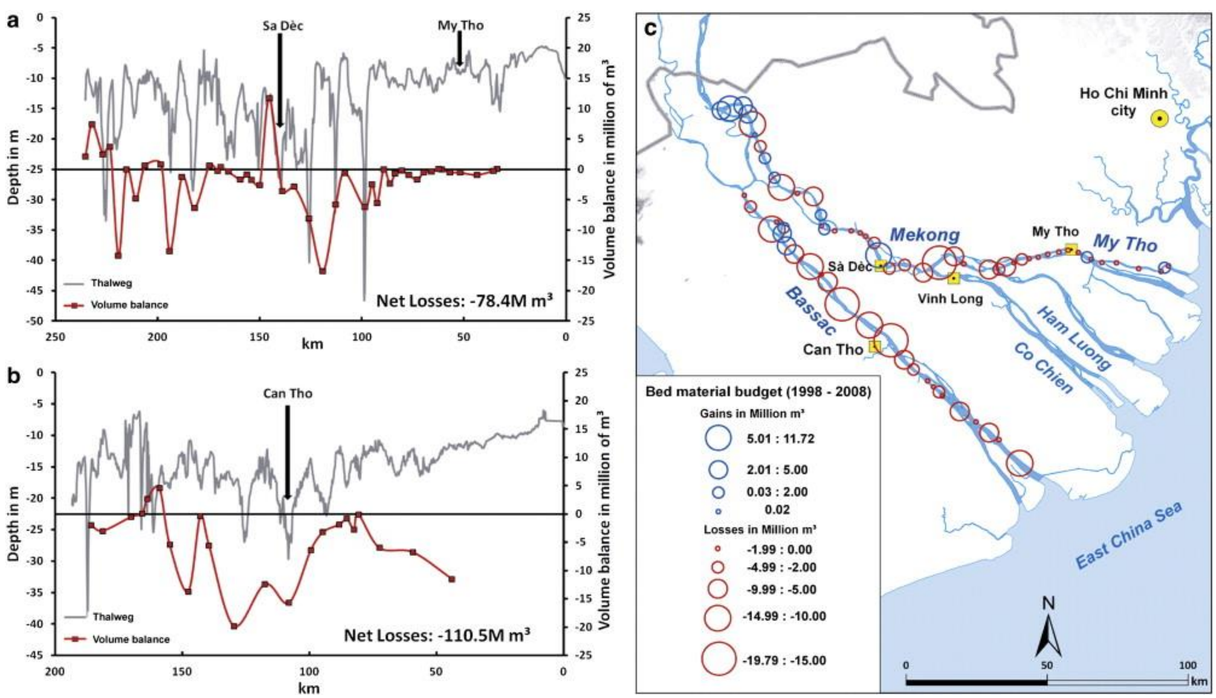

Figure 2.13 Changes in the river thalweg along (a) the Tien River, (b) the Hau River, and (c) the aggradation and degradation in the Tien and Hau Rivers between 1998 and 2008. Source: (Brunier et al., 2014).

The coastline of the VMD has been rapidly retreated due to dam-induced sediment reduction, and likely due to, to some extent, land use change and mangrove forest reduction in the VMD coastline (Allison et al., 2017b). Over the past 8,000 years, the Mekong Delta accreted rapidly up to 16 km^2/yr (Kondolf et al., 2018), equivalent to 16-26 m/yr. However, over 50% of 600 km of the VMD coastline has been under serious erosion during 2003-2012 (during the boom of river-damming in the MRB), equal to over 5 km^2 land loss (2.3 km^2/yr) with retreat rates commonly exceeding 50 m/yr in places (Anthony et al., 2015). Fig. 2.14 shows the spatial and temporal evolution of the erosion/accretion of the VMD coastline during 1973-2015 which is retrieved from (Li et al., 2017b).

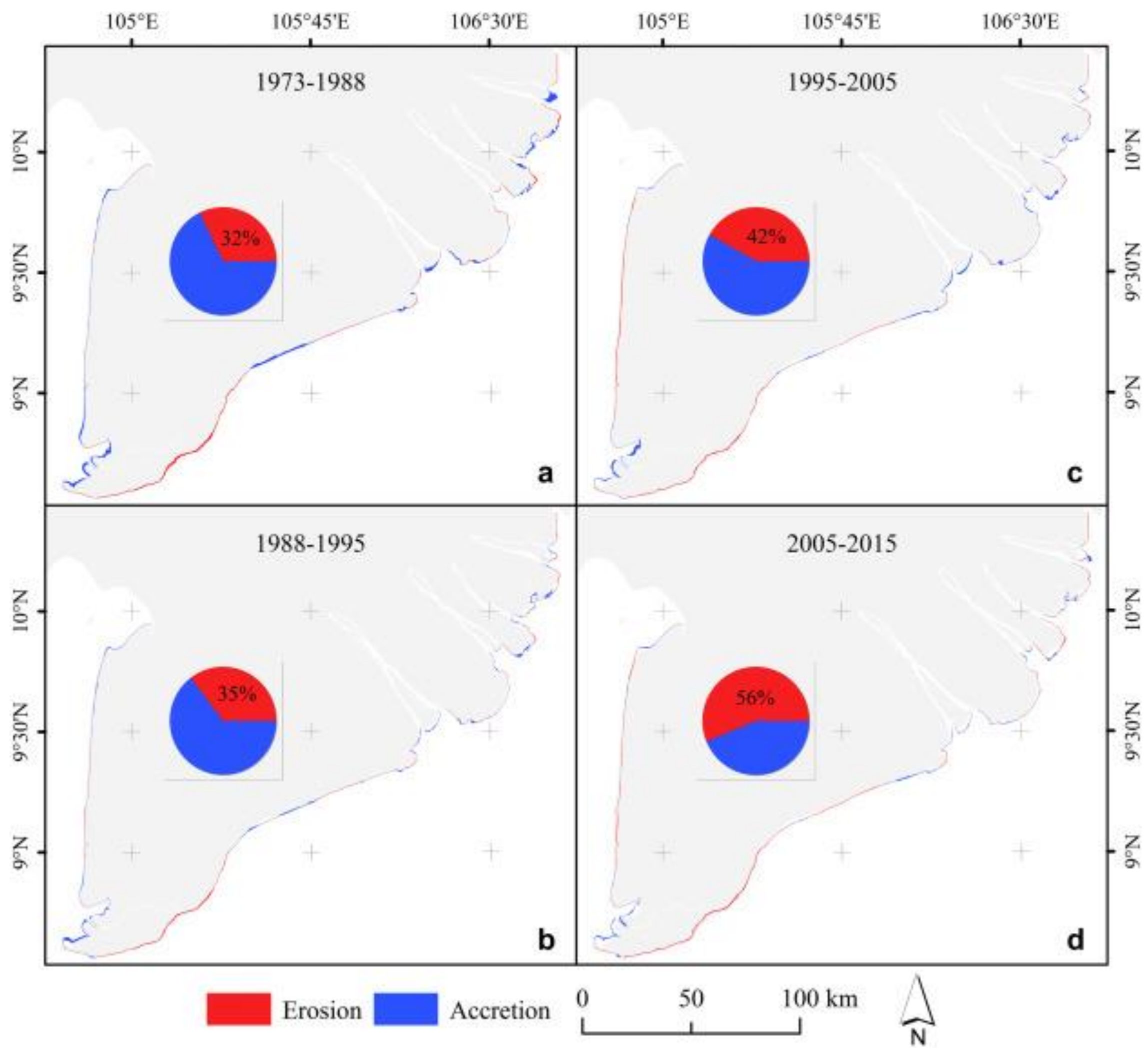

Figure 2.14 Spatial-temporal evolution of the VMD coastline during 1973-2015. Source: (Li et al., 2017b).

Chapter 3 Cumulative impacts of hydropower dams on long-term alterations of flow regimes of the Mekong River and proposing adaptation strategies for the Vietnamese Mekong Delta

3.1 Introduction

The annual flood pulses characterized by the distinct low-flow and high-flow seasons are the primary driving forces for the productivity of ecosystems in the MRB (Räsänen et al., 2017). The flood pulse provides water and nutrient-rich sediment to sustain the extensive floodplains in the lower MRB and the TSL, which support one of the largest agriculture, fishery, and wetland ecosystems in the world. The TSL plays as an important role as a natural reservoir to regulate the flood pulse of its downstream floodplains in Cambodia and Vietnam by receiving flows from the MR during the high-flow and releasing water back to the MR during the low-flow (Pokhrel et al., 2018). However, the annual flood pulse, as well as the flow regimes of the MR, has been significantly altered by hydropower dams, which reduce the amplitude of the annual flood pulse, disrupting the connectivity between rivers and floodplains. Hydropower dams also trap sediment, reducing the volume of sediment that can be transported downstream to maintain river channels and coastal landforms (Kondolf et al., 2014). Moreover, fish migration paths are blocked by dams built across the rivers. All these factors lead to a degradation of the integrity of ecosystems in the MRB (Arias et al., 2014).

The flow regimes of the MR have been significantly altered by hydropower dams in the MRB (Manh et al., 2015). Although climate change is known to be one of the drivers of the flow alterations, its impacts on the alterations of the flow regimes in the MR is considered to be much smaller than those caused by hydropower dams (Arias et al., 2014; Lauri et al., 2012). In general, dams decreased high-flows while increased low-flows (Lauri et al., 2012), as observed in many rivers worldwide. For the period 2000-2010, only about 0.57% of the area experienced the land use change, leading Li et al., (2017) to conclude that hydropower dams contributed to 62% of the flow regime changes from 1952-1991 to 2010-2014. The low-flows (evaluated by 1-, 3-, and 7-day minimum values) decreased in the postdam period (1992-2010) from the predam period (1960-1991) while the high-flows (evaluated by 1-, 3-, and 7-day maximum values) decreased, and the mean July discharge increased 15% while the mean August discharge decreased 9% (Lu et al., 2014b). Recently, Räsänen et al., (2017) reported that discharges in March-May 2014 increased by 121-187% while those in July-August 2014 reduced by 32-46% at Chiang Saen, compared to average discharges. At Kratie, the degree of the flow alterations is smaller with an increase of 41-74% in March-May and a reduction of 0-6% in July-August (Räsänen et al., 2017).

Future impacts of planned dams in the MRB were assessed by (Räsänen et al., 2012) using a combined hydrological model and dynamic optimization model to predict impacts of hydropower dams in the Lancang cascade, and found that at Chiang Saen, December-May discharges increased 34-155% while July-September discharges decreased 29-36%. Lauri et al., (2012) predicted that planned mainstream and tributary dams would increase the low-flows by 25-160% and reduce the flood peaks by 5-24% at Kratie.

Understanding historical alterations of the flow regimes along the MR is of crucial importance for scientists and stakeholders, to inform sustainable integrated water management strategies and to improve decisions to share benefits from the transboundary MR in the coming decades. Any decision from stakeholders based on a short-term flow analysis may lead to unsustainable development. For that, the functioning of existing high-dike systems and salinity control sluice gates in the VMD are heavily debated and revised. Many scientists argue against these structures because they may worsen the situations. High-dike systems may destroy soil properties and wetland ecosystems because nutrient-rich fine sediment is blocked to access to the wetlands and agriculture areas. Additionally, salinity control sluice gates may increase the intrusion length land-ward because of reducing buffering zones near the estuaries. We argue that these structures were suitable at the time of building but become a constraint in recent years because of unexpected flow regime alterations that outrange the design values. Therefore, investigation of the long-term flow regime alterations plays a fundamental reference for sustainable water resources management strategies.

However, the long-term flow alterations along the entire lower MR, especially the VMD have not been fully understood. Such limitations are associated with difficulty in the collection of the historical data throughout the MRB, especially the VMD. The aim of this research is, therefore, to comprehensively assess the long-term alterations of various components of the flow regimes (i.e., maximum, minimum, monthly, seasonal, and annual) along the entire lower MR associated with driving factors, including hydropower dams and climate change. Long-term adaptive strategies for the flood control, irrigation water intakes and salinity intrusion control in the VMD based on the analyzed long-term flow regime alterations are proposed and discussed. The outcome of this research can be referred by stakeholders to make sustainable long-term decisions.

3.2 Materials and methods

3.2.1 Data collection

Table 3.1 shows the available data used in this research. Daily discharges and water levels were collected during 1960-2015 at Chiang Saen and Kratie, and annual discharges were available during the 1960s-2013 at Chiang Saen, Luang Prabang, Nong Khai, and Pakse in the middle MRB (Fig. 2.1). Daily discharges and water levels at Tan Chau, Chau Doc, Vam Nao, My Thuan, and Can Tho in the VMD (Fig. 2.2) were available during 1980-2015. Monthly maximum salinity concentration at Tra Vinh and Cau Quan (Fig. 2.2) were provided by local agencies during 1990-2016. Daily precipitation at seven stations along the MRB, namely, Lincang, Simao, Lancang, and Jinghong in the upper MRB, and Chiang Saen, Nong Khai, and Pakse in the middle MRB were collected for a period of 1954-2016.

Table 3.1 Available data of the discharge, water level, SSC, SSL, precipitation, and salinity concentration in the MRB.

Station	Discharge	Water level	SSC	SSL	Precipitation	Salinity concentration
Licang					1954-2010	
Simao					1954-2010	
Lancang					1954-2010	
Jinghong					1954-2010	
Chiang Saen	1960-2013	1960-2015		1961-2013	1966-2016	
Luang Prabang	1962-2013			1961-2013		
Nong Khai	1969-2013			1961-2013	1973-2016	
Pakse	1961-2013			1961-2013	1950-2016	
Kratie	1960-2015	1960-2015				
Tan Chau	1980-2015	1980-2015	1980-2015			
Chau Doc	1980-2015	1980-2015	1980-2015			
Vam Nao	1987-2015	1985-2015	1987-2015			
My Thuan	1999-2015	2009-2015	2009-2015			
Can Tho	2000-2015	2009-2015	2009-2015			
Vung Tau		1980-2014				
Tra Vinh						1990-2016
Cau Quan						1990-2016

The main sources of the collective data are the Mekong River Commission (MRC) and the Vietnamese national Center for Hydrometeorological Data. Data were also collected from published reports and journal papers (e.g., Ta et al., 2002; Lu and Siew, 2006; Wang et al., 2011; Koehnken, 2014; Lu et al., 2014; Manh et al., 2014; Wang et al., 2016; Räsänen et al., 2017).

Water level, discharge, and SSC have been monitored annually by the Vietnamese National Center for Hydro-meteorological Data under the MRC framework. Hourly water levels at stations in the VMD are monitored using automatic water level recorders, namely Steven A-71 of Steven Water Monitoring System, Inc., USA (e.g., at Tan Chau, Chau Doc, and Can Tho) and ValDai of Valdai Experimental Laboratory, Russia (e.g., at Vam Nao and My Thuan). Recorded water levels are cross-checked twice a day (i.e., at 7:00 and 19:00 o'clock) using national installed leveling system. Before releasing the usable data to the society, water levels are validated using HYDTID software, developed by the Vietnamese national Center for Hydrometeorological Data, to detect and treat noise spikes. The ultimate water levels use Vietnam national datum at Ha Tien. Hourly discharges were then estimated based on the established stage-discharge rating curves at each station by the Vietnamese national Center for Hydrometeorological Data. To guarantee the reliability, the stage-discharge rating curves were periodically updated three to four times a year, depending on the station, by using discharges that are measured by acoustic Doppler current profiler (ADCP). For instance, three times a year at Vam Nao and four times a year at Can Tho and My Thuan (Ha et al., 2018).

3.2.2 Estimating missing discharges in the VMD using stage-discharge rating curves

At Tan Chau and Chau Doc, daily discharges were not continuously measured during 1980-1995. Therefore, missing discharges must be estimated using stage-discharge rating curves to be able to conduct further long-term analysis. To the best of authors' knowledge, rating curves are only available from a study by WUP-JICA (2004). Their study used limited data of discharges and water levels from 1997 to 2001 (5 years) to generate the stage-discharge rating curves. Rating curves were developed in the dry and wet seasons, corresponding to the water levels above and below 2.0 m, respectively. However, such rating curves using the short time period (5 years only) are not sufficient to extrapolate discharges during 1980-1995 in this research. Therefore, it is necessary to develop new rating curves at these two stations, using all available data from 1980-2015 which have a wider range in terms of time and values. In the attempt to develop rating curves, it is recommended to split the data sets into time periods, during which stable hydraulic conditions are satisfied (Rantz, 1982). Therefore, the stage-discharge rating curves in the VMD are created for in the rising stage (April-September) and falling stage (October-March) separately.

The rating equations are developed using polynomial regression analysis with least squares method. The rating equations for the rising and falling stages at Tan Chau are provided by Eqs. 3.1 and 3.2 respectively, while respective equations at Chau Doc are given by Eqs. 3.3 and 3.4 as follow:

$$Q = -0.0913H^2 + 92.433H - 1060.7 \quad (3.1)$$

$$Q = -0.0592H^2 + 77.11H - 1643.7 \quad (3.2)$$

$$Q = -0.0174H^2 + 25.32H - 484.5 \quad (3.3)$$

$$Q = -0.0075H^2 + 24.531H - 796.9 \quad (3.4)$$

where Q: discharge (in m^3/s) and H: water level (in cm).

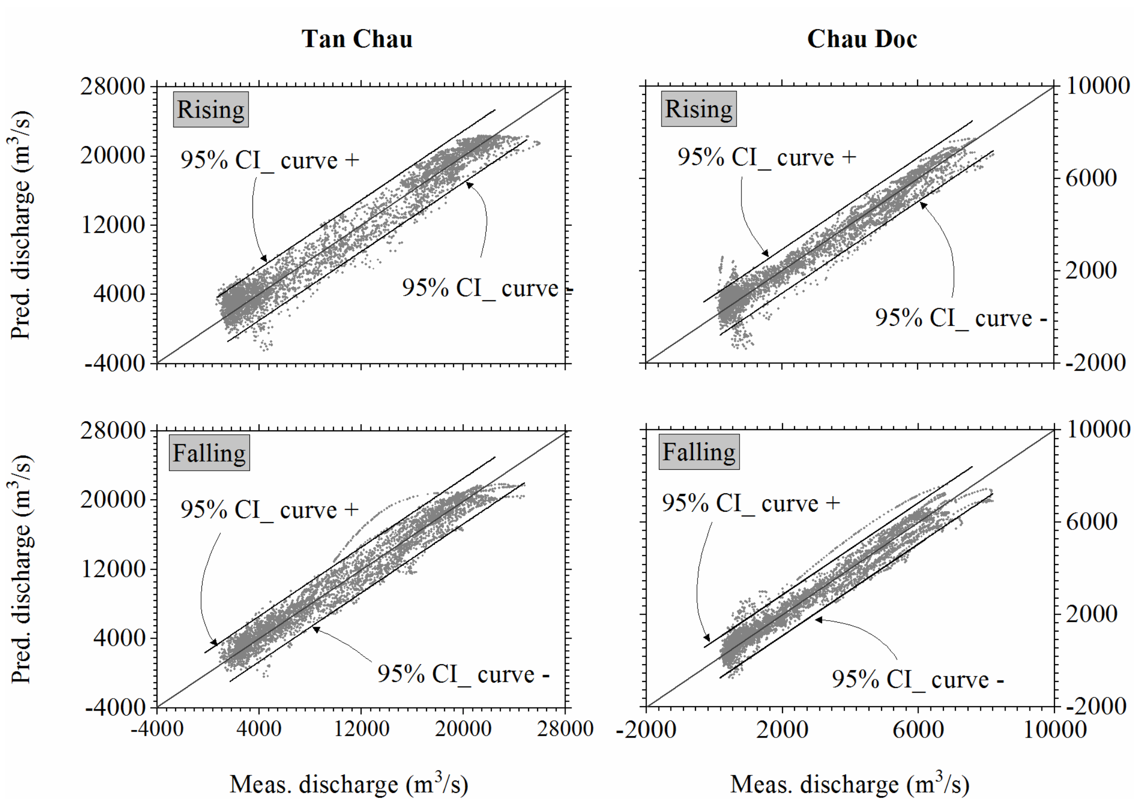

Figure 3.1 Stage-discharge rating curves at Tan Chau and Chau Doc. CI is the confidence interval.

By dividing the flow into rising and falling stages, discharges are well-predicted by proposed rating equations with high coefficients of determination, R^2 (0.95-0.96), which are much better than those of rating curves proposed by WUP-JICA (2004), having correlation coefficients ranging from 0.825 to 0.918. Most of the values fall within 95% confidence intervals, showing a strong agreement between measured and predicted discharges (Fig. 3.1). Noticeably, some values of the extreme drought year 2015 are underestimated in the rising stage while on the other hand, discharges during the exceptional flood year 2000 are likely overestimated in the falling stage. Therefore, the limitations of these rating curves should be taken into consideration when conducting additional studies.

Rating curves in this study are developed using 36 years of data (from 1980-2015), covering extreme drought in 2015 and 1998 and exceptionally high flood in 2000 and 2011. The developed equations are more comprehensive and representative, compared to those used in WUP-JICA (2004) considering the length of the data used (36 years in our study compared to only 5 years in their study) and better performance with higher correlation coefficients. Although parts of the extreme high and low flows are under or over-estimated by developed curves, they are useful in predicting missing discharges from 1980-1995 at Tan Chau and Chau Doc. It is worth mentioning that rating curves are not unique as these curves are dynamic and heavily depend on changes in river geometry. In other words, these rating curves need to be updated when new data become available and accurate prediction of discharges is required.

3.2.3 Methods

a. Trend analyses

Long-term historical flow discharges in the lower Mekong River were analyzed using two trend tests, Mann-Kendall, Sens' Slope and Pettitt tests at 5% significance level (α = 0.05). First, changes in the trend of historical data were detected using the Mann-Kendall test (Kendall, 1938; Mann, 1945). When trends were detected, we identified inflection points in time series using the Pettitt test (Pettitt, 1979). These two tests are non-parametric approaches. Finally, the Sens' slope method (Sen, 1968) was employed to estimate the rate of change (the slope) of the data. These three methods have been successfully employed by some researchers in the past hydrometeorological studies (i.e., Zhang and Lu, 2009). The results of trend tests allowed us to partition the long-term data into periods having a similar behavior under cumulative impacts of a group of dams. Theory of these statistical methods were detailed in Appendix A.

b. Flood-frequency analysis

Changes in the magnitude and frequency of annual extreme discharges (maximum and minimum) among periods were investigated using flood-frequency analysis. The historical data were ranked in the descending order. The probabilities associated with the ranked values were then estimated using the Hazen equation (Bartkes et al., 2016). Predicted probabilities are then estimated using the Pearson Type III probability distribution fitted using the method of moments as proposed by (USGS, 1982). Finally, flood-frequency curves in each period at all stations were established. Detail of this method was presented in Appendix A.

c. Seasonality of discharge hydrographs

All daily discharges at each station (Chiang Saen, Kratie, Tan Chau, and Chau Doc) for the period of 1980-2015 were used to classify the discharge hydrographs into three categories: high-flow (discharges ≥25 percentile), transition-flow, and low-flow (discharges ≤75 percentile). Figure 3.2 shows discharge hydrographs deriving from mean daily discharges over 1980-2015 at stations along the lower Mekong River, and discharge thresholds distinguishing three seasons at each station. Number of months in each season at stations along the lower Mekong River are shown in Table 3.2. In general, the high-flow season upstream of the VMD starts one month earlier than that inside the VMD. On the other hand, the low-flow season upstream of the VMD ends one month before that inside the VMD (Table 3.2). The high-flow transports a majority of the annual flow, for example, 62% at Chiang Saen and 74% at Kratie.

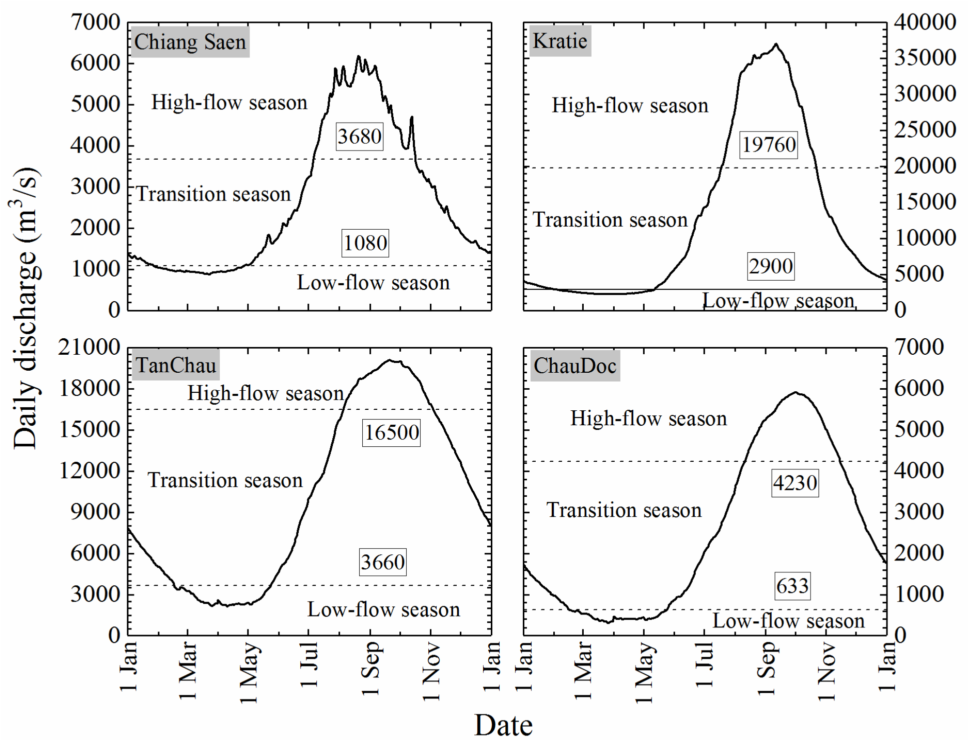

Figure 3.2 Discharge hydrographs showing three seasons at four stations along the lower MR.

Table 3.2 Seasonal classification of discharge hydrographs at stations along the MR.

Station	Low-flow season	Transition season	High-flow season
Chiang Saen	February-April	May-June and November-January	July-October
Kratie	February-April	May-June and November-January	July-October
Tan Chau	February-May	June-July and November-January	August-October
ChauDoc	February-May	June-July and November-January	August-October

Note: high-flow season: discharges $\geq 25^{th}$ percentile; low-flow season: discharges $\leq 75^{th}$ percentile; transition season: discharges in between high-flow and low-flow season.

d. Methods investigating flow regime alterations

Changes in the flow magnitudes of these seasons among periods associated with hydropower dam development were assessed by using Indicators of Hydrologic Alteration (IHA), and Range of Variability (RVA) approaches (Richter et al., 1997). The IHA and RVA methods are among the most popular metrics used for assessing the alterations of 33 hydrological indicators of the flow regimes. Also, the index of alteration to the hydrological regime (*FQ*) proposed by Alcayaga et al., (2012) was adapted to assess alterations of the frequency and duration in three seasons. Details of these methods were presented in Appendix A. Moreover, IHA and RVA approaches were also used in conjunction with other methods (trend tests, flood-frequency analysis) to quantify the alterations of annual maximum, minimum, mean, and monthly discharges at stations analyzed.

3.3 Results

3.3.1 Partition of the long-term discharges in the lower MR

Trend tests show that the annual minimum discharges at Chiang Saen have statistically reduced since 1992 (Table A3.2). The annual mean, maximum, and monthly discharges have also changed since 2008 although these changes are not statistically significant. The general trends were increases in the low flows and decreases in the high flows. These change years were related to the reservoir infilling of Manwan (1993) – the first dam in the Lancang cascade, and Xiaowan (2008) – the second largest dam in the Lancang cascade. The annual mean, maximum, minimum, and monthly discharges at downstream stations (Kratie, Tan Chau, and Chau Doc) have also changed during the 1992-2008 period (Table A3.3-A3.5). The time series data at stations along the lower MR were therefore divided into three periods to investigate the cumulative impacts of dams in the mainstream and tributaries: no-dam (1980-1992), low-dam development (1993-2008), and high-dam development (2009-2015). The low-dam development consists of four mainstream dams in the Lancang cascade (Manwan, Daochaoshan, Xiaowan, and Jinghong) and 21 dams in the tributaries. The high-dam development includes additional two mainstream dams in the Lancang cascade (Gongguoqiao and Nuozhadu – the largest dams in the MRB) and an additional 35 dams in the tributaries. The years of infilling reservoirs of the Lancang cascade were in Table 2.1.

3.3.2 Alterations in the annual mean discharges

Although not statistically significant, the annual mean discharges at Chiang Saen, Kratie, Tan Chau, and Chau Doc have reduced (Table A3.2-A3.5). The maximum reduction was at Kratie with a rate of 4.4 m^3/s/yr since 1993. In the low-dam development, the annual mean discharges at all four stations have increased by 1.1-12.0% compared to those in the no-dam period. The maximum increase was at Kratie (from 12,040 m^3/s in the no-dam to 13,490 m^3/s in the low-dam), followed by Chiang Saen (from 2,580 m^3/s in the no-dam to 2,750 m^3/s in the low-dam). However, the high-dam development has caused reductions at all four stations, ranging from 1.8-7.9%, with a maximum reduction at Chiang Saen (from 2,580 m^3/s in the no-dam to 2,380 m^3/s in the high-dam).

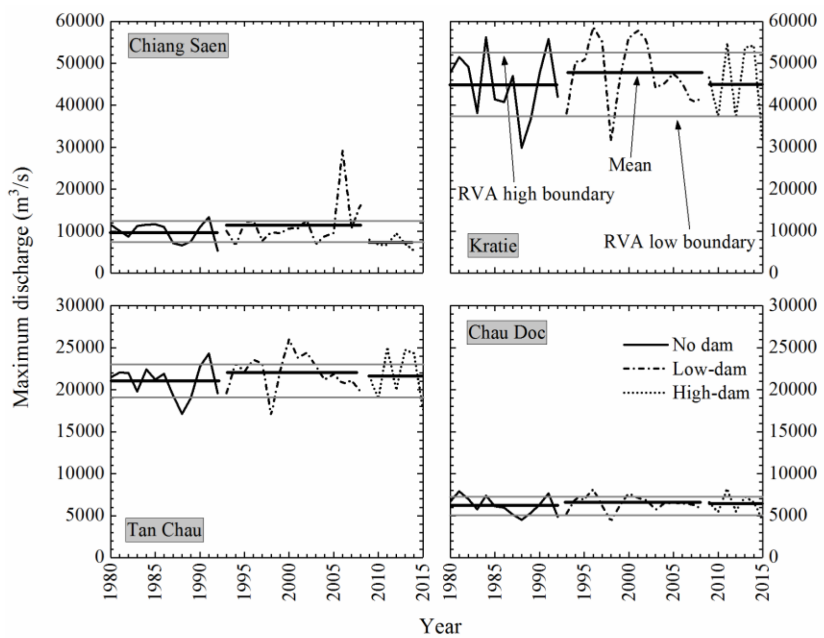

Figure 3.3 Long-term variations of the annual maximum discharges along the MR.

3.3.3 Alterations in the annual maximum discharges

Fig. 3.3 compares annual maximum discharges at four stations along the lower MR for three periods reflecting different levels of dam development in the MRB, based on IHA and RVA analyses. Clearly, the annual maximum discharges significantly increased in the low-dam development compared to the no-dam period. The increased rates at Chiang Saen, Kratie, Tan Chau, and Chau Doc were 18.0%, 6.3%, 5.0%, and 4.2%, respectively. Frequency curves (Fig. 3.4) also show increases in the annual maximum discharges at four stations at almost all exceedance probabilities: 11.0-162.5% at Chiang Saen, 5.2-18.9% at Kratie, 4.6-9.2% at Tan Chau, and 0-60.4% at Chau Doc (Table A3.6-A3.9).

However, the annual maximum discharges in the high-dam development had different trends among four stations: reduced at Chiang Saen and increased at Kratie, Tan Chau, and Chau Doc

(Fig. 3.3). Trend tests showed a reduced rate of 56.3 $m^3/s/yr$ since 2008 at Chiang Saen (Table A3.2) and an increased rate of 28.3 $m^3/s/yr$ since 1993 at Tan Chau (Table A3.4). Such trends among four stations were also captured in frequency curves (Fig. 3.4). The annual maximum discharges at 0.2-50% exceedance probabilities reduced 24.8-39.9% at Chiang Saen and increased 3.6-11.0% at Kratie, 3.8-13.7% at Tan Chau, and 1.5-5.0% at Chau Doc (Table A3.6-A3.9).

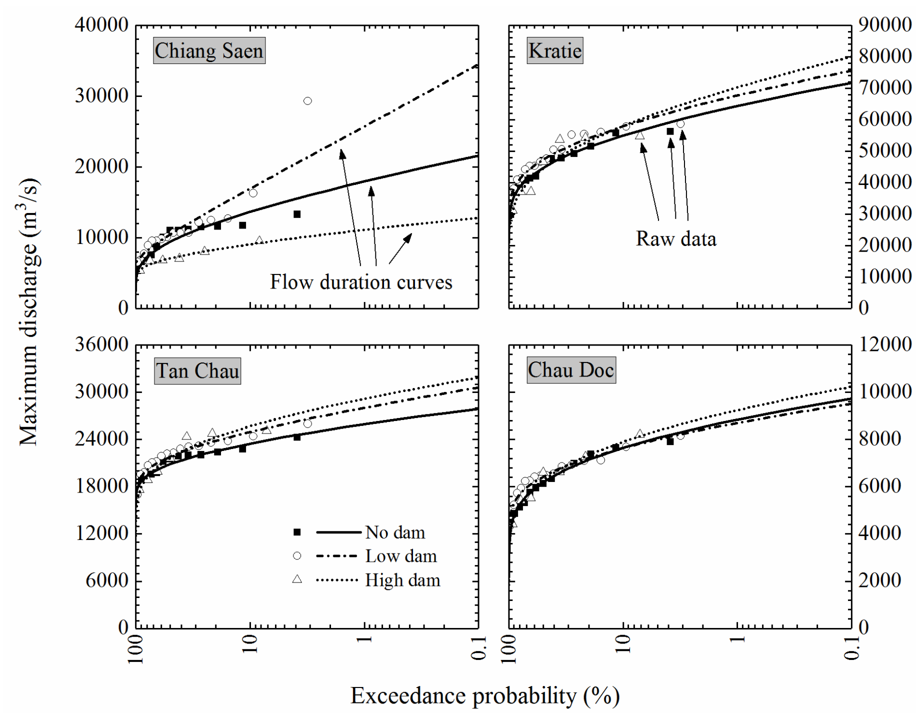

Figure 3.4 Frequency curves of the maximum discharges along the MR.

Fig. 3.5 shows long-term daily discharges of 36 years during 1980-2015 at Tan Chau. Annual maximum and minimum discharges are highlighted. The figure shows that the annual maximum discharges reduce in the predam period. However, their trends vary in the postdam periods due to some exceptional high flood peaks, i.e., in years 2011, 2013, and 2014. The decreasing tendency of discharges in the predam period at Tan Chau are directly related to the reduction of the flow at upstream stations in the MR's mainstream, such as Chiang Saen and Pakse (Lu and Siew, 2006). These decreasing trends may be due to the reduction in the annual rainfall in the MRB because the river discharges are mainly driven by the rainfall when hydraulic structures (i.e. hydropower dams) have not appeared in the predam period.

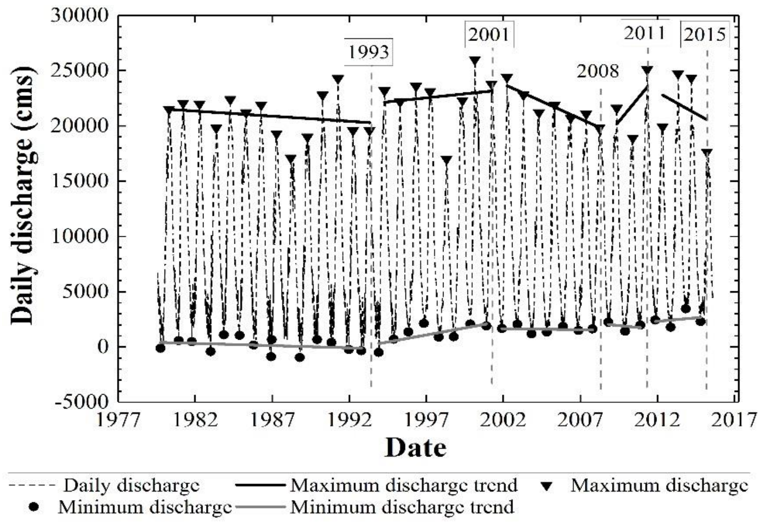

Figure 3.5 Long-term daily discharges at Tan Chau in the VMD.

3.3.4 Alterations in the annual minimum discharges

Alterations in the annual minimum discharges at Chiang Saen were different from those at downstream stations (Fig. 3.6 and 3.7). At Chiang Saen, the annual minimum discharges in the low-dam and high-dam development decreased by 25.1% and 1.9%, respectively, from the no-dam period. Reduced rates at all non-exceedance probabilities derived from frequency curves (Fig. 3.7) were 18.8÷68.9% in the low-dam and 0.1÷55.4% in the high-dam development (Table A3.10). On the other hand, the annual minimum discharges at Kratie, Tan Chau, and Chau Doc markedly increased in both low-dam and high-dam development (Fig. 3.6). Fig. 3.5 shows that the annual minimum discharge at Tan Chau decreases in the predam period but increases significantly in the postdam periods. At Tan Chau, minimum discharges increased from 50 m^3/s in the no-dam period to 1,270 m^3/s and 2,230 m^3/s in low-dam and high-dam development, respectively (Fig. 3.6). Increased rates at Kratie and Chau Doc were 180.4% and 40.7% respectively, from the no-dam to high-dam development periods. Frequency curves show that the high-dam development had higher increased rates than the low-dam development at most of non-exceedance probabilities (Fig. 3.7). Increased rates ranged from 2.2-65.8%, 4.7-941%, and 49-179.3% in the low-dam development to 9.9-80.2%, 32.7-1,566%, and 71.6-192% in the high-dam development at Kratie, Tan Chau, and Chau Doc, respectively (Table A3.11-A3.13).

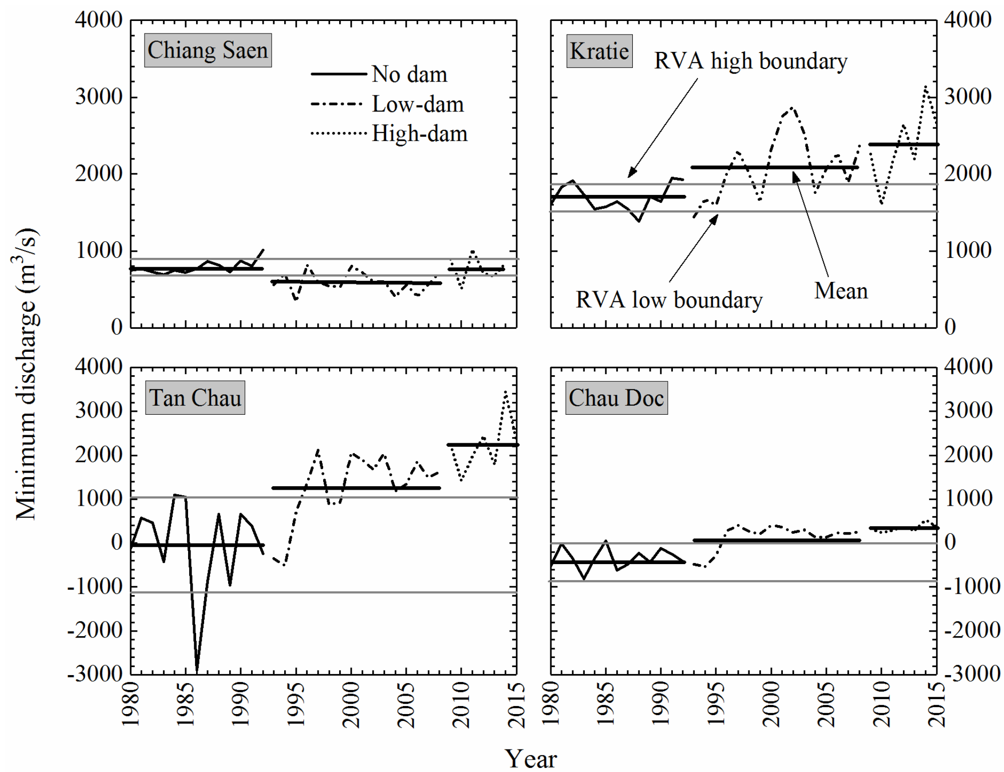

Figure 3.6 Long-term variations of the annual minimum discharges along the MR.

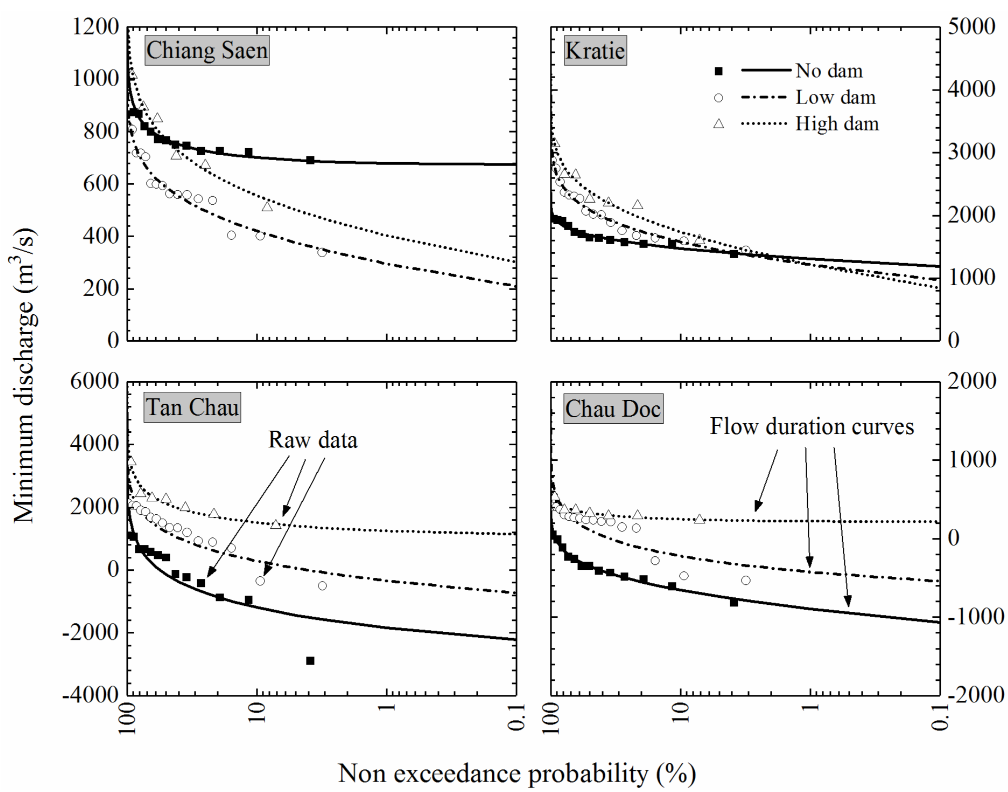

Figure 3.7 Frequency curves of the minimum discharges along MR.

3.3.5 Alterations in the seasonal and monthly discharges

a. Alterations in the high-flow discharges

In the low-dam development period (1993-2008), the high-flow discharges at all four stations along the lower MR increased (Table 3.3). The increased rates at stations Chiang Saen (0.5-15.9%) and Kratie (4.5-18.9%) were higher than those at Tan Chau (2.7-6.7%) and Chau Doc (4.9-14.6%). August was the month having the maximum increased discharges at Chiang Saen, Tan Chau, and Chau Doc, and the maximum increased discharges at Kratie was in July. Trend tests revealed that August discharges at Kratie, Tan Chau, and Chau Doc have increased since 1993, with increased rates of 77.3, 31.2, and 17.1 $m^3/s/yr$, respectively (Table A3.3-A3.5). The duration of the high-flow (calculated using Eq. A3.11) at Tan Chau and Chau Doc increased by 12% and 15%, respectively.

Table 3.3 Changes of the high-flow discharges (m3/s) in the no-dam, low-dam, and high-dam development periods at four stations along the MR.

Month	No-dam	Low-dam		High-dam	
	Discharge	Discharge	Change (%)	Discharge	Change (%)
1. At Chiang Saen station					
July	4,460	5,130	+14.9	3,320	-25.6
August	5,480	6,350	+15.9	4,810	-12.2
September	4,960	5,690	+14.8	4,330	-12.7
October	3,890	3,910	+0.5	2,990	-23.1
2. At Krate station					
July	18,140	21,570	+18.9	17,470	-3.7
August	31,930	36,310	+13.7	30,990	-2.9
September	33,430	37,930	+13.5	31,560	-5.6
October	22,260	23,270	+4.5	22,920	+3.0
3. At Tan Chau station					
August	17,250	18,410	+6.7	17,790	+3.1
September	19,610	20,140	+2.7	19,050	-2.9
October	18,420	18,910	+2.7	19,010	+3.2
4. At Chau Doc station					
August	4,180	4,790	+14.6	4,440	+6.2
September	5,560	5,830	+4.9	5,250	-5.6
October	5,430	5,810	+7.1	5,580	+2.8

In the high-dam development period (2009-2015), discharges in the high-flow generally decreased (Table 3.3) at four stations along the lower MR. Reduced rates were high at upstream stations, then reducing downstream. The strongest reductions were in July at Chiang Saen (25.5%), and in September at Kratie (5.6%), Tan Chau (2.9%), and Chau Doc (5.6%) (Table 3.3). Trend tests revealed that the starting year of the reduction at Chiang Saen was 2008 with a maximum reduced rate of 25.1 m^3/s/yr in July (Table A3.2). On the other hand, the October discharges at Kratie, Tan Chau, and Chau Doc increased by about 3.0% at each station (Table 3.3).

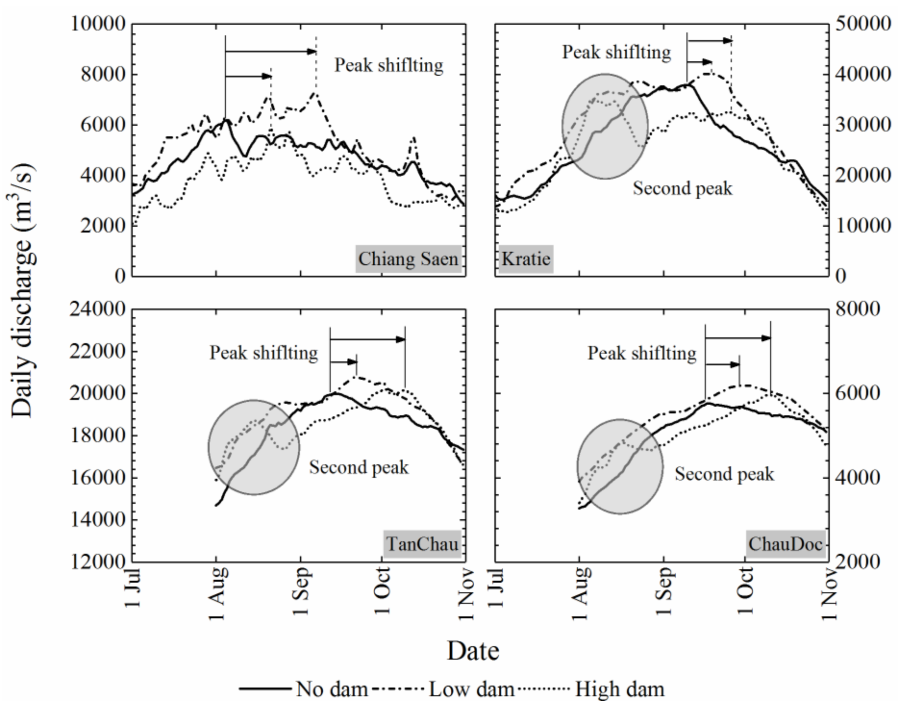

Figure 3.8 Hydrographs of the mean daily discharges in the high-flow season in the no-dam, low-dam, and high-dam development periods at four stations along the MR.

Not only the magnitude, but but the patterns of the discharge hydrographs also altered. Fig. 3.8 shows that the peak discharges at Chiang Saen, Kratie, Tan Chau, and Chau Doc were shifted to occur late in the low-dam and high-dam development periods compared to the no-dam period. For instance, the peak discharges have delayed by 17 days at Chiang Saen (from August 4th in the no-dam to August 21st in the high-dam) and 20 days at Tan Chau (from September 13th in the no-dam to October 3rd in the high-dam). Moreover, the second peak in August appeared at Kratie, Tan Chau, and Chau Doc in the high-dam development which was not seen in the no-dam and low-dam development periods (Fig. 3.8).

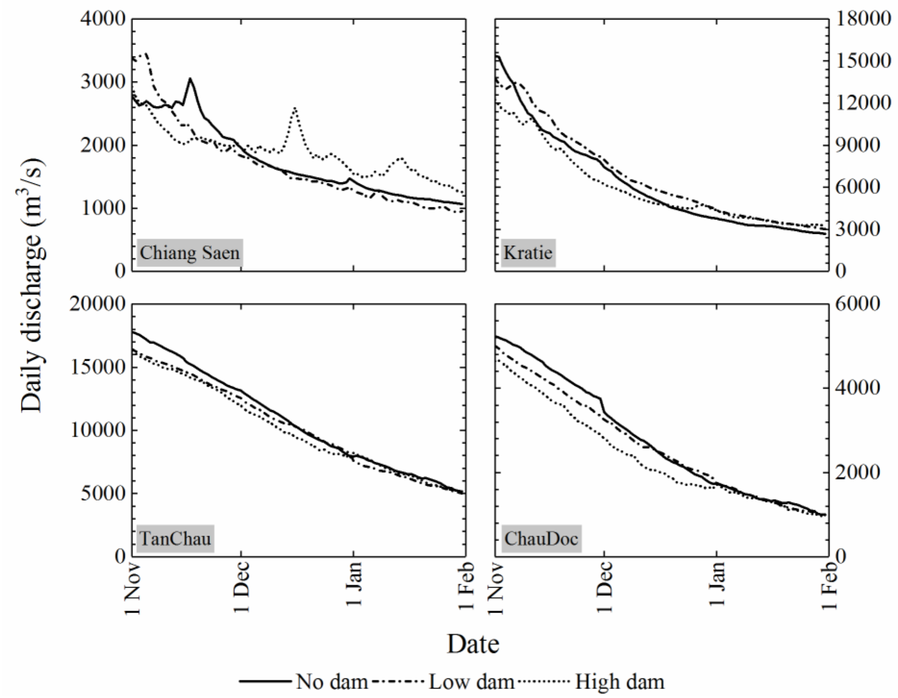

Figure 3.9 Hydrographs of the mean daily discharges in the transition-flow season in the no-dam, low-dam, and high-dam development periods at four stations along the MR.

b. Alterations in the transition-flow discharges

At Chiang Saen, the transition-flow discharges generally decreased in the low-dam development but increased in the high-dam development (Fig. 3.9). For instance, the January discharges reduced by 9% in the low-dam development but increased by 15.9% in the high-dam development. At Tan Chau and Chau Doc, discharges of all months in the transition-flow significantly reduced in the high-dam development while slight reductions in the low-dam development were found (Fig. 3.9). At Chau Doc, for example, the December discharges reduced by 17.9% in the high-dam development compared to only 0.7% in the low-dam development.

c. Alterations in the low-flow discharges

At Chiang Saen, the low-flow discharges in the low-dam development reduced by 5.5-8.5% (Fig. 3.10 and Table 3.4). The maximum reduction was in February. However, the low-flow discharge increased by 22.9-39.4% in high-dam development. The maximum increase was in March. The low-flow discharges in the high-dam development have started increasing since 2007 with a rate of 2.0÷6.9 m^3/s/yr (Table A3.2). The duration of the low-flow significantly reduced, especially in high-dam development, with a rate of 100%.

Table 3.4 Changes of the low-flow discharges (m3/s) in the no-dam, low-dam, and high-dam development periods at four stations along the MR.

Month	No-dam	Low-dam		High-dam	
	Discharge	Discharge	Change (%)	Discharge	Change (%)
1. At Chiang Saen station					
February	980	900	-8.5	1,210	+22.9
March	880	830	-5.5	1,230	+39.4
April	970	900	-7.6	1,320	+35.4
2. At Krate station					
February	2,420	2,820	+16.5	2,920	+20.8
March	2,000	2,410	+20.4	2,720	+36.1
April	1,840	2,500	+35.6	2,990	+62.1
3. At Tan Chau station					
February	4,060	3,950	-2.71	4,110	+1.4
March	2,530	2,520	-0.12	2,990	+18.5
April	2,110	2,185	+3.46	2,900	+37.5
May	2,800	3,100	+10.7	3,740	+33.4
4. At Chau Doc station					
February	675	725	+7.4	755	+11.9
March	310	450	+44.2	520	+67.3
April	360	420	+16.9	525	+47.5
May	430	580	+36.6	660	+55.2

At Kratie, Tan Chau, and Chau Doc, the low-flow discharges statistically increased in both low-dam and high-dam development periods since 1994-1995 (Fig. 3.10 and Table 3.4, A3.3-A3.5). Increased rates ranged from 16.5-35.6%, 3.5-10.7%, and 7.4-44.2% in the low-dam development to 20.8-62.1%, 1.4-33.4%, and 11.9-67.3% in the high-dam development at Kratie, Tan Chau, and Chau Doc, respectively (Fig. 3.10 and Table 3.4). The duration of the low-flow at Kratie, Tan Chau, and Chau Doc significantly reduced, especially in the high-dam development, with rates of 41%, 9%, and 19%, respectively. In the VMD, the low-flow discharges at Chau Doc increased more than those at Tan Chau (Table 3.4). Moreover, the low-flow season at Tan Chau and Chau Doc in the high-dam development started earlier than that in the no-dam period (Fig. 3.10). It was five days at Tan Chau and eight days at Chau Doc.

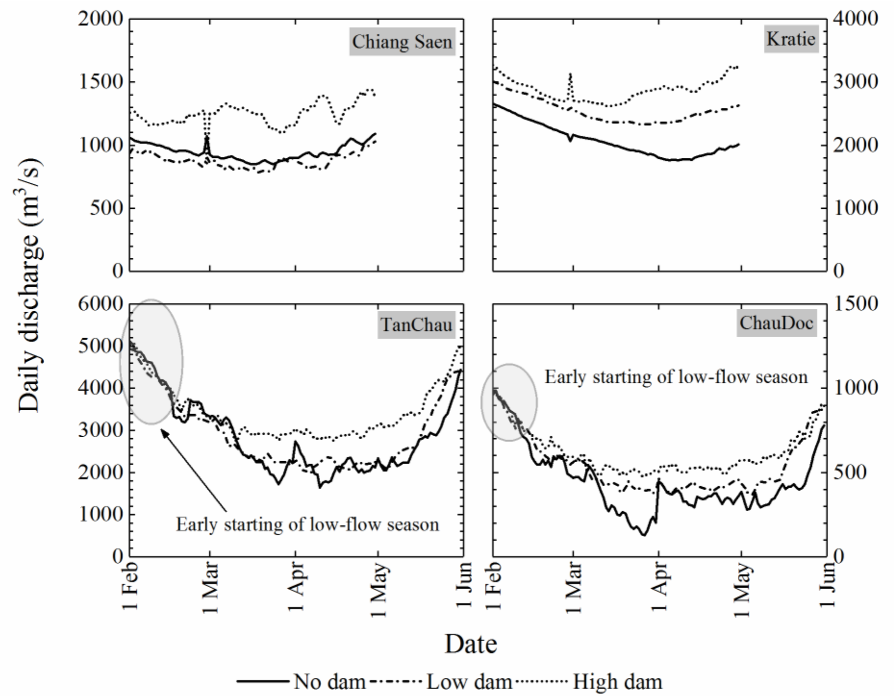

Figure 3.10 Hydrographs of the mean daily discharges in the low-flow season in the no-dam, low-dam, and high-dam development periods at four stations along the MR.

3.3.6 Alterations in water levels

The long-term mean annual water levels increased at Chiang Saen and Kratie, and decreased at Tan Chau and My Thuan (Fig. 3.11). My Thuan is the lowermost station which is about 100 km from the river mouth (Fig. 2.2). The increased rates at Chiang Saen and Kratie were 1.9 cm/yr and 1.2 cm/yr, respectively, and the decreased rates were 0.7 cm/yr at Tan Chau and 0.4 cm/yr at My Thuan. In the low-dam development, the mean annual water levels at Chiang Saen, Kratie, and Tan Chau increased by 15.9%, 9.3%, and 3.8%, respectively while those at My Thuan decreased by 5.6%, from the no-dam period. Furthermore, the mean water levels at Tan Chau and My Thuan in the high-dam development decreased by 13.6% and 22.8%, respectively, from the no-dam period.

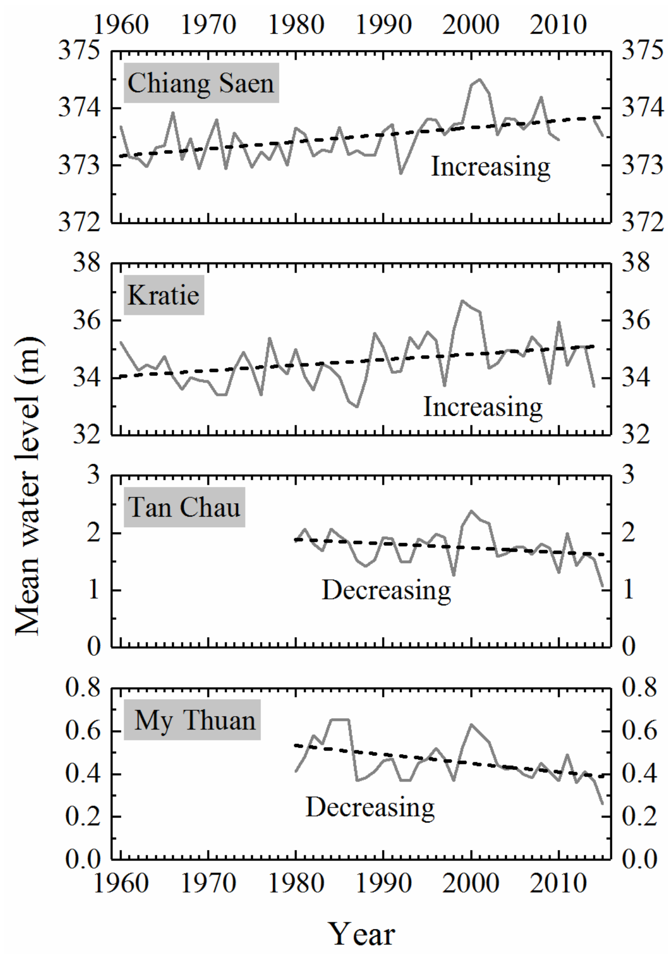

Figure 3.11 Long-term mean water levels along the MR.

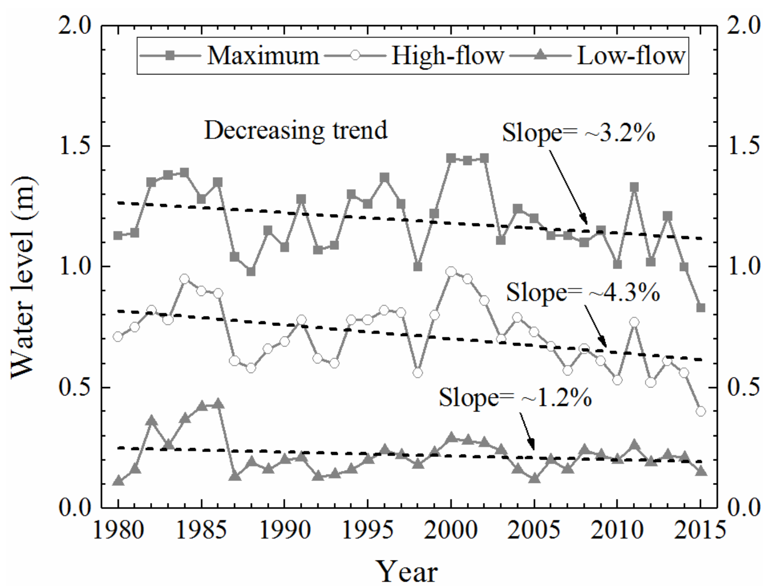

Figure 3.12 Long-term maximum, high-flow and low-flow water levels at My Thuan.

The maximum and high-flow water levels have important implications for flood control while the low-flow water levels are of crucial importance in mitigating and managing salinity intrusion in the VMD. At My Thuan, the long-term maximum, high-flow and low-flow water levels reduced (Fig. 3.12), with the reduced rates of 0.4 cm/yr, 0.6 cm/yr, and 0.2 cm/yr, respectively. Compared to the no-dam period, the maximum and high-flow water levels increased by 2.7% and 0.7%, respectively while the low-flow water levels decreased by 14.2% in the low-dam development. In the high-flow development, the maximum, high-flow, and low-flow water levels reduced by 10.2%, 23.4%, and 13.3%, respectively, from the no-dam period.

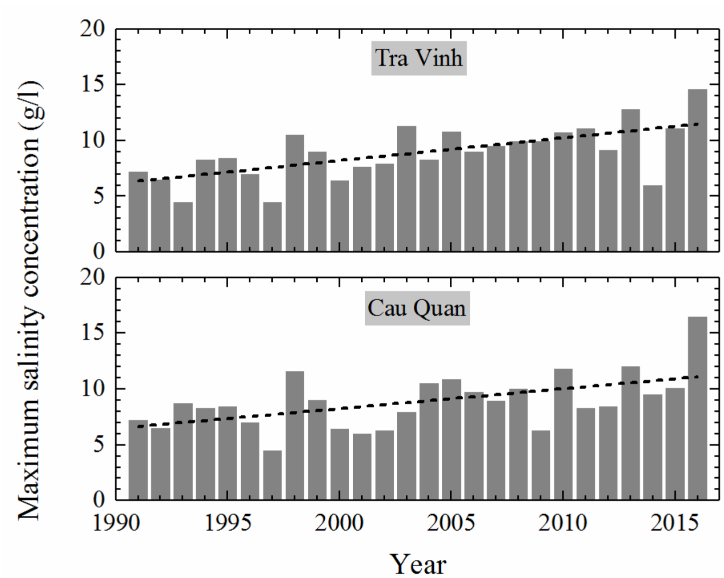

Figure 3.13 Long-term maximum salinity concentrations at Tra Vinh in the Tien River and at Cau Quan in the Hau River.

3.3.7 Alterations in the salinity intrusion

Controlling and mitigating salinity intrusion is of strategic importance to maintain and increase agriculture production in the VMD. However, the long-term salinity concentrations in the VMD have increased (Fig. 3.13). The maximum salinity concentrations at Tra Vinh in the Tien River and Cau Quan in the Hau River (Fig. 2.2) increased with a rate of approximately 0.2 g/l during 1990-2016. More seriously, the severe salinity intrusion frequently occurred in recent years. The maximum salinity concentration at Cau Quan in 2016 was about 1.4 times larger than that measured in 1998 (16.5 g/l for the former and 11.6 g/l for the later). The intrusion lengths of 4 g/l in 2016 were 65 km in the Tien River and 60 km in the Hau River which were approximately 20-25 km longer than the long-term average values. Not only the magnitude but also has the intrusion pattern changed. Salinity intrusion has shifted to begin earlier in recent years than the past (Fig. 3.14). For instance, the occurrence of the maximum salinity concentration in 2016 was about 1-2 months earlier than that in previous years. At Cau Quan, the maximum salinity concentration occurred in February 2016 while in April 1998 and March 2010 (Fig. 3.14).

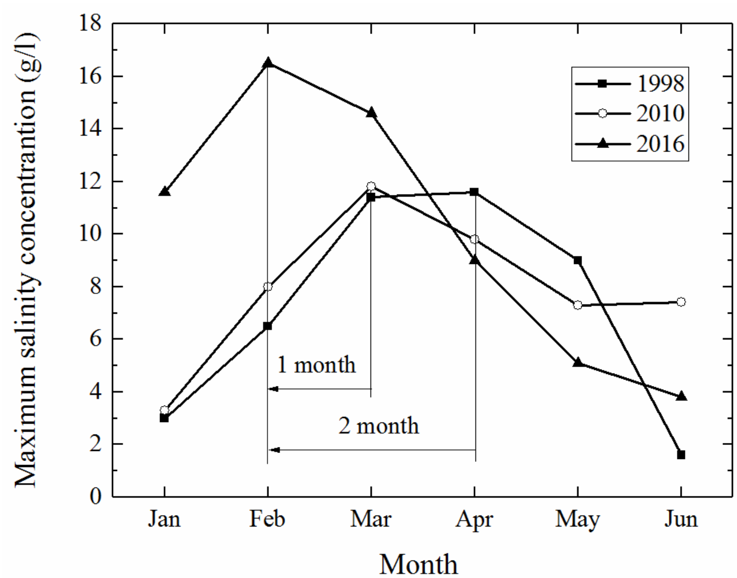

Figure 3.14 Maximum monthly salinity concentrations at Cau Quan in the Hau River.

3.3.8 Impacts of Lancang cascade dams on the low-flow season flows in the VMD

Discharges and water levels in the postdam periods, especially since 2009 when three largest dams were in operation, are significantly reduced in January-February while increased in March-June compared to those in predam period (Fig. 3.15). These findings clearly show that the low-flow season flows are shifted to begin earlier in the postdam periods. That may cause difficulty in irrigating the winter-spring crop, which is the most productive and important among the three crops in the VMD (Xuan, 1975).

Fig. 3.16 demonstrates the similarity in the tidal patterns of the VungTau (about 100 km Northward from the estuary of the Tien River) and Tan Chau stations using the mean water levels in 2012 and 2013. The river flows are more fluctuating in the postdam periods comparing to that of the predam (Fig. 3.15). This fluctuation has the same pattern with the variations of the tide (Fig. 3.16).

Due to the Lancang cascade dams, the maximum tidal amplitude at Tan Chau increases from 0.19 m in the predam to 0.33 m in 2009-2011 (4 dams) and 0.44 m 2012-2015 (6 dams), corresponding to an increase of 1.7 and 2.3 times, respectively. This indicates that the tide carrying saltwater has gradually increased propagating upstream as the number of completed dams increase.

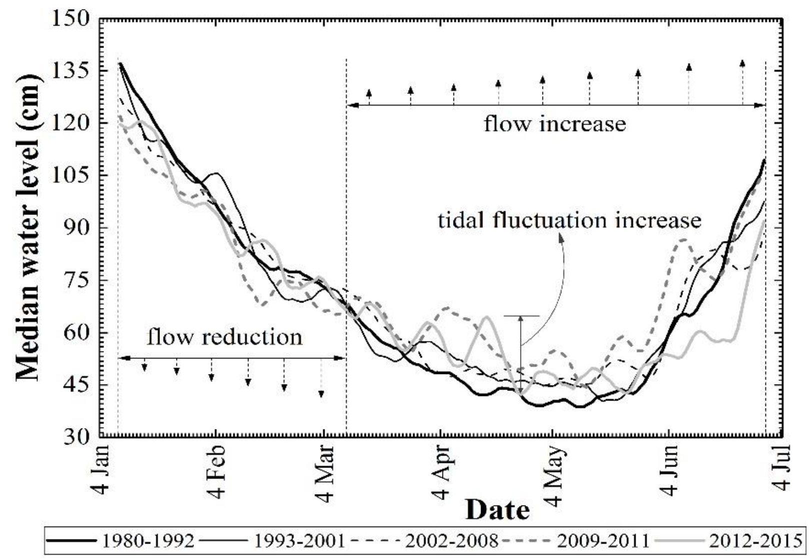

Figure 3.15 Median water levels in dry season at TanChau.

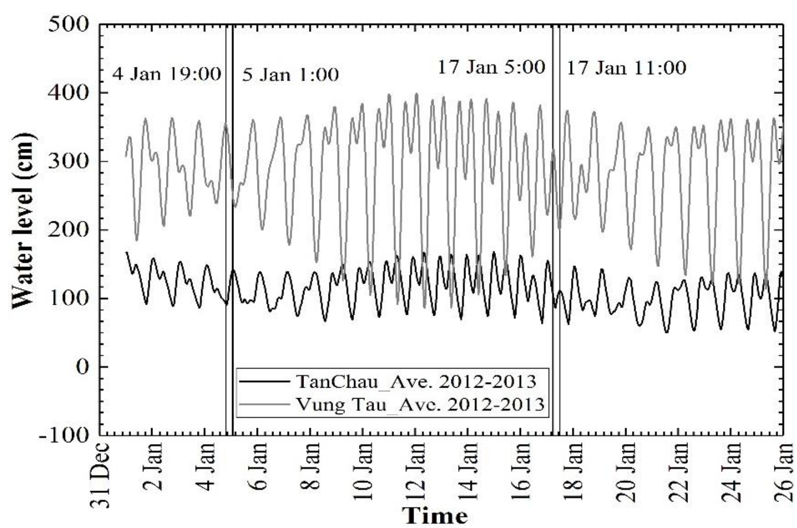

Figure 3.16 Hourly water levels at Vung Tau and Tan Chau.

As shown in Fig. 3.17, changed patterns of the median discharges between the postdam periods up to 2009-2011 and the predam period are not clear. This is linked with no statistical trend in the mean water levels in the dry season at the Jiuzhou station (Li and He, 2008) (Fig. 3.18) which is upstream of the Lancang cascade (Fig. 2.1**)**. Water levels from 1980-2003 (not available since 2004) at Jiuzhou are used for the comparison because discharge data are not publicly available upstream of the Lancang cascade dams. It indicates that impacts of the Lancang cascade dams on the low-flows in the VMD by the year 2011 are not obvious, the possible reason may be due to a relatively small reservoir capacity of the first four dams in the cascade compared to the MR flow. However, the median discharge during 2012-2015 (4,037 m^3/s) when all six Lancang cascade dams were in operation significantly increases compared to that of the predam period (3,708 m^3/s). Fig. 5.15 also reveals that the minimum discharges significantly increase as the number of Lancang cascade dams increase, from 1,519 m^3/s in the predam period to 2,935 m^3/s during 2012-2015 (+93.2%), equivalent to 1.9 times. This is commonsense because hydropower dams discharge water for electricity generation during the low-flow season. In contrast, the median and minimum water levels generally reduce when the number of Lancang cascade dams increase.

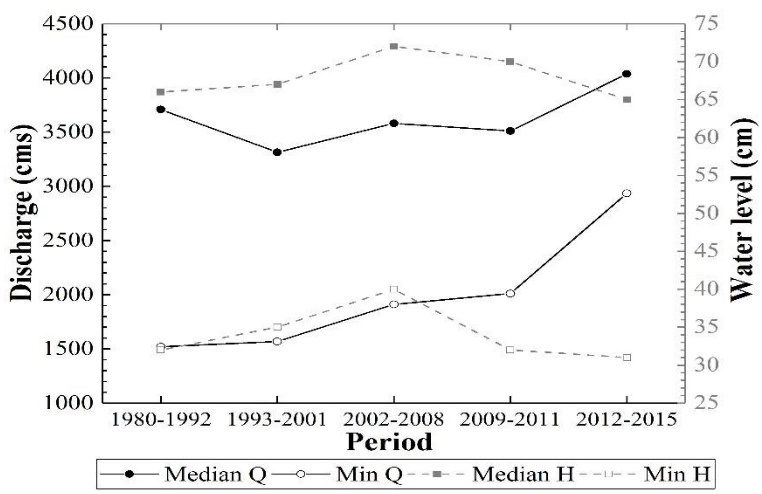

Figure 3.17 Discharges and water levels in the low-flow seasons at Tan Chau.

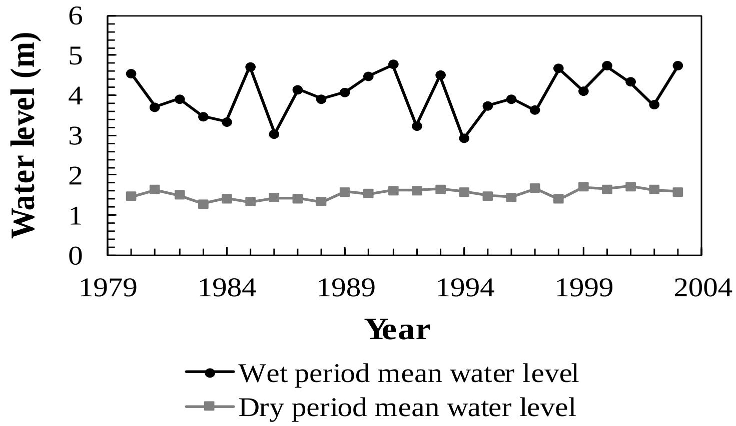

Figure 3.18 Mean water levels in the high and low-flow seasons at Jiuzhou.

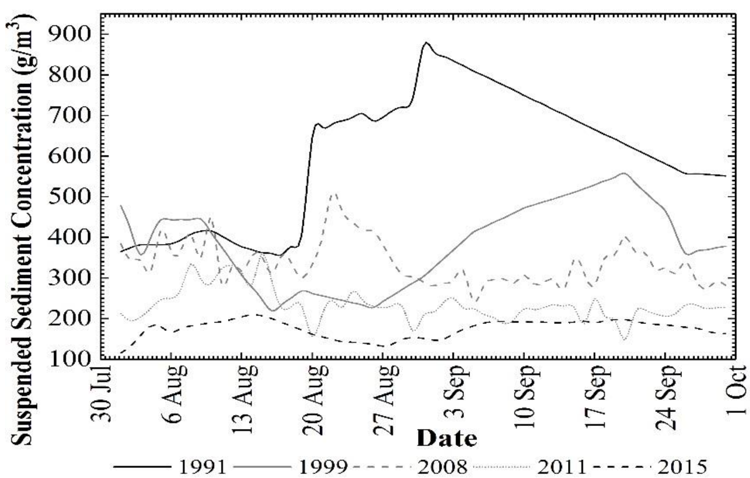

Figure 3.19 Daily suspended sediment concentrations at Tan Chau.

Obviously, the discharges and water levels at Tan Chau have opposite trends under the impacts of the Lancang cascade dams. Discharges tend to increase while water levels tend to decrease (Fig. 3.17). When the inflow is high, the tide is kept far seaward, therefore the water level is low and vice versa. This phenomenon can be explained through a reduction in sediment supply from the UMB due to the Lancang cascade dams (Fig. 3.19). The figure shows that the suspended sediment concentrations in August and September at Tan Chau are gradually reduced as the number of dams increases, from about 600 g/m^3 in 1991 (predam) to about 175 g/m^3 in 2015 when six dams in the Lancang cascade completed (about 340% reduction). Moreover, Kondolf et al (2014) revealed that dams in the upper MRB trap about 83% of sediment generated in this region, equivalent to about

40% of the total sediment generated in the MRB. Such a huge reduction may result in an increase in river bed incision, causing an increase in the influence of the tide. More seriously, such increased tidal influence may lead to more salinity intrusion to the VMD, damaging agriculture, aquaculture, ecosystem, and livelihood of local citizens (Kantoush et al., 2017).

3.3.9 Impacts of Lancang cascade dams on the high-flow season flows in the VMD

Although there are some fluctuations, the mean water levels in the high-flow season at Jiuzhou from 1980-2003 do not statistically follow any trend (Fig. 3.18). Consequently, the trends in the median and maximum discharges and water levels at Tan Chau in the high-flow season between the pre-and-postdam periods, up to the year 2011, are not clear (Fig. 3.20). Thus, the impacts of the Lancang cascade dams on the high-flows at Tan Chau by the year 2011 are not obvious. This is because the reservoir capacity of the first four dams is still relatively small compared to the total flow budget of the MR.

However, both discharges and water levels during 2012-2015 (six Lancang cascade dams completed) significantly decrease compared to those of predam period (Fig. 3.20). The median and maximum discharges reduce by -13.5% and –4.6%, respectively. Similarly, the median and maximum water levels decrease by -19.6% and -20.2%, respectively. Such reductions are due to the fact that reservoirs in the Lancang cascade dams store flood water for electricity generation in the next low-flow season.

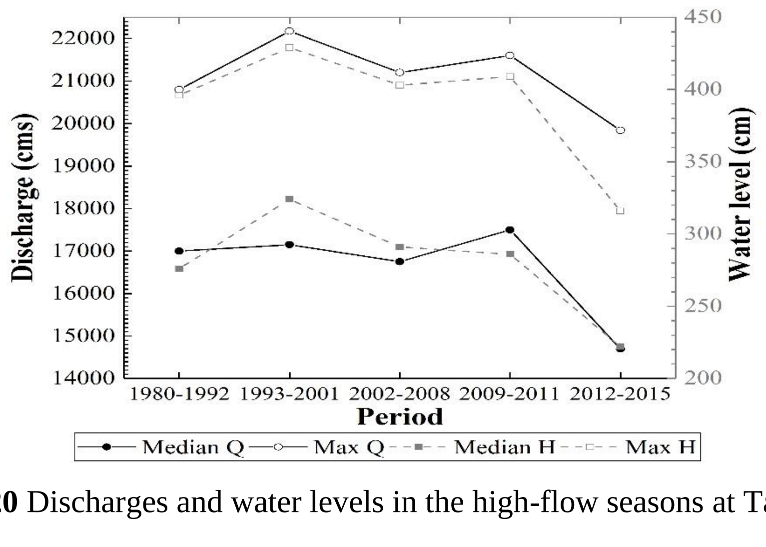

Figure 3.20 Discharges and water levels in the high-flow seasons at Tan Chau.

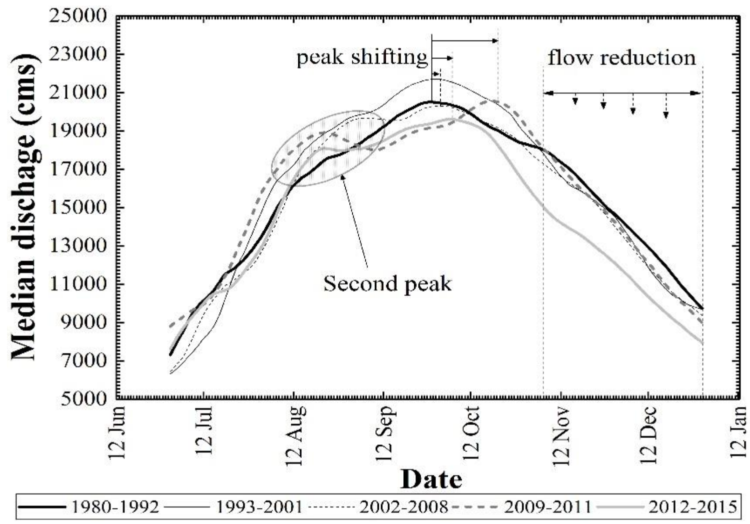

Figure 3.21 Median daily discharges in the high-flow seasons at Tan Chau.

Flow reductions in the high-flow seasons due to Lancang cascade dams are somehow helpful for the VMD by reducing losses caused by floods, i.e. from infrastructure, human lives. However, unexpected huge reductions in high-flow flows become significantly negative because the VMD needs floods for its development. Floods provide fisheries and rich natural fertilizers, remove contaminants, and maintain biodiversity and ecosystem. The best water levels at Tan Chau are 0.35-0.45 m (MRC, 2005). At these levels, damages caused by floods are acceptable while benefits are advantageous. The maximum water levels of 0.32 m during 2012-2015 (0.8 m smaller than that in the predam period) is lower than these limits; therefore, Lancang cascade dams may have negative impacts on high-flows in the VMD.

Lancang cascade dams not only change the magnitudes but also shift the peaks and patterns of the flood flow in the VMD (Fig. 3.21). The figure shows that the timing of the flood peak is shifted to happen lately due to reservoir regulation. For instance, the flood peak occurred on October 11 in 2009-2011 compared to September 20 in the predam period. Seriously, the hydrograph appears a second peak in August in the postdam periods instead of one peak in September in the predam. This second peak may additionally inundate and damage the second rice crop (April/May-July/August) in some areas which are not protected by dike systems because local people used to be familiar with single-peak floods in the predam. Meanwhile, the flows from November to December in the postdam periods significantly reduce due to reservoir regulations, causing difficulty in irrigating the winter-spring rice crop.

3.3.10 Impacts of planned mainstream dams in the lower MR and climate change on the hydrodynamics of the VMD

a. Model setup and scenarios

The prediction of hydrological changes in the VMD under the development of 11 planned dams in the lower MR in Thailand, Laos, and Cambodia along with sea level rise is performed using Mike 11 hydrodynamic model developed by DHI (DHI, 2009). The model solves the 1-D Saint Venant equations using an implicit finite difference scheme (see Appendix A). The model was set up for the whole VMD, including 2,551 branches with 13,429 points as in Fig. 3.22. In the model, hourly discharges at Tan Chau and Chau Doc are used as upstream boundaries whereas hourly water levels at seven stations along the coast, including My Thanh, Ben Trai, Vam Kenh, Ganh Hao, Song Doc, Binh Dai, and Rach Gia are prescribed as downstream boundary conditions. One hundred and fourty-five (145) cross sections describing the geometry of the Tien River from Tan Chau to My Thuan are updated to 2014 whereas cross sections measured in 2010 are applied elsewhere.

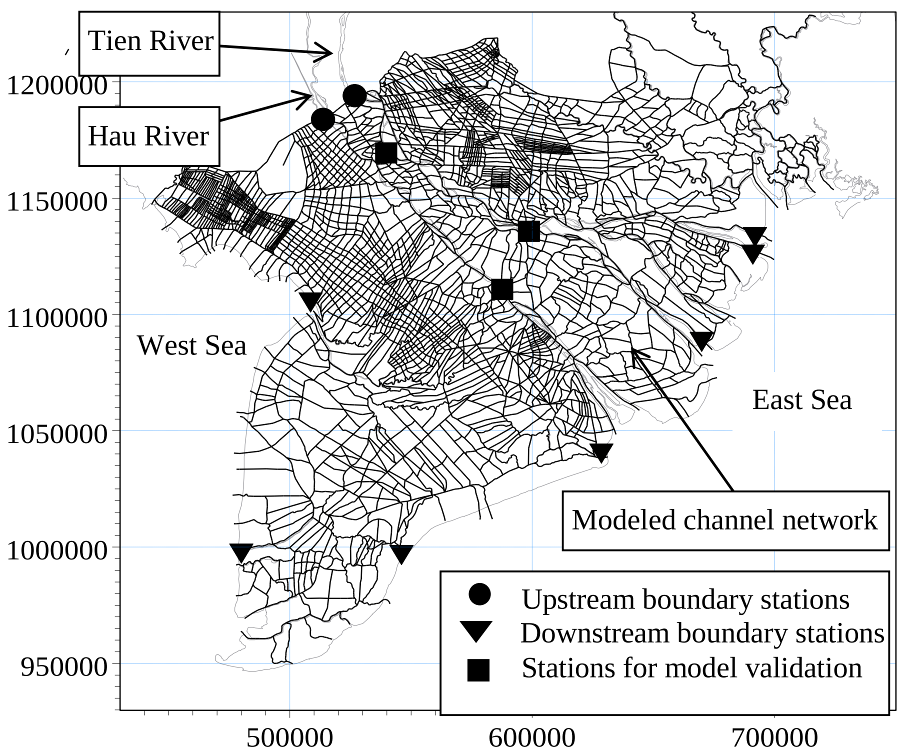

Figure 3.22 1-D hydrodynamic model setup.

Table 3.5 Simulation scenarios considering influence of 11 planned mainstream dams in the lower MR and climate change.

Scenarios	Description of boundary condition	Remark
Baseline (Sc0)	- Upstream: discharge hydrograph of 2015 - Downstream: water level stage of 2015	*Without dam and without sea level rise*
Scenario 1 (Sc1)	- Upstream: discharge hydrograph of 2015, considering 11 proposed dams - Downstream: water level stage of 2015	*With dam and without sea level rise* - Jan. – May: -1.9% at Tan Chau and -2.5% at Chau Doc - Jun.: -0.5% at both Tan Chau and Chau Doc
Scenario 2 (Sc2)	- Upstream: discharge hydrograph of 2015, considering 11 proposed dams - Downstream: water level stage of 2015, considering sea level rise 47 cm	*With dam and with sea level rise* - Jan.–May: -1.9% at Tan Chau and -2.5% at Chau Doc - Jun.: -0.5% at both Tan Chau and Chau Doc - Water level of 2015 + 47cm (high emission scenario - A1F1 – increasing 5.5mm/year)

Three scenarios are used to simulate changes of hydrology in the VMD (Table 3.5). The baseline (Sc0) refers to discharges and water levels of the drought year 2015. Scenario 1 (Sc1) considers the impact of 11 dams. In scenario 1, discharges at Tan Chau and Chau Doc are reduced by 1.9% and 2.5% (DHI-HDR, 2015), respectively, in between January and May and by 0.5% in June (DHI-HDR, 2015) compared to the baseline (Table 3.5), but water levels remain unchanged. Scenario 2 (Sc2) is similar to Sc1 but sea level rise is considered at the downstream ends. According to (Doyle et al., 2010), the sea level increases by 5.5 mm/year under the high emission scenario. Therefore, the water levels of scenario 2 are those of 2015 increased by 47 cm as the total increase in the water level up to the year 2100.

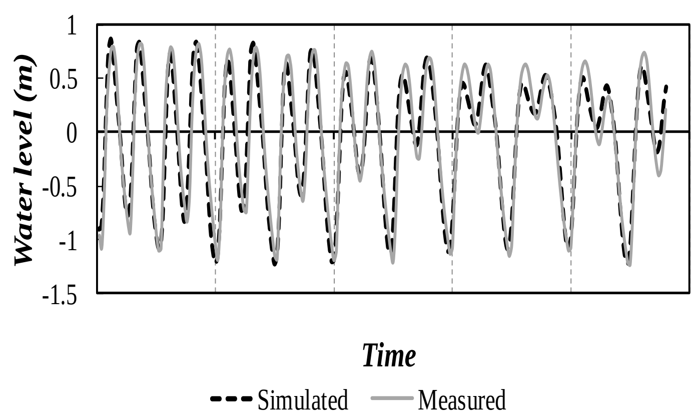

Figure 3.23 Predicted and measured water levels at Can Tho.

Table 3.6 Values of two performance indicators at three stations.

Station	Vam Nao	My Thuan	Can Tho
Calibration (2015)			
R^2	0.913	0.936	0.978
E_f	0.807	0.862	0.913
Validation (1998)			
R^2	0.877	0.97	0.95
E_f	0.727	0.912	0.890

b. Model validation and results

Water levels at the Vam Nao and My Thuan stations in the Tien River and the Can Tho station in Hau River (see Fig. 2.2) of the year 2015 are used to calibrate the model. The model is validated using water levels measured at the same stations during the drought year 1998. Computed versus measured water levels at the Can Tho station are plotted in Fig. 3.23. The accuracy of the numerical results is evaluated using correlation coefficient (R^2) and Nash-Sutcliffe coefficient (E_f) (Table 3.6). Based on these performance indicators, one can see that a satisfactory model-data agreement is obtained.

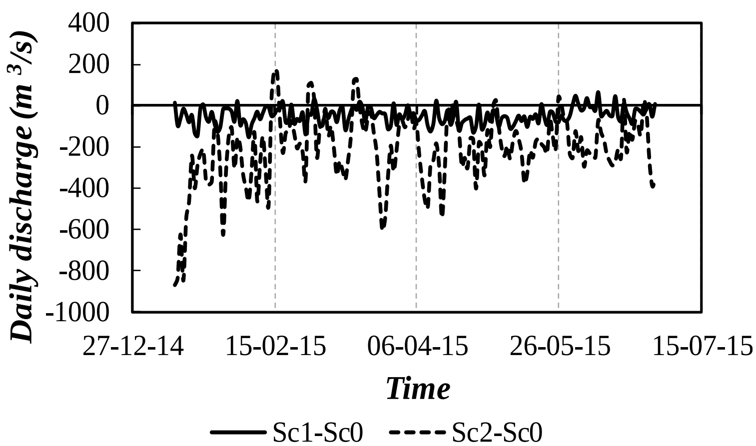

Figure 3.24 Discharge reduction of scenario 1 and 2 compared to the baseline in solid and dash lines at Long Xuyen.

Hydrological parameters of the VMD are directly affected by changes in the upstream discharges at Tan Chau and Chau Doc and downstream water levels along the coast. Table 3.7 shows the reduction in the mean simulated discharges and the increase in mean simulated water levels within the studied period (Jan.–Jun.) under different scenarios. Moreover, Fig. 3.24 shows a comparison between the difference in Sc1 and Sc2. The difference between scenarios is calculated as follow in equations 3.5 and 3.6:

$$(Scx - Sc0) = \frac{\sum_{i=1}^{N}(A_{Scx\_i} - A_{Sc0\_i})}{N} \tag{3.5}$$

$$P(\%) = \frac{\sum_{i=1}^{N}[(A_{Scx\_i} - A_{Sc0\_i})/A_{Sc0\_i}.100]}{N} \tag{3.6}$$

where (*Scx-Sc0*) is the difference of discharges or water levels in absolute values between scenario *x* (*x=1: scenario 1 and x=2: scenario 2*) and the baseline (*Sc0*); A_{Scx_i}, A_{Sc0_i} are discharge or water level of scenario *x* and the baseline, respectively, at day i^{th}; *P(%)* is the difference of discharge or water level between scenarios and the baseline in percentage; *N:* number of days within Jan.–Jun. If (*Scx-Sc0*) (or *P*(%)) is positive, discharge or water level will increase, vice versa they will decrease.

Table 3.7 Mean discharge reductions and water level increases within the simulated period (Jan.– Jun.) in the VMD under different simulation scenarios at eight measurement stations.

Statio	**TanChau**	**VamNao**	**MyThuan**	**MyTho**	**ChauDoc**	**LongXuyen**	**CanTho**	**DaiNgai**
				Discharge reduction (m³/s)				
(Sc1-	-63.8	-31.6	-27.0	-9.6	-13.8	-50.6	-50.0	-17.1
P (%)	-1.7	-2.2	-1.2	-0.5	-2.1	-2.8	-2.9	-3.6
(Sc2-	-63.8	-24.1	-34.8	-16.3	-13.8	-213.8	-260.2	-22.2
P (%)	-1.7	-1.0	-2.8	-2.7	-2.1	-11.6	-14.9	-4.6
				Water level increase (cm)				
(Sc2-	0.423	0.436	0.456	0.467	0.436	0.452	0.458	0.467
P (%)	94.6	127.1	75.5	221.2	139.2	172.6	162	25.7

Under the reduction of discharges at Tan Chau and Chau Doc (Sc1), flow discharges at Vam Nao, My Thuan and My Tho in the Tien River and at Long Xuyen, Can Tho, and Dai Ngai in the Hau River are reduced by 0.5 to 3.6% in average (Table 3.7). In the Tien River, the maximum reduction of discharge is obtained at Tan Chau with a mean value of 63.8 m^3/s, while in the Hau River, it is Long Xuyen that experiences the maximum reduction (50.6 m^3/s). More seriously, the discharges in VMD are even more reduced in Sc2 which further considers the influence of the sea level rise. For example, mean discharge at Can Tho drops by 260 m^3/s, corresponding to 14.9% - the maximum reduction among stations (Table 3.7). In contrast, water levels at all stations in the VMD are increased, a clear example from My Tho is shown in Fig. 3.25. The water levels in stations near the sea increase faster than those in upstream sections (Table 3.7). Among these, the water levels at My Tho increase the most with over 220% (Fig. 3.25).

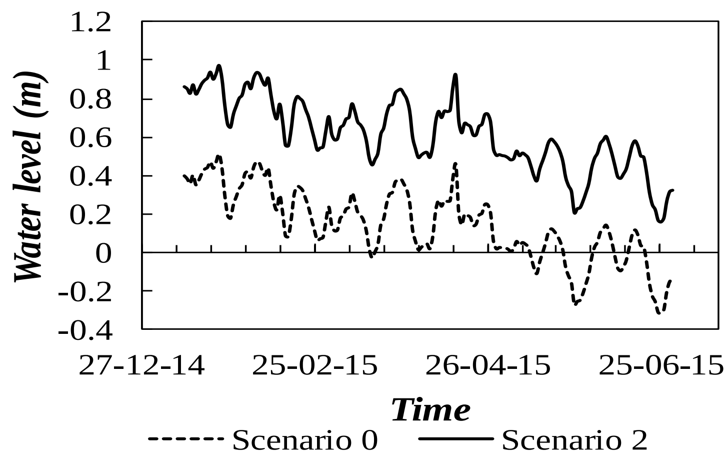

Figure 3.25 Increases in the water level of scenario 2 compared to the baseline at My Tho.

Because of the geographical location, hydrology of VMD is strongly dependent on activities of upstream countries such as dam construction and irrigation development. Chinese dams are more likely the main cause of the water decrease in the VMD. More seriously, two drought events happened just after the first and the last dams, in 1998 and 2015. Recently, there are other eleven dams proposed by Thailand, Lao PDR, and Cambodia in the mainstream of the MR. Results from scenario 1 show that these eleven dams will cause flow discharge declining in the VMD from 0.5 to 3.6%. The Hau River experiences higher reduction than the Tien River. Moreover, the further the areas from the Vietnam-Cambodia border is, the more the reduction in the flow discharges will be. Importantly, these proposed dams together with existed ones in China may lead to the disappearance of floods in the upper parts of the VMD, which is extremely crucial to livelihoods of millions of people there.

Low discharges observed at the upper part of the VMD during the drought event 2015-2016 caused saltwater intruding deeply into lands, thereby resulting in detrimental impacts on the agriculture and aquaculture. The drought 2015-2016 has led to total damages of 31,198.94 ha (approximately 2.2 million US dollars) in the Soc Trang province. Many regions, where paddy fields with 27,004.16 ha were affected, have reduced their agricultural productivity (Fig. 3.26).

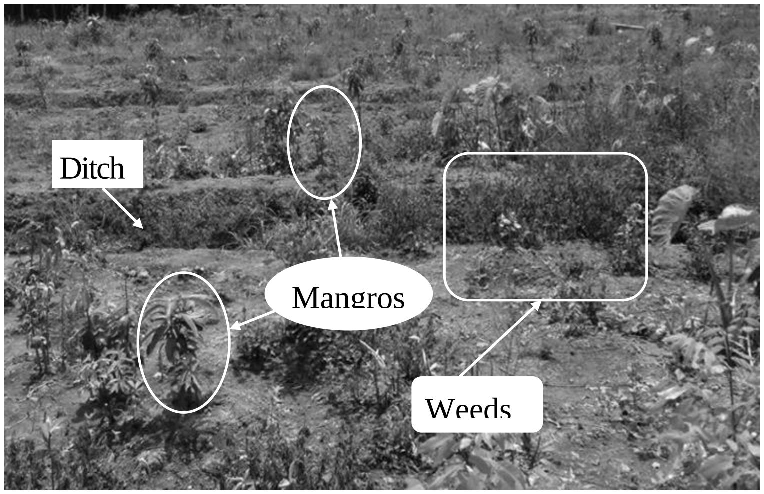

Figure 3.26 Damaged fruit-garden in the Ke Sach district – Soc Trang province. Dead mangosteen was replaced by new mango.

As predicted by scenario 2, flow discharges are much reduced and water levels are increased in the VMD (Table 3.7). Discharges at Can Tho decrease the most with 14.9% while My Tho faces an increase of more than 220% in the water level. This causes saltwater significantly to intrude into the upper parts. It means that more areas, including regions having not been affected before, will be covered by the saline water with higher concentration.

Sea level rise may also increase the flooding in coastal regions of VMD (Hoa et al., 2007). Furthermore, because of decreasing discharges and increasing water levels, the flow velocity will be reduced in the channels. Nutrient-rich sediment will deposit preferentially in the rivers instead of conveying into the floodplains that may lead to a reduction of the agricultural productivity in the near future.

3.4 Discussions

3.4.1 Drivers of the flow regime alterations upstream of Chiang Saen

In undisturbed river systems, the climate condition is the key driver controlling the river flow regimes. However, the mechanism will be more complicated if anthropogenic interventions such as hydropower dams appear in river systems. At Chiang Saen, the mean annual, maximum, and high-flow discharges in the low-dam development increased, which cannot be attributed to decreased annual precipitation intensity (0.5%) in the upper MR for a period of 1993-2008, from the no-dam period (Fig. A3.1 and Table 3.8). Xue et al., (2011) reported a no significant change in the precipitation over the past 50 years in the MRB. Although the mean annual precipitation contributed from tropical cyclones in the upper MRB, 7.7% of the annual flow passing Vientiane (Darby et al., 2013), has spatially reduced for the period of 1996-2005 (the low-dam development period) from the pre-1990 (no-dam period) (Darby et al., 2016), the shifting in the timing of tropical cyclones may, the most convincing, explain for the increases in the maximum and high-flow discharges at Chiang Saen because the precipitation derived from tropical cyclones largely falls during, or just after, monsoon months, when subsoil layers are already wetted or even saturated; therefore effective in forming runoff (Darby et al., 2016). Small storage capacity of hydropower dams in the upper MRB in the low-dam development period (4.1% of mean annual water flux at Kratie) may intensify the maximum and high-flow discharge increases through reservoir operations in the context to which tropical cyclones occur when reservoirs almost or already full; therefore, dam regulators have to release water as fast as possible for safety reason. Changes in the seasonality of the monsoon may also be the cause; however, further studies about this topic should be conducted to clarify. Reductions in the low-flow discharges in the low-dam development are mainly attributable to hydropower dams due to irregular releases during the low-flow (i.e., Manwan and Dachaoshan) (Hecht et al., 2019), that the released water from power generation may be less than the baseflows in the natural conditions.

Table 3.8 Changes in the annual precipitation (mm) in the no-dam, low-dam, and high-dam development periods at seven rain gauges in the MRB.

Month	No-dam	Low-dam		High-dam	
	Precipitation	Precipitation	Change (%)	Precipitation	Change (%)
Lincang	1155.1	1158.8	+0.3	1151.5	-0.3
Simao	1517.5	1481.6	-2.4	1379.8	-9.1
Lancang	1619.8	1601.0	-1.2	1454.8	-10.2
Jinghong	1163.2	1188.3	+2.2	1388.4	+19.4
Upper Mekong basin	1363.9	1357.4	-0.5	1343.6	-1.5
Chiang Saen	1761.3	1733.7	-1.6	1758.7	-0.1
Pakse	1837.5	2065.2	+12.4	1778.2	-3.2
Nong Khai	1049.5	1297.6	+23.6	1592.4	+51.7
Lower Mekong basin	1689.7	1698.8	+0.5	1709.8	+1.2

Note: Change (%) = [High-dam (or low-dam) – no-dam]/no-dam *100%. “+”: increase and “-”: decrease.

In the high-dam development period, hydropower dams drive flow regime alterations at Chiang Saen, exceeding the impacts of climate conditions. At least two prior researches (Lyon et al., 2017; Räsänen et al., 2017) had the same conclusion. Large storage capacity of hydropower dams in the upper MRB in the high-dam development period (after the completion of Xiaowan and Nuozhadu) has led to reductions in the maximum and high-flow discharges at Chiang Saen. The total storage capacity of the six existing Lancang cascade dams is equivalent to 49% of the annual runoff at Chiang Saen, which can extensively regulate the flow regimes at Chiang Saen. Mean annual precipitation in the high-dam development (decreased by 1.5%) likely cause discharge reductions at Chiang Saen but less compared to dam impacts. Moreover, dam operations control the increases in the low-flow discharges at Chiang Saen. In general, hydropower dams are the main driver of decreasing maximum and high-flow discharges and increasing low-flow discharges at Chiang Saen (Table A3.2 and Fig. 3.3-3.4 and 3.6-3.7). This conclusion is in good agreement with at least four prior studies by (Li et al., 2017; Lu et al., 2014b; Räsänen et al., 2017, 2012). For instance, in our analysis, the February-April discharges increased by 22.9-39.4% and the July-October discharges reduced by 12.2-25.6%, which are compatible to respective 25.9-55.2% increase and 22.3-32.9% decrease, respectively, reported by (Li et al., 2017).

3.4.2 Drivers of the flow regime alterations downstream of Chiang Saen to the VMD

Following the upper MRB, the highland areas in Laos, Thailand, and Vietnam such as the 3S (Sekong, Sesan, Srepok) and Mun-Chi sub-basins are the main sources of the water runoff of the lower MR. The high-flow discharges at Kratie increased by 4.5-18.9% (Table 3.3) in the low-dam development, compatible to increases of 0.7-11.5% in the July-September discharges at Stung Treng (just downstream of Kratie) for a period of 1992-2009, found by Li et al., (2017). Although not statistically significant, the long-term annual precipitation in the lower MRB in the low-dam development period increased (Fig. A3.1), with a mean (among Chiang Saen, Pakse, and Nong Khai) of 0.5% and a maximum of 23.6% at Nong Khai (Table 3.8). Therefore, the increased precipitation in the low-dam development period is likely the main driver of increases in the maximum and high-flow discharges in the lower part of the lower MR. Although not increase in the intensity (Darby et al., 2016), shifting the timing and pattern of tropical cyclones in the lower MRB (e.g., more concentrated during a short time) may contribute to increasing the maximum and high-flow discharges in the lower MR. Hydropower dams in the mainstream and tributaries with a relatively small reservoir capacity may intensify the maximum and high-flow discharges by exceptionally releasing large volumes of the water during the heavy rainfall and/or cyclones for dam safety operations. However, hydropower dams in tributaries are the main factor of the increased minimum and low-flow discharges of the lower MR through power generation.

In the high-dam development period, mainstream hydropower dams in the Lacang cascade were the main driver of reductions in the high-flow discharges in the lower part of the lower MR and the VMD (Table 3.3) due to their large reservoir capacity, capable of regulating the large floods, generated in the upper MRB. Räsänen et al., (2017) reported a reduction of 21% in the September discharge at Kratie during 2010-2014 from the 1960-1990 period, which is in line with our findings. Moreover, diversions may additionally reduce the flow discharges downstream of dams, such as the Nam Theun 2 dam and extensive diversions for the irrigation in the Mun-Chi basin in the northeastern of Thailand (Hecht et al., 2019). However, the increased precipitation intensity in the lower MRB (Table 3.8) that exceeds the capacity of hydropower dams in tributaries may increase the irregular released discharges in August and October in the VMD (Table 3.3). The delay of the high-flow (delay in the start, peak, and end) was also mainly driven by operations of mainstream dams in the Lancang cascade, which is partially compensated by the tributary dams. All hydropower dams in the MRB synthetically substantially increased the magnitude and reduced the duration of the low-flow discharges along the lower MR up to the VMD (Table 3.4), in which the former may permanently inundate the riverbank gardens (54% of the MR mainstream) and the later are critical for the fisheries (Hecht et al., 2019). We found that hydropower dams in the MRB have the strongest impact on the April flow. One important finding is that the maximum discharges at Kratie, Tan Chau, and Chau Doc in the high-dam development period increased, attributed to the climate change that causes increases in the frequency and magnitude of severe floods (Hoanh et al., 2010). Therefore, the design of future hydraulic structures must pay special attention to this mechanism.

In the upcoming decades, hydropower dams in the MRB (existing and planned) and the climate change are expected to continue driving the hydrology of the lower MR. Although future climate change is projected to increase the impacts, all existing and planned dams in the MRB will remain as the largest key factor driving the alterations in the flow regimes of the lower MR until the 2040s as concluded by at least three studies (Arias et al., 2014; Keskinen et al., 2015; Lauri et al., 2012). We are expecting that soon after the completion of the 11 planned and under construction dams in the mainstream of the lower MR in Laos, Thailand, and Cambodia, the Mekong Delta (Cambodian and Vietnamese) will be negatively impacted in terms of the altered flow regimes, fishery, environment, and ecosystems.

The TSL (8,800km^2) is of crucial importance in naturally regulating the flow regimes of the VMD: reducing the high-flow and increasing the low-flow discharges. The TSL could reduce the high-flow flood depth in the Mekong Delta by 0.5 m which could reduce the flooded area by 400-900 km^2 while the TLS may increase the low-flow water levels by 0.2-0.6 m (Pokhrel et al., 2018). In the time scale of our analyses (1980-2015), the TSL may help, to some extent, attenuate the impacts of hydropower dams and climate change on flow regimes of the Mekong Delta; however, this topic should receive more researches to be quantified. Despite the important role of the TSL, its functioning in harmonizing the flow regimes of the Mekong Delta may be lost if more dams will be built in the future as planned (Arias et al., 2014; Keskinen et al., 2015). Kummu and Sarkkula, (2008) found that an increase of 17-40% of the permanent lake area due to increased low-flow water levels, induced by hydropower dams, would reduce the capacity of the TSL in reducing the flood flows in the VMD.

The results also revealed that the mean and low-flow water levels in the VMD (typical at Tan Chau and My Thuan) significantly decreased (Fig. 3.11-3.12) even though the discharges increased. A possible reason for such mechanism is reservoir sediment trapping; for instance, reservoir trapping efficiencies of Xiaowan and Nuozhadu were estimated as 89% (Kummu et al., 2010). The sediment supply from the MR which formed the Mekong Delta has reduced due to the reservoir trapping, leading the VMD from accretion to erosion (Li et al., 2017b); therefore, the riverbed under a process of degradation. Sand mining is another main factor causing riverbed degradation in the VMD (Kondolf et al., 2018). As a consequence of the riverbed degradation, the water levels reduced even the discharges increased. The reduced low-flow water levels pose a serious threat in obtaining the intake water for farming.

3.4.3 Consequences of the socio-economic activities and ecosystems due to the flow regime alterations

The benefits of hydropower dams include energy for the increasing needs of the society, and as a side effect, reduce the wet-season flooding and increase dry-season baseflows, which may help mitigate salinity intrusion and support irrigation. Six mainstream dams in the Lancang cascade reduced the annual maximum and high-flow discharges in the upper part of the lower Mekong River, which could reduce damages from flooding. However, flood pulse is important for the society by benefiting fisheries and floodplain agriculture, estimated as $8-10 billion in the lower Mekong River basin which is more than hundred times greater than damages caused by flooding, estimated as $60-70 million (Hecht et al., 2019). While countries that own hydropower dams benefit from power generation, and depending on the context, potentially from increased trade, foreign investments, navigation, and irrigation (Räsänen et al., 2012), neighboring (especially downstream) countries can experience negative impacts, such as reduced sediment and nutrient loads to downstream reaches. The dams have also disrupted the river's sediment continuity and connectivity between the floodplains and main rivers, preventing nutrient-rich sediment from depositing on floodplains, with negative consequences for ecosystems (e.g., fish spawning) and agriculture productivity. Hydropower dams also block fish migration path, reducing fish species and population, and consequently affect food security in the Mekong River basin because fisheries and other aquatic animals provide important protein for over 56 million people in the Mekong River basin, especially in Cambodia and Vietnam (Hortle, 2007). Example of the tradeoff between hydropower dam's benefits and damages in the Mekong River basin is that dams benefit $6-32 billion to the operators while its potential damages to capture fisheries only was estimated $2-13 billion, mainly in Cambodia and Vietnam (Hecht et al., 2019).

3.4.4 Stakeholder's strategic adaptation policies for sustainable development of the VMD

a. Adaptive flood control policies

Historically, people's livelihoods in the VMD closely depended on the natural flow regimes of the MR. Local people adapted with that by a so-called *living together with floods*. However, the Vietnamese government oriented the VMD becoming a *rice bowl* of the country that supported Vietnam to become the second largest rice exporter in the world. As a result, large-scale low-dike systems have been constructed since 1996 to convert floating rice to irrigated rice farming (Triet et al., 2017). The low-dike policy has proved its advantages with twofold: protecting the agricultural farming from early floods in July-August to grow lands of the double rice crops while providing retention areas for the flood control during the flood peak in September-October. Allowing the flood water flowing into the large-scale floodplains during the flood peak benefits the local people, especially the poor, from fisheries as the second important income source. Low-dike systems are also friendly to the environment and ecosystems, allowing the nutrient-rich fine sediment accessing the large-scale floodplains which may help recover and enrich the soil properties for the next cultivation crops. Other benefits of the low-dike systems were well discussed in (Tran et al., 2018). The Vietnamese government again changed the policies and concept of the flood control and rice farming after tremendously suffering the most severe flooding occurred in the year 2000. Large-scale high-dike systems have been built since then to completely control the flood peak and the 2000-flood became the standard of high-dike constructions. The high-dike systems extensively converted from double to triple rice crops in the VMD, helping increase rice productivity. However, the high-dike posed many serious problems to the livelihoods of the local people, the environment and ecosystems. One of the largest negative impacts of the high-dike is to totally block the fine sediment approaching into the floodplains, that gradually degrades the soil properties; and consequently, may reduce, in the long-term, the total income of the farmers due to increasing using costly artificial fertilizers and toxic pesticides. Other negative impacts of the high-dike systems were extensively discussed in (Dang et al., 2016; Tran et al., 2018; Triet et al., 2017).

Linking the period of high-dike constructions with the flow regime alterations in the VMD during the low-dam development (1993-2008) provided an important finding that stakeholders made a prompt decision to build the high-dike systems after suffering a severe flood in 2000. Such a decision was suitable during that time but not sustainable under the changing climate and the upstream hydropower dam development. Both discharges and water levels in the VMD in the high-dam development (2009-2015) reduced substantially. Therefore, the flood control in modern years do not need such costly high-dike systems, instead, the low-dike rings are preferable to easily receive the flood water, which contains the fine sediment. Stakeholders are therefore recommended to carefully conduct a long-term holistic investigation to comprehensively understand the nature of the future floods in the VMD under high degrees of upstream developments (i.e. dams, irrigation systems) and climate change before making important decisions, which would lead the VMD to fall into the *collapsed state* or to return to the modified *Holocene condition state*, accordingly (Tran et al., 2018). Results from our analyses, therefore, serve as an important fundamental for stakeholders to refer.

We here propose a concept for the flood control in the VMD, including two directions for the people and the economy-ecosystem separately. In residential areas, the ground level should be heightened above the peak water levels and the local governments should encourage people settling in those safe places, instead of sparsely settling inside the floodplains near their cultivated lands, which would cause difficulties for sustainable management. In important cities like Can Tho, the close cooperation between water resources management agencies and other sectors such as transportation and housing is a prerequisite to controlling the urban flooding. Combining the high-dike rings and pumping stations alongside with wise arrangement of roads, sewage systems, and housing would effectively control the urban flooding. Constructions of underground retention reservoirs inside cities which successfully tested in the Ho Chi Minh city by a Japanese company is also a good alternative for not only the urban flood control but also the groundwater recharge. For rice farming, we recommend to totally stop building new high-dike systems. Cultivating lands inside the existing high-dike systems should be converted from triple to double crops by permanently opening the sluice gates under existing the high-dikes, which can recover soil properties, flush out contaminants, support wetland ecosystems, and provide more retention capacity for the flood control in cities. Alternatively, periodic openings of the sluice gates under the high-dikes during the flood months (for instance, every 3 or 5 years) should be considered and firstly tested to justify the solution. Finally, the water resources management must be long-term investigated and implemented at a delta-scale but not provincial or local-scales.

b. Adaptive policies for obtaining intake water for the irrigation and for salinity intrusion control

Among three rice crops in the VMD, the Winter-Spring crop, cultivated from November/December to February/March is the most productive and important. The timing of this crop is in the period of the low-flow season. Although the low-flow discharges in the VMD increased, the low-flow water levels reduced (Fig. 3.12), resulted from riverbed incision and river bank erosion induced by reduced sediment supply from the MR. Such sediment supply reduction is possibly driven by the reservoir sediment trapping (Kummu et al., 2010) and sand mining (Kondolf et al., 2018). The sediment budget of the MR reduced from 160 Mt/yr in the predam (Kondolf et al., 2014) to 40 Mt/yr in 2012-2013 (Nowacki et al., 2015). Chapter 4 will provide more detail about dam impacts on the sediment budget of the MRB and VMD. Reductions in the low-flow water levels pose two critical problems. The first problem is the difficulty in obtaining intake freshwater to irrigate rice crops, especially the Winter-Spring crop. Reduced low-flow water levels may drop below the water intakes that farmers cannot operate the gravitational irrigation systems, instead, dynamical systems such as pumping stations are required. Such dynamical systems would increase the costs and reduce the benefits in the cost-benefit relation of rice farming. Secondly, reduced low-flow water levels may cause increased salinity intrusion in the VMD, causing lack of freshwater for domestic use, negatively impacting livelihoods of the people distributing near the estuaries, and damaging agricultural and aquaculture farming. In fact, the saltwater has increasingly intruded in the VMD recently (Fig. 3.13) and its pattern and timing have also shifted to occur earlier (Fig. 3.14).

Sustainable water resources management under reduced water levels and increased salinity intrusion is an urgent need in the VMD. Buffering zones such as ponds and small natural-like reservoirs should be allocated for the purpose of agricultural irrigation and salinity intrusion mitigations. Indeed, buffering zones also provide more room for the flood control in the high-flows. Both structural and non-structural measures to prevent the riverbed incision and river bank erosion should be investigated and implemented with care. Techniques to reduce reservoir sedimentation and to increase the sediment discharge from reservoirs should be used to retrofit the existing dams and designed for the planned dams. Locations of the sand mining must be carefully managed to not overexploit riverbed sand. With a good management policy, problems related to the reduced water levels and increased salinity intrusion can be sustainably solved.

Another hot issue in the salinity intrusion control in the VMD is widespread of sluice gate constructions. Salinity control sluice gates have been increasingly built and planned near the estuaries along the Tien and Hau Rivers over the last decade. These sluice gates effectively control the saltwater for the protected areas near the coast but increase the salinity intrusion land-ward along the rivers because the saltwater cannot enter into buffering zones near the estuaries. For this, we strongly recommend the stakeholders to suspend building the planned salinity control sluice gates along the main rivers in order to evaluate the functioning of the operating gates, which is a promising topic for further researches. Moreover, shifting land use from agriculture to aquaculture in areas intruded by saltwater may be an effective alternation to gain the people income and to adapt to the new flow regime conditions. Ca Mau Province is a good model. However, aquaculture farming practices must be friendly to the environment and ecosystems.

3.5 Conclusions

Long-term discharges were analyzed along the lower MR from Chiang Saen, Thailand, to Tan Chau and Chau Doc in the VMD for the period of 1980-2015, during which time all six mainstream hydropower dams in the Lancang cascade completed. Long-term water levels and salinity concentrations in the VMD were also analyzed. Main drivers of the flow regime alterations in each part of the lower MR using trend tests (Mann-Kendall, Pettitt, and Sen's Slope), indicators of hydrologic alterations, the range of variability, frequency analysis, and alteration index of hydrological regime were identified. The main findings are as follow:

(1) The climate conditions controlled the flow regimes in the low-dam development period (1993-2008) while hydropower dams in the MRB intensified the impacts.

(2) The operations of hydropower dams in the MRB were the main driver of the flow regime alterations in the high-dam development period (2009-2015), and dam impacts are expected to dominate through the 2040s.

(3) Mainstream dams manipulated the maximum and high-flow discharges while tributary dams controlled the minimum and low-flow discharges in the lower MR.

(4) For the flood control, considering economy and ecosystem sustainability, the high-dyke systems should not be further built while the existing high-dikes should be permanently or periodically opened during flood months (i.e., every 3 or 5 years) to receive the nutrient-rich fine sediment to recover and enrich the soil properties and to support the wetland ecosystems.

(5) The planned salinity control sluice gates along the main rivers in the VMD should be suspended, waiting for a comprehensive evaluation of the functioning and possible impacts of the existing sluice gates. Where applicable, converting lands from agriculture to aquaculture should be considered if it can increase the people income while ensuring environmentally friendly.

(6) The water resources management must be long-term investigated and implemented at a delta-scale but not provincial or local-scales.

(7) Finally, sharing data, knowledge, and benefits from the MR and cooperating among riparian countries under an integrated water resources management scheme are strongly recommended.

Chapter 4 Long-term discharge and sediment budget alteration in the Vietnamese Mekong Delta due to upstream dam development and adaptive measures

4.1 Introduction

Since the 1950s, hydropower dams have been increasingly built and planned in the MRB. Hydropower dams have significantly altered the flow regimes and reduced the sediment budget of the MR. In general, the flood flow decreased, but the low flow increased. The completion of the Manwan dam reduced the sediment budget at the Gajiu station by more than 60% (Fu et al., 2008), and more than 50% of the sediment budget at Chiang Saen (Lu and Siew, 2006). Six mainstream dams in the upper MR were predicted to trap as much as 83% of the sediment generated from the upper MRB, which is equivalent to 40% of the total sediment budget of the MR (Kondolf et al., 2014). This number can reach 94% (Kummu and Varis, 2007). Kondolf et al., (2014) predicted that only 4% of the MR sediment would reach the Mekong Delta annually if all 133 planned dams are constructed in the future. Sediment reduction is likely to cause riverbed incision and bank erosion along downstream reaches at different rates and time scales (reaches closer to the dams are affected sooner and at faster rates). Using remote sensing in Vientiane-Nong Khai area, Kummu et al., (2008) estimated the MR bank erosion of 0.8 and 1.0 m/yr (for the main channel) and 2.4 and 4.8 m/yr (for the islands) during the 1961-1992 and 1992-2005 periods, respectively.

The sediment budget of the VMD has significantly reduced during the past 3,000 years from 144 Mt/yr (Ta et al., 2002) to 40 Mt/yr during 2012-2013 (Nowacki et al., 2015). While not the sole reason, such a sediment budget reduction could cause riverbed incision, river bank erosion in major rivers and channels and coastline retreat (Li et al., 2017b), which may in turn create difficulties in obtaining intake water for irrigation and may increase salinity intrusion in the VMD (Binh et al., 2018a). For instance, the riverbed of the Hau River measured in 2008 in the VMD was degraded by 1-5 m more than that measured in 1998, with an average incision of 1.4 m (Allison et al., 2017a). On 22 April 2017, a 130-m-long and 30-m-wide river bank of the Vam Nao diversion channel collapsed, which was partly due to the reduced sediment supply from the MR. Approximately 50-66% of the current VMD coastline is experiencing rampant erosion (Anthony et al., 2015; Li et al., 2017b), which shifted from an accretionary phase of 10.6 m/yr during 1973-1979 to an erosional phase of -2.1 m/yr during 2010-2015 (Li et al., 2017b). The reduction in the

MR sediment supply to the VMD may also worsen the ecosystem functions and adversely affect local communities.

The understanding on which the hydropower dams in the MRB affect the long-term flow and sediment budgets in the large-scale VMD has been not fully quantified, due to lack of historical data. Therefore, quantification of dam impacts on the morphological changes, which are affecting the livelihoods of thousands of riparian people, especially the poor and homeless, in the VMD remains a challenge (Brunier et al., 2014). Some researchers (i.e., Anthony et al., 2015; Ha et al., 2018; Li et al., 2017b) tried to link dam impacts to the flow and sediment regimes in the VMD, but in the short-term and at small scales. Some other studies assessed dam impacts on the long-term flow and sediment alterations in the lower MR (i.e., Koehnken, 2014; Kummu et al., 2010; Kummu and Varis, 2007; Lu et al., 2014a), but they limited their study areas upstream of the Kratie station in Cambodia.

Therefore, the main objective of this chapter is to link hydropower dam development in the MRB and other factors, such as climate change and sand mining, to long-term discharge and sediment budget alterations in the VMD over the 36-year period of 1980-2015. To achieve concrete conclusions, long-term discharge and sediment data from some stations along the lower MR were also analyzed over 53 years during 1961-2013. Morphological changes during 1998-2017 in the Tien River were also analyzed to determine one of the consequences of the reduced sediment supply from the MR. The results of this study could help to close the knowledge gap and comprehensively understand the impacts of dams on the entire lower MR. Additionally, the findings of this study are important for the sound management of water conservancy, flood control, river navigation, salinity control, and agricultural development in the VMD.

4.2 Materials and methods

4.2.1 Data collection

Only the suspended sediment data were analyzed in this study due to a lack of bedload data in the MRB. The main sources of sediment data used in this study were the MRC for stations from Chiang Saen to Pakse and the Vietnamese National Hydro-meteorological Data Center for stations in the VMD (Fig. 2.1-2.2). Data were also collected from published reports and journal papers (e.g. Koehnken, 2014; Lu et al., 2014; Lu and Siew, 2006; Manh et al., 2014; Ta et al., 2002; Wang et al., 2011). Seven precipitation stations, six discharge and sediment stations were analyzed. The data range discharge, precipitation, SSCs and SSLs are given in Table 3.1. Precipitation stations are located in both the UMB and LMB. Discharge and sediment data were gathered for two periods in the LMB: pre-dam (pre-1992) and post-dam (2009-2013) when all mainstream dams completed. We re-examined the historical annual sediment loads at four stations: Chiang Saen, Luang Prabang, Nong Khai, and Pakse in the pre-dam period from Wang et al. (2011) who estimated annual sediment loads using four methods of SSC-discharge rating curves. These pre-dam sediment loads were compared with post-dam sediment loads (2009-2013) collected from Koehnken, (2014). It should be mentioned that historical sediment data at Mukdahan and Khong Chiam for pre- and post-dam periods were available. However, the annual sediment loads at these stations were overestimated due to the limitation of the devices used to collect water samples (Koehnken, 2014); therefore, they were excluded from this analysis.

The MR has discharged 144 Mt of sediment annually during the past thousands of years (Ta et al., 2002). Considering a 13.6% of the sediment at Vietnam-Cambodia border was deposited along Tien and Hau Rivers before reaching to the sea (Manh et al., 2014), the annual sediment load entering the VMD in the pre-dam period was estimated to be as 166.7 Mt yr^{-1}. This value is comparable to 160 Mt yr^{-1} as pre-dam sediment budget at Kratie station reported in a recent study (Bravard and Gaillot, 2013).

The measurements of SSCs at stations in the VMD are conducted by ships (Fig. 4.1), applying depth-integration method using isokinetic samplers. The sampled water is filtered on the blue filters, having a porosity of 8 μm (Ha et al., 2018), then weighted. In the low-flow season, the SSCs are measured twice a day, one in the ebb tide and one in the flood tide at all stations. In the high-flow season, SSCs are measured twice a day at My Thuan and Can Tho (one in the ebb tide and one in the flood tide) while once a day at Tan Chau, Chau Doc, and Vam Nao (in the morning). Normally, the SSCs are measured at a representative profile at each cross-section (this representative profile is usually around the thalweg of the river). The daily mean cross-sectional SSCs are estimated using the established linear rating curves between the representative SSCs and the mean cross-sectional SSCs measured at several profiles (five profiles at Vam Nao, six profiles at Tan Chau and Chau Doc, and four profiles at My Thuan and Can Tho) which periodically updated several times a year (for instance, three times a year at Vam Nao and four times a year at My Thuan and Can Tho) (Ha et al., 2018).

Figure 4.1 Ships used for SSC measurement at stations in the VMD. Photos were taken by Binh D.V. in February 2016.

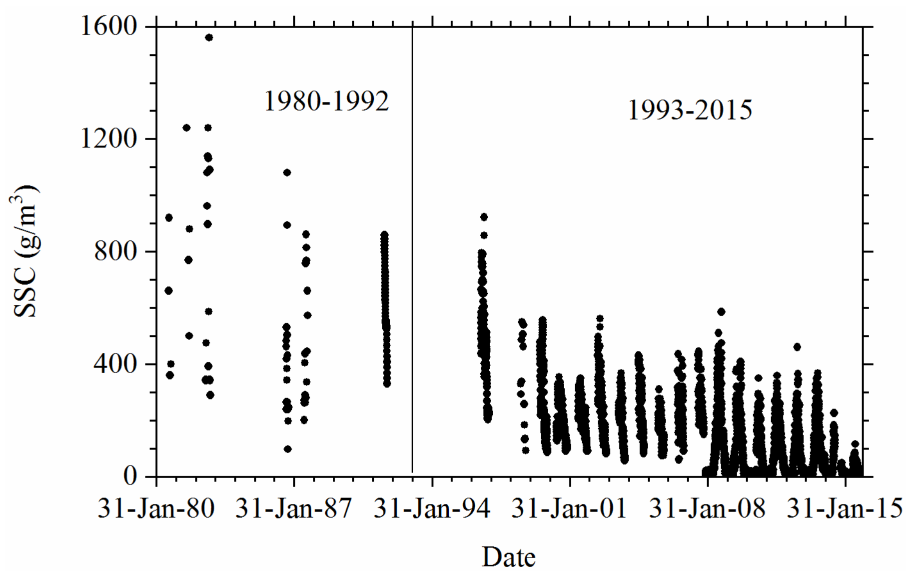

Figure 4.2 Measured daily suspended sediment concentrations at Tan Chau.

4.2.2 Estimating missing SSCs in the VMD using discharge-SSC rating curve and sediment load estimates

Fig. 4.2 shows that daily SSCs at Tan Chau during 1980-1992 were significantly higher than those during 1993-2015. Therefore, the discharge-SSC rating curves at Tan Chau and Chau Doc were established separately for these two periods to estimate the missing SSCs. During 1980-1992, the missing daily SSCs at Tan Chau were first estimated using the discharge-SSC rating curve by compiling all available data in this period. Then, missing daily SSCs at Chau Doc during 1980-1992 were the product of corresponding daily SSCs at Tan Chau and a factor of 13.3%, which was the mean percentage of the SSLs at Chau Doc compared to those at Tan Chau during 1993-2015. This estimating method yields a mean annual sediment budget in the VMD of 166.7±33.3 Mt/yr for the 1980-1992 period (sum of Tan Chau and Chau Doc), which is comparable to 160 Mt/yr widely reported in the literature (Meade, 1996; Kondolf et al., 2014a). Additionally, the product of 144 Mt/yr, the annual sediment load entering the VMD over the past 3,000 years (Ta et al., 2002), and 13.6%, which is the fraction of suspended sediment deposited along the Tien and Hau Rivers from the Vietnam-Cambodia border before reaching sea (Manh et al., 2014), yields a mean annual sediment budget in the VMD of 166.7 Mt/yr during the predam period, which fits our estimate perfectly. On the other hand, the mean annual discharges at Tan Chau and Chau Doc during 1980-2015 were 9,940 m^3/s and 2,490 m^3/s, respectively. These hydrographs were divided into the rising stage from April to September and the falling stage from October to March of the following year. Fig. 4.3 shows that the discharge-SSC relations in the VMD have a clockwise hysteresis and that the SSCs were higher during the rising stage than in the falling stage under the same discharge amounts. Thus, the missing SSCs during 1993-2015 at Tan Chau and Chau Doc were estimated based on the discharge-SSC rating curves, which were established separately for these rising and falling stages. The discharge-SSC rating curves were generated and fitted using a power relationship:

$$SSC = a \times Q^b \tag{4.1}$$

Then, the daily SSLs were computed as a product of daily SSCs and corresponding daily discharges:

$$SSL = \frac{86{,}400 \times SSC \times Q}{10^6} \tag{4.2}$$

where Q is the discharge; *a* and *b* are two dimensionless coefficients; 86,400 is the total seconds in a day; 10^6 is the conversion factor. The units of Q, SSC, and SSL are m^3/s, g/m^3, and t/day (ton/day), respectively. Then, the daily SSLs were used to examine the monthly SSLs and annual suspended sediment budgets. The suspended sediment budget of the VMD was the summation of the Tan Chau and Chau Doc station SSLs. Analyses and discussions on the variations in suspended sediment budgets in the VMD were based on daily, monthly and annual data.

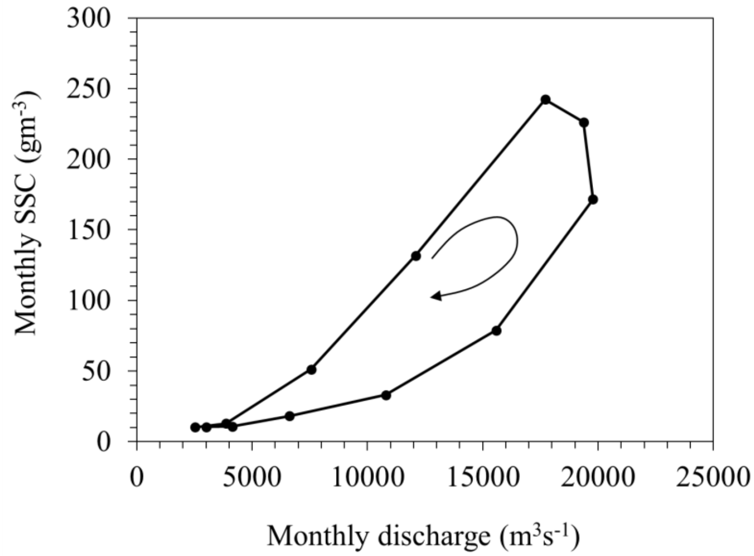

Figure 4.3 Clockwise hysteresis relations of discharges and SSCs at Tan Chau using mean 2008-2014 hydrological-year data.

4.2.3 Methods

Mann-Kendall with Sen Slope and Pettitt tests at 5% significance ($\alpha = 0.05$) level were used to analyze the trends and changes in the long-term precipitation and sediment budget of the MRB under the impacts of the mainstream and tributary dams. Mann-Kendall test (Kendall, 1938; Mann, 1945) was employed to detect changes in the trend of historical data. When a change of the trend was detected, Pettitt test (Pettitt, 1979) was then used to find the change point in the time series. These two tests are non-parametric approaches. Finally, Sen's slope method (Sen, 1968) was used to estimate the slope (or rate of change) of the data. Sen's slope method is unaffected by non-normal distribution, missing data, and outliers (Zhang and Lu, 2009). Detail of these methods were provided in Appendix A. These three methods have been widely employed by many researchers in the past hydro-meteorological studies. Zhang and Lu (2009) used these methods to investigate changes in the long-term discharge and sediment load of the lower Xijiang, China.

4.3 Results

4.3.1 Daily SSCs at Tan Chau during the pre and postdam periods

Over 85% of the suspended sediment entering the VMD from the MR is transported in the Tien River (monitored at Tan Chau); therefore, the behavior of the suspended sediment at Tan Chau well describes the VMD sediment dynamics. Daily SSCs at Tan Chau were largely seasonal and interannual variations (Fig. 4.4). The maximum daily SSC during the flood season reached 1,560 g/m^3, while the minimum value during the dry season was nearly zero (0.0018 g/m^3). The year 2010 had the lowest mean daily SSC (54.9 g/m^3), while the year 1981 had the largest mean daily SSC (377.5 g/m^3). The Mann-Kendall test revealed a significant decreasing trend in the mean daily SSCs during 1980-2015 ($p=1.36x10^{-7}$), and the year 1992 was the change point detected by the Pettitt test ($p=2.77x10^{-5}$). Fig. 4.4 graphically shows that the daily SSCs have significantly reduced since 1993, when the Manwan dam was completed in the MR mainstream. The SSC time series was divided into four periods according to the completion years of mainstream dams in the MR: the predam period (pre-1992) when only some small tributary dams existed, and therefore, the sediment regime was relatively pristine and the three postdam periods of 1993-2001, 2002-2011, and 2012-2015. Due to dam impacts, the mean daily SSCs reduced from 316.8 g/m^3 during the predam period to 108.6 g/m^3 during 1993-2001 (65.7%), 90.2 g/m^3 during 2002-2011 (71.5%), and 74.3 g/m^3 during 2012-2015 (76.6%).

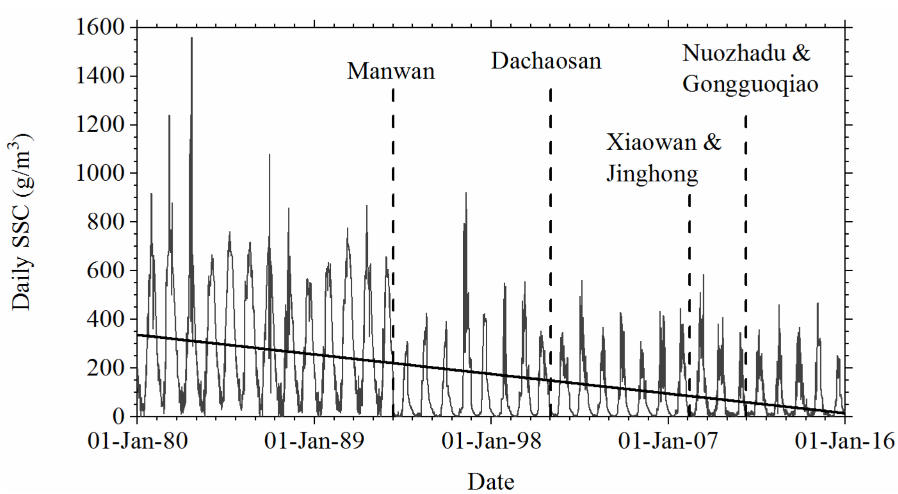

Figure 4.4 Long-term daily SSCs at Tan Chau.

4.3.2 Daily discharges and SSLs at Tan Chau during the pre and postdam periods

Fig. 4.5 depicts the long-term daily discharges and SSLs at Tan Chau during 1980-2015, which show high degrees of seasonal and interannual variations. Daily discharges varied from 2,890 m^3/s to 26,000 m^3/s with a mean of 9,940 m^3/s, and daily SSLs ranged from 2.9 Mt/day to 5.5 kg/day with a mean of 234,600 t/day. Daily discharges varied on the order of 9, while daily SSLs varied on the order of almost 520 million. Although the year 2000 had the maximum mean daily discharge of 12,090 m^3/s over 1980-2015, the year with the maximum mean daily SSL was 1981 at 523,960 t/day. The lowest mean daily discharge (7,170 m^3/s) and SSL (60,030 t/day) occurred in 1998, although the lowest mean daily SSC of 54.9 g/m^3 occurred in 2010.

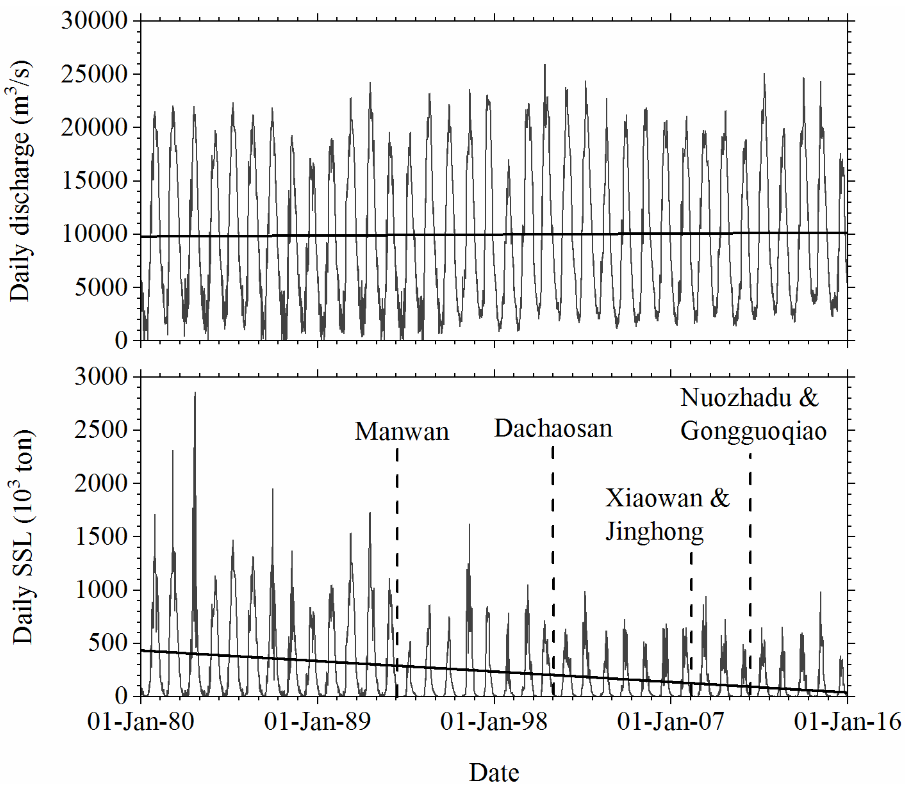

Figure 4.5 Long-term daily discharges and SSLs at Tan Chau.

The Mann-Kendall test revealed that the mean daily discharge at Tan Chau was nonsignificantly reduced during 1980-2015, while the mean daily SSL was significantly reduced at a rate of 10,780 t/year ($p=1.57 \times 10^{-7}$). The change point occurred in 1992, as detected by the Pettitt test ($p=3.22 \times 10^{-5}$). Graphically, the daily SSL clearly decreased beginning in 1993 (Fig. 4.5). Figs. 4.5 and 4.6 show that while the mean daily discharge did not significantly change, although the minimum daily discharge stably increased, the mean daily SSL significantly decreased, from 401,960 t/day during the predam period to 165,300 t/day during 1993-2001 (58.9%), 129,780 t/day during 2002-2011 (67.7%), and 104,290 t/day during 2012-2015 (74.1%). The minimum daily SSL did not clearly change during the pre and postdam periods, whereas the maximum daily SSL significantly reduced from 2.9 Mt/day during the predam to 1.6 Mt/day during 1993-2001 and approximately 1.0 Mt/day during both 2002-2011 and 2012-2015.

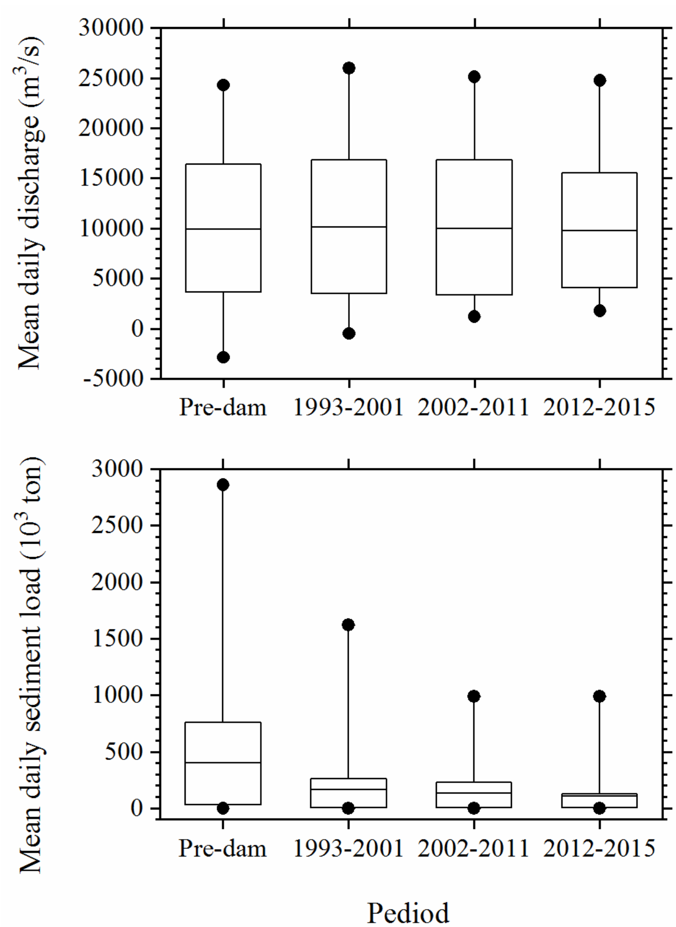

Figure 4.6 Box-whisker plots of mean daily discharges and sediment loads at Tan Chau during the pre and postdam periods, including the mean, 25^{th} percentile, 75^{th} percentile, and minimum and maximum values.

4.3.3 Monthly water flux and suspended sediment budget of the VMD during the pre and postdam periods

The flow and sediment transport in the VMD (based on the data for the 1980-2015 period) was mainly concentrated during July-December, accounting for 80.1% and 94.5% of the annual water flux and sediment budget, respectively (Fig. 4.7). A total of 61.4% of the annual water flux and 80.7% of the annual sediment budget were conveyed during August-November. The largest volumes of water (65.7 km^3) and sediment (24.2 Mt) were transported in September. On the other hand, a negligible volume of sediment (2.6%, equivalent to 3.3 Mt) and a relatively small volume of water (14.6%, equivalent to 57.1 km^3) were transported during January-May.

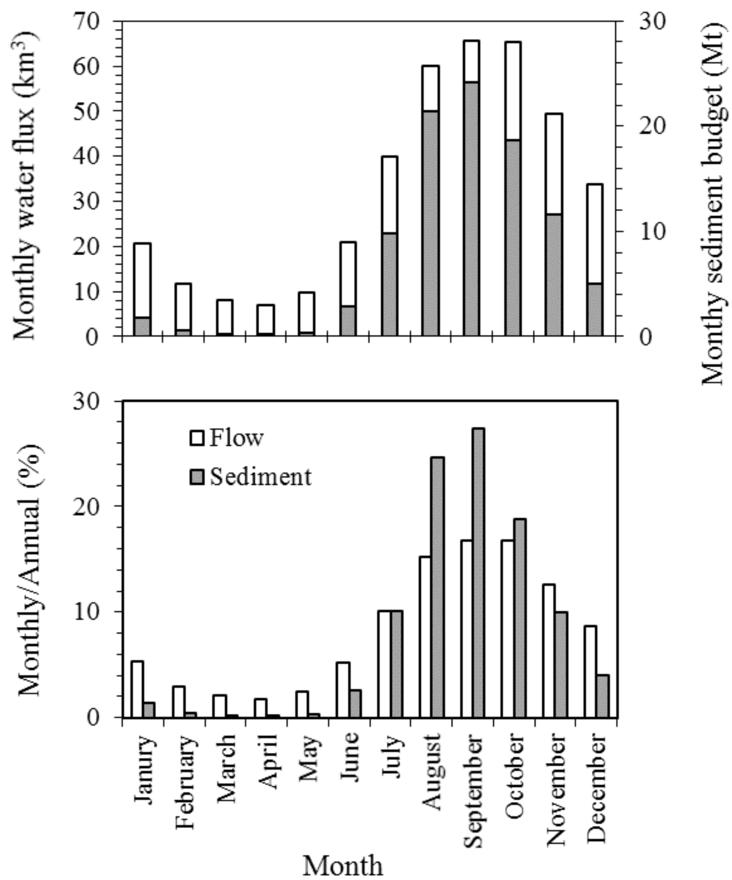

Figure 4.7 Monthly water flux and sediment budget of the VMD.

Fig. 4.8 shows the long-term monthly water and sediment budgets of the VMD (sum of Tan Chau and Chau Doc) for the 1980-2015 period, including completion years of the mainstream hydropower dams in the Lancang cascade. Clearly, the long-term water and sediment budgets varied intra and interannually. The Mann-Kendall test revealed that the monthly water flux in the VMD changed nonsignificantly over 1980-2015 (except for May when the monthly water flux increased significantly beginning in 1998 at the 5% significance level according to the Pettitt test), and the sediment budgets of all months significantly decreased beginning in 1992 at the 1% significance level (Table 4.1). The most reductions occurred in September and October, with a reduced rate of nearly 1 Mt/yr, and April was the month experiencing the least reduced rate (6,600 t/yr).

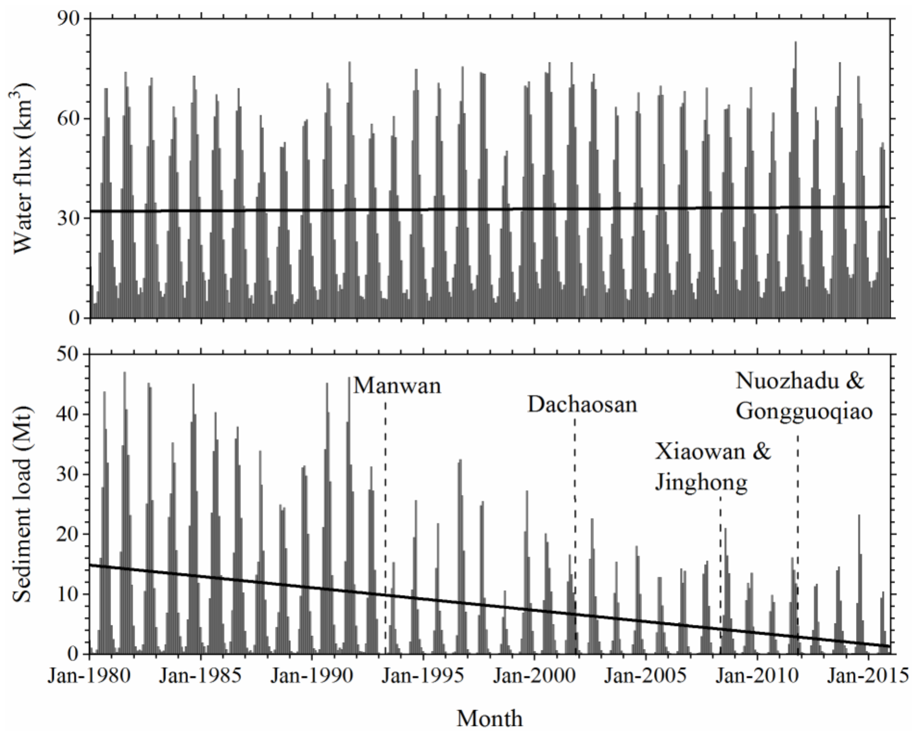

Figure 4.8 Long-term monthly water fluxes and sediment loads of the VMD.

Table 4.1 Statistical tests in evaluating changes in the long-term monthly and annual SSLs in the VMD over 36 years (1980-2015).

Month	n	Man-Kendall trend test				Sen's Slop estimator	Pettitt test to find changing point			
		S	Z	p	Trend	(Mt)	K_T	t	p	Shift
January	36	-326	-4.427	$9.57x10^{-6}$	-	-0.1118	299	1992	$2.77x10^{-5}$	-
February	36	-290	-3.936	$8.27x10^{-5}$	-	-0.0375	299	1992	$2.77x10^{-5}$	-
March	36	-214	-2.901	$3.72x10^{-3}$	-	-0.0146	299	1992	$2.77x10^{-5}$	-
April	36	-232	-3.146	$1.65x10^{-3}$	-	-0.0066	299	1992	$2.77x10^{-5}$	-
May	36	-250	-3.392	$6.95x10^{-4}$	-	-0.0198	279	1992	$1.18x10^{-4}$	-
June	36	-234	-3.174	$1.51x10^{-3}$	-	-0.0982	219	1992	$4.95x10^{-3}$	-
July	36	-274	-3.719	$2.00x10^{4}$	-	-0.3503	235	1992	$2.00x10^{-3}$	-
August	36	-316	-4.291	$1.78x10^{-5}$	-	-0.6484	261	1992	$3.97x10^{-4}$	-
September	36	-394	-5.353	$8.65x10^{-8}$	-	-0.9692	302	1992	$2.21x10^{-5}$	-
October	36	-338	-4.590	$4.43x10^{-6}$	-	-0.9517	297	1992	$3.21x10^{-5}$	-
November	36	-372	-5.053	$4.34x10^{-7}$	-	-0.7578	295	1992	$3.73x10^{-5}$	-
December	36	-406	-5.517	$3.45x10^{-8}$	-	-0.3605	295	1992	$3.73x10^{-5}$	-
Annual	36	-388	-5.271	$1.36x10^{-7}$	-	-4.4596	297	1992	$3.22x10^{-5}$	-

Table 4.2 Changes in the mean monthly water flux and SSL in the pre and postdam periods in the VMD over 36 years (1980-2015).

Index	Month	Period						
		Predam	1993-2001		2002-2011		2012-2015	
		Magnitude	Magnitude	Change (%)	Magnitude	Change (%)	Magnitude	Change (%)
Water flux (km^3)	Jan	21.26	20.26	-4.69	20	-5.91	21.66	+1.89
	Feb	11.92	11.05	-7.28	11.47	-3.75	12.8	+7.41
	Mar	7.6	7.93	+4.37	7.91	+4.04	10.7	+40.7
	Apr	6.12	6.9	+12.8	6.83	+11.6	9.91	+61.9
	May	8.38	9.84	+17.4	10.37	+23.7	11.97	+42.8
	Jun	20.64	22.08	+6.99	21.07	+2.08	19.74	-4.36
	Jul	39.6	43.65	+10.2	37.86	-4.37	38.1	-3.79
	Aug	57.4	63.1	+9.93	60.26	+4.99	60.22	+4.92
	Sep	65.23	68.46	+4.95	65.49	+0.4	61.78	-5.29
	Oct	63.87	66.68	+4.39	67.35	+5.45	61.69	-3.42
	Nov	51.5	49.18	-4.5	49.31	-4.24	42.19	-18.07
	Dec	34.71	35.18	+1.37	33.5	-3.48	28.53	-17.8
Sediment load (Mt)	Jan	4.2	0.42	-89.97	0.38	-91	0.44	-89.54
	Feb	1.54	0.12	-92.26	0.13	-91.35	0.13	-91.25
	Mar	0.68	0.05	-92.88	0.06	-90.55	0.09	-86.44
	Apr	0.4	0.05	-86.85	0.05	-87.92	0.1	-75.59
	May	0.85	0.19	-78.23	0.15	-82.58	0.12	-86.43
	Jun	5.5	1.94	-64.69	1.14	-79.24	0.94	-82.97
	Jul	15.85	7.76	-51.01	5.85	-63.12	4.83	-69.52
	Aug	30.98	18.14	-41.43	14.74	-52.4	14.47	-53.28
	Sep	37.8	20.7	-45.24	14.03	-62.89	13.34	-64.71
	Oct	33.77	10.63	-68.51	11.33	-66.47	5.94	-82.41
	Nov	23.86	5.94	-75.11	4.5	-81.13	2.03	-91.49
	Dec	10.99	2.47	-77.56	1.36	-87.67	0.7	-93.65

Change (%) = (post-pre)/pre*100. "+": increase and "-": decrease

From the predam period, more than 60% of the monthly sediment budgets of the VMD (except for August, 53.3%) decreased during2012-2015 when 64 dams were completed in the MRB, with exceptionally high reductions during November-December and January-February (over 90%) (Table 4.2). Compared to predam conditions, the postdam monthly water flux generally increased during the low-flow season (January-May) and decreased during the high-flow season (June-December), while postdam monthly sediment budgets significantly decreased in all months (Table 4.2). Increasing the number of hydropower dams in the MRB led to a greater increase in the low-flow season and a greater decrease in high-flow season water fluxes. However, more dams completed in the MRB would cause more reductions in monthly sediment budgets in the VMD. Interestingly, the majority (> 70%) of the monthly sediment budget reductions during the low-flow season from the predam period in the VMD occurred in the 1993-2001 period (Table 4.2). On the other hand, more dams completed during 2002-2011 and 2012-2015 caused more reductions in the sediment budgets in the high-flow season. For instance, the July sediment budget decreased from 15.9 Mt during the predam period to 7.8 Mt during 1993-2001 (51.0%), 5.9 Mt during 2002-2011 (63.1%) and 4.8 Mt during 2012-2015 (69.5%).

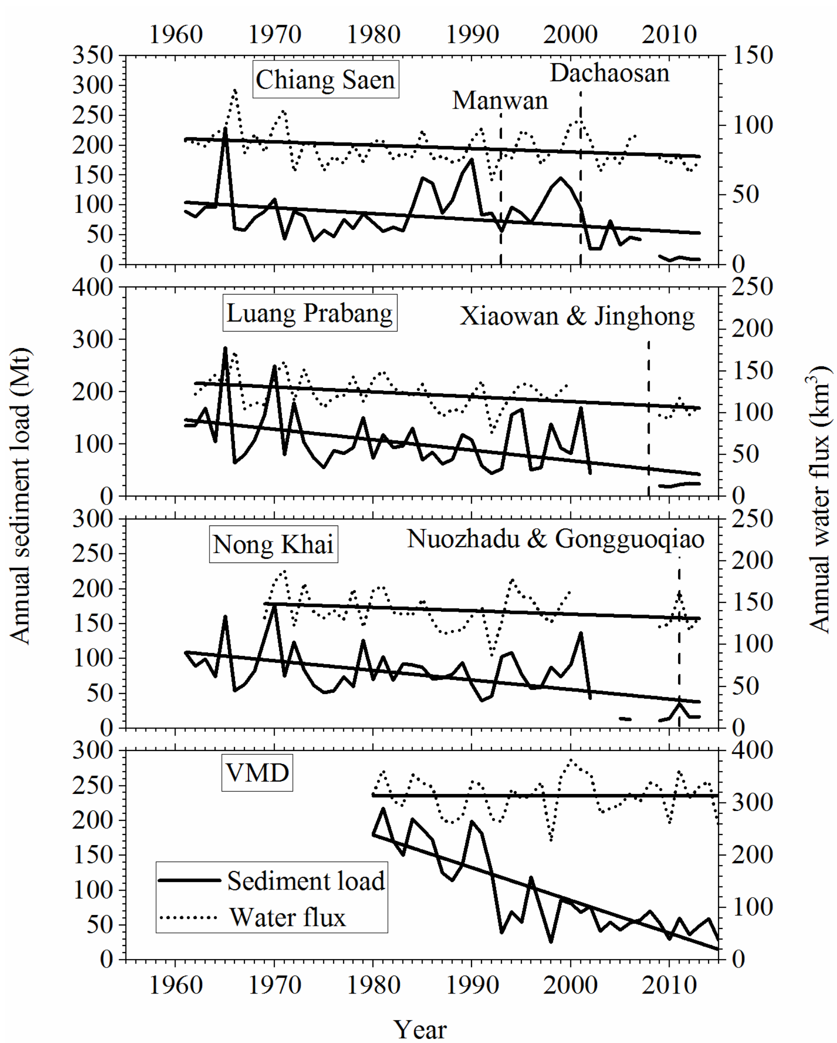

Figure 4.9 Long-term annual water fluxes and sediment loads at 4 stations along the lower MR.

Table 4.3 Changes in annual water flux and suspended sediment budget in the pre and postdam periods at five stations along the MR.

Station	Period	Water flux		Sediment load	
		Magnitude km^3	Change (%)	Magnitude Mt	Change (%)
Chiang Saen	Predam	85.13		90.39	
	1993-2001	87.26	+2.5	100.24	+10.89
	2002-2011	80.11	-5.89	31.56	-65.09
	2012-2015	70.11	-17.64	9.47	-89.52
Luang Prabang	Predam	125.02		110.35	
	1993-2001	123.86	-0.93	107.19	-2.86
	2002-2011	102.25	-18.21	26.47	-76.02
	2012-2015	103.1	-17.54	24.69	-77.63
Nong Khai	Predam	140.13		85.13	
	1993-2001	149.28	+6.53	88.3	+3.72
	2002-2011	136.22	-2.79	21.81	-74.38
	2012-2015	124.66	-11.04	16.64	-80.46
Pakse	Predam	307.88		161.31	
	1993-2001	319.9	+3.91	124.01	-23.12
	2002-2011	322.71	+4.82	92.64	-42.57
	2012-2015	296.2	-3.79	65.92	-59.13
VMD	Predam	389.24		166.42	
	1993-2001	403.8	+3.74	68.41	-58.9
	2002-2011	390.63	+0.36	53.71	-67.72
	2012-2015	378.81	-2.68	43.13	-74.09

Change (%) = (post-pre)/pre*100. "+": increase and "-": decrease

4.3.4 Annual water flux and suspended sediment budget of the VMD during the pre and postdam periods

The long-term annual water flux and suspended sediment budget at Chiang Saen, Luang Prabang, Nong Khai, and the VMD significantly decreased, especially in 1992, 2002, and 2009 after the completion of the Manwan, Dachaoshan, and Xiaowan and Jinghong dams, respectively (Fig. 4.9). For instance, at Chiang Saen, the sediment budget decreased more than 68% after completion of the Manwan dam, from 177 Mt in 1990 to 56.4 Mt in 1993, and more than 70% after completion of the Dachaoshan dam, from 94 Mt in 2001 to 26.9 Mt in 2002. Similarly, the sediment budget at Luang Prabang decreased by more than 50% after completion of the Manwan dam, from 108.5 Mt in 1990 to 52.8 Mt in 1993. Notably, by comparing the slope of the trend lines, the sediment budget decreased faster than the water flux (Fig. 4.9). Additionally, more dams completed in the MRB caused greater reductions in the annual water flux and sediment budget at stations along the lower MR. For instance, at Luang Prabang, the sediment budget decreased by 77.6% during 2012-2015 when 64 dams were completed, and only a 2.9% reduction occurred during 1993-2001 when 17 dams completed (Table 4.3).

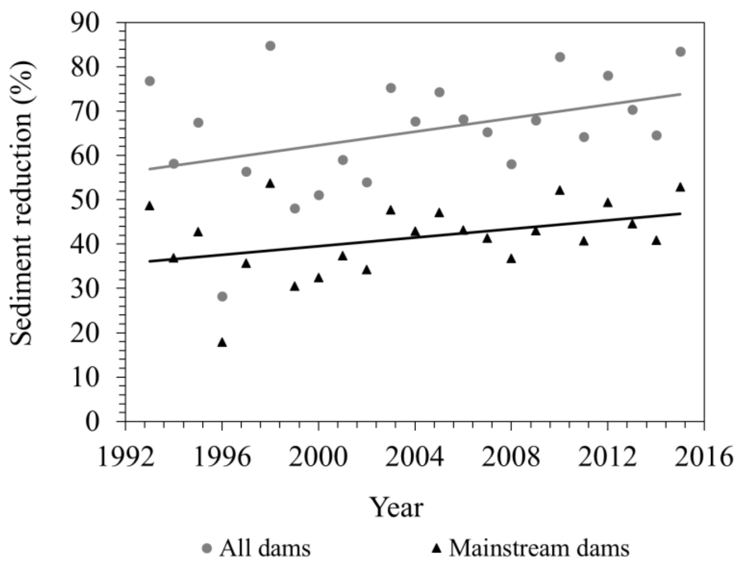

Figure 4.10 Annual sediment reduction rate in the VMD caused by all 64 dams in the MRB and by mainstream dams in the Lancang cascade.

In the VMD, the annual sediment budget sharply decreased, whereas the annual water flux slightly decreased (Fig. 4.9). The Mann-Kendall and Pettitt tests showed that the VMD's annual sediment load has statistically decreased ($p<0.01$) since 1992, which was the completion year of the Manwan dam, with a rate of 4.5 Mt/yr, as determined by the Sen's slope test (Table 4.1). In total, 74.1% of the annual sediment budget of the VMD decreased during 2012-2015 as a consequence of all 64 dams in the MRB, and 58.9% occurred during 1993-2001 (Table 4.3). During the predam period, the upper MRB contributed 54.3% of the VMD sediment budget (the proportion of the Chiang Saen sediment load (90.4 Mt) to the VMD sediment load (166.7 Mt)), indicating that out of a 74.1% total reduction in the VMD sediment budget, 40.2% was caused by the six mainstream dams in the upper MR, and 32% was a consequence of the Manwan and Dachaoshan dams alone. Annual sediment reductions in the VMD caused by all 64 dams and mainstream dams are shown in Fig. 4.10. The annual sediment budgets of the VMD in the postdam period (1993-2015) were even smaller than those at Chiang Saen. Both stations had decreased trends, while the annual sediment budget in the upper MR at Jiuzhou station, upstream of the

Lancang cascade, substantially increased (Fig. 4.11). This finding clearly indicates that a significant sediment volume was trapped by the mainstream reservoirs in the upper MR instead of being discharged downstream.

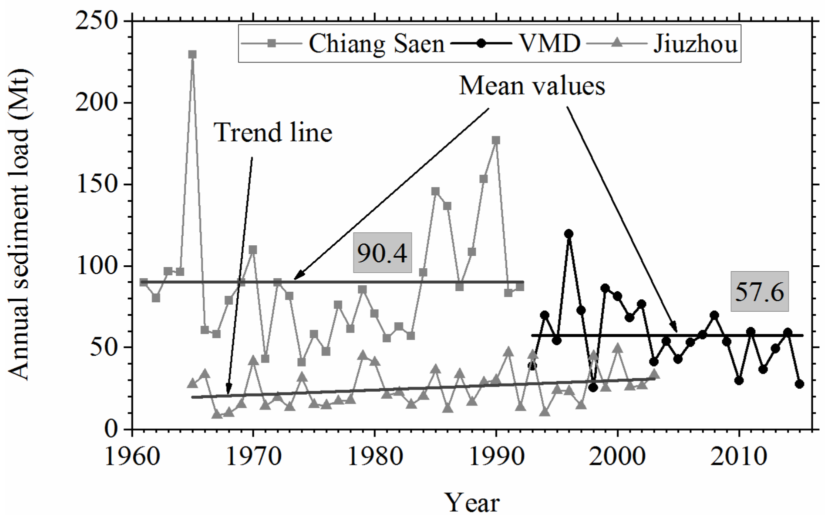

Figure 4.11 Annual sediment load in the upper (Jiuzhou), middle (Chiang Saen), and lower MR (VMD).

4.4 Discussions

4.4.1 Change in sediment sources

The largest sediment source delivered to the MR during the predam period was the upper MRB, contributing most of the sediment at Chiang Saen, 82% at Luang Prabang, and 54.3% in the VMD. However, the upper MRB became a minor sediment contributor to the lower MR during the postdam periods because a large volume of the sediment was trapped by the mainstream reservoirs; for example, there is a projected 94% trapping efficiency of the eight mainstream dams in the upper MR (Kummu and Varis, 2007). Instead, the Nong Khai-Pakse section (including the 3S river basin) became the largest sediment source of the VMD during postdam periods (over 70%).

Riverbank erosion and riverbed resuspension along the lower MR (especially from Nong Khai to Pakse) due to "hungry water" were likely considerable sources of the postdam sediment that compensated for what was diminished by the mainstream dams. This phenomenon is common in the world's rivers; for instance, during the postdam period of the Mississippi River, the sediment locally resuspended from the riverbed during the high-flow season contributed a considerable amount of the sediment downstream (Allison et al., 2017b). Darby et al., (2013) reported mean annual rates of river bank erosion at Ang Nyay (near Nong Khai) during 1913-2010 and at Pakse during 1923-2010 as 0.68±0.11 m/yr and 0.64±0.16 m/yr, respectively. Lu and Siew, (2006) found that the areas surrounding Vientiane (near Nong Khai) contributed a considerable sediment volume from either tributaries or bank erosion during the postdam periods.

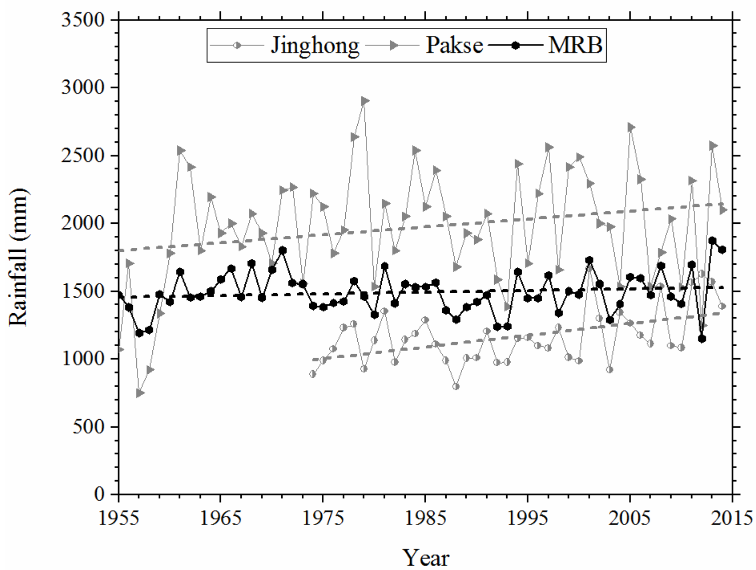

Figure 4.12 Long-term variation of the annual precipitation in the MRB.

4.4.2 Drivers of the flow and suspended sediment alterations along the lower MR

There was no clear change in the VMD monthly discharges during 1993-2001 (Table 4.2 and Fig. 4.8), which is attributed to the relatively small reservoir capacity of the existing dams; therefore, climate conditions, especially tropical cyclones (Darby et al., 2016), controlled the flow regimes during that period. However, decreased high-flow discharges and increased low-flow discharges at stations along the MR during 2012-2015 (Table 4.2 and Fig. 4.9) were mainly driven by hydropower dams in the MRB due to their large reservoir capacity. Although the long-term mean annual precipitation at seven stations (Fig. 2.1) in the MRB did not significantly change (Fig. 4.12), which was also reported by Xue et al., (2011), shifting in the timing and intensity of tropical cyclones is likely a considerable driver.

However, daily, monthly, and annual SSLs at stations in lower MR significantly reduced (Table 4.2 and Figs. 4.4-4.6 and 4.8-4.9), beginning from the completion of the Manwan dam in 1992, which were detected by the Pettitt test at $p<0.01$ (Table 4.1). Importantly, while the long-term sediment budget at Jiuzhou, the station upstream of the six mainstream dams, increased over the

1965-2003 period (Fig. 4.11), the sediment budgets at all stations along the entire lower MR significantly decreased (Fig. 4.9), providing evidence that such reduced sediment budget was trapped by the mainstream dams. Owing to the relatively stable long-term precipitation of the MRB, the mainstream dams in the Lancang cascade were the main driver of sediment reductions in the MR upstream of Nong Khai because most of the tributary dams are concentrated in the Nong Khai-Mukdahan and Pakse-Stung Treng (3S river basin) sections (Fig. 2.1). Cumulatively, six mainstream dams were the direct cause of 89.5% of the sediment reduction at Chiang Saen during 2012-2015, from the predam period, which was compatible with the 94% trapping efficiency reported for these six dams by Kummu and Varis, (2007). In addition, a decreasing intensity of tropical cyclones in the MRB during the postdam period before 2005 (Extended Data Fig. 5 in Darby et al., (2016)) also played a key role in contributing to sediment reduction in the MR.

From Pakse to the VMD, a decreasing tropical cyclone intensity can be partly attributed to sediment reductions during 1993-2001. However, how tropical cyclones changed after 2005 is unclear (from the studied period of Darby et al., (2016) and no other studies have focused on this topic); however, tropical cyclones seemed to increase in intensity due to climate change (Hoanh et al., 2010), which increased the sediment yield. Therefore, significant sediment reductions at Pakse and the VMD during 2012-2015 (Table 4.3) were mainly caused by the cumulative impacts of 64 dams in the MRB. Manh et al., (2015) concluded that hydropower dams in the MRB were the largest contributors to changes in sediment dynamics in the Mekong Delta when numerically compared to climate change and sea level rise influences. Among the 74.1% total sediment reduction in the VMD, 40.2% was induced by six mainstream dams, and 32% of this reduction was caused by the Manwan and Dachaoshan dams alone. Our findings are comparable with the results of Kondolf et al., (2014), who numerically estimated that all mainstream dams in the upper MRB would cause a 40% reduction in the sediment budget of the lower MR. Hydropower dams were also responsible for a 74% reduction in the annual sediment discharge to the East Sea of Vietnam, from 144 Mt/yr during the predam period (Ta et al., 2002) to 37.7 Mt/yr during 2012-2015, based on our data from the My Thuan and Can Tho stations. Similar to the MR, dam-induced sediment reductions are common all over the world, such as in the Red River of Vietnam (Lu et al., 2015), Yangtze River of China (Tena and Batalla, 2013), Colorado River of the USA (Tena and Batalla, 2013), Nile River of Egypt (Milliman and Syvitski, 1992), and São Francisco River of Brazil (Walling, 2006).

The demand for food security in riparian countries in the MRB has increased due to rapid population growth, socioeconomic development, and urbanization, forcing a rapid conversion from forest cover to cultivated lands. Deforestation for expansion of cultivated lands would increase the total sediment yield. However, our analysis reported a significant decrease in the sediment budget of the entire lower MR, especially during 2012-2015, indicating that land use change in the MRB is likely not a key driver. Hoang et al., (2019) found that the impacts of hydropower dams in the MRB exceed those caused by irrigation expansion and land use change.

We collected suspended sediment samples along the Tien River during our field survey in August 2017 to determine the grain size distribution. The grain size distribution at the Mang Thit and My Thuan stations depicted in Fig. 5.5 clearly shows that approximately 95% of the suspended sediment is composed of silt and clay. Approximately 90% of the bed material composition is sand, and the sand is mined from the riverbed. Therefore, sand mining is likely not the main driver of reductions in the suspended sediment budget in the VMD. If sand mining has an influence, the mining activities would increase the SSCs (through mud content in the sand bed) in areas surrounding the mined points due to mechanical resuspension, which would lead to an increased suspended sediment load, but this result is not the case in the VMD. For instance, during our field survey in August 2017, we recorded the exceptional high SSCs just downstream of the mining area, locating at 83 km from the river mouth in the Tien River. The mean cross-sectional SSCs downstream of the mining area (1,132 g/m^3) is more than three times larger than that upstream of the mining area (356 g/m^3) (the flow was seaward during the survey time).

4.4.3 Consequences of sediment deficits

The construction of hydropower dams creates many problems for societies. Dams themselves block the migration paths of fish species; therefore, the populations of these fish are at high risk if more dams are completed in the MR mainstream. The habitats of many living species in the lower MRB may be vulnerable due to the lack of upstream sediment supply, which may lead to various negative alterations to the ecology and ecosystem. The ecosystems of the TSL and the VMD are most likely the strongest impacted areas. Lower high-flow discharges and reduced sediment supplies induced by dams may reduce the wetland biodiversity in the Mekong Delta. Importantly, agricultural production, i.e., in the VMD, is expected to decrease due to sediment deficiency caused by river-floodplain disconnectivity, leading to increased use of artificial fertilizers, and this change may aggravate the soil properties. In turn, food security and human livelihoods may be threatened in the countries of the lower MRB, including Vietnam, and many environment-related problems may occur.

4.4.4 Delta dynamics due to sediment reduction and adaptive strategies

Although the low-flow discharges in the VMD increased due to dam operations, the low-flow water levels were significantly reduced due to riverbed incision resulting from a reduced sediment supply from the MR and sand mining. Xue et al., (2011) reported significant reductions in minimum water levels since 1994 at Can Tho and My Thuan in the VMD during 1979-2006. For instance, the mean minimum water levels at Can Tho decreased from 0.65 m during 1979-1993 to 0.4 m during 1994-2006. Water level reductions in the VMD may result in difficulty in obtaining intake water for irrigation. Farmers alternatively use pumping stations to irrigate rice crops because they are not able to operate gravitational irrigation systems, which would increase the costs and therefore reduce the ultimate income of farmers. To address this difficulty, high-dike systems (which operate as water intake barriers) are strictly recommended for flood control in the VMD and low-dike systems should be used instead. Buffering zones and artificial storage ponds should be allocated to store water during the high-flow season for use in the low-flow season. Moreover, investment in creating new rice varieties that can advantageously adapt to drier conditions is encouraged.

In addition, reduced low-flow water levels in the VMD would increase salinity intrusion, leading to damage to agriculture and aquaculture in affected areas and thus negatively influencing people's livelihoods. Buffering zones in coastal areas may help mitigate salinity intrusion impacts. Additionally, constructions of salinity control sluice gates along the Tien and Hau Rivers should not be implemented without comprehensive investigation of their side effects because such sluice gates are more likely to enhance salinity intrusions further inland due to reduced buffering zones in coastal areas. Importantly, converting from agriculture to aquaculture, where applicable, is a good solution if this action increases farmer incomes while reducing stresses on fresh-salt water management conflicts.

4.4.5 Strategic reservoir sediment management for current and planned dams and reservoirs in the MRB

Similar to other river basins worldwide, in the MRB, a sustainable reservoir sediment management plan should be implemented for current and planned dams, deriving from a fact that dam owners need to reduce reservoir sedimentation to prolong reservoir lifespans whereas downstream reaches need sediment for the environment and ecosystem. Therefore, we provided a conceptual method (Fig. 4.13) which can prolong the lifespans of reservoirs to be several hundred or thousand years instead of 100 years as tradition. Our concept can be applied to hydropower dams in the MRB with two components: current and planned dams. Firstly, for existing dams, urgent measures (i.e. excavation) can be considered to urgently dredge the accumulated sediment in reservoirs to deliver downstream. Meanwhile, a comprehensive study is needed to determine the most suitable method among conventional solutions to route the inflowing sediment downstream (i.e. drawdown flushing, bypassing, sluicing) (Fig. 4.13) to avoid sediment accumulation in reservoirs. For instance, the life span of Nunobiki reservoir in Japan can be extended about 30-500 years by implementing reservoir sedimentation management (Sumi et al., 2004). Secondly, for planned dams (such as 11 proposed dams in the mainstream of the lower MR in Thailand, Laos, and Cambodia), alternative locations and designed configurations of dams should be revised in order to minimize the reservoir sedimentation. Then conventional sediment management measures (drawdown flushing, bypassing, sluicing) to route sediment through or bypass reservoirs should be considered at the design stage (Fig. 4.13). Furthermore, advanced sediment management techniques such as hydro-suction, dam asset management (Sumi et al., 2009), dam rehabilitation and retrofitting (Kondolf et al., 2014) can be employed. Annandale (2012) proposed alternatives for Sambor dam in Cambodia (the last dam in the 11 proposed mainstream dams in the lower MR) as re-siting, implementing drawdown flushing, and providing a diversion weird with a bypass channel to improve fish and sediment passages. As estimated, only 5% of the inflowing sediment can be accumulated in the reservoir. It is worth noting that the implementation of sediment management in reservoirs from the beginning is much cheaper than dam retrofitting after construction. Moreover, removing accumulated sediment in reservoirs is normally much more expensive than routing sediment through or bypass reservoirs.

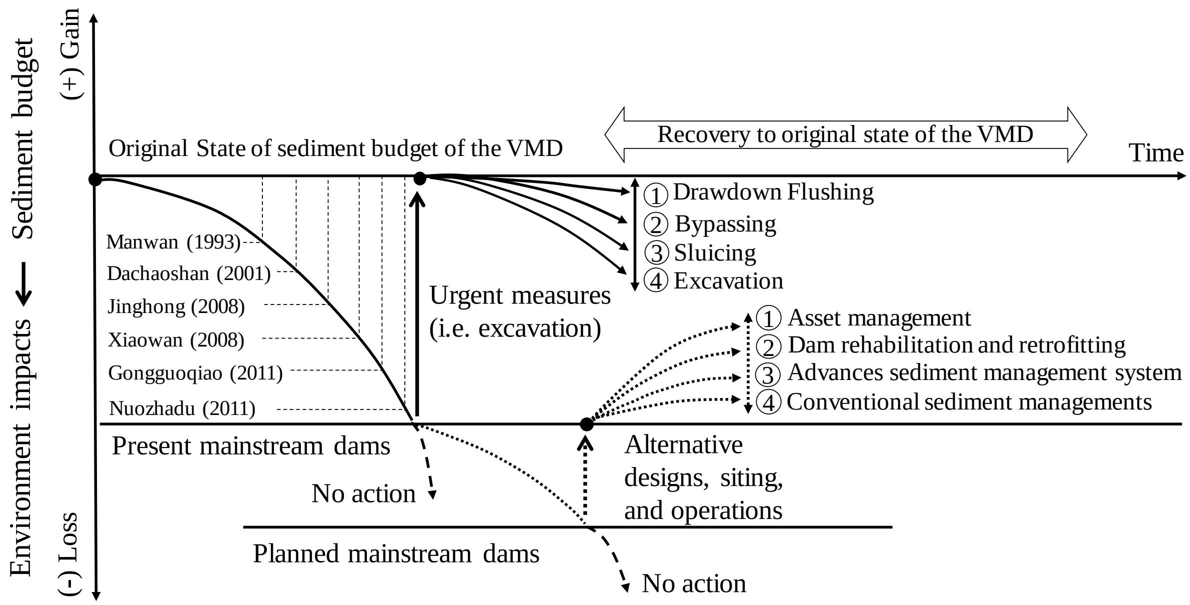

Figure 4.13 Strategic reservoir sediment management for the mainstream dams in the MRB.

4.5 Conclusions

Suspended sediment plays an important role in structuring river basin morphology, hydrology, and ecosystems. Similar to the world's large river basins, the flow and sediment budgets of the MR have been significantly altered due to natural processes and anthropogenic activities, including river damming. In this chapter, the long-term discharges and suspended sediment budgets along the entire lower MR from Chiang Saen to the VMD were analyzed in daily, monthly, and annual quantities using various statistical methods and associated driving factors were linked to flow and sediment alterations. Climate conditions controlled the MR flow and sediment regime during the predam period (pre-1992) and together with hydropower dams, remained one of the main flow and sediment alteration drivers from 1993-2001. However, from 2012-2015 in the MRB, sixty-four completed hydropower dams were the main cause of sediment reductions along the entire lower MR. Due to river damming, the annual suspended sediment budgets at Chiang Saen, Luang Prabang, and Nong Khai, decreased from the predam period by 89.5%, 77%, and 80.5%, respectively, from 2012-2015. The sediment was reduced by 74.1% in the VMD; 166.7±33.3 Mt/yr occurred during the predam period and 43.1 Mt/yr occurred during 2012-2015, and 40.2% was caused by six mainstream dams in the Lancang cascade, where the Manwan and Dachaosan dams alone directly accounted for 32% of the reduction. The annual sediment reduction rate in the VMD was 4.5 Mt/yr at the 1% significance level ($p=1.36x10^{-7}$) since the Manwan dam completion in 1993. Similarly, the annual sediment discharge from the MR to the East Sea of Vietnam has reduced by 74% from 144 Mt/yr during the predam period to 37.7 Mt/yr during 2012-2015. The findings of our study are helpful for furthering the research related to sediment issues in the VMD, such as agricultural production and salinity intrusion, and these results serve as a basic reference for the sound management of water conservancy, flood control, river navigation, salinity control, and agricultural development in the VMD.

Chapter 5 Field measurements of hydro-sediment-morphodynamics and long-term morphological changes in the Vietnamese Mekong Delta

5.1 Introduction

In the catchment scale, river channels play a role as a conveyor to transport sediment from erosion spots (mainly bare soil on hill slopes) to the deposition sites downstream (Kondolf, 1997). Global rivers export 13 Gt/yr of sediment to oceans (Mclachlan et al., 2017). Such sediment forms large river deltas and maintains the coastlines. River deltas where the river slopes are small receive eroded sediment from the upstream through the interactive processes between the flows and sediment. Increasingly accumulative sediment has expanded river deltas, i.e. Nile River Delta, Mississippi River Delta, Mekong River Delta, for centuries. The sediment supply (through erosion process upstream) therefore governs the river morphology and shoreline landscape (Anthony et al., 2015).

The estimated sediment budgets of global river basins were widely based on the suspended sediment discharges measured at the upriver stations where the tidal influence is limited or nil. Therefore, the net sediment export to oceans is somewhat smaller than the reported amount as the sediment usually deposits along the channels within the river deltas when moving seaward. For example, 13.6% of the sediment budgets at the Vietnam-Cambodia border is deposited along the VMD's channels before reaching the East Sea of Vietnam (Manh et al., 2014).

In the VMD, the predam sediment budget of 160 Mt/yr was recorded at Kratie station which is approximately a thousand kilometers from the river mouth (Lois Koehnken, 2014). Since 2009, gauging stations My Thuan and Can Tho in the Tien and Hau Rivers, respectively, which locate in the tidal areas of the VMD can better represent the net sediment outflow (rivers to the sea) and inflow (sea to the inland) through a twice-a-day sediment measurement schedule: once in the ebb tide and once in the flood tide. However, these stations are still far from the river mouths (~100 km and 80 km respectively). Therefore, the realistic net sediment export to the sea of the MR is still unclear although some studies reported various values based on their field surveys' data (Allison et al., 2017a; Nowacki et al., 2015; Unverricht et al., 2013; Wolanski et al., 1998, 1996). The limitation of these researches is (1) based on short-term measurement data and (2) considered small spatial scale (two branches among eight branches); therefore, their reported values were more likely not representative.

The SSCs at the VMD hydrological stations are not hourly measured, instead, twice a day; therefore, do not well represent the influence of the tide. Moreover, the number of existing hydrological stations in the VMD are limited. The bathymetric data are not homogeneous and not frequently surveyed. Therefore, studies on the VMD related to water resources issues remains difficulties in terms of available data. For that, we installed additional SSC monitoring stations and two field surveys to collect long-term and large-scale homogeneous flow, sediment and bathymetric data. The objectives of the monitoring and field surveys are (1) to comprehensively understand the temporally-spatially fluvial-tidal interactive processes of the hydro-sediment-morphodynamics along the main rivers and distributaries in the VMD, and (2) to evaluate the representativeness of the measured SSCs under the MRC framework to propose whether it is necessary to implement hourly (or less) measurements of the SSCs in the VMD so that the influence of the tide on the SSC variation can be captured. In addition, the new dataset will be then used as boundary conditions for a 2-dimensional coupled numerical hydro-sediment-morphodynamics model to investigate morphological changes and associated challenges to irrigation water intake in the VMD.

5.2 Field works

5.2.1 Why are additional monitoring stations and field surveys needed?

Monitoring stations in the VMD under MRC program measure hourly water levels and discharges which can well describe the tidal variations. However, the SSCs are not hourly measured, instead, twice a day; therefore, not well represent the influence of the tide on the sediment dynamics. Moreover, the spatial coverage of monitoring stations is sparse. Therefore, monitored data, together with data collected from field surveys that were conducted by some other researches under several projects, are not enough to fully understand the characteristics of the hydro-sediment-morphodynamics of the VMD. As a result, many researchers have used numerical simulations instead. However, another issue arises, related to the lack of river bathymetric data. No holistic river bathymetry data is available for the whole, or even the main, rivers in the VMD. Therefore, most of the researchers collected segmented topographic and cross-section data which were measured at different time-scales according to their projects. Noticeably, many researchers are still using bathymetric data measured during 1998-2000 for their simulation which are far different from the current situation. Given such a critical lack of the temporal-spatial flow and sediment data, two campaigns to install additional stations to monitor the SSCs and two field surveys to measure flow, sediment, and bathymetric data in the VMD were conducted. Two monitoring campaigns were carried out in February 2016 and February 2017. The first field survey was conducted in August 2017 (high-flow season) to measure the discharge, velocity, water levels, river bathymetry, and SSCs while the second field survey was in March-April 2018 (low-flow season) to measure the vertical and longitudinal SSCs along approximately 570 km of the Tien, Hau Rivers and Vam Nao channel.

5.2.2 Two campaigns installing additional SSC monitoring stations

Under JASTIP project, we conducted two campaigns to install instruments for turbidity and salinity measurement outspread over the VMD. The turbidity meters were installed in the upper part of the VMD while salinity meters were set up in the lower part (Fig. 5.1). In the first campaign taken during February 26-28, 2016, two turbidity meters were installed at the Tan Chau and Vam Nao stations and the location of a salinity meter was in An Lac Tay, Soc Trang province (Fig. 5.1). The An Lac Tay station locates in the Hau River right bank, looking downward. It is about 50 km from the East Sea.

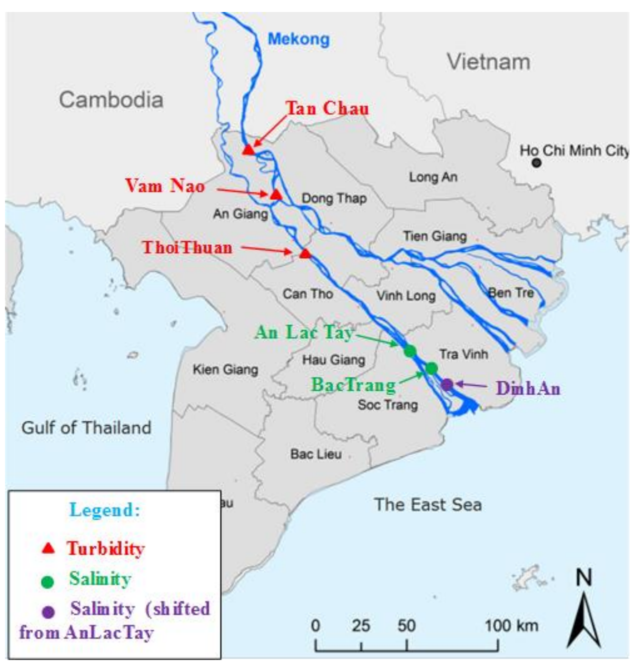

Figure 5.1 Location map of installed additional turbidity and salinity stations.

The second campaign was conducted during February 10-11, 2017, about one year after the first campaign. One turbidity and one salinity were installed. The turbidity meter was installed in the Hau River in the Thoi Thuan commune, Thot Not district, CanTho city (Fig. 5.1). It is about 120 km downstream of the Chau Doc station. The installed location of the salinity meter was on the left bank of the Hau River, at the Bac Trang station, which is about 25 km from the river mouth and around 25 km downstream of the An Lac Tay station (Fig. 5.1). The salinity concentration at the An Lac Tay station was too small in 2017, therefore it was shifted downstream to the Dinh An station, which is also in the Hau River to be able to continuously measure salinity concentrations. The Dinh An station is about 20 km from the estuary (Fig. 5.1). Fig. 5.2 shows field activities in installing the turbidity and salinity stations.

Figure 5.2 Field activities in installing additional turbidity and salinity stations. Photos were taken by Binh D.V. during the field trip in February 2016.

The installed turbidity and salinity meters are Infinity-ATU75W2-USB and Infinity-ACTW-USB, respectively (Fig. 5.3). The instruments used 4 pieces of one-time-use battery which can be used up to 5 months of continuous measurement. The turbidity meters record the values once every

15 minutes and 30 minutes were set up for the salinity meters. To overcome the potential errors, ten values were recorded at each reading time, at which the time interval is 1 s. Then the 10 values at each reading are averaged. The position of the turbidity sensors is changeable between the low-flow and high-low seasons so that the sensors must be at about 2 m below the water surface. Periodical field investigations (3 times a year) are implemented to collect the measured data and observe real changes by photographs. The first time is in the dry season in January/February. The second time is during the rising stage of the flow hydrograph, usually in June/July. The third time is during the high stage of the flood flow, normally in September/October.

Our strategy for those installed turbidity stations is twofold: (1) to use our high resolution data to check the reliability of existing data provided by the Vietnamese National Hydro-meteorological Data Center under MRC framework and (2) to investigate sediment dynamics in the VMD at the hourly interval.

Figure 5.3 The installed turbidity meter (right) and salinity meter (left) in the VMD.

5.2.3 Two campaigns of the field surveys

The first boat-based field survey was conducted in August 2017 (high-flow season) along about 570 km in main rivers in the VMD, including Tien, Hau rivers and Vam Nao channels (Fig. 2.2) to measure the river depths, velocities, discharges, water levels, and turbidity. Various instruments were used such as Trimble GPS-equipped ADCP, Garmin GPS, and turbidity meters. Each instrument used will be described in subsequent sub-sections. In total, 200 cross sections were measured with the distance between adjacent cross-sections ranging from hundreds to thousands of meters. The handheld Garmin GPS was used to double-check the reliability of the Trimble GPS. In addition, hourly water levels at eleven hydrological stations along the Tien and Hau Rivers (namely Tan Chau, Vam Nao, Cao Lanh, My Thuan, Tra Vinh, Ben Trai, Chau Doc, Long Xuyen, Can Tho, Dai Ngai, and My Thanh) were collected during the period of the field survey to derive river bed elevations from river depths measured by the ADCP. These stations are operated by the Southern Regional Hydrometeorological Center, belonging to Vietnam National Centre for Hydrometeorological Forecasting. The second boat-based field survey was conducted in March-April 2018 (low-flow season) along the same pathway of the first survey. In this survey, we measured longitudinal and vertical turbidity using turbidity meters. The positions of measured profiles were recorded by a Garmin GPS.

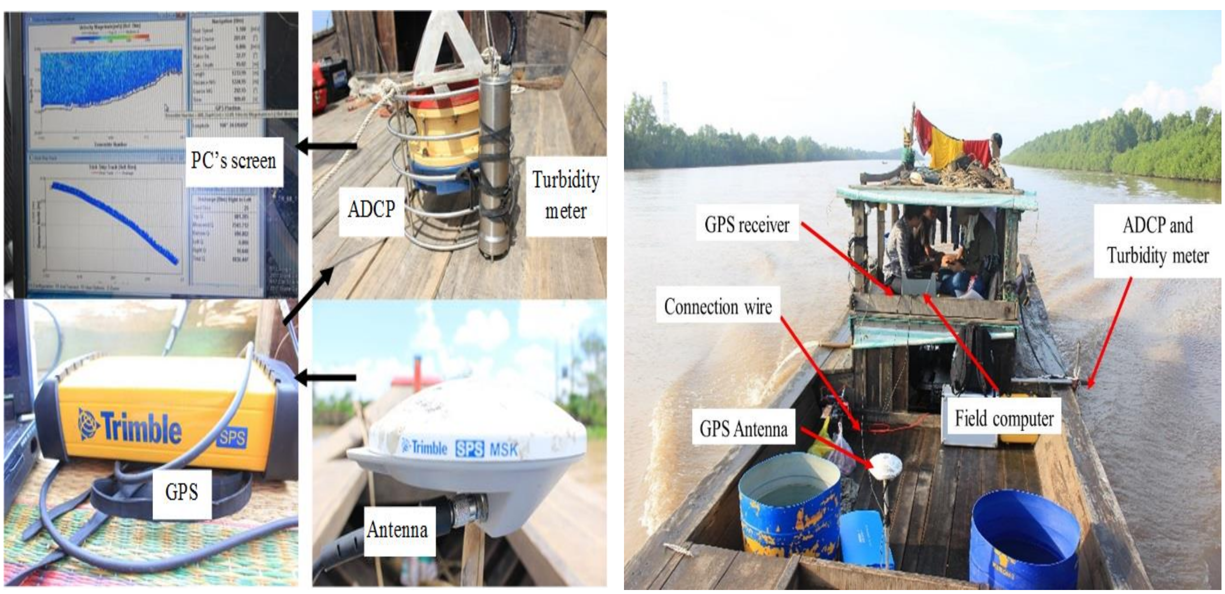

Figure 5.4 The measurement instrument used in the field survey.

a. The ADCP

The ADCP was used in the first field survey in August 2017. We used a boat to move along the Co Chien, Dinh An (in the Tien River), Dinh An, and Tran De (in the Hau River) to the upper parts up to the Tan Chau and Chau Doc stations (Fig. 2.2). A pole-mounted GPS-equipped Teledyne RD Instruments Workhorse Rio Grande 600 kHz ADCP was used to measure the river depths and

2-dimensional velocities. The ADCP was mounted at 0.3 m under the water surface on the boat side. A Trimble GPS with an antenna was combined with the ADCP (Fig. 5.4). These devices connected to a field computer to control the speed and direction of the boat. The boat moved longitudinally and transversally.

b. The turbidity meter

In the first field survey, an Infinity-ATU75W2-USB turbidity meter (Fig. 5.3) was attached aside the ADCP (Fig. 5.4) to longitudinally and transversally measure the turbidity along the Tien River from river mouths (Co Chien and Dinh An branches) to the Tan Chau station (Fig. 2.2). The turbidity meter recorded the turbidity once every 2 minutes. Ten readings were set up for each recording with an interval of 1s. The results of the measurement are spatially-distributed instantaneous turbidity along the Tien River. Besides that, time series of the turbidity were also available at several points along rivers where we were at rest and/or sleeping. This kind of data can capture half of a daily tidal circle.

In the second field survey, the same turbidity meter that was used in the first field survey was mounted aside the boat to measure the turbidity along the Tien and Hau Rivers from the river mouths to the Tan Chau and Chau Doc stations (Fig. 2.2). The interval of the measurement was 1 minute at which ten readings were recorded every recording. The boat moved longitudinally and transversally along rivers.

5.3 Data processing for measured flow and suspended sediment data

5.3.1 Bathymetric data processing

The acquired ADCP raw bathymetric data were checked and the noise spike points due to boat movement were filtered. Then, the cross-sectional river depths were processed using Teledyne RD Instruments WinRiver II software. In the meantime, water surface elevations at each cross-section at the time of the measurement were interpolated in a matrix of time and distance using hourly water levels at adjacent hydrological stations. Finally, riverbed elevations were obtained by subtracting the water surface elevations to the corresponding river depths. Products of such data processing of the two field surveys were maps to obtain a spatial river bathymetric distribution, which were used to examine riverbed incision and associated controlling drivers.

5.3.2 Cross-sectional velocity and discharge profiling using ADCP

The acquired ADCP raw flow velocity data were quality checked to remove spurious recordings. Then, the flow velocities were processed using Teledyne RD Instruments WinRiver II software. The flow instantaneous velocities were achieved after processing considering the boat position, heading, and velocities which were measured by internally-equipped Trimble GPS. The flow instantaneous velocities were extracted at every 0.4-1.5 m depth, depending on the river depth at each cross section. In general, about 0.4-0.6 m interval near the river mouths where the rivers are shallow and 0.8-1.5 m interval in the upper river where the rivers are deep. Unmeasured areas near the water surface were linearly extrapolated while unmeasured areas near the bottom and banks were extrapolated assuming a no-slip condition, using a power function. The measured flow velocities and riverbed elevations were then used to estimate the cross-sectional flow discharges.

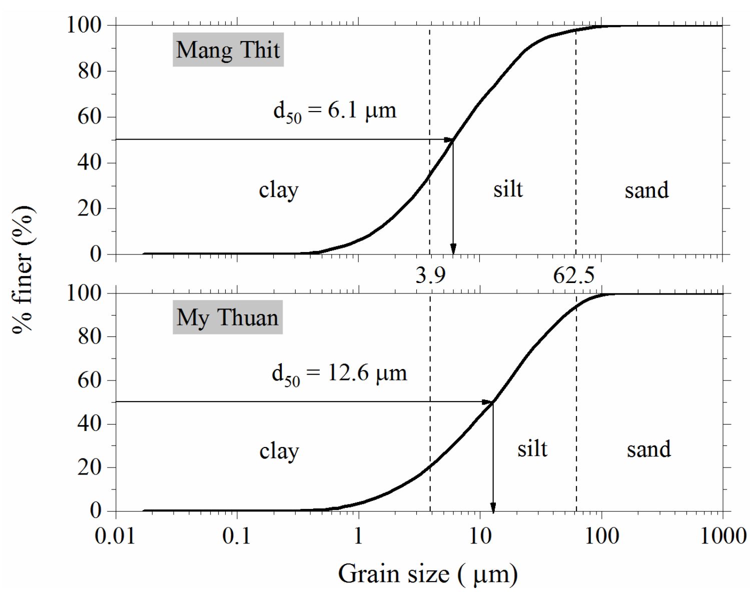

Figure 5.5 Grain size distribution of the suspended sediment at My Thuan and Mang Thit (100 and 65 km from the river mouth, respectively) in the Tien River. The sediment samples were taken during the field survey in August 2017.

5.4 Results

5.4.1 Suspended sediment grain size distribution

The suspended sediment was sampled at My Thuan and Mang Thit which are approximately 100 and 65 km from the river mouth of the Tien River, respectively (Fig. 2.2). These samples were analyzed to determine the grain size distribution using Shimadzu SALD-2300 Laser Diffraction

Particle Size Analyzer which can measure particles from 17 nm to 2,500 μm. These samples were collected at 1 m from the water surface. Fig. 5.5 shows the grain size distribution of these samples. Median suspended sediment diameters of these samples are 12.6 μm and 6.1 μm at My Thuan and Mang Thit, respectively. These median grain sizes are equivalent to settling velocities of 0.052 mm/s and 0.012 mm/s, respectively, by applying Stocks' law. Our measured median diameters are comparable to d_{50}= 10-15 μm by Hung et al., (2013) who measured suspended sediment diameters over 12 sediment traps in the upper part of the VMD's floodplain and to d_{50}= 2.5-3.9 μm near the water surface in the freshwater region of the Hau River estuary by Wolanski et al., (1996) in their field surveys. Fig. 5.5 also clearly shows that approximately 95% of the suspended sediment is composed of silt and clay.

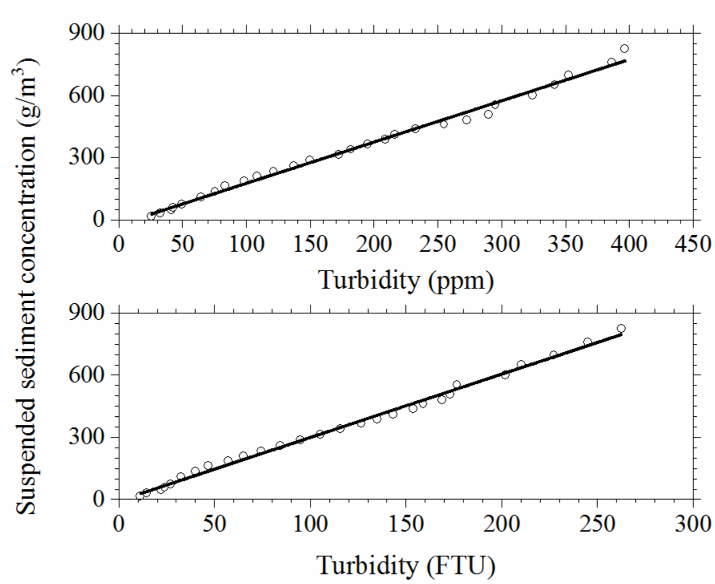

Figure 5.6 Relationship between the SSC and turbidity in the VMD.

5.4.2 Turbidity and suspended sediment concentration relations

During the field surveys, we also recorded the longitudinal and vertical turbidity distribution using the Infinity-ATU75W2-USB. We also took water samples to measure the SSCs to make a relationship between the turbidity and the SSC. The SSCs were well correlated with the turbidity in a linear relation (Fig. 5.6). The correlation equations are as follow:

$$SSC\ (g/m^3) = 1.9922 \times Turbidity\ (ppm) - 23.981\ (R^2=0.9925) \quad (5.1)$$

$$SSC\ (g/m^3) = 3.0572 \times Turbidity\ (FTU) - 6.8179\ (R^2=0.9945) \quad (5.2)$$

5.4.3 Water level fluctuations and variations

Seasonal variations in the precipitation induced by monsoon drive the seasonal fluctuations of flow discharges which control the seasonal fluctuations of water levels. In the upper part of the VMD (at Tan Chau and Chau Doc), the seasonal variation of water levels is about 3 m (Fig. 5.7). In the high-flow season (August-October), the water level fluctuation is controlled by the inflow from the MR with a little influence of the tide. The tide-induced water level fluctuation in the high-flow is ranging from centimeters to decimeters. However, in the low-flow season (January-May), the tide has a significant influence on the water level fluctuation, up to 1 m or more (Fig. 5.7).

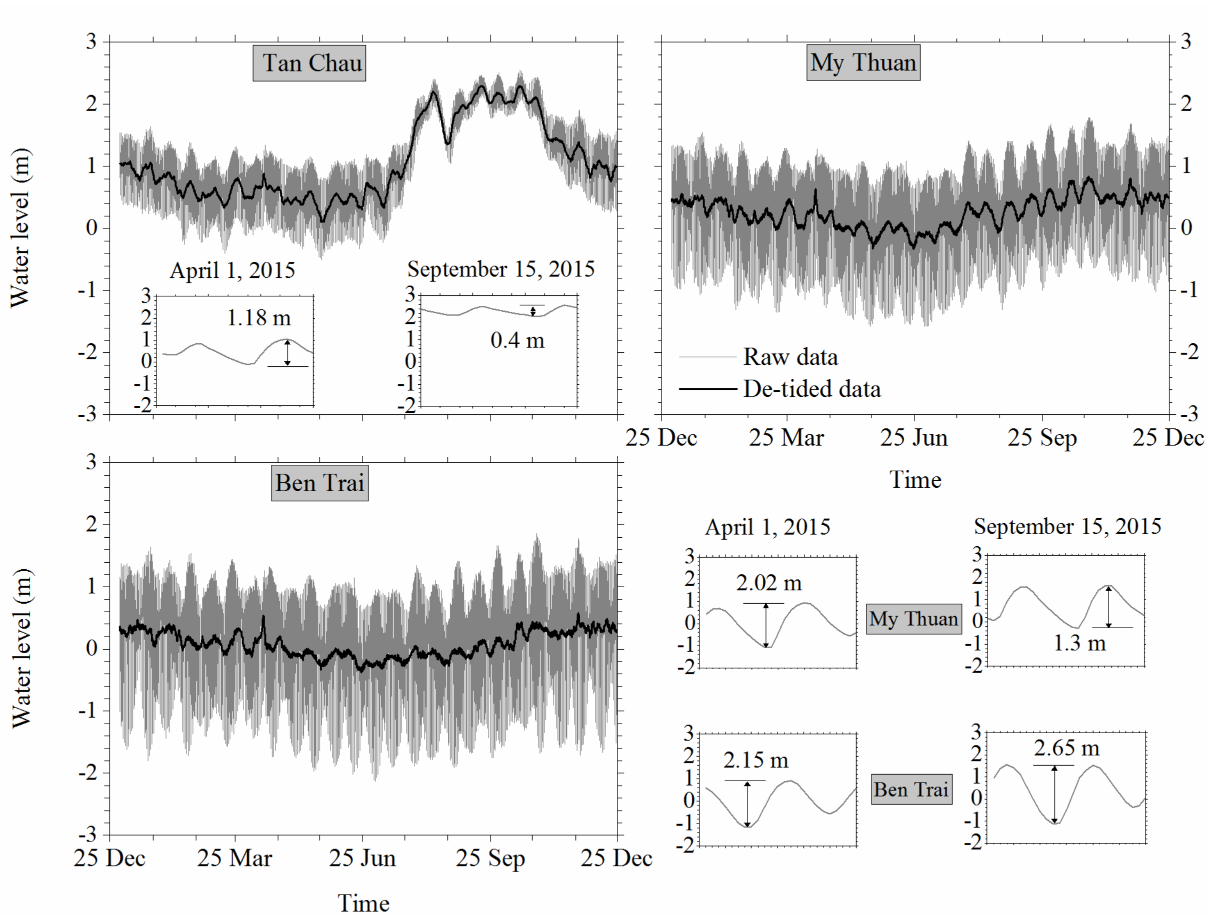

Figure 5.7 Water level fluctuations along the Tien River in 2015.

In the middle part of the VMD (at My Thuan and Can Tho), the seasonal water level variation is about 3.5 m. In this region, the influence of the tide on the water level fluctuation increases. The tide-induced water level fluctuation in the high-flow season is up to 1.5 m while up to 2 m in the low-flow season. The tidal signal in the water level appears all year round (Fig. 5.7).

In the river mouth area (at Ben Trai and My Thanh), the water level fluctuation is controlled by the tide. The maximum tidal range is almost similar throughout the year, up to 4 m. The influence of the river flow from the MR nearly disappears in the low-flow season while not significant in the high-flow season. The mean tidal range is 2.2-2.7 m (Fig. 5.7).

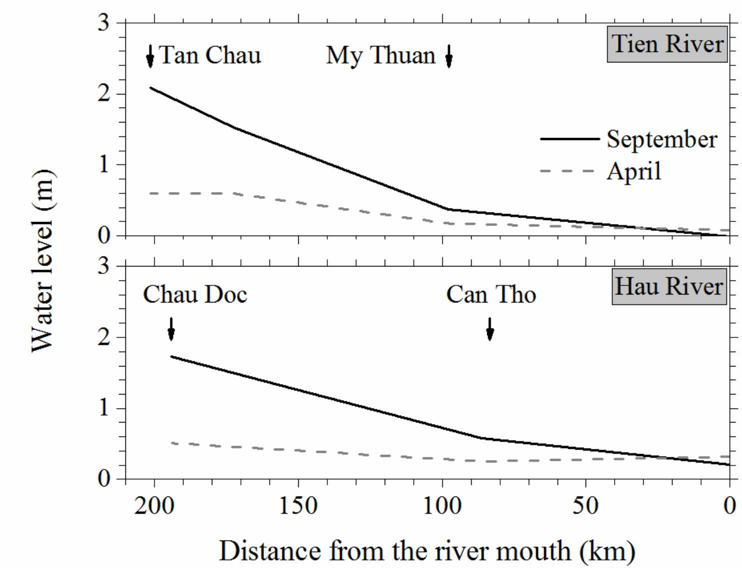

Figure 5.8 Variations in water surface slopes in the Tien and Hau Rivers in the high and low-flow seasons in 2015.

Fig. 5.8 depicts mean longitudinal variations of the water levels in the Tien and Hau Rivers. Not only the magnitude, but also the slope of the water level in the high-low season is larger than that in the low-flow season. The water surface slope in the upper part (from Tan Chau/Chau Doc to My Thuan/Can Tho) is larger than that in the lower part (from My Thuan/Can Tho to the sea). In the low-flow season, the water surface slope is very mild throughout the entire Tien and Hau Rivers.

In terms of water level fluctuations and variations, the Tien and Hau Rivers are divided into two reaches. The upper reach is from the Vietnam-Cambodia border to My Thuan/ Can Tho, characterized by inflow dominance with steep water surface slopes and low tide-induced water level fluctuations during the high-flow season but moderate tide-induced water level fluctuations during the low-flow season. The lower reach is from downstream of My Thuan/ Can Tho to the East Sea, characterized by tide dominance with mild water surface slopes, large tide-induced water level fluctuations throughout the year and little effect of the inflow from the MR during the low-flow season.

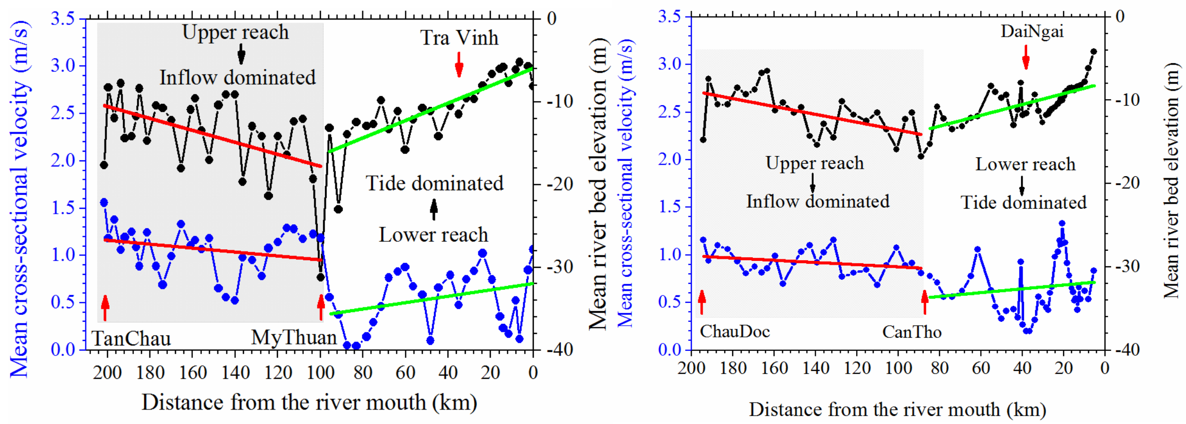

Figure 5.9 Longitudinal variations in the mean riverbed elevation and velocity in the Tien River (left panel) and Hau River (right panel).

5.4.4 Longitudinal, transversal, and vertical flow discharge and velocity distribution

The field survey took place for several days which captured several tidal cycles. Therefore, it is not concrete to compare the instantaneous cross-sectional discharges and velocities along the Tien and Hau Rivers. However, despite such discrepancy, there are relatively different trends in the mean cross-sectional discharges and velocities in the upper and lower reaches (Fig. 5.9). Mean cross-sectional discharges and velocities in the upper reach is higher than those of the lower reach. For example, the mean cross-sectional velocity at Tan Chau is 1.56 m/s while that at the river mouth of the Co Chien distributary is only 1.05 m/s. Both cross-sectional discharges and velocities in the upper reach are decreased seaward while those in the lower reach are increased seaward. These trends are similar to the riverbed elevations as discussed above.

In general, the flow velocity is high in the upper zone of a cross-section (0-0.4h, where *h* is water depth) and lower near the riverbed. According to the cross-section shape, the cross-section velocity distribution is different between the upper and lower reaches. The velocity is high in the upper reach than the lower reach. In the upper reach, high velocities concentrate on the thalweg side (Fig. 5.10). On the other hand, high velocities in the lower reach appear in the middle of a cross-section (Fig. 5.10). At cross-sections having a forming island, high velocities concentrate near the riverbanks and the velocity is low on top of the forming island (Fig. 5.10). Relatively, the ratios between lowest velocity (near the riverbed) and highest velocity (near the water surface) of a cross-section are around 0.6 and 0.4 in the upper and lower reaches, respectively.

In terms of the flow velocity, the Tien and Hau Rivers are distinguished by two reaches. High velocities are in the upper reach, decreasing seaward. The cross-sectional velocity is asymmetric with high velocities in the thalweg side. Lower velocities are in the lower reach, increasing seaward. The cross-sectional velocity is symmetric with high velocities concentrating in the middle of the cross-section. Cross-sections having a forming island near the river mouth have low velocity on top of the island while high velocity is near the riverbanks.

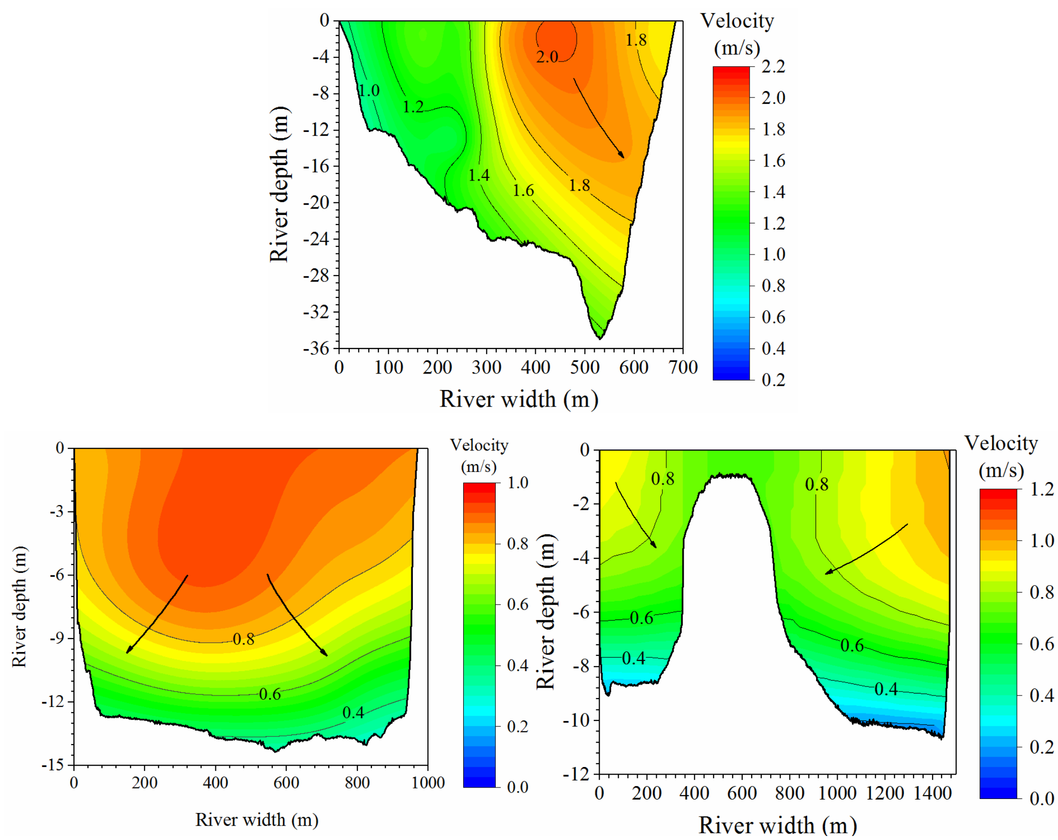

Figure 5.10 Typical cross-sectional velocity distribution in the upper reach (upper panel) at Tan Chau in the Tien River and lower reach (lower panels). Lower left panel: symmetric velocity distribution at a location of 65 km from the river mouth of the Hau River; lower right panel: velocity distribution at a cross-section, having a forming island, at a location of 19 km from the river mouth of the Tien River.

5.4.5 Temporal and spatial variations of the SSC

a. Seasonal variation

The SSC (turbidity) in the VMD is seasonally changeable. It is very high in the high-flow season (around 1,300 g/m^3, recorded by the turbidity meter under JASTIP project, installed at Tan Chau) and very low in the low-flow season (5-70 g/m^3), except for regions appearing turbidity maximum (at around Tra Vinh in our measured data) under the effect of the wind, making local resuspension, and flood tide turbidity current (Fig. 5.11). At Tan Chau, the SSC in August 2017 was 645 g/m^3 which is 14 times larger than that in April 2018 of 45 g/m^3. Similarly, at My Thuan, the SSC August 2017 was 463 g/m^3 compared to 34 g/m^3 in April 2018 (more than 13 times larger). In regions appearing the turbidity maximum during the low-flow season due to the wind and tide effects, there is minor difference in the SSC between the high-flow and low-flow seasons. For example, at Tra Vinh, the SSCs in the high-flow and low-flow seasons were 364 g/m^3 (in August 2017) and 295 g/m^3 (in April 2018), respectively (about 1.2 times difference).

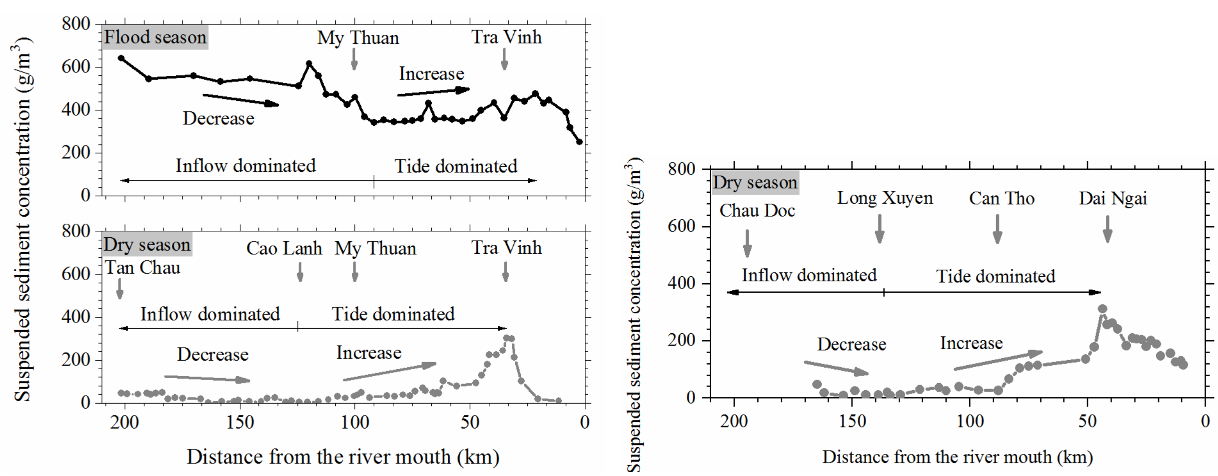

Figure 5.11 Longitudinal SSC variations of the Tien River in the high-flow and low-flow seasons (left panel) and the Hau River in the low-flow season (right panel). High-flow values are in August 2017 and low-flow values are in March-April 2018.

b. Longitudinal variations

Comparison of the longitudinal variations of the SSC in the Tien and Hau Rivers is based on the SSCs measured at around 1 m below the water surface. In the high-flow season, the SSC is highest at Tan Chau (645 g/m^3) and lowest near the river mouth 250 (g/m^3), 2.6 times difference. In the Tien River (we did not measure in the Hau River), the SSC is higher from Tan Chau to some kilometers downstream of My Thuan, decreasing seaward while it is lower from My Thuan to the river mouth, increasing seaward (Fig. 5.11). In the last 10 km from the river mouth, the SSC is lower than the other parts and decreasing seaward.

In the low-flow season, the highest SSC appears within the turbidity maximum which is at around Tra Vinh (295 g/m^3) in the Tien River and at around of Dai Ngai (313 g/m^3) in the Hau River (Fig. 5.11). The SSCs are always higher in the vicinity of the turbidity maximum compared to other segments. In the Tien River, the SSC is high from Tan Chau to Cao Lanh, decreasing seaward and low from Cao Lanh to before the turbidity maximum (at around downstream of My Thuan), increasing seaward (Fig. 5.12). In the Hau River, we did not measure the SSC from a location 165 km from the river mouth to Chau Doc. However, the extrapolated trend of the SSC is expected to increase landward (Fig. 5.11). Therefore, the SSC is high from Chau Doc to Long Xuyen, decreasing seaward and low from Long Xuyen to before the turbidity maximum (at around Can Tho), increasing seaward. Downstream of the turbidity maximum at both rivers, the SSC decreases seaward.

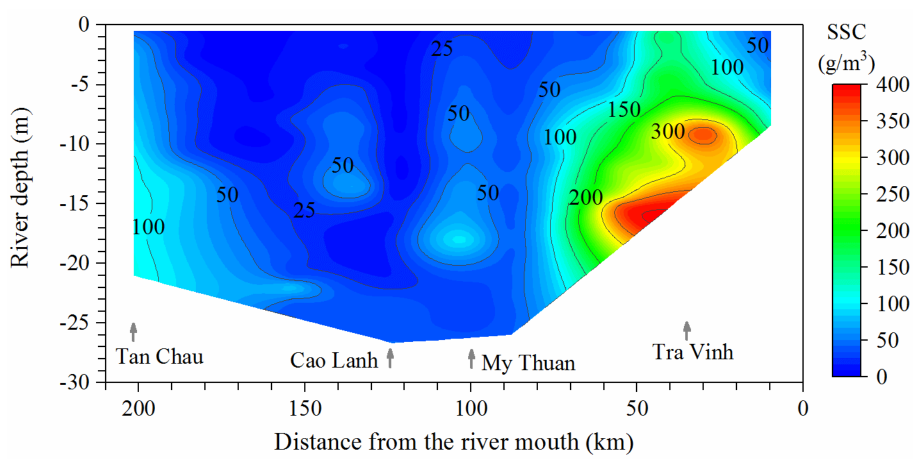

Figure 5.12 Two dimensional SSC distribution along the Tien River in the low-flow season.

In the Tien River, the Cung Hau distributary has higher SSCs than the Co Chien distributary in both high and low-flow seasons (Fig. 5.13). In the high-flow season, the maximum SSC in Cung the Hau distributary reaches 540 g/m^3 while the maximum SSC in the Co Chien distributary is 470 g/m^3. Among the Co Chien, Cung Hau (Tien River), and Tran De (Hau River) distributaries, the highest SSCs were recorded in the Tran De distributary in the low-flow season. Unfortunately, it is not possible to compare the SSCs during the high-flow season among these three branches due to lack of measured data in the Tran De distributary. On the other hand, the Dinh An distributary in the Hau River (Fig. 2.2) has higher SSCs than the Tran De distributary both in the low and high-flow seasons (Allison et al., 2017a).

In terms of longitudinal variations of the SSC, the Tien and Hau Rivers are characterized by two reaches. In the Tien River, the upper reach is from Tan Chau to My Thuan in the high-flow season and from Tan Chau to Cao Lanh in the low-flow season. In the Hau River, although we did not measure the SSC in the high-flow season, based on the similarity between the Tien and Hau Rivers and relative locations of My Thuan and Can Tho allows us to draw a conclusion that the upper reach is from Chau Doc to Can Tho in the high-flow season and from Chau Doc to Long Xuyen in the low-flow season. In both rivers, the SSC is high in the upper reach, decreasing seaward and low in the lower reach, increasing seaward. The turbidity maximum appears in the lower reach in the low-flow season. Downstream of the turbidity maximum, the SSC decreases seaward.

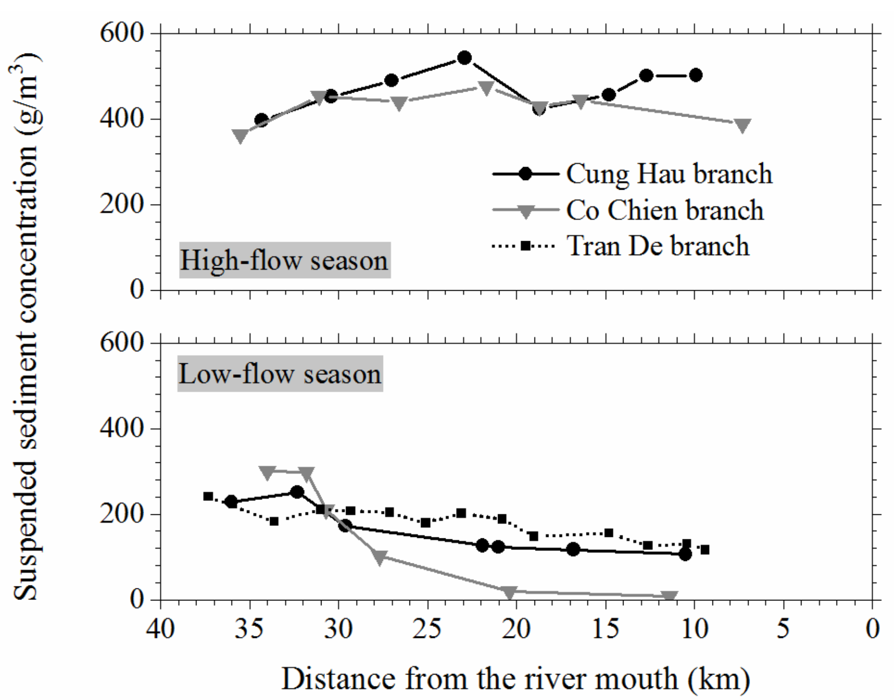

Figure 5.13 Comparison of the longitudinal SSCs between the Co Chien, Cung Hau, and Dinh An distributaries.

c. Vertical and transversal distribution

In the second field survey in March-April 2018, we measured the vertical velocities and SSCs at some representative cross-sections in both upper and lower reaches. At each cross-section, 3-6 profiles were measured, depending on the river width. Normally, three profiles in the upper reach and five profiles in the lower reach. At each profile, the instantaneous SSCs and velocities were measured at a vertical interval of 1-2 m, depending on the river depth. The instantaneous SSCs were used to linearly interpolate the vertical and transversal distribution of the cross-sectional SSCs. In general, the SSC is high near the bottom and low near the water surface. Moreover, high SSCs concentrate in the deeper part of a cross-section (Fig. 5.14 and 5.15). The difference between the highest and lowest values in each cross-section ranges in orders of 3 or 4. Additionally, the vertical distribution of the SSC in the low-flow season in the VMD can be well described by Rouse profile (García, 2008), using a parabolic diffusion coefficient (see Eq. B6.12 in Appendix B).

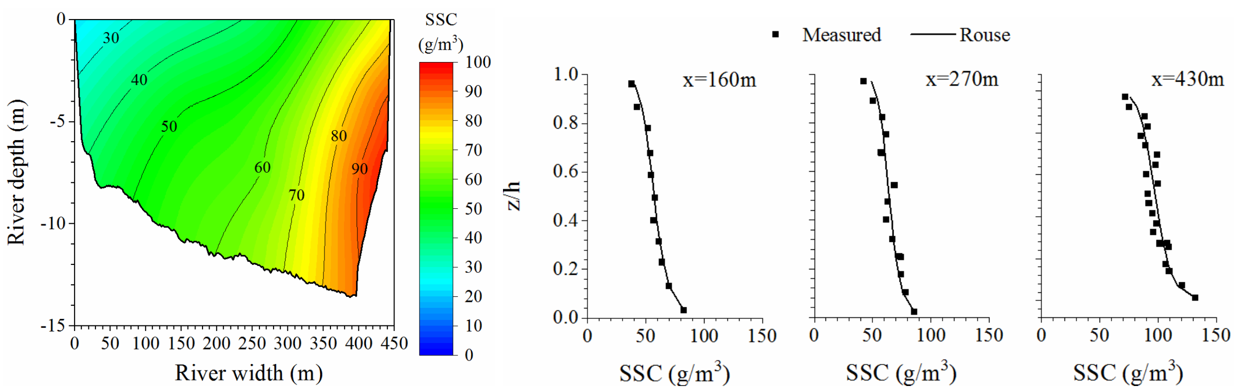

Figure 5.14 Vertical and transversal distributions of the SSC in the upper reach of the Hau River. *x*: the distance from the left bank. Vertical distribution is well fitted by Rouse equation.

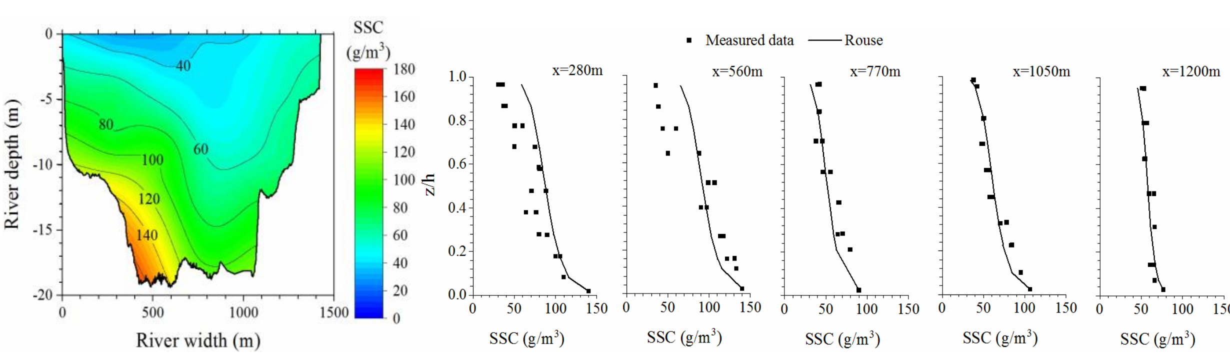

Figure 5.15 Vertical and transversal distributions of the SSC in the lower reach of the Tien River. *x*: the distance from the left bank. Vertical distribution is well fitted with Rouse equation.

In terms of the vertical and transversal SSC distribution, the Tien and Hau Rivers are divided into two reaches, following the longitudinal division of the cross-section shape. In the upper reach, the SSC is asymmetric with high values in the thalweg side, decreasing to the other bank. In the lower reach, the SSC is symmetric with high values in the middle and decreasing onto two banks.

d. Differences between the SSCs under the MRC framework and JASTIP project

The SSC is changeable not only seasonally but also within a day, which was recorded by the Infinity meter under the JASTIP project in an hourly interval measurement (Fig. 5.16). In the low-flow season, due to substantial influence of the tide, the flood tide SSC (80-90 g/m^3) is much different from that in the ebb tide (30-50 g/m^3) during March 5-9, 2016. It is approximately 2-3 times difference. Such a large range in the SSC fluctuation was under-measured under the MRC framework, using isokinetic sampler (Fig. 5.16). In the high-flow season, the flow in the VMD is controlled by the MR runoff; therefore, the tidal influence is small in the upper reach of the VMD. Within a day, the SSC slightly varies between the flood and ebb tides (about 1.1-1.3 times difference from the data during August 26-29, 2016) (Fig. 5.16). Although the range of the SSC fluctuation measured under the MRC framework is lower than that measured under the JASTIP project, the difference between the two is relatively small.

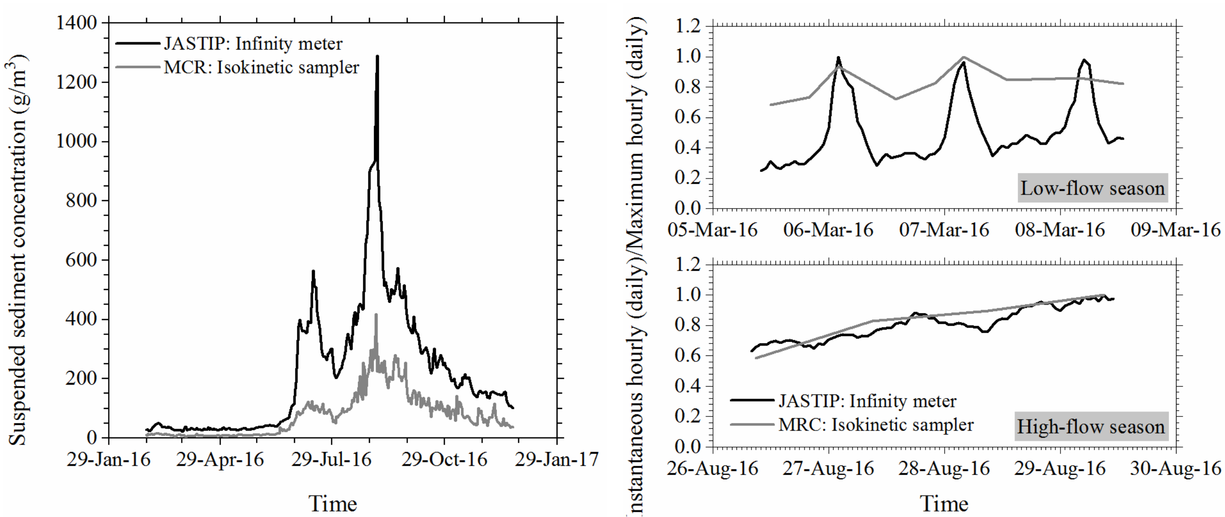

Figure 5.16 Comparison of the SSCs measured under the JASTIP project and the MRC framework in terms of magnitude (left), phase, and fluctuation range (right).

The phases of the SSC fluctuation between the two data sources are similar (Fig. 5.16). However, in terms of the magnitude, the SSCs measured under the JAPSTIP significantly larger than those measured under the MRC. The JASTIP's SSCs are approximately 1.4-7.6 and 1.2-5.9 times larger than the MRC's SSCs during February-June and July-December, 2016, respectively.

5.4.6 River bathymetry and cross-sectional geometry

The riverbed elevation of the Tien and Hau Rivers is very much variable, ranging from several meters near the river mouths to more than 30 meters in the upper parts (Fig. 5.9). The deepest point in the Tien River is at a location of approximately 2 km upstream of the My Thuan station (-46 m deep) while the deepest riverbed in the Hau River is just upstream of the Can Tho station (-31 m deep). The riverbeds are shallowest around the last 15 km near the river mouths (Fig. 5.9). When reaching the deepest points in both Tien and Hau Rivers, the riverbeds become shallower as moving seaward.

The Tien and Hau Rivers are distinguished by two clear reaches in terms of riverbed elevation and cross-section shape. The dividing points are at the My Thuan station in the Tien River and at the Can Tho station in the Hau River. The upper reach is deep and narrow (normally less than 1,000 m wide). The riverbed elevation decreases seaward. The cross-section in the upper reach is asymmetric with the thalweg appearing either on the left or the right bank (Fig. 5.17). In the upper reach, the slope of the riverbed of the Tien River (0.013%) is steeper than that of the Hau River (0.0088%). On the other hand, the lower reach is shallow and wide (the maximum width can reach 3,000 m near the river mouth). The riverbed elevation increases seaward. The cross-section in the lower reach is symmetric (Fig. 5.17). In the last 35 km from the river mouths of the Tien and Hau Rivers, islands are usually formed in the middle of the river (Fig. 5.17). Commonly, islands appear at regions having cross-section larger than 1,000 m in the Tien River and larger than 2,000 m in the Hau River. In the lower reach, the riverbed of the Tien River is slightly steeper than that in the Hau River with a mean slope of 0.019% for the former and 0.013% for the latter.

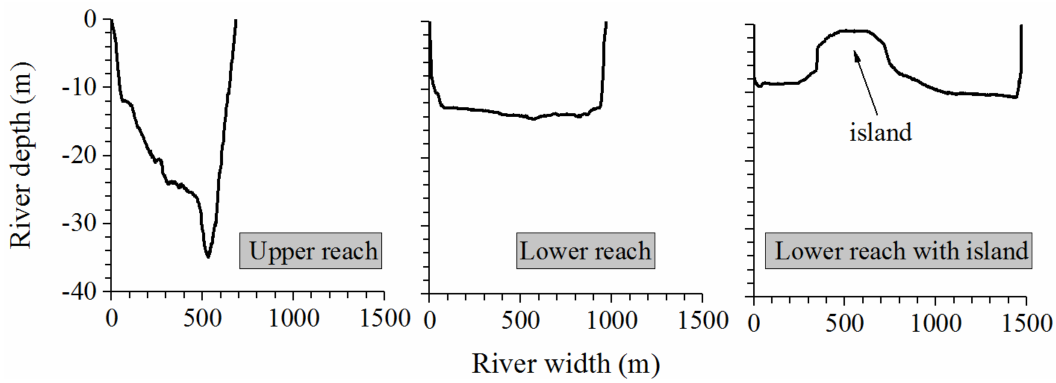

Figure 5.17 Representative cross-section geometry in the upper and lower reaches of the VMD.

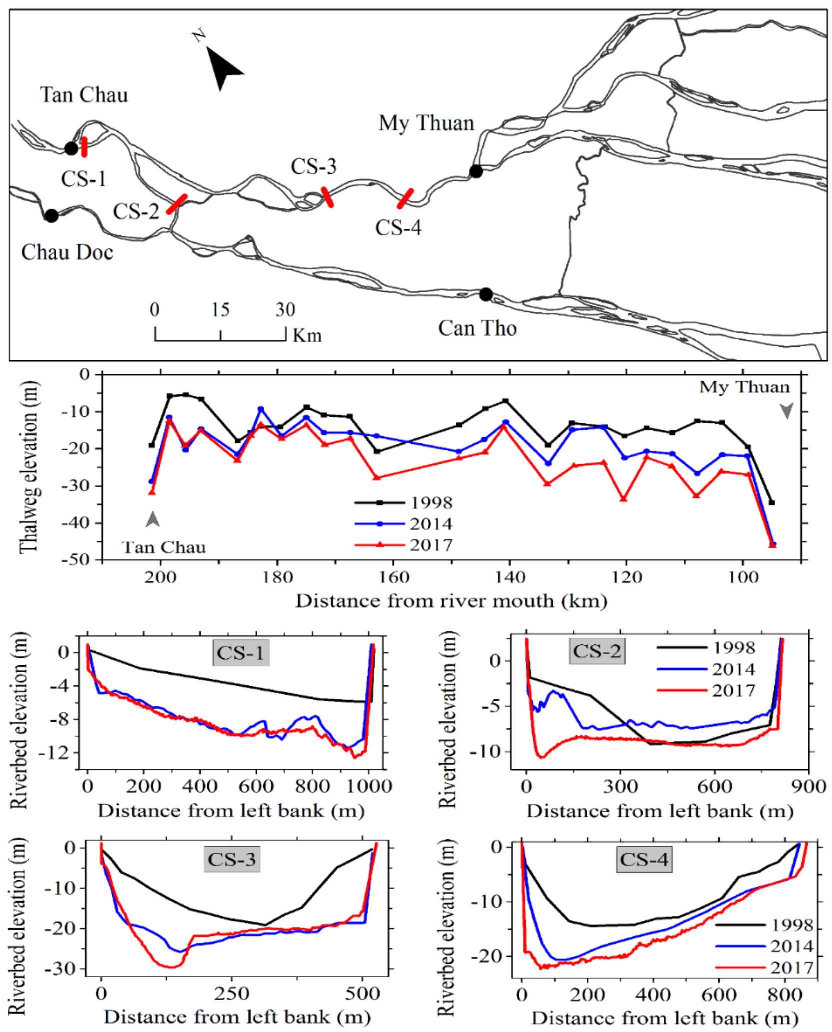

Figure 5.18 Longitudinal and cross-sectional riverbed incision along the Tien River between the Tan Chau and My Thuan stations.

5.4.7 Morphological changes

Fig. 5.18 shows evidence of a critical riverbed incision in the VMD during 1998-2017. The river thalweg was significantly incised, ranging from -0.43 m to -14.87 m deep, with a mean value of -5.2 m during 1998-2014. In other words, the incision rates ranged from -0.03 to -0.93 m/yr, with a mean value of -0.33 m/yr. During the three years between 2014 and 2017, the mean river thalweg incision was -3.73 m, varying between -0.45 and -11.37 m. These incisions were equivalent to -1.24 m/yr (for the mean incision) and between -0.15 m/yr and -3.79 m/yr (for the minimum and maximum incisions, respectively). In total, the maximum and mean river thalweg incisions were -20.28 m and -8.92 m, respectively, during 1998-2017. Four typical cross-sections along the Tan Chau-My Thuan section confirmed a significant riverbed incision (Fig. 5.18).

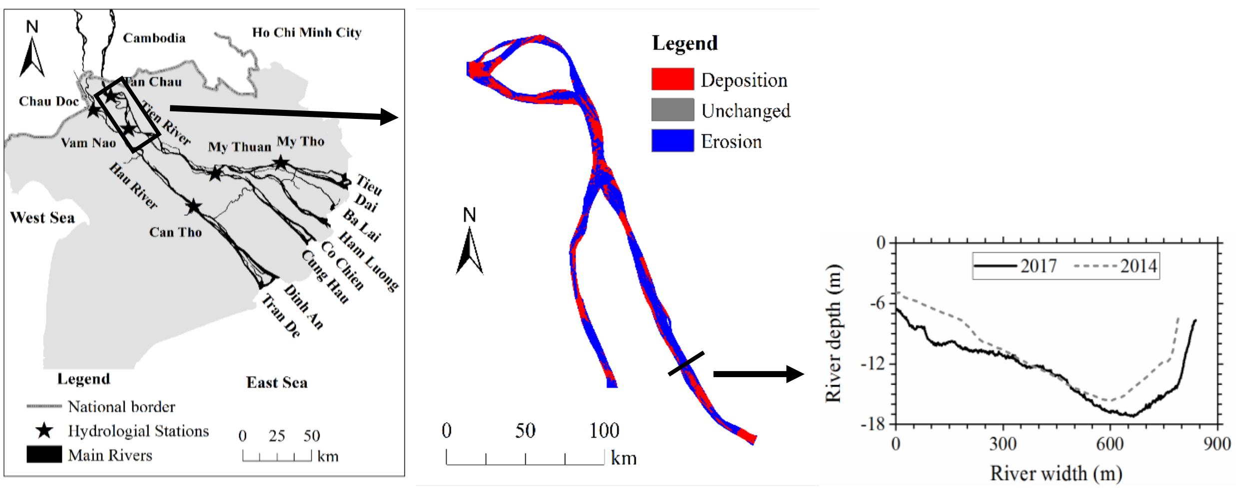

Figure 5.19 Erosion and deposition patterns of river bathymetry between 2014 and 2017.

To clarify more detail a rapid morphological change, the river bathymetry measured in August 2017 from the first field survey was compared with the one measured in 2014 in the upper part of the Tien River in three dimensions (Fig. 5.19). The figure shows that erosion occupies about two third of the region. The total eroded volume was 145.5 Mm^3 over an area of 37 km^2, leading to a mean erosion depth of -4 m. Similarly, the total deposited volume was 66.9 Mm^3 over an area of 21.4 km^2, resulting in a mean deposition depth of +3.1 m. By subtracting the total erosion volume to the total deposition volume and dividing by the total area, the region was, on average, eroded by about -1.5 m. Noticeably, the maximum erosion depth can reach 8.3 m at a cross-section of 5.4 km downstream of Tan Chau on the left channel. Besides, riverbanks were also eroded significantly. The maximum bank erosion can reach 50 m over these three years. Such erosion of the riverbed and banks was mainly due to a reduction in the sediment supply from the MR which was mostly trapped by upstream hydropower dams.

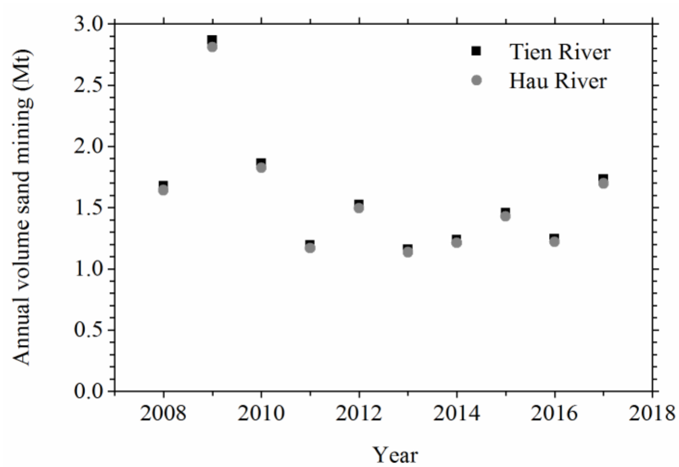

Figure 5.20 Amount of annual mined sand during 2008-2017 in the upper part of the Tien and Hau Rivers, from Tan Chau/ Chau Doc to My Thuan/ Can Tho.

5.5 Discussions

5.5.1 Morphological changes in the VMD as a consequence of river damming and sand mining

The river thalweg incision rate in the Tien River from Tan Chau to My Thuan during 2014-2017 (-1.24 m/yr) is nearly four times larger than that during 1998-2014 (-0.33 m/yr) (Fig. 5.18). Additionally, we estimated that the riverbed of the Tien River from Tan Chau to Vam Nao has been incised by an average of -1.5 m during 2014-2017 at a mean rate of -0.5 m/yr, which is double the mean riverbed incision rate of -0.25 m/yr over a decade during 1998-2008, which had an absolute mean incision of -2.47 m (Brunier et al., 2014). Such riverbed incisions were likely mainly driven by hydropower dams that trap most of the bedload, including sand (riverbed material of the VMD consists mainly of sand, i.e., 90%). For instance, current and planned dams in the 3S river basin trap 91% and 97% of the sand load, respectively (Schmitt et al., 2018). The riverbed incision in the VMD is much faster in recent years than in the past (twofold faster over a much shorter period). This finding can be explained by the fact that reworked sediment, which was deposited in pools during the predam period, and/or riverbank erosion in areas downstream of hydropower dams in the postdam period delivered a considerable volume of sediment to the VMD and therefore hindered the impact of the dams. Over two decades following the first dam completion when such deposited sediment is likely almost exhausted and riverbanks of such areas may reach new equilibrium conditions, the impacts of hydropower dams on the VMD riverbed incision was already initiated at a tremendous rate. The riverbed incision rate is predicted to be even faster in the future when more dams will be completed.

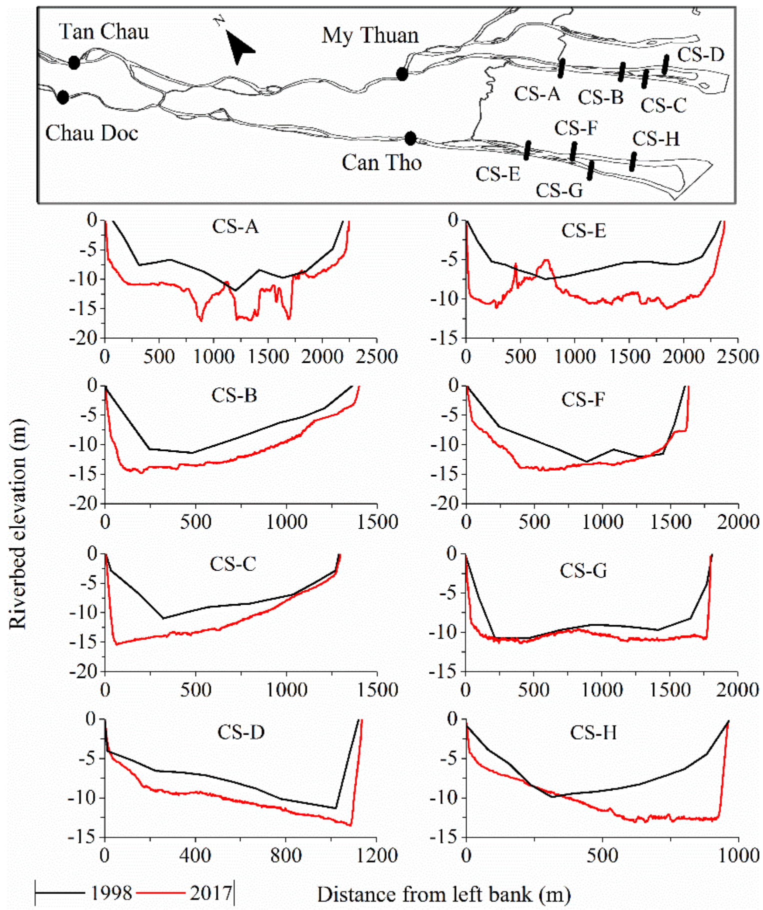

Figure 5.21 Typical riverbed incision during 1998-2017 along 50 km from the river mouths of the Tien and Hau Rivers.

Additionally, sand mining is also a key driver of the riverbed incision. Annually, sand mining in the VMD is approximately 8 Mt/yr (Bravard et al., 2013). Our data collected from local authorities show that the mean annual sand mining in the upper part of the Tien and Hau Rivers (upstream of Can Tho and My Thuan) during 2008-2017 is 1.7 Mm^3 or 2.8 Mt/yr when considering an aggregate density of 1.6 t/m^3, and mining in the Tien River contributed 50.5% compared to 49.5% in the Hau River. Fig. 5.20 shows the annual volume of mined sand during 2008-2017, indicating that sand mining might be strictly authorized since 2011 due to increasing complains on its impacts on recently severe riverbank erosion from the community. We argued that while sand mining causes riverbed incision at the local scale, hydropower dams are responsible for large-scale morphological changes. Fig. 5.21 differentiates the riverbed degradation caused by local sand mining and by large-scale hydropower dams. At cross-sections appearing sand mining (e.g., CS-A), the riverbed geometry is irregular, characterized by deeply mined pits, while other cross-sections experience riverbed incision, with regular shape, even without the appearance of sand mining. Allison et al., (2017a) found that sand mining was not the main cause of thalweg deepening in the area between Can Tho and the river mouth of the Hau River.

Figure 5.22 Typical severe river bank erosion in the VMD. Photos were taken by Binh D.V. during the field survey in April 2018.

Hydropower dams and sand mining are also driving riverbank erosion, which spreads over the VMD, especially the upper part of the Tien River from Tan Chau to Vam Nao. Fig. 5.22 shows the typical riverbank erosion, which was obtained during the VMD field survey in August 2017. Furthermore, land subsidence induced by hydropower dams and sand mining largely occurred in the VMD due to over-extraction of groundwater for domestic, agricultural, and industrial uses (Kondolf et al., 2018). Similarly, the VMD coastline has rapidly retreated due to dam-induced sediment reduction and to some extent is likely due to land use change and mangrove forest reduction along the VMD coastline (Allison et al., 2017b). Over the past 8,000 years, the Mekong Delta accreted rapidly up to 16 km^2/yr (Kondolf et al., 2018), which is equivalent to 16-26 m/yr. However, over 50% of the 600 km of VMD coastline has been experiencing serious erosion during 2003-2012 (during the boom of river damming in the MRB), which is equal to over 5 km^2 in land loss (2.3 km^2/yr), and the retreat rates commonly exceed 50 m/yr in some places (Anthony et al., 2015). Therefore, countermeasures against riverbank and coastal erosion are urgently needed to mitigate the negative effects of erosion on the environment and human livelihoods.

5.5.2 Division of the Tien and Hau Rivers based on morpho-hydrodynamics and fine-sediment dynamics

The hydro-sediment-morphodynamics in the fluvial to marine transition zone (Gugliotta et al., 2017) are one of the most complicated research fields in hydraulics engineering as various controlling factors (i.e., fluvial flow, tide, wave, and social development) involve in the interactive processes. The backwater effect extends more than 600 km up-river from the river mouths (Allison et al., 2017a), from which the VMD entirely locates in the fluvial to the marine transition zone. In the high-flow season, the fluvial flow controls the hydro-sediment processes; its influence can protrude tens of kilometers into the shore. Results analyzed in this chapter revealed that the fluvial processes do not influence the water level fluctuation but dominate the inflow-outflow discharge and sediment balances at the river mouths, leading to the net flow and sediment outputs to the East Sea (Stephens et al., 2017), which was in agreement with Gugliotta et al., (2017). In the low-flow season, tidal processes fully control the hydro-sediment dynamics seaward of the fluvial-marine interface. The tidal influences can extend hundreds of kilometer landward; for example, the tidal component of the water level at Tan Chau/Chau Doc can reach up to 1 m or more (Fig. 5.7).

There are clear trends in the hydro-sediment-morphodynamics along the VMD main rivers. The Tien and Hau Rivers can be distinguished by two reaches. The upper reach from Tan Chau/ Chau Doc (maybe from the Vietnam-Cambodia border) to My Thuan/ Can Tho and the lower reach from My Thuan/Can Tho to the river mouths. However, the division locations may vary between the high-flow and low-flow season, relatively in between Cao Lanh/ Long Xuyen and My Thuan/ Can Tho (Fig. 2.2). In the upper reach, the rivers are deep and the riverbed elevation decreases seaward. The river widths are narrow and the riverbed slopes are steep. The rivers are sinuous (Gugliotta et al., 2017). River cross-sections are asymmetric with the thalweg being deflected toward one side of the riverbank. Natural levees are dominant. The upper reach is dominant by the fluvial processes with steep water surface slopes and low (high-flow season) to moderate (low-flow season) tide-induced water level fluctuations. The velocity is high, decreasing seaward. The cross-sectional velocity and SSC distributions are asymmetric followed the asymmetry of the cross-section geometry. The SSCs are high, decreasing seaward. The suspended sediment is silt with d_{50} = 12.6 μm, within the range of 10-15 μm by Hung et al., (2013). The riverbed materials are dominant by fine sand, with grain size decreasing seaward, and the mud content is low, about 5% (Gugliotta et al., 2017).

In the lower reach, the rivers are shallower and the riverbed elevation increases seaward. Rivers are wide, straight, and symmetric. Mangroves are dominant (Gugliotta et al., 2017). The flow is tide-dominated while the fluvial influences are nearly disappeared in the water level fluctuations. The flow velocity is smaller than the upper reach, increasing seaward. Saltwater intrudes up to 40-60 km, depending on the inter-annual variations of the inflow that is driven by the monsoon. The flow and SSC distributions are symmetric. The SSCs are low, controlled by marine processes such as the tide, salinity, and wind. The estuaries of the Tien and Hau Rivers have a salt wedge during the high-flow and is partially well-mixed during the low-flow (Wolanski et al., 1996). The suspended sediment is silt with d_{50} = 6.1 μm, comparable to d_{50} = 3.5-6 μm near the bottom in the freshwater region (Wolanski et al., 1996). The bed materials are uniformly fine sand and mud content is high (Gugliotta et al., 2017).

Within the last 35 km from the river mouths, islands are alternately formed in the middle of the river where the rivers are wide and straight, and the flow velocity is reduced compared to the upper reach. Island formation stems from the residual flow and sediment fluxes supplied by the MR during the high-flow season. Islands which are usually formed at a cross-section of approximately 20 km landward from the river mouth of the Dinh An distributary were more likely to be generated by lateral convergence of the sediment from the ebb-dominated and flood-dominated channels due to the tidal asymmetry (Nowacki et al., 2015).

Within the last 50 km from the river mouths, the saltwater zone has larger d_{50} and higher clay fraction than the freshwater zone. Flocculation occurs and such flocs are settled during the slack water. Flocs sizes are larger in the freshwater than the saltwater zones with d_{50} = 50-200 μm (Wolanski et al., 1996). In the low-flow season, a turbidity maximum zone is formed with its position changeable between the ebb and flood tides. The turbidity maximum is obviously not a product of the upstream MR sediment flux while other drivers may contribute. First, the tide (accompanied by the wind) pumps up-river the fine sediment with high concentrations, which was deposited within 20 km seaward of the river mouths during the previous high-flow seasons. In fact, approximately 95% of the suspended sediment from the MR is exported to the East Sea during the high-flow season, of which approximately 5% is transported up-river with the salt wedge (Wolanski et al., 1996). Second, the riverbed resuspension may contribute considerable fine sediment, which is carried onto the turbidity maximum zone. Third, the riverbank erosion may be a substantial source of the fine sediment of the turbidity maximum. During the second field survey in April 2018, we observed critically eroded banks in between 35-130 km from the river mouths. Last but not least, the fine sediment resuspended from sand mining activities is a compromised source, contributing to the turbidity maximum. Sand mining was mainly found to be on the forming island.

5.5.3 Reliability of monitored SSCs under MRC program

Under the MRC framework, hourly monitored water levels and discharges satisfactorily represent the tidal influence. However, twice-a-day monitored SSCs under-describe the range of the suspended sediment variability during the low-flow season while are acceptable during the high-flow season (Fig. 5.16). In terms of the magnitude, the SSCs measured under the MRC framework using isokinetic samplers are under-recorded compared to those measured under the JASTIP project using turbidity meter (orders of 1.1-7.6 times). Using a filter having a porosity of 8 μm more likely excludes a considerable amount of the silt and clay in the collected sample as our grain size analysis showed that the suspended sediment in the VMD consists of a large amount of silt and clay fractions and the d_{50} near the river mouth is even smaller than the filter porosity (Fig. 5.5). Koehnken, (2014) reported that the silt and clay contribute 98% of the suspended sediment at Tan Chau and Chau Doc and our finding is approximately 95%. It is worth noting that SSC measurement under the JASTIP project may over-record the SSC values during the low-flow season to some extents because the installed positions of the turbidity meters are relatively close to the riverbank (about 20-40 m) therefore may be impacted by human activities and reflected waves. However, such human and wave influences during the high-flow season should be negligible because of high water levels. Moreover, the spatial coverage of the SSC monitoring stations is very sparse. Therefore, we recommend to (1) install more flow and SSC monitoring stations along main rivers, especially near the river mouths of Tien and Hau distributaries so that the realistic net sediment inflow and outflow from the MR can be monitored, (2) monitor the SSC at hourly interval so that monitored data can well describe the sediment dynamics in the VMD, and (3) use automatic instruments with high accuracy to monitor the hourly SSCs.

5.5.4 Effect of upstream dam development on the VMD's dynamics

Historically, the sediment discharging into the East Sea from the MR was large, of approximately 144±36 Mt/yr over the past 3,000 years (Ta et al., 2002). This sediment deposited in the subaqueous VMD within the 20 km seaward of the river mouths (Wolanski et al., 1996). Part of this sediment is transported up-river and part is transported southward to the Cape Ca Mau, helping balance the flow-wave-human-induced erosion processes in the rivers and protect the coast from wave-induced erosion (Wolanski et al., 1998). However, the suspended sediment budget of the MR has been critically reduced due to upstream dam development (Koehnken, 2014; Kondolf et al., 2014; Kondolf et al., 2018; Kummu et al., 2010). Our data showed that the SSC budget of the MR entering the VMD has reduced by 83% in 2015 (28 Mt/yr) from the predam condition (166.7 Mt/yr). Near the river mouths, Nowacki et al., (2015) estimated that the net outflow of the suspended sediment of eight river distributaries into the East Sea was 40 Mt/yr using their field data, collected during August 2012-April 2013. Reductions in the sediment supply from the MR will encounter a cutting process (from wave-induced erosion) of the deposited subaqueous VMD; therefore, the VMD landscape is expected to be at critical retreats in a long-term (hundreds of years) and in the worst case, may disappear if no countermeasure action is implemented to improve the sediment discharge from upstream hydropower dams and to protect the delta from erosion.

5.6 Conclusions

The flow and sediment fluxes from the MR are of crucial importance to sustain the VMD, helping the Delta survive from natural and anthropogenic erosion processes. However, a full understanding of the hydro-sediment-morphodynamics of the whole VMD is lacking due to poor temporal-spatial monitoring stations under the MRC framework. To partly overcome this kind of difficulty, two campaigns to install additional SSC monitoring stations in February 2016 and February 2017 and two field surveys in August 2017 and March-April 2018 under the JASTIP project were conducted, supported by Kyoto University. Dataset from this project include temporal-spatial 3D velocities and SSCs, discharges, water levels, river bathymetry, and geometry. Main findings of this chapter are:

(1) In terms of hydro-sediment-morphodynamics, the Tien and Hau Rivers are distinguished into two reaches. The division locations are changeable in between Cao Lanh/Long Xuyen and My Thuan/Can Tho (Fig. 2.2), depending on the seasons. The upper reach is dominated by the fluvial

processes while the lower reach is dominated by the tide. In the upper reach, the rivers are narrow, sinuous, and deep, decreasing seaward. River cross-sections, flow velocities, and SSCs are asymmetric. SSCs are high, decreasing seaward and bed materials are fine sand with low mud content. In the lower reach, the rivers are wide, straight, and shallow, increasing seaward. River cross-sections, flow velocities, and SSCs are symmetric. SSCs are low, increasing seaward and bed materials are uniformly fine sand with high mud content. Turbidity maximum zone occurs during the low-flow season due to the saline water cycle. Mid-river islands commonly appear within the last 35 km from river mouths.

(2) Owing to poor temporal-spatial monitored data, obtained from monitoring stations under the MRC framework, scientists have difficulties in understanding the realistic hydro-sediment dynamics; therefore, stakeholders have difficulties in sustainably planning and developing the VMD. We recommend installing more monitoring stations of the flow and sediment along VMD rivers, especially near the river mouths. Using modern automatic instruments with high accuracy to monitor the SSCs is strongly recommended.

(3) Combing results of long-term flow (in Chapter 3) and sediment (in Chapter 4) budget alterations and long-term morphological changes in the VMD analyzed in this chapter, it can be concluded that hydropower dams have caused large-scale morphological changes in the VMD as they trapped most of the inflowing sediment, while sand mining caused local riverbed incisions. Hydropower dams and sand mining have already had short to intermediate-term influences on morphological degradation in the VMD, but long-term effects of climate change are projected.

Chapter 6 Establishment of two-dimensional numerical models in simulating hydro-sediment-morphodynamics and morphological changes in the Vietnamese Mekong Delta

6.1 Introduction

Fig. 3.17 of Chapter 3 shows that mean discharges during 2012-2015 have increased whereas mean water levels have significantly reduced, from the 1980-1992 (predam) period. Specifically, the median discharge increases by 10% but the median water level decreases by 2% by comparing the two periods of 1980-1992 (predam) and 2012-2105 (six mainstream dams are in operation). These two periods are compared because it is necessary to understand the cumulative impacts of all mainstream dams, of which Nuozhadu (completed in 2011) is the largest, having the total storage capacity of 22.37 km^3, on the future flows of the VMD, based on the historical changes between the postdam and predam flows. Such opposite trends in discharges and water levels may be due to the morphological degradation caused by reductions in the sediment supply from the MR, which is evidenced in Chapter 4 and 5. Fig. 6.1 conceptually interprets the effects of the increased flow discharges and degraded riverbed on water levels in rivers, especially during the low-flow season. Specifically, water levels are controlled by inflow discharges (Fig. 6.1a). When inflow discharges increase, water levels will increase accordingly under an unchanged riverbed bathymetry (Fig. 6.1b). However, when the riverbed is degraded with a rate that is greater than the rate of increased water levels, resulted from the increased inflow discharges, water levels ultimately decrease (Fig. 6.1c). Consequently, the reduction in water levels, especially during the low-flow seasons, leads to difficulty in obtaining the intake water for irrigating the agricultural crops.

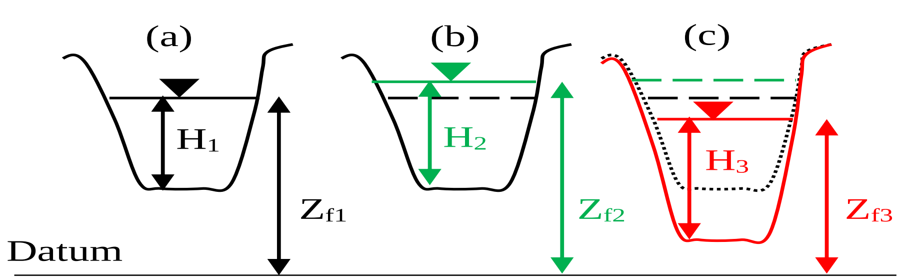

Figure 6.1 Conceptual effects of increased flow discharge and degraded riverbed on water depth (H) and water level (Z_f): (a) initial condition, (b) increased flow discharge, (c) increased flow discharge with degraded river bed. $H_1 < H_2 < H_3$ but $Z_{f3} < Z_{f1} < Z_{f2}$.

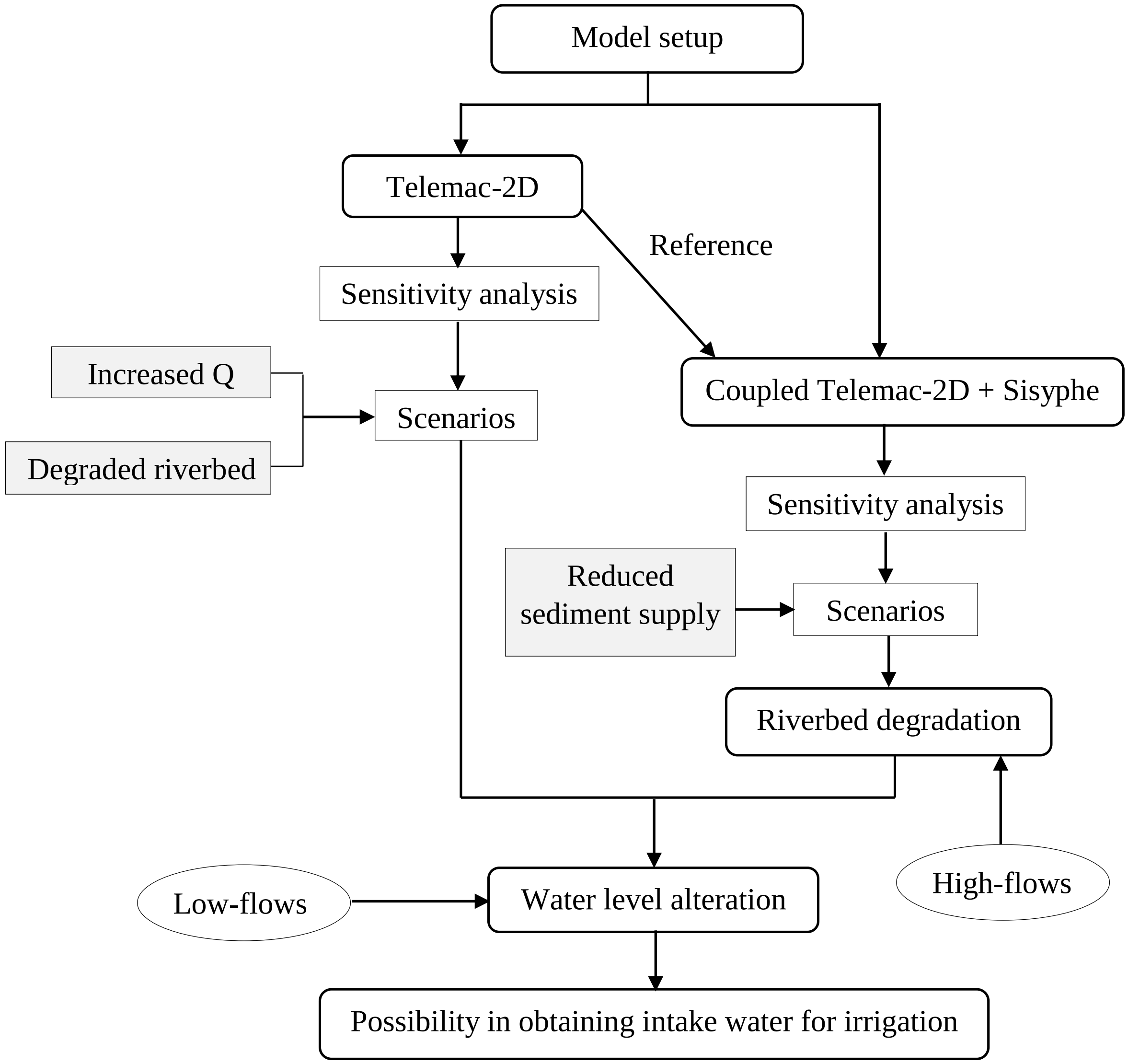

Figure 6.2 Procedure of numerically simulating effects of water levels alterations on the possibility in obtaining intake water for irrigation in the low-flow season.

Numerical applications have been widely used in many world's large river systems to investigate the hydro and sediment dynamics necessary for river management practices because of limited monitoring data which are not enough to provide a full understanding of the flow and sediment behaviors. Due to data limitation, modelers have to analyze the sensitivity of all governing physical and numerical parameters, which affect the model results. First, they roughly run a number of simulations to determine the most sensitive parameters. Then more simulations are conducted to find the best value of each sensitive parameter which can well reproduce a real flow and sediment dynamics of river systems. Sensitivity analysis using hydrodynamics and sediment transport models have been widely conducted. In the VMD, Manh et al., (2014) analyzed the sensitivity of some physical parameters in the 1-D flow and sediment transport models (Mike 11).

The goal of this chapter is to establish two-dimensional models that are applicable to simulate hydro-sediment-morphodynamics and morphological changes in the VMD's rivers, which are the product of reductions in the sediment supply from the MR. The procedure in Fig. 6.2 is designed. For that, two models are established. A single Telemac-2D is to simulate the low-flow alterations under dam impacts. A coupled Telemac-2D and Sisyphe model is to predict the riverbed evolution during the high-flow season due to reduced sediment supply from the MR and then the altered simulated riverbed will be input into the single Telemac-2D to simulate the low-flow water alterations. This chapter presents sensitivity analysis in establishing the single Telemac-2D and coupled Telemac-2D and Sisyphe models while the remaining steps in Fig. 6.2 (results of simulations) are analyzed in Chapter 7.

6.2 Background of Telemac-2D and Sisyphe

6.2.1 Telemac-2D

The Telemac-2D is an open source (a component of Telemac Mascaret system), developed by the National Hydraulics and Environment Laboratory of Electricité de France (EDF). The Telemac-2D solves the depth-averaged free surface flow equations or Saint-Venant equation. The main results of each node of the computation mesh are the water depth and depth-averaged velocities in x and y-direction (longitudinal and transversal directions, respectively) (Ata et al., 2014). The Telemac-2D is applicable in riverine and maritime hydraulics. It can take into consideration of various phenomena, including propagation of long waves, friction on the bed, the effect of the Coriolis force, the turbulence effect, supercritical and subcritical flows, dry areas in the tidal flats and floodplains, dike breaching (Ata et al., 2014). The Telemac-2D can be coupled with the sediment transport model (Sisyphe), wave model (Tomawac), and water quality module. The Telemac-2D can be able to simulate the flow around the port structure, the effect of the submersible dikes, dredging, weirs, tubes, dam breaks, flooding, and tracer transport. The advantage of the Telemac system is to be able to run in parallel mode, which may reduce much of the simulation time, therefore, reducing the simulation cost. This allows simulating complex geometry domains with fine mesh and more simulation scenarios can be considered. The simulation solutions can be finite element or finite volume schemes. More details of governing equations, inputs, and output of Telemac-2D are presented in Appendix B.

6.2.2 Sisyphe

Sisyphe is, a module of Telemac Mascaret system, the sediment transport and bed evolution model (Pablo, 2018). The Sisyphe model can simulate complex morphodynamic processes in rivers, lakes, estuaries, and coastal environment. The sediment transport can be bedload, suspended load or total load (bedload + suspended load). Cohesive sediment (diameter ≤ 62.5 μm), non-cohesive sediment (diameter > 62.5 μm), and sand-mud mixtures can be simulated. The non-cohesive sediment can be uniform or non-uniform (graded sediment). For the suspended sediment, multiple grain sizes can be simulated. Similarly, multiple vertical layers of the riverbed can be considered. The influence of secondary current in meandering rivers, bed slope effect, and non-erodible bed is incorporated in the Sisyphe. Details of Sisyphe are described in Appendix B.

6.2.3 Coupled Telemac-2D and Sisyphe model

The Sisyphe can be externally or internally coupled with Telemac-2D. In case of external coupling (chaining method), hydrodynamic and morphodynamic models are run independently. The hydrodynamic model from the Telemac-2D is first simulated with the assumption of a fixed riverbed. The results, mainly the water depths and flow velocities, of the hydrodynamic model will be then used as inputs for the morphodynamic model in Sisyphe to simulate the riverbed evolution. The external coupling method can be used for relatively simple flows. In case of internal coupling, at each time step, the estimated bed shear stresses and other relevant hydrodynamics variables achieved by solving governing continuity and momentum equations of theTelemac-2D are sent to the sediment transport model in the Sisyphe to calculate the sediment transport rate and update the bed geometry which is then sent back to the Telemac-2D to estimate hydrodynamics variables in the next time step.

6.3 Evaluation of numerical model performance

To evaluate the performance of the numerical model, coefficient of determination (R^2), Nash-Sutcliffe number (*NSE*), and root mean square error (*RMSE*) are used.

Coefficient of determination is computed as follow:

$$R^2 = \left(\frac{n\sum_{i=1}^{n}(y_i \times f_i) - \sum_{i=1}^{n} y_i \sum_{i=1}^{n} f_i}{\sqrt{n\sum_{i=1}^{n} y_i^{\,2} - \left(\sum_{i=1}^{n} y_i\right)^2} \sqrt{n\sum_{i=1}^{n} f_i^{\,2} - \left(\sum_{i=1}^{n} f_i\right)^2}} \right)^2 \tag{6.1}$$

where y_i, i=1, 2, …n are the observed data with n values; f_i, i=1, 2, …n are the estimated data which are associated with y_i. The range of R^2 is in between 0 and 1.0. The high the values of R^2, the more reliable the model is developed.

The Nash-Sutcliffe number which indicates how well the simulated data match the corresponding observed values. *NSE* is computed as follow:

$$NSE = 1 - \frac{\sum_{i=1}^{n}(y_i - f_i)^2}{\sum_{i=1}^{n}(y_i - \bar{y}_i)^2} \tag{6.2}$$

in which $\bar{y}$ is the mean of observed values, computed as follow:

$$\bar{y} = \frac{\sum_{i=1}^{n} f_i}{n} \tag{6.3}$$

The *RMSE* compares the errors of the model and observed data. Its value is from 0 to positive infinity. The smaller values (close to 0) indicate a good established model. The *RMSE* is computed:

$$RMSE = \frac{\sum_{i=1}^{n}(y_i - f_i)^2}{n} \tag{6.4}$$

6.4 Establishing a single Telemac-2D model for the VMD

In Chapter 5, the Tien and Hau Rivers are divided into two reaches: the upper reach is inflow-dominated while the lower reach is tide-dominated. These two reaches are seasonally separated in between Cao Lanh and My Thuan in the Tien River and in between Long Xuyen and Can Tho in the Hau River. Considering the complexity of the lower reach due to the tide, wave, and saltwater effects, the upper reach of VMD is selected as the study domain. It includes part of the Tien River from Tan Chau to My Thuan, part of the Hau River from Chau Doc to Can Tho and the entire Vam Nao channel (Fig. 2.2).

6.4.1 Model setup

The simulated domain includes a 1-2 km floodplain wide. The triangle finite element method is used to generate the mesh, which has a grid spacing of 80 m in the rivers and 150 m in the floodplains (Fig. 6.3). The mesh consists of 111,416 nodes and 219,397 elements. The mesh is then incorporated with river bathymetric and floodplain DEMs to produce a geometry mesh for the model. The 2017 measured bathymetric DEM and 2013 SRTM floodplain DEM are used to create the geometry mesh for the study domain. Because the distance between two adjacent cross-sections is relatively large, various interpolation methods are tested using a geostatistical tool in ArcGIS. As a result of more than 100 trials, Universal Kriging is selected as the best interpolation method.

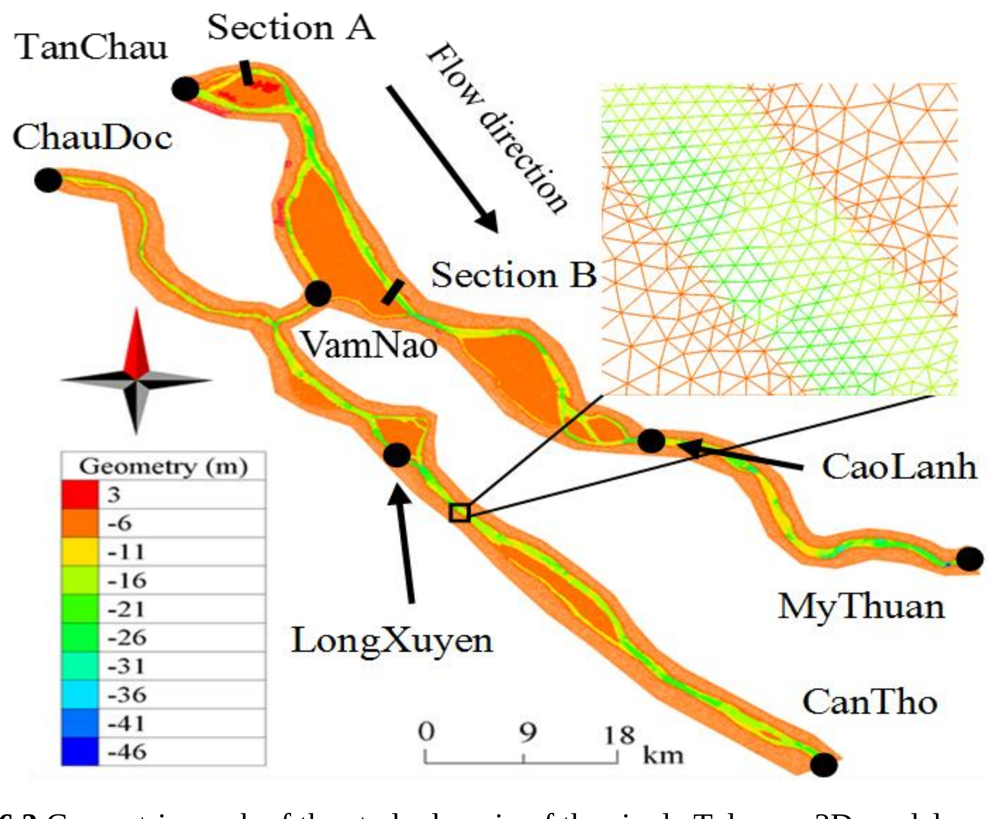

Figure 6.3 Geometric mesh of the study domain of the single Telemac-2D model, using 2017 river bathymetric and 2013 SRTM floodplain DEMs.

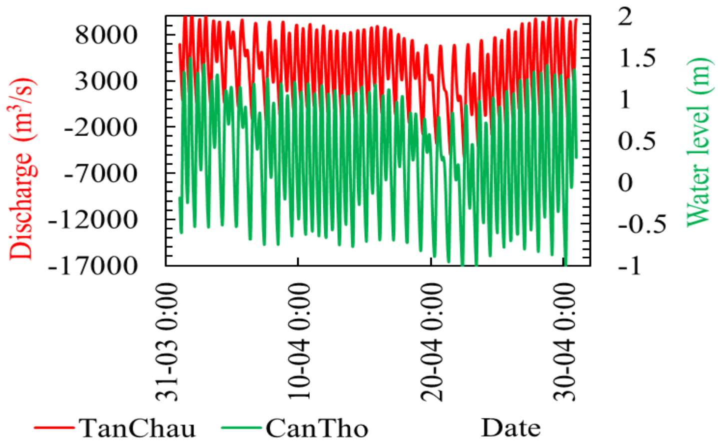

Figure 6.4 Boundary conditions: daily discharges at Tan Chau and water levels Can Tho in April 2017.

6.4.2 Boundary and initial conditions

There are four open boundaries in the study domain. Two upstream boundaries (at Tan Chau and Chau Do) use imposed hourly flow discharges and two downstream boundaries (at My Thuan and Can Tho) use imposed hourly water levels (Fig. 6.3). Typical time series of boundary conditions are shown in Fig. 6.4. The study domain is inflow-dominated but influenced by the tide during the low-flow season such as in April.

Constantly imposed discharges and water levels in the upstream and downstream boundaries were simulated for 10 days to achieve steady conditions (hotstart), which is used as the initial conditions for the real simulations. In terms of model calibration and validation, hourly water levels at Vam Nao, Cao Lanh, and Long Xuyen are used. Due to lack of data, the model is not calibrated and validated using discharges at these stations.

6.4.3 Sensitivity analysis

The single Telemac-2D model was calibrated by testing various values of different physical and numerical parameters, including time step (Δt), friction coefficient (Manning law, *n*), turbulent model, velocity diffusivity (ν), and solver option. In total, twenty-two trials were simulated to find the best value of each parameter. The constant viscosity model and the conjugate residual solver were selected. Velocity diffusivity was tested in the range of 0.5-5. Increasing the velocity diffusivity reduces the water level range, such that the peak is shifted downward and the trough is shifted upward. A uniform constant friction coefficient was first applied to the whole domain. Then various zones with different values were tested to obtain the best value. Finally, three zones were selected. The upper zone covers both the Tien and Hau Rivers, from Tan Chau/ Chau Doc to a location of approximately 40 km seaward. The second and third zones are in the remaining lower parts of the Tien and Hau Rivers, respectively. In each zone, the friction coefficient was tested in the range of 0.008-0.1. In general, increasing friction coefficient reduce the magnitude and range of water level fluctuations and vice versus. The time step was tested in between 1-30 second. Reducing the time step results in more accurate simulation but increases substantially the simulation time. Moreover, the study domain is influenced by the tide. Therefore, the tidal flat was applied to consider the drying and wetting effects. Table 6.1 shows the best values of each parameter of the single Telemac-2D for the study domain as a result of the sensitivity analysis.

The simulated water levels at Cao Lanh and Long Xuyen are in good agreement with the corresponding measured values with high correlation coefficients of 0.91 and 0.95, respectively, and Nash-Sutcliffe efficiency of 0.82 and 0.84, respectively. Fig. 6.5 shows a typical simulated versus measured water levels at Long Xuyen.

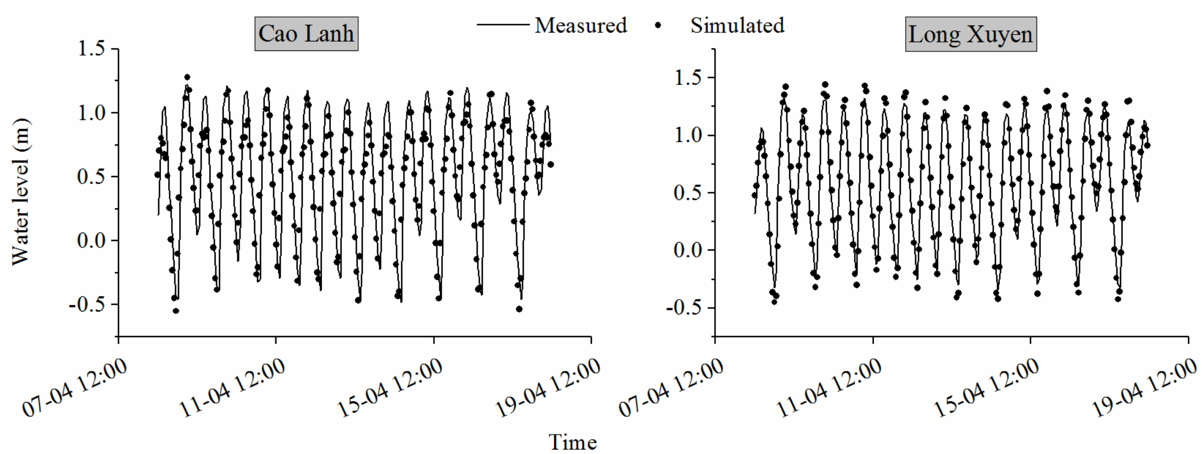

Figure 6.5 Measured versus simulated water levels at Long Xuyen.

Table 6.1 Set of best Telemac-2D's parameters.

Δt (s)	n			Turbulent model	ν (m²/s)	Solver option
	Upper	Lower Tien River	Lower Hau River			
10	0.42	0.14	0.24	1	2	2

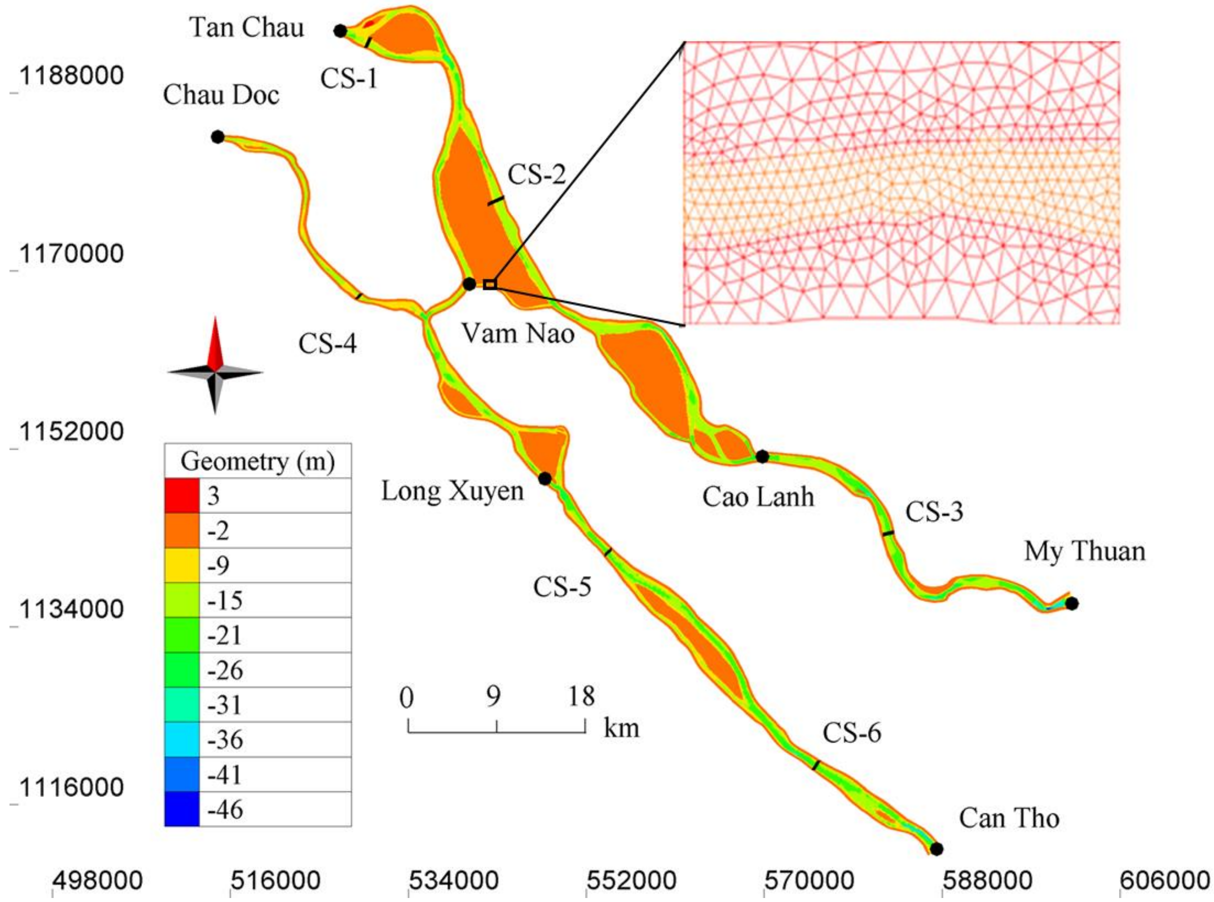

Figure 6.6 Model setup of the coupled Telemac-2D and Sisyphe model, including boundaries, geometric mesh, and calibration stations.

6.5 Establishing a coupled Telemac-2D and Sisyphe model for the VMD

6.5.1 Model setup

Similar to the single Telemac-2D model established above, the study domain of the coupled Telemac-2D and Sisyphe model is from Tan Chau/ Chau Doc to My Thuan/ Can Tho in the Tien and Hau Rivers, and the entire Vam Nao channel (Fig. 6.6). 200-300m floodplain wide is considered to make the model stabilized. The simulated domain uses triangle mesh generated by finite element method. The mesh has a grid spacing of 80 m in the main rivers and floodplains, and 30-40 m in the narrow channels (Fig. 6.6). By that, the domain consists of 106,413 nodes and 206,455 elements. The established mesh sizes are much finer than those in Thanh et al., (2017) who used Delta3D model with mesh sizes ranging from 100-200m in the connecting channels and 300-600 m in the main rivers to simulate the suspended sediment dynamics in the VMD. Xing et al., (2017) applied Delta3D with a grid size of about 180 m (40 m for the detailed study) in the Hau River estuary to investigate the sand dynamics. The coupled Telemac-2D and Sisyphe model uses the 2014 river bathymetric DEM and 2013 SRTM floodplain DEM as input geometry. It then uses the 2017 river bathymetric DEM for model calibration.

6.5.2 Boundary and initial conditions

Similar to the single Telemac-2D model as described above, the coupled Telemac-2D and Sisyphe model has four boundaries. Two upstream boundaries (at Tan Chau and Chau Doc) use hourly flow discharges and daily SSCs of cohesive sediment and two downstream boundaries (at My Thuan and Can Tho) use hourly water levels and free flow of the suspended sediment (Fig. 6.6). The model simulates only the suspended load and bed evolution while the bedload transport is not considered. Typical time series of hourly discharges and water levels at upstream boundaries are shown in Fig. 6.4. Fig. 4.4 shows a typical time series of daily SSCs at Tan Chau.

More than 95% of the suspended sediment in the VMD is composed of silt and clay (Fig. 5.5) while more than 90% of the riverbed material is sand. Therefore, the Sisyphe model uses mixed sediment transport to simulate the sediment dynamics and riverbed evolution. Detail of the mixed sediment transport model is described in Appendix B. According to (Gugliotta et al., 2017), less than 5% of the riverbed material is mud while fine sand is dominant in between the Vietnam-Cambodia border to around My Thuan/ Can Tho. Therefore, in the mixed sediment model, only cohesive sediment is simulated for the imposed suspended sediment. The initial fractions of the riverbed material are 95% of the non-cohesive sediment (fine sand) and 5% of the cohesive sediment. Uniform median diameters (d_{50}) are used to specify the grain size of both cohesive (d_{50} = 12.63 μm) and non-cohesive sediment (d_{50} = 214 μm according to (Gugliotta et al., 2017)).

Initial conditions of the coupled model are obtained by simulating for 10 days, using constantly imposed discharges, water levels, and SSCs at boundaries to achieve the steady condition, which is used as the hotstart for the real simulations. In the hotstart simulation, the bed evolution model is not activated.

6.5.3 Existing sediment transport model’s parameters in the VMD

There are several numerical studies investigating the hydro-sediment-morphodynamics and morphological changes in the VMD. Table 6.2 summarizes the flow and sediment characteristics in the VMD that were analyzed and applied in the prior numerical studies. The value ranges of these parameters are considered as the starting point of the established coupled Telemac-2D and Sisyphe model. Interestingly, previous studies mainly used Mike and Delta3D packages while the application of the Telemac packages in the VMD has not existed in the literature.

Table 6.2 Flow and sediment characteristics in the VMD that were applied in previous numerical studies.

Author	Parameter						
	ρ_s (kg/m^3)	d_{50} μm	ω_s (m/s)	u_*^{cr} (m/s)	M (kg/m^2/s)	τ_{ce} (N/m^2)	Bed mud concentration (kg/m^3)
(Letrung et al., 2013)			$1x10^{-4}$-$3x10^{-4}$	$8.9x10^{-3}$-$1.1x10^{-2}$	$5x10^{-6}$-$1x10^{-4}$	0.15-1.5	120-600
(Hung et al., 2013a)	2.65	10-15 30-40	$2.16x10^{-4}$-$1.85x10^{-03}$	$4.5x10^{-3}$-$5.3x10^{-3}$	$5.13x10^{-6}$-$8x10^{-6}$	0.028-0.044	
(Manh et al., 2014)	2.65		$1x10^{-4}$-$1.3x10^{-3}$	$4.4x10^{-3}$-$5x10^{-3}$			
(Thanh et al., 2017)		15	$5x10^{-5}$-$3.3x10^{-4}$	1.0	$2x10^{-5}$	0.2	

Manh et al., (2014) classified the Manning coefficient into 8 zones in the VMD, ranging from 0.016-0.034 with a fixed value of 0.016 in the coastal zone. They applied a time step of 3-5 minutes for the mesh size of 700 m to control the stable Courant number. Letrung et al., (2013) used Manning coefficient of 0.025-0.05 and time step of 0.01-30 s to control the Courant number less than 0.8 to ensure the model stability. They used flexible mesh but the range of the mesh size was not mentioned.

6.5.4 Sensitivity analysis

The sensitivity of various physical and numerical parameters of the hydrodynamics component of the coupled Telemac-2D and Sisyphe model is tested, including floodplain size, Manning coefficient (n), velocity diffusivity (ν), time step (Δt), type of advection (TA), free surface compatibility (FSC), and implicitation for depth (IMD) and velocity (IMV), in which time step and the Manning coefficient are the most sensitive.

Then different physical and numerical parameters of the mixed sediment transport and bed evolution components of the coupled model are also sensitively simulated, including critical shear stress for erosion (τ_{ce}), critical shear velocity for deposition (u_*^{cr}), setting velocity (ω_s), Krone-

Partheniades constant (M), option for dispersion, dispersion coefficient, and solver for suspension, in which, M and τ_{ce} are the most sensitive parameters to the erosion flux and ω_s is the most sensitive parameter to the erosion flux.

In the calibration of the hydrodynamic model, water levels at Vam Nao, Cao Lanh and Long Xuyen were used. The SSCs at Vam Nao were used for calibrating the cohesive sediment transport. Additionally, six cross-sections (CS-1 to CS-6), in which three cross-sections in each river that evenly distribute along the river, were used for calibrating the riverbed evolution. Fig. 6.6 shows these locations.

a. Effect of floodplain size on hydrodynamics

Thanh et al., (2017) overestimated the high-flow water levels and discharges in the Tien and Hau River because they did not include the floodplain in their simulation. On the other hand, their low-flow water levels and discharges were well predicted. Those suggested that the inclusion of the floodplains in the model will improve the simulated results.

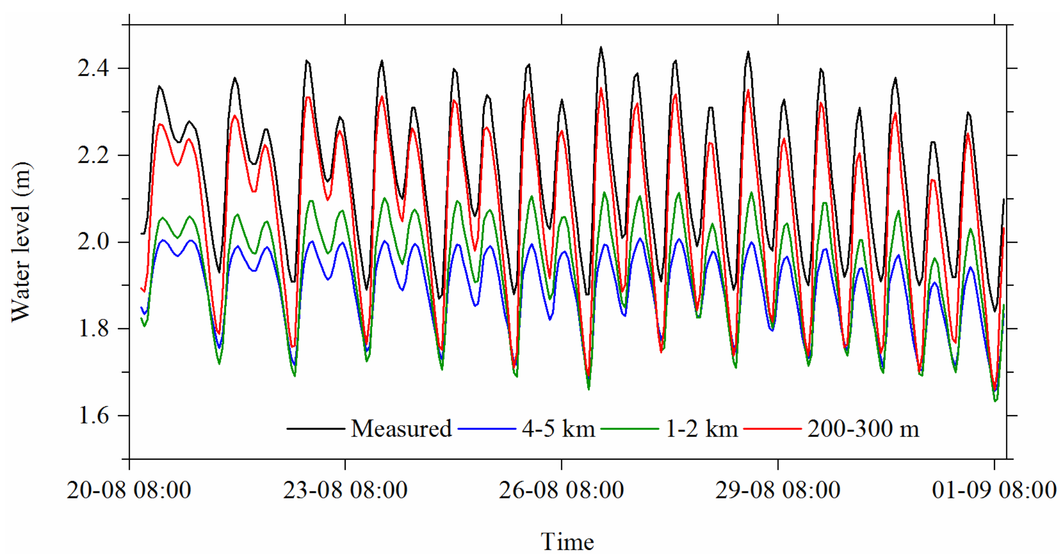

Figure 6.7 Effect of floodplain size on water levels in the main rivers at Vam Nao in 2014.

Some tens of kilometers downstream of Tan Chau and Chau Doc, the Tien and Hau Rivers receive the overflow through the floodplains during the high-flow season from the Vietnam-Cambodia border. In the established coupled model, this overflow is not considered. The imposed discharges are set at Tan Chau and Chau Doc only. Therefore, the flow direction is from the main rivers to the floodplains instead of from the floodplains to the main rivers as the reality. This simplified consideration may exert some errors. Therefore, different sizes of the floodplains, i.e., 4-5 km, 2-3 km, and 200-300 m wide, were tested to optimize the model.

Fig. 6.7 shows that the 4-5 km floodplain wide reduces significantly the water level in the main rivers because the floodplains receive a substantial volume of the water that should be transported downstream in reality. Reducing the floodplain width to 2-3 km increases the water levels in the main rivers, however, the effect is still small. When continue reducing the floodplain width to 200-300 m, the simulated water levels in the main rivers are well fitted with the measured values (Fig. 6.7). This can be explained that the smaller size of the floodplain receives a little volume of water from the rivers, that does not markedly reduce the main river's water levels while can stabilize the model. Therefore, 200-300 m floodplain wide was selected.

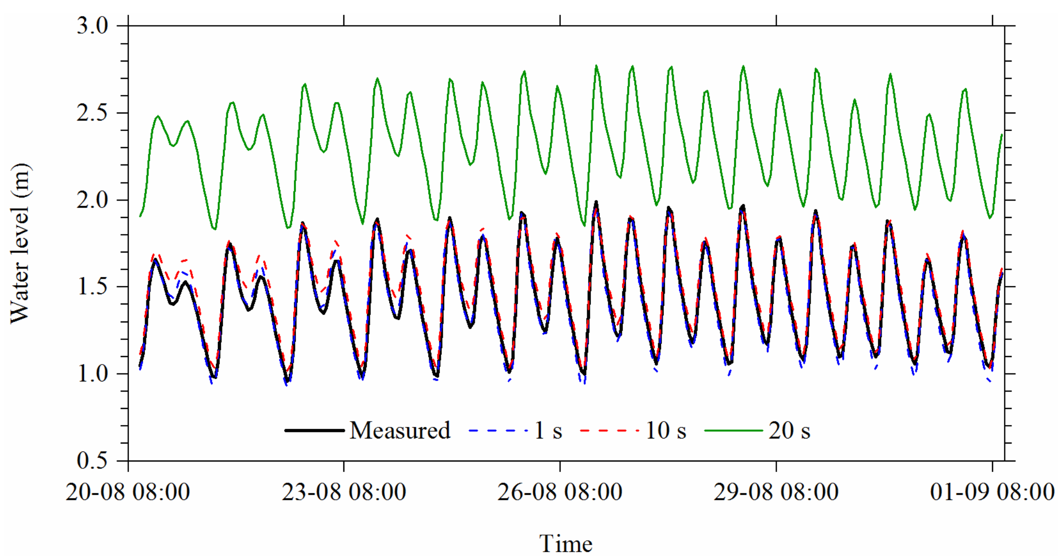

Figure 6.8 Effect of time step on water levels in the main rivers at Long Xuyen in 2014.

b. Effect of time step on hydrodynamics

The time step Δt = 1, 5, 8, 10, and 20 s were tested to determine the most suitable value in terms of accuracy and simulation time. In general, increasing the time step reduces the simulation time but significantly reduces the accuracy of the model. Fig. 6.8 depicts the time series of the water levels under different time steps. Fig. 6.9 shows that the accuracy is relatively similar while the simulation time is significantly different when the time step is within 1-10 s. When Δt = 20 s, although the simulation time significantly reduces but the accuracy is very low (Fig. 6.8-6.9). Therefore, Δt = 10 s is selected, leading to the maximum Courant number of 0.78.

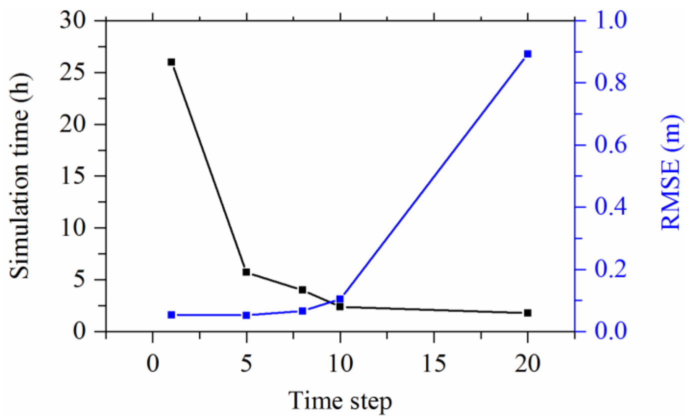

Figure 6.9 Sensitivity of time step on the model accuracy and simulation time at Long Xuyen.

c. Effect of friction coefficient on hydrodynamics

The Manning coefficient significantly affects the results of the hydrodynamics which further affects the results of the sediment transport and riverbed evolution models. Based on the results of the single Telemac-2D model established before, three zones of the Manning coefficient were selected as the starting point. Then based on the obtained results, more divisions of the Manning coefficient were tested. Various values of the Manning coefficients in the range of 0.01-0.15 were tested for the floodplains, channels, and rivers. Finally, the Manning coefficient of the floodplain was 0.15, based on a suggestion of Mtamba et al., (2015) and the Manning coefficient in the range of 0.015-0.04 was spatially assigned to the channels and rivers (Fig. 6.10).

In general, increasing Manning coefficient reduces the magnitude and range of water level fluctuations and vice versus. Fig. 6.11 shows time series of water levels under different Manning coefficient. It is clear that the water level is shifted upward when increasing the Manning coefficient.

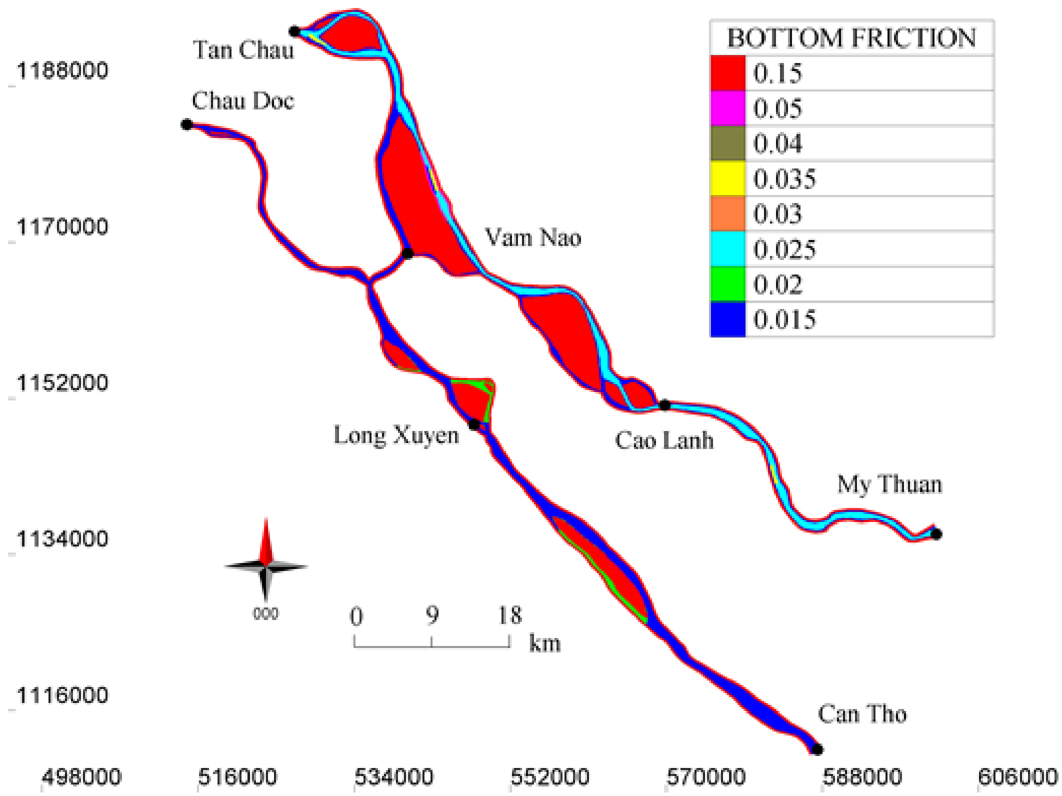

Figure 6.10 Spatial distribution of the Manning coefficient in the coupled model.

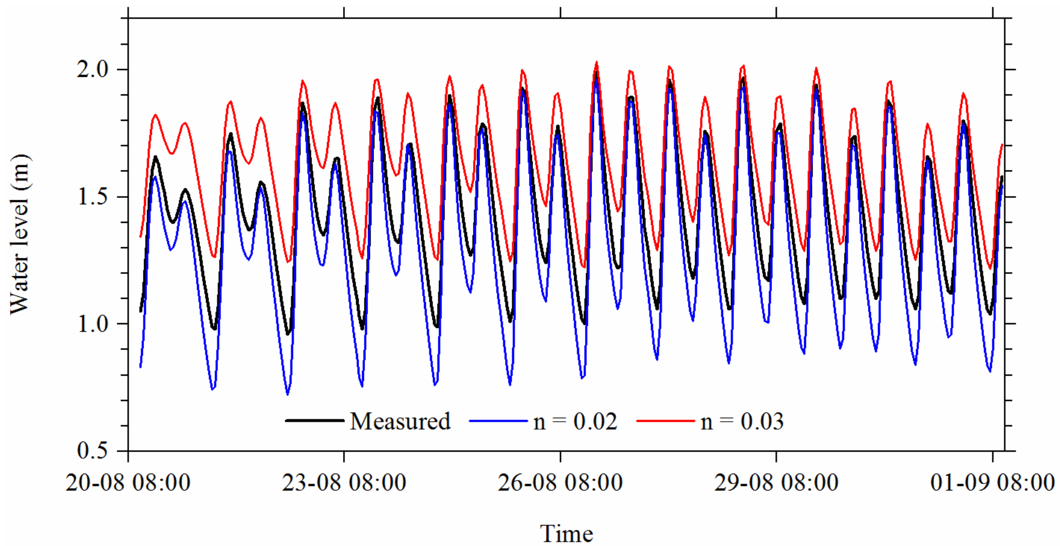

Figure 6.11 Effect of Manning coefficient on water levels in the main rivers at Long Xuyen in 2014.

d. Effect of Partheniades number and critical shear stress for erosion on cohesive sediment transport and riverbed evolution

For cohesive sediment, the Eq. B6.16 (Appendix B) indicates that M and τ_{ce} have an opposite influence on the erosion flux. Increasing M increases the riverbed erosion, leading to increasing the SSCs because such eroded sediment becomes resuspension (Fig. 6.12). Values of M in the range of 1-5x10^{-6} were tested and M = 1x10^{-6} was selected.

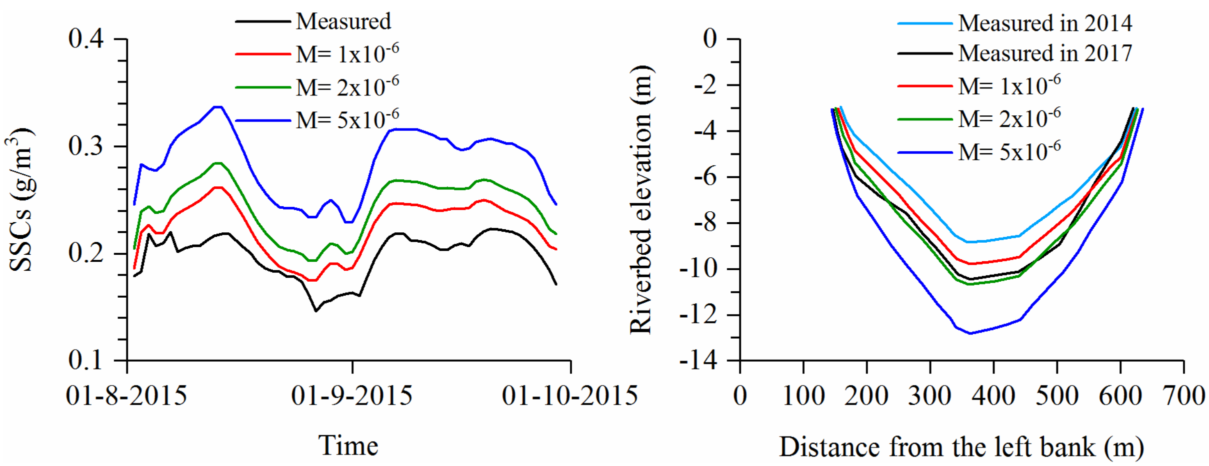

Figure 6.12 Effect of M on the erosion flux of cohesive sediment transport and bed evolution. Left panel: SSCs at Vam Nao. Right panel: bed elevation at CS-4.

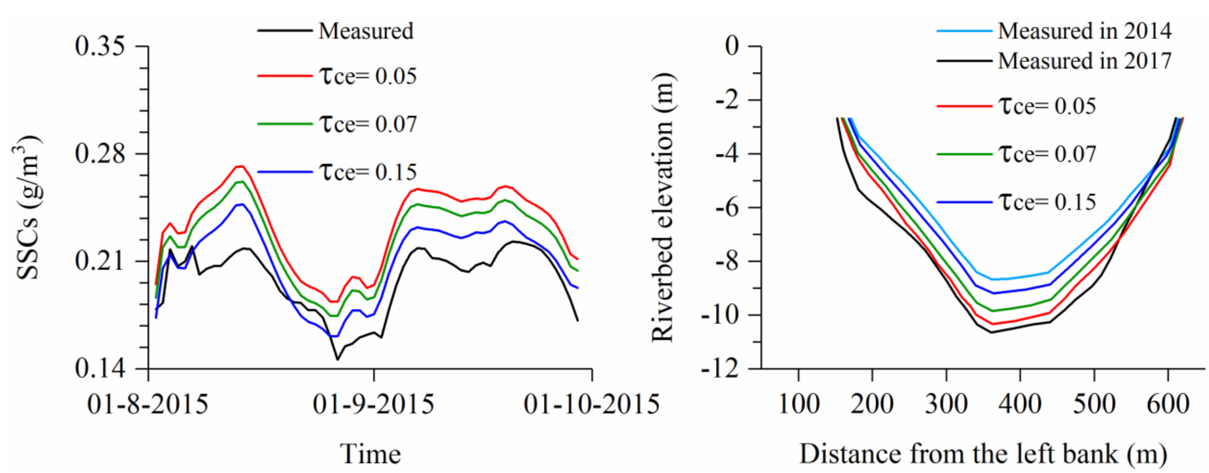

Figure 6.13 Effect of τ_{ce} on the erosion flux of cohesive sediment transport and bed evolution. Left panel: SSCs at Vam Nao. Right panel: bed elevation at CS-4.

In contrast, increasing τ_{ce} reduces the riverbed erosion rate because the shear strength of the sediment particles increases (Fig. 6.13: right panel). As a result, the amount of the SSCs that are transited from the re-suspended sediment is small (Fig. 6.13: left panel). The values of τ_{ce} in the range of 0.02-0.25 were tested and τ_{ce} = 0.15 was selected. This value is compatible with Letrung et al., (2013).

e. Effect of critical shear velocity for deposition and settling velocity on cohesive sediment transport and riverbed evolution

Different values of u_*^{cr} in the range of 0.03-0.001 were tested to find the most suitable value. It was found that the model is not markedly sensitive to a wide range of u_*^{cr} (Fig. 6.14). Increasing u_*^{cr} increases the deposition flux, leading to reduction of the SSCs. u_*^{cr}= 0.03 was selected. Fig. 6.15 shows that the model is more sensitive to changes of ω_s which was tested in the range of $4.3x10^{-6}$-$6x10^{-4}$. More sediment become deposited when increasing ω_s, therefore, the riverbed become less eroded, that reduces the SSCs. The most suitable value of ω_s is $6.6x10^{-5}$.

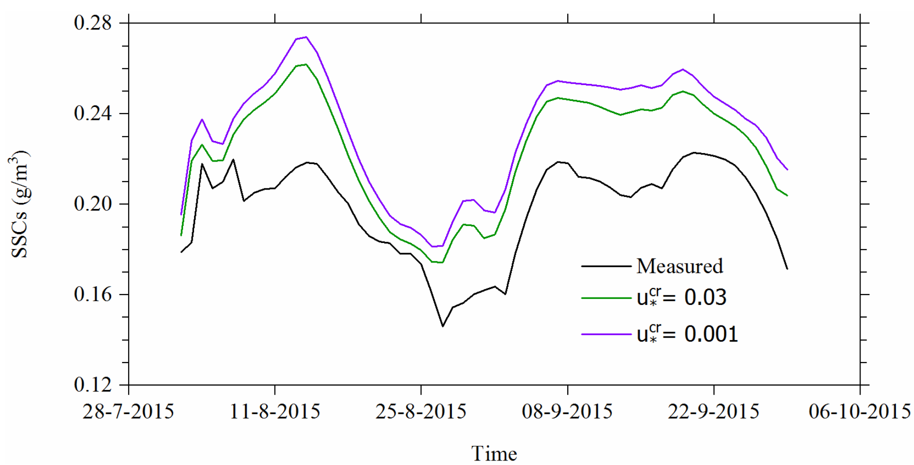

Figure 6.14 Effect of u_*^{cr} on the deposition flux of cohesive sediment transport.

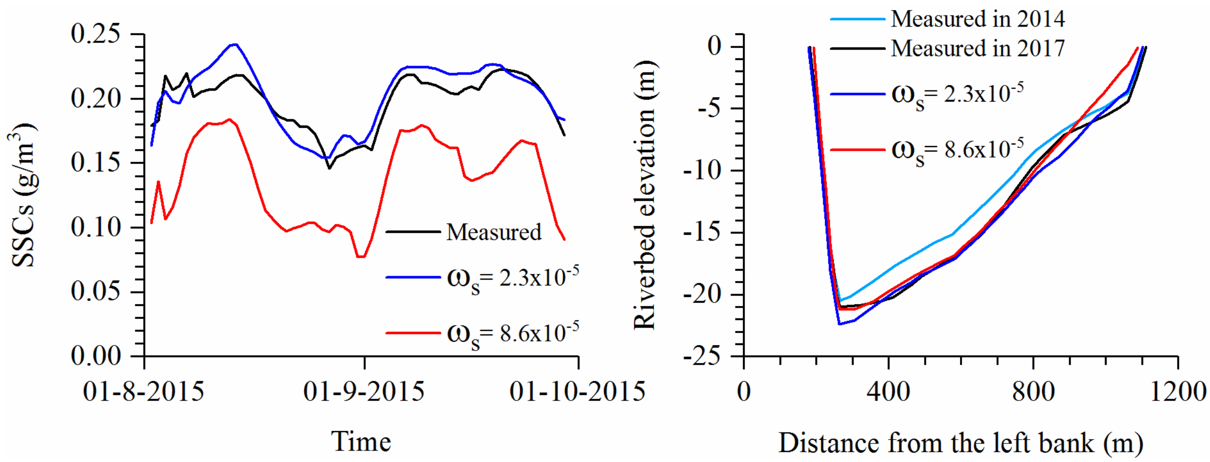

Figure 6.15 Effect of ω_s on the deposition flux of cohesive sediment transport and bed evolution. Left panel: SSCs at Vam Nao. Right panel: bed elevation at CS-3.

Table 6.3 Best values of the coupled model parameters.

Parameters	Value	Parameters	Value
Floodplain size (m)	200-300	M ($kg/m^2/s$)	$1x10^{-6}$
Δt (s)	10	τ_{ce} (N/m^2)	0.15
ν (m^2/s)	10^{-6}	u^{cr}_* (m/s)	0.03
Type of advection	14;5	ω_s (m/s)	$6.6x10^{-5}$
FSC	0.5	C_{eq}	Zyserman-Fresoe
n in floodplain ($m^{1/3}/s$)	0.15	k_s	2.5
n in rivers ($m^{1/3}/s$)	0.015-0.04	ρ_s (kg/m^3)	1,590
IMD/IMV	1/1	Dispersion coefficient (σ)	0.1

Table 6.4 Evaluation of the model performance.

Stations	Water level			SSCs		
	RMSE (m)	NSE	R^2	RMSE (g/m^3)	NSE	R^2
Vam Nao	0.12	0.81	0.89	0.04	0.69	0.83
Cao Lanh	0.09	0.94	0.94			
Long Xuyen	0.07	0.96	0.98			

f. Best model parameters

More than 100 runs have been simulated to evaluate the sensitivity of the coupled model to various physical and numerical parameters, of which the most sensitive parameters among the others were analyzed above. Table 6.3 shows the best value of each parameter. The performance of the model through evaluation indicators are shown in Table 6.4. Fig. 6.16 and 6.17 compare the measured and simulated SSCs and riverbed elevation, respectively, of the coupled model after calibration.

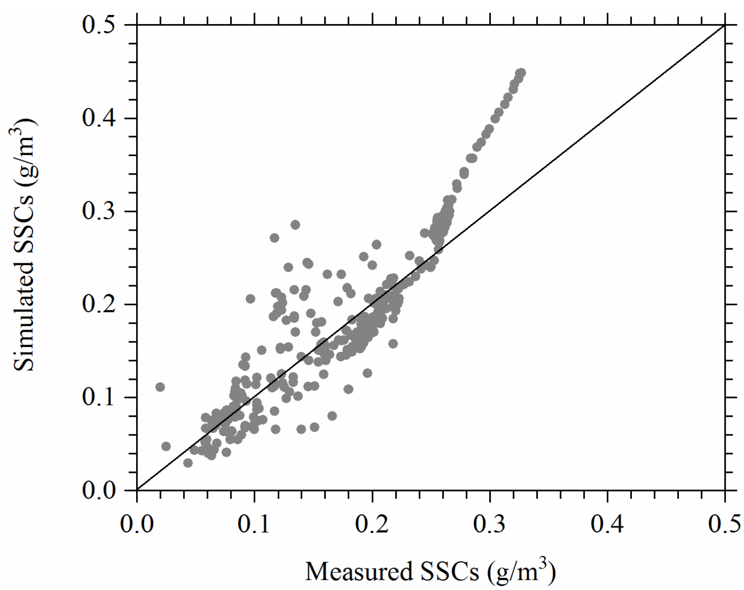

Figure 6.16 Measured versus simulated SSCs after calibration of the coupled model.

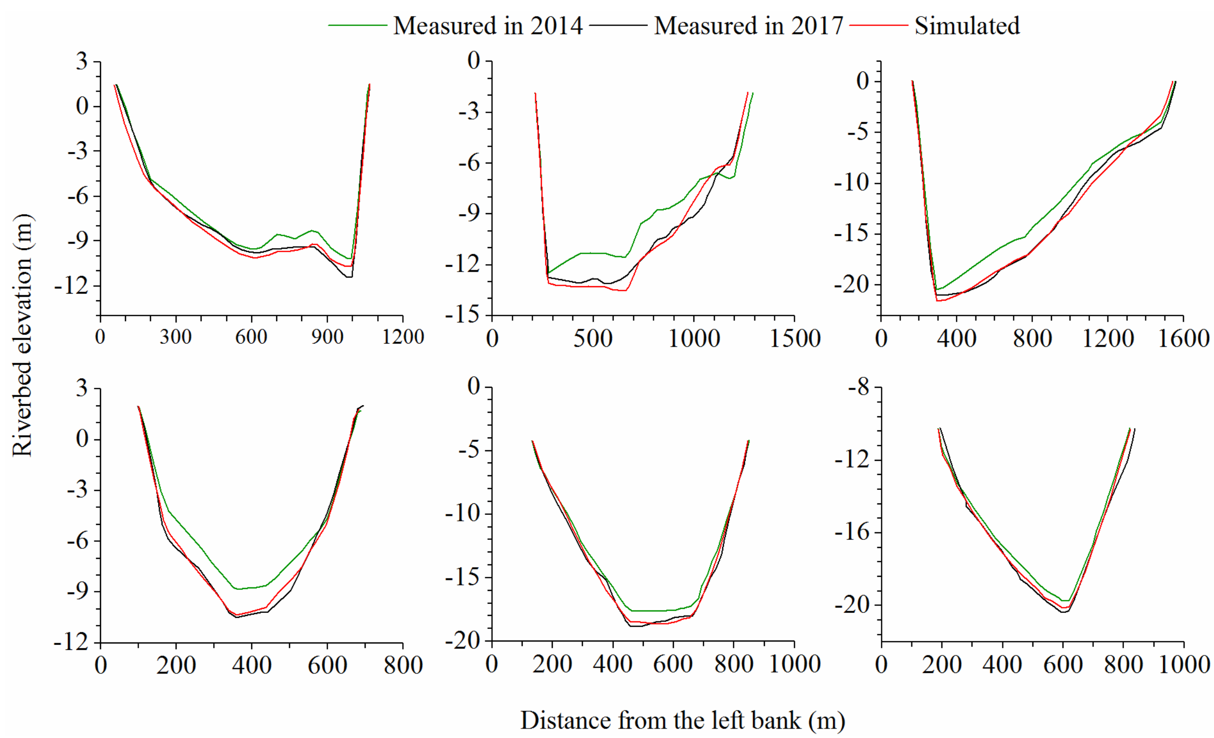

Figure 6.17 Measured versus simulated riverbed elevation after calibration of the coupled model.

6.6 Conclusions

In this chapter, two numerical models are established. The single Telemac-2D model simulates the flow alterations in the low-flow season under imposed changes in the flow conditions and riverbed degradation which are supposed due to dam impacts. More realistic, the coupled Telemac-2D and Sisyphe model first simulate the riverbed evolution during the high-flow season under dam impacts. The altered river geometry is then input into the single Telemac-2D model to simulate the water level alteration during the low-flow season. The results of these two models are analyzed in Chapter 7.

Both single and coupled models were sensitively evaluated by considering various physical and numerical parameters involved in affecting the model result. The influence of each parameter was tested for a wide range of value, of which the starting value was usually based on the results of prior researches. From sensitive analysis, resulting in high values of evaluation parameters (e.g., R^2, NSE, and RMSE), both single and coupled models are reliable to be used to evaluate dam impacts on the possibility in obtaining the intake water for irrigation in the VMD that is strongly controlled by morphological changes induced by upstream hydropower dams.

Chapter 7 Impacts of upstream dam development on long-term morphological changes and associated impacts on the irrigation possibility in the low-flows in the Vietnamese Mekong Delta

7.1 Introduction

The suspended sediment budget in the VMD has been significantly reduced since completions of numerous hydropower dams in the MRB, which were long-term analyzed in Chapter 4. Reductions in the sediment supply from the MR may, in turn, lead to the alterations in the geomorphologic characteristics and hydraulic geometric behavior of the VMD rivers, which were analyzed in Chapter 5. Riverbed is at risk from degradation and riverbank is vulnerable to be eroded, as can be seen in Fig. 5.18-5.19 and 5.21-5.22. Once the geomorphology is degraded, the water levels in the rivers become lower even the discharge may increase that may disrupt the connectivity between the rivers and floodplains, leading to difficulty in obtaining intake water for irrigation and in getting naturally fertile suspended sediment for the agricultural crops in the floodplains.

Two numerical models were established in Chapter 6, including a single Telemac-2D to simulate the hydrodynamics in the low-flow season and a coupled Telemac-2D and Sisyphe model to simulate the hydro-sediment-morphodynamics and morphological changes during the high-flow season of the VMD under effects of hydropower dams. The ultimate goal of this chapter is to evaluate the effects of the altered morphology of the VMD rivers (resulted from the coupled model) on the possibility in obtaining intake water for irrigation during the lowest water months, e.g., April so that countermeasures are then proposed to overcome the problems.

The single model investigates the effect of imposed increased flow discharges and degraded riverbed on low-flow water levels. The results of the single model motivate the establishment of the coupled model which is more complicated and realistic. There are two main purposes of the coupled model. First, it predicts long-term morphological changes of the VMD rivers under reduced sediment supply from the MR due to dam impacts. Second, the altered morphology is input into the single model to simulate the low-flow water level alterations that may affect the irrigation possibility in the VMD. Subsequent sections are the results of the established models.

Table 7.1 Nineteen simulated scenarios by increasing inflow discharges and lowering river bed in the single Telemac-2D model.

Bed elevation (Z_b)	Discharge (Q)				
	Q0	Q0+10%	Q0+20%	Q0+25%	Q0+50%
Z_b0	Sc0	Sc4	Sc9		Sc14
Z_b0-0.75m	Sc1	Sc5			Sc15
Z_b0-1.5m	Sc2	Sc6	Sc10	Sc13	Sc16
Z_b0-3m		Sc7	Sc11		Sc17
Z_b0-6m	Sc3	Sc8	Sc12		Sc18

7.2 Results of the single model: low-flow water level alterations due to regulated flow discharges and degraded riverbed in the VMD

7.2.1 Simulation scenarios

The nineteen scenarios in Table 7.1 are proposed to evaluate the impacts of water level changes under increased flow discharges and riverbed degradation on the possibility of rice crop' irrigation. The worst conditions for changes in water levels are in April 2017, as the recorded water levels were the lowest during this year under different scenarios of discharges and bathymetry.

The baseline (Sc0) considers the discharges, water levels and bathymetry of April 2017. Four options of the increased flow discharges by 10%, 20%, 25% and 50% at upstream boundaries (Tan Chau and Chau Doc) are considered. These scenarios are designed based on the median discharge in the flow-flow season at Tan Chau that increased by 10% in the postdam period (2012-2015) compared to the predam period (1980-1992) (Fig. 3.17). Fig. 5.18-5.19 and 5.21-5.22 show that the riverbeds in the VMD are both degraded and aggraded. However, the degradation is dominant throughout the study domain while the aggradation occurred near banks in limited areas and magnitudes. Moreover, the river bank erosion is also taken place in various locations in the delta. However, due to a lack of data, the effect of river bank erosion is not considered in this chapter. As a hypothesis, four options of the riverbed degradation of 0.75 m, 1.5 m, 3 m, and 6 m associated with 2017 bathymetry are simulated. The four scenarios are related to low (degradation < 1.5 m), moderate (1.5 m ≤ degradation ≤ 3 m), and high (3 m < degradation ≤ 6 m) river bed degradation. These considerations are based on an average reduction in the riverbed of 1.5 m in between 2017 and 2014 as analyzed Chapter 5. Such a uniform degradation applied throughout the study domain is not really realistic but acceptable because the general mechanism of the water level changes responding to the riverbed degradation is intentionally investigated. The more realistic simulations of the riverbed changes due to the reduced sediment supply from the MR, that will affect the water level alterations, is considered in the coupled Telemac-2D and Sisyphe model.

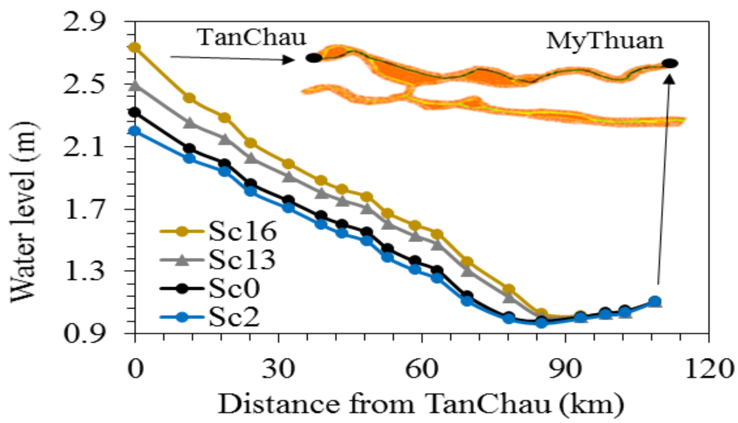

Figure 7.1 Mean daily maximum water levels along the Tien River, having the same river bathymetry with different discharges.

Table 7.2 Changes of the water levels (%) at Tan Chau, comparing scenarios to the baseline (Sc0). "+": increase; "-": decrease.

Reduced riverbed (m)	Increased discharge				
	0	10%	20%	25%	50%
0	0	7	14		23
0.75	-3	2			20
1.5	-4	0	5	8	18
3.0		-2	2		14
6.0	-11	-6	-3		8

7.2.2 Influence of regulated flow discharges

In order to assess the influence of the increased flow discharges due to dam operations on the water level in the VMD, a reduction of 1.5 m of the originally measured bathymetry in 2017 is considered as a representative geometry. Fig. 7.1 depicts that the water levels in April in the VMD increase by increasing the flow discharge under the same domain geometry. Table 7.2 shows that, the mean water levels in April at Tan Chau, on average, increase by 4%, 9%, 12%, and 22% if the flow discharges increase by 10%, 20%, 25% and 50%, respectively (Sc6, Sc10, Sc13, and Sc16 compared to Sc2). The amplitude of the water level increase reduces longitudinally to downstream locations due to the effect of the simulated constant water levels at the downstream boundaries. As a result, the influence of the increased river discharge diminished with the increased distance from the upstream at 90 km (Fig. 7.1).

7.2.3 Influence of riverbed degradation

Under the same discharge, the cross-sectional area will increase if the riverbed is degraded. This leads to a reduction in the water level accordingly. For example, the mean water levels in April at Tan Chau, on average, decrease by 3%, 5%, 9%, and 15% under reductions of 0.75 m, 1.5 m, 3 m, and 6 m, respectively, of the riverbed by comparing Sc15, Sc16, Sc17, and Sc18, respectively, to Sc14 (Table 7.2).

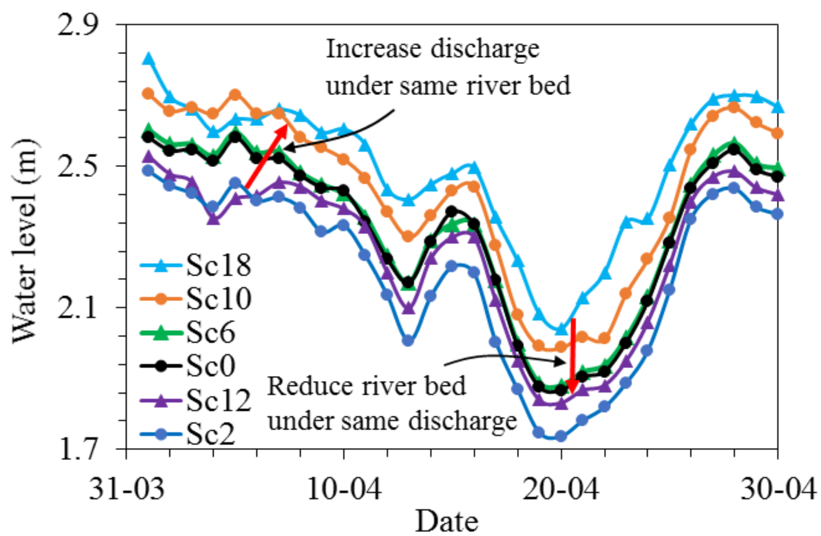

Figure 7.2 Changes of the mean daily maximum water levels at Tan Chau under various scenarios.

7.2.4 Combined impacts of the increased flow discharge and degraded riverbed on the water levels

Table 7.2 and Fig. 7.2 show that, compared to the baseline (Sc0), the mean water level in April at Tan Chau reduces by 4% when the riverbed degrades by 1.5 m (Sc2). It then gradually increases by 4% and 9% under the increases of 10% and 20% of the flow discharge, respectively (Sc6 and Sc10 compared to Sc2). Reversely, the water level reduces by 8% with further degradation of 4.5 m of the riverbed (Sc12 compared to Sc10). However, a further increase of 30% discharge helps increase the water level by 11% (Sc18 compared to Sc12).

If the riverbed degrades by 1.5 m, an increase of 10% in the flow discharge will help conserve the water level (Sc6 compared to Sc0) (Table 7.2 and Fig. 7.6). Table 7.2 also indicates that to maintain the water level unchanged when the riverbed degrades by 4.5 m, the flow discharge should be increased by 25% (compared Sc18 to Sc13).

Another important result from Table 7.2 is that when the riverbed degrades by 6 m (Sc12), an increase of 20% of the flow discharge is not enough to conserve the water level as same as the baseline. However, an increase of 50% of the flow discharge is advantageous (Sc18).

Table 7.3 Simulation scenarios of the coupled model under reduced sediment supply from the MR due to dam impacts.

Scenarios	Discharge	Water level	SSC	Total change of sediment budget (2026 vs 2017) (%)
ScA	Same as 2017	Same as 2017	Same as 2017	--
ScB	Same as 2017	Same as 2017	Based on long-term sediment reduction in Chapter 6 **2017** → **2026**	-17.5%
ScC	Same as 2017	Same as 2017	Based on Kondolf et al., (2014) **2017** → **2019** → **2020** → **2026**	-84.8%

7.3 Results of the coupled model: hydro-sediment-morphodynamics, morphological changes, and associated influence on irrigation water intake in the VMD under reduced sediment supply from the MR due to upstream dam development

7.3.1 Simulation scenarios

In simulating the riverbed evolution of the coupled model under upstream dam impacts, the 2017 geometric data which were measured during the field survey in August-September 2017 were used. Impacts of dams on riverbed evolution last for a long period, i.e., in decades. Therefore, the effects of reduced sediment supply from the MR induced by hydropower dams on riverbed evolution are assessed for the projected 10-year period of 2017-2026. The boundary conditions are discharge, water levels, SSCs, and river geometric data of 2017.

Table 7.4 Monthly sediment reduction in the VMD under ScB.

Month	% of the year	Predam SSL (Mt/yr)	Sediment reduction rate (Mt/yr)	% reduction of annual SSL
June	2.5	4.2	-0.1	-2.3
July	10.0	16.7	-0.35	-2.1
August	24.3	40.6	-0.65	-1.6
September	27.1	45.2	-0.97	-2.1
October	19.4	32.3	-0.95	-3.0
November	10.0	16.6	-0.76	-4.6
December	4.1	6.7	-0.36	-5.3

There are three scenarios being considered (Table 7.3). ScA considers the flow and sediment conditions of 2017 which are kept unchanged till 2026. ScB considers the unchanged flow conditions of 2017 till 2016. The monthly sediment budget is reduced with rates analyzed in Chapter 4, which are shown in Table 4.1. Noticeably, the coupled model simulates for the high-flow season, from June to December, during which 97.4% of the annual sediment budget of the MR is transported. Eq. 7.1 calculates the boundary condition of the SSC of the considered year based on the previous year with annual reduction rates of the monthly suspended sediment budget shown in Table 7.4. In Table 7.4, the predam suspended sediment budget entering the VMD is 166.7 Mt/yr which was estimated in Chapter 4.

$$Daily\ SSC\,(year_{i+1}) = Daily\ SSC\,(year_i) \times \%\,reduction \tag{7.1}$$

If 133 planned dams in the MRB are built by 2020, the sediment budget of the MR that reaches the VMD is only 4% of the predam condition (Kondolf et al., 2014). For that the sediment budget of the VMD in 2020 will be 4%x166.7 = 6.7 Mt/yr. It implies that 84.8% of the SSL of the VMD in 2017 (43.9 Mt/yr) will be reduced if such 133 dams are built by 2020. Therefore, stemming from this hypothesis, ScC considers unchanged flow conditions of 2017 till 2026. The sediment budget of 2017 is kept unchanged until 2019 with an assumption that the basin development is not significant during this period. Considering 133 dams are completed by 2020, the sediment budget of 2019 is reduced by 84.8%, then remains unchanged till 2026 (Table 7.3).

7.3.2 Sediment dynamics in the VMD

Temporal variations, i.e., daily, monthly, and annual of the suspended sediment dynamics in the VMD, were analyzed in Chapter 4. Therefore, the spatial distribution of the suspended sediment is analyzed in this section through the analysis of the SSCs resulted from the coupled model. Fig. 7.3 depicts the spatial distribution of the SSC in the upper part of the VMD in the high-flow season. Generally, the SSCs in the Tien River are much higher than those in the Hau River. Close to the inlets (at Tan Chau and Chau Doc), the SSC in the Tien River is more than double that in the Hau River while the corresponding number is approximately more than unity close to the outlets (at My Thuan and Can Tho). In the Tien River, the SSC slightly reduces longitudinally from Tan Chau to My Thuan. In particular, the SSC at My Thuan is approximately 85% of that at Tan Chau. In the Hau River (Fig. 7.3), the SSC is low in the Chau Doc- Point C section. Downstream of Point C, the SSC sharply increases, almost double. Such increased SSC is diverted from the Tien River via the Vam Nao channel. From Point C to Can Tho, the SSC gradually decreases.

The spatial distribution of the SSC in the transition-flow season is shown in Fig. 7.4. Clearly, the transition-flow SSCs are significantly lower than the high-flow SSCs. Particularly, the mean SSC along the Tien River on August 11, 2014 is more than 8 times larger than that on November 5, 2014. The corresponding number for the Hau River is more than 4 times (Fig. 7.3 vs Fig. 7.4). There is no significant difference in the SSC between the Tien and Hau River in the transition-flow season. The general patterns of the SSC in both rivers are a longitudinal reduction.

Table 7.5 shows the sediment distribution at the vicinity of Point A and C confluences in the Tien and Hau Rivers. In other words, the table shows how much the Tien River diverts the suspended sediment to the Hau River via the Vam Nao channel. During June-December of 2014-2017, the Tien River diverts 40-50% of the suspended sediment to the Vam Nao channel while the remaining transports downstream, heading to My Thuan. During 2014-2017, the Tien River diverts, on average, approximately 44% of its suspended sediment to the Vam Nao channel in both high-flow (August-October) and transition-flow seasons (June-July and November-December). On the other hand, the Vam Nao channel contributes 60-80% the Hau River's suspended sediment (at Point C) during June-December of 2014-2017 (Table 7.5). On average, the Vam Nao channel contributes 72% and 75% of the Hau River's suspended sediment in the high-flow and transition-flow, respectively, during 2014-2017. The suspended sediment of the Vam Nao channel that contributes to the Hau River is from the Tien River and from resuspended sediment through riverbed incision.

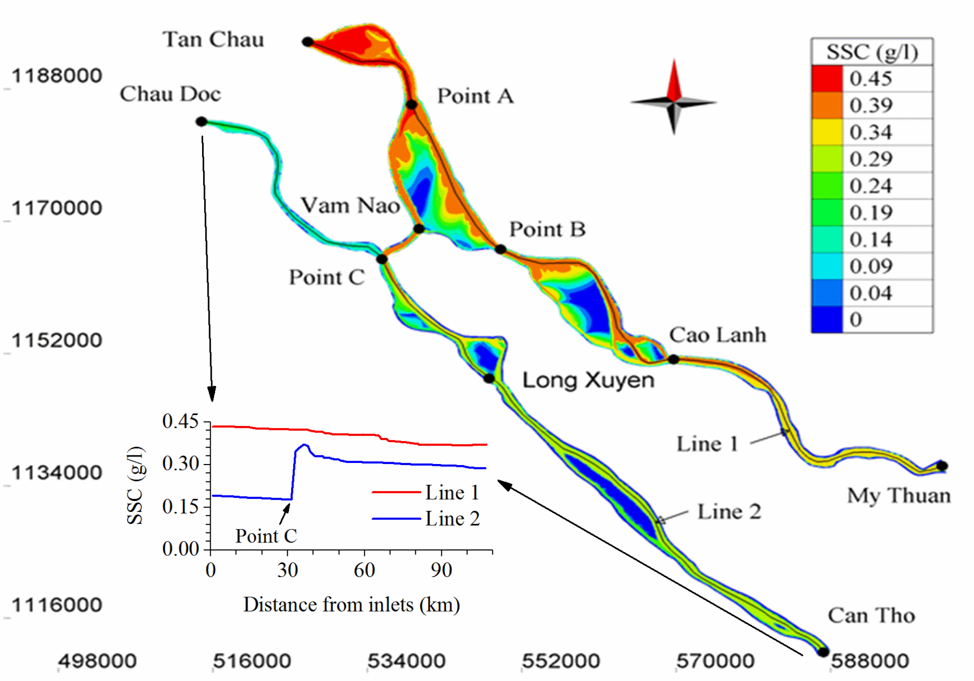

Figure 7.3 Simulated SSC distribution in the VMD in the high-flow season on August 11, 2014.

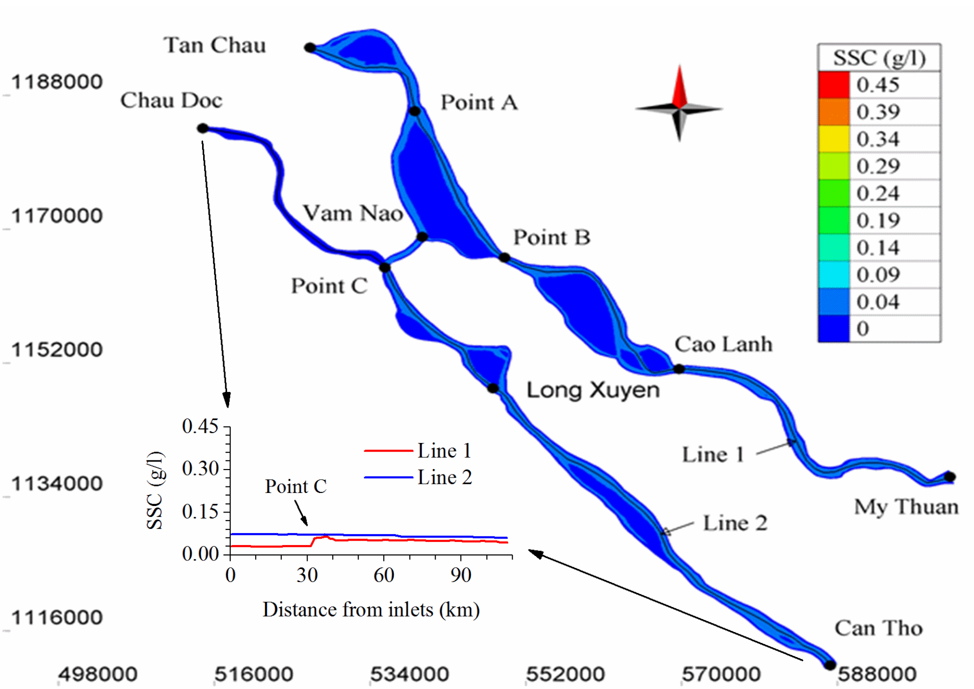

Figure 7.4 Simulated SSC distribution in the VMD in the transition-flow season on November 5, 2014.

Table 7.5 Suspended sediment discharges (m^3/s) at Poin A and Poin C confluences, showing the diversion from the Tien River to the Hau River. Values in the parentheses show the percentage (%) of sediment distribution. TR_upper A = TR_lower A + VN_lower A; HR_lower C = HR_upper C + VN_upper C. TR: Tien River, HR: Hau River, and VN: Vam Nao. A, B, and C are point A, B, and C, respectively.

Year	Month	Location					
		TR_upper A	TR_lower A	VN_lower A	HR_upper C	VN_upper C	HR_lower C
2014	June	0.28 (100)	0.16 (57.1)	0.12 (42.9)	0.08 (24.2)	0.25 (75.8)	0.33 (100)
	July	1.7 (100)	0.95 (55.9)	0.75 (44.1)	0.32 (20.6)	1.23 (79.4)	1.55 (100)
	August	4.21 (100)	2.38 (56.5)	1.83 (43.5)	0.91 (25.8)	2.62 (74.2)	3.53 (100)
	September	3.19 (100)	1.79 (56.1)	1.4 (43.9)	0.74 (27)	2 (73)	2.74 (100)
	October	1.32 (100)	0.74 (56.1)	0.58 (43.9)	0.65 (39.4)	1 (60.6)	1.65 (100)
	November	0.52 (100)	0.29 (55.8)	0.23 (44.2)	0.18 (27.7)	0.47 (72.3)	0.65 (100)
	December	0.14 (100)	0.07 (50)	0.07 (50)	0.04 (22)	0.14 (77.8)	0.18 (100)
2015	June	0.07 (100)	0.04 (57.1)	0.03 (42.9)	0.03 (25)	0.09 (75)	0.12 (100)
	July	0.35 (100)	0.19 (54.3)	0.16 (45.7)	0.07 (20)	0.28 (80)	0.35 (100)
	August	1.74 (100)	0.98 (56.3)	0.76 (43.7)	0.31 (21.5)	1.13 (78.5)	1.44 (100)
	September	1.96 (100)	1.1 (56.1)	0.86 (43.9)	0.38 (23.9)	1.21 (76.1)	1.59 (100)
	October	0.92 (100)	0.52 (56.5)	0.4 (43.5)	0.22 (24.7)	0.67 (75.3)	0.89 (100)
	November	0.23 (100)	0.13 (56.5)	0.1 (43.5)	0.06 (26.1)	0.17 73.9)	0.23 (100)
	December	0.05 (100)	0.03 (60)	0.02 (40)	0.02 (25)	0.06 (75)	0.08 (100)
2016	June	0.09 (100)	0.05 (55.6)	0.04 (44.4)	0.04 (36.4)	0.07 (63.6)	0.11 (100)
	July	0.72 (100)	0.4 (55.6)	0.32 (44.4)	0.12 (19.4)	0.5 (80.6)	0.62 (100)
	August	1.17 (100)	0.65 (55.6)	0.52 (44.4)	0.23 (23)	0.77 (77)	1 (100)
	September	2.17 (100)	1.2 (55.3)	0.97 (44.7)	0.49 (26.2)	1.38 (73.8)	1.87 (100)
	October	1.51 (100)	0.83 (55)	0.68 (45)	0.49 (30.8)	1.1 (69.2)	1.59 (100)
	November	0.8 (100)	0.44 (55)	0.36 (45)	0.27 (31.4)	0.59 (68.6)	0.86 (100)
	December	0.35 (100)	0.19 (54.3)	0.16 (45.7)	0.08 (22.9)	0.27 (77.1)	0.35 (100)
2017	June	0.61 (100)	0.34 (55.7)	0.27 (44.3)	0.1 (20.4)	0.39 (79.6)	0.49 (100)
	July	1.47 (100)	0.8 (54.4)	0.67 (45.6)	0.28 (21.9)	1 (78.1)	1.28 (100)
	August	2.34 (100)	1.27 (54.3)	1.07 (45.7)	0.65 (28.5)	1.63 (71.5)	2.28 (100)
	September	2.01 (100)	1.09 (54.2)	0.92 (45.8)	0.65 (32.2)	1.37 (67.8)	2.02 (100)

7.3.3 Morphological changes during 2014-2017 in the VMD

Fig. 7.5 shows the simulated result of the riverbed changes in the upper part of the VMD between September 2017 and September 2014. In general, the riverbed of the Vam Nao channel is the most incised. The Tien River is more incised and less deposited than the Hau River (Fig. 7.6). Fig. 6 also shows a good agreement between simulated and measured river thalweg along the Tien River. Generally, riverbed incision mainly occurs in the meandering and riffle areas and in the middle of the channel where the velocity is high while deposition mostly happens at the tail of the islands and secondary channels where the velocity is low (Fig. 7.5 and 7.7). The maximum incision depth reaches 5.5 m while the maximum deposition depth approaches 1 m. In the Tien

River, the most riverbed incision areas are from Tan Chau to Vam Nao and from Cao Lanh to My Thuan (Fig. 7.6). In the Hau River, riverbed is more incised in the upper part from Chau Doc to Long Xuyen, especially from the Hau River- Vam Nao channel confluence (at Point C in Fig. 7.4).

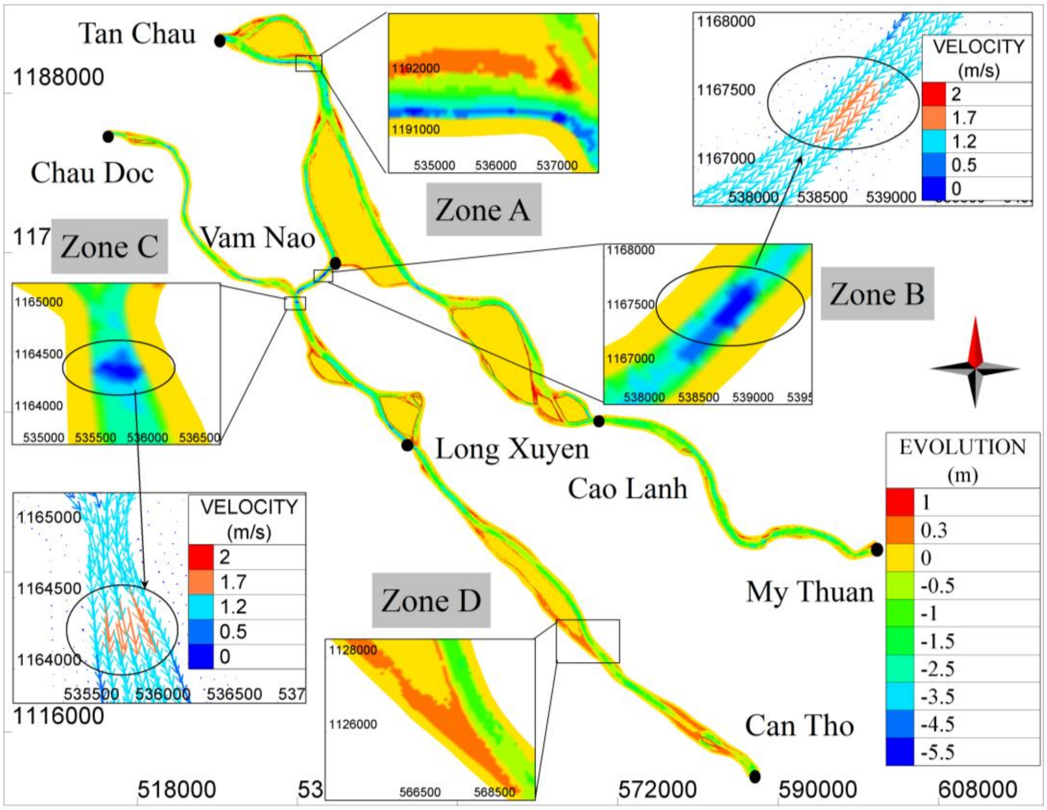

Figure 7.5 Simulated riverbed evolution of the upper VMD during 2014-2017. It shows typical local scour holes and time evolution of riverbed changes.

Annually simulated riverbed incision volume during 2014-2017 in the study domain is 79.2 Mm^3 (148.6 Mm^3 incision volume versus to 69.4 Mm^3 deposition volume) which is 5.8% underestimated compared to the measured data, having an annual incision volume of 84.1 Mm^3. On average, the mean simulated riverbed incision of the Tien River is -0.42 m over the 2014-2017 period or the incision rate is -0.14 m/yr, which are more than those in the Hau River where the mean simulated riverbed incision and incision rate are -0.31 m and -0.1 m/yr during 2014-2017. Fig. 7.6 shows typically mean longitudinal riverbed incision depths along mainstream of the Tien and Hau Rivers. In the Vam Nao channel, the mean riverbed incision and the incision rate are -2.38 m and -0.79 m/yr. The left bank of the Vam Nao channel is more prone to erosion than the right bank due to high velocity (Fig. 7.5 and 7.7). A high degree of riverbed incision in the Vam Nao channel can be attributed to recently rapid riverbank collapse which destroyed houses and harmed people lives and their properties.

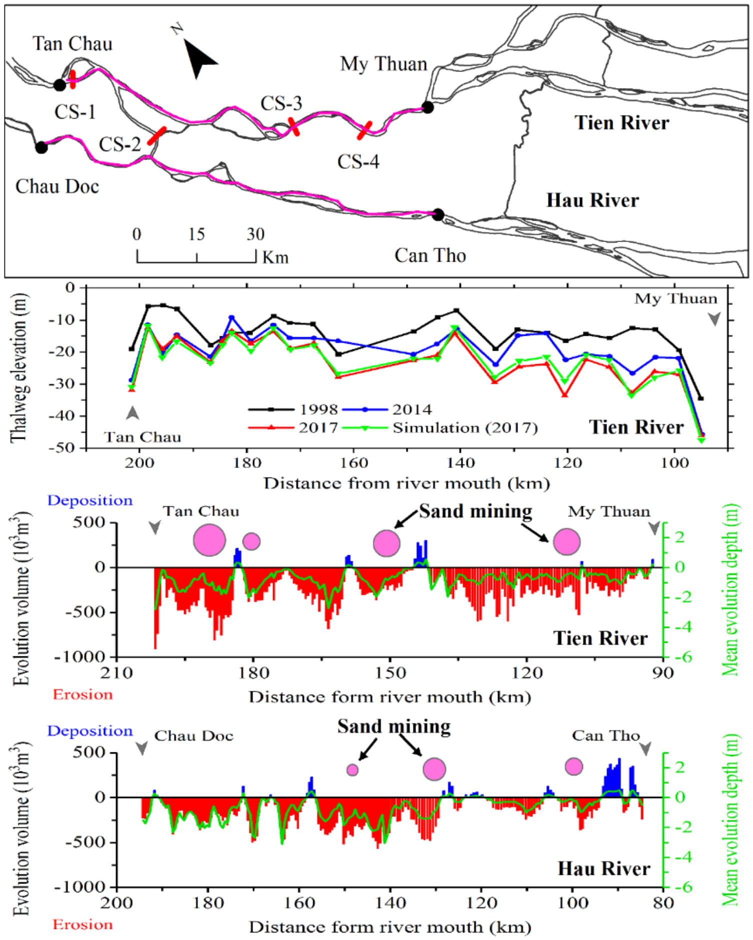

Figure 7.6 Simulated erosion and deposition volumes and mean longitudinal riverbed incision depths in Tien and Hau Rivers.

Several scour holes were developed over the simulation period, such as in zone A, B, and C in Fig. 7.7. At these scour holes, the incision rate is smallest in 2015 during which the flow and sediment discharges are lowest among the simulated years. Importantly, it appears a deep scour hole in the Hau River at zone C, just about 500-1,000 m downstream of the Hau River- Vam Nao channel confluence (Fig. 7.7). This scour hole is at around the location of the riverbank collapse that happened on 22 April 2017, being 130 m long and 30 m wide, which was widely broadcasted.

Therefore, such severe riverbank erosion is more likely the consequence of the developed scour hole.

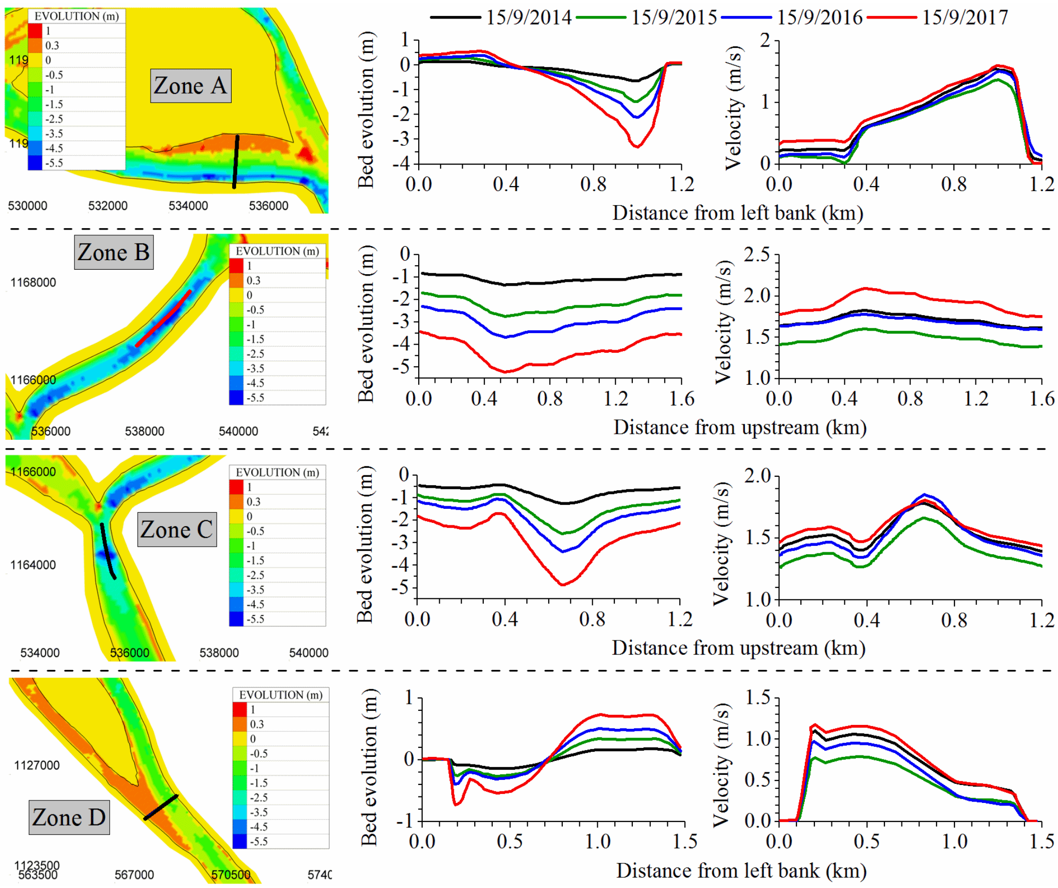

Figure 7.7 Typical locations of riverbed evolution during the simulated 2014-2017 period and associated flow velocity distributions. Locations of Zone A-D are shown in Fig. 8.3.

7.3.4 The role of sand mining in morphological changes

Fig. 7.8 shows the annual volume of sand mining in the VMD from the 2015 field survey. Sand mining mostly concentrates in the upper and middle parts of the VMD with a total volume of approximately 28 Mm^3. The figure also includes the mean annual sand mining volume which was estimated by the coupled Telemac-2D and Sisyphe model. To estimate sand mining volume from the simulation, we assumed that (1) riverbed incision by comparing the measured 2014 and 2017 bathymetries is caused by combined upstream dams and sand mining effect and (2) riverbed incision during 2014-2017 from the simulation is due to upstream dams alone because we did not incorporate sand mining effect in the coupled model. Therefore, the difference in riverbed incision between measured data and simulated results during 2014-2017 is due to sand mining alone. In general, the simulated sand mining in the upper reach of the VMD is overestimated by comparing with that from the field survey. Particularly, sand mining volume in the upper reach of the VMD from the field survey was approximately 16 Mm^3 compared to approximately 19.4 Mm^3 from the simulation. In other words, sand mining volume from the simulation was about 21.3% greater than that from the field survey.

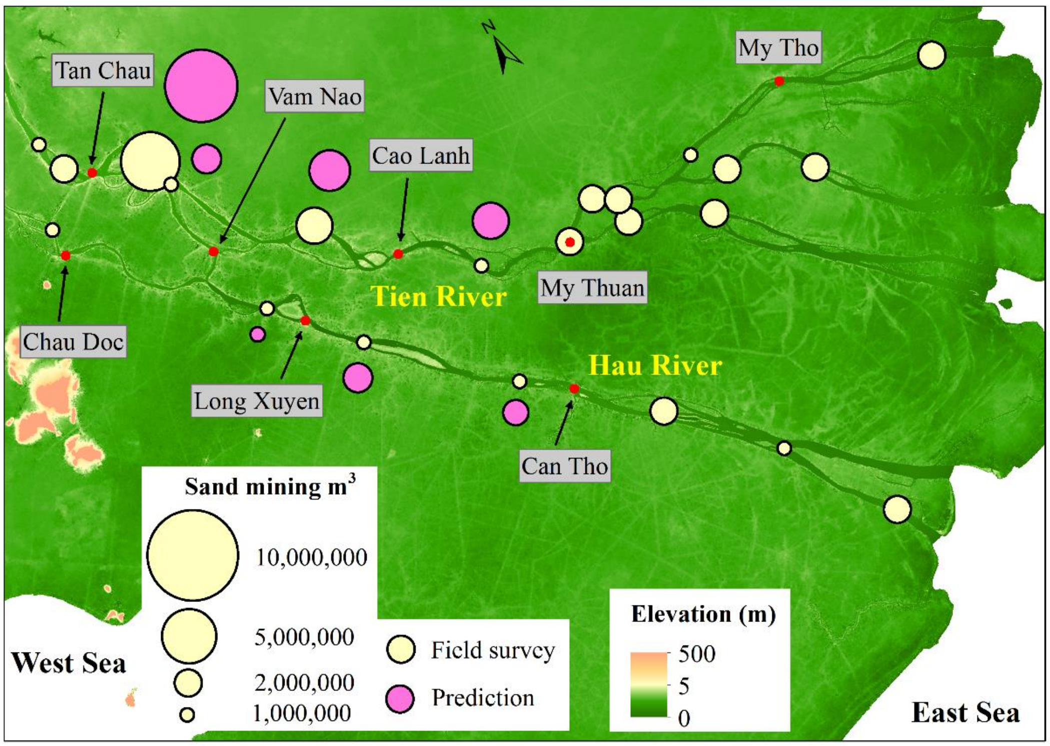

Figure 7.8 Annual volume of sand mining in the VMD estimated from field survey in 2015 and from the coupled Telemac-2D and Sisyphe model during 2014-2017.

There are likely two main possibilities for the difference between the simulated and licensed sand mining volumes. First, the resolution of the measured bathymetric data in 2014 and 2017 was not high, therefore, the difference between the two measured bathymetric data in 2017 and 2014 may have limitations, and thus the input geometric data for the model may remain some uncertainties. Second, the volume of sand mining that was provided by local authorities and/or sand miner during field surveys is more likely underestimated with two main reasons: (1) the mining companies extracted a much greater amount of sand than the licensed volume, and (2) illegal individual miners may extract a great volume of sand that was not recorded by the authorities or any organization. Given these, the simulated amount of sand mining of 19.4 Mm^3/yr during 2014-2017 in the upper reach of the VMD (Fig. 7.8) from the simulation is relatively reasonable. Even overestimated, sand mining is responsible for 23.1% of the riverbed incision in the upper reach of the VMD while the remaining 76.9% is attributed to the effect of upstream hydropower dams that trapped most of the bedload and great amount of suspended load. Importantly, sand mining is more concentrated in the upper reach of the VMD, therefore, sand mining is more likely responsible for less than 20% of riverbed incision in the whole VMD. Reminding from Chapter 4 that hydropower dams are the main driver of 74.1% suspended sediment reduction in the VMD during 2012-2015, from the predam period. Therefore, it can be concluded that hydropower dams cause large-scale morphological degradation in the VMD while sand mining causes local scours on a much smaller scale.

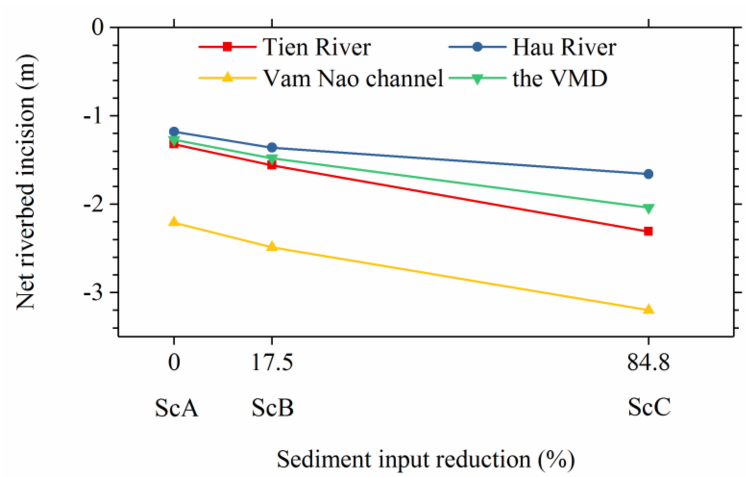

Figure 7.9 Net mean riverbed incision in the VMD rivers under different scenarios of hydropower dam-induced sediment supply reductions.

7.3.5 Effect of dam-induced sediment reduction on morphological changes in the VMD

Although the current sediment supply to the VMD remains unchanged during 2017-2026 (ScA), the riverbeds will be significantly incised over the next ten years, by 2026 (Fig. C7.1). This indicates the transport capacity of the VMD rivers already exceeded and will continue exceeding the sediment supply from the MR by 2026. Riverbed incision largely occurs in all rivers. The riverbed incision is signified under reductions of 17.5% (ScB) and 84.8% (ScC) (Fig. C7.2-C7.3).

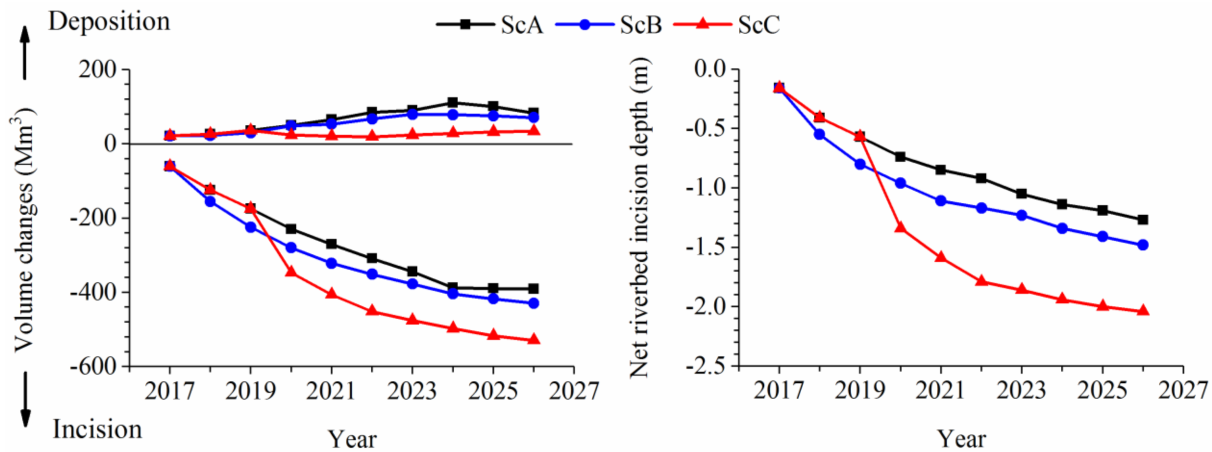

Figure 7.10 Annually simulated mean riverbed changes in the VMD under different scenarios of sediment supply reductions.

Fig. 7.9 depicts the net mean riverbed incision depths (the difference between incision and deposition) in the Tien, Hau and Vam Nao rivers and the VMD under different scenarios. The most severe incision is the Vam Nao channel, followed by the Tien River. From Tan Chau/ Chau Doc to the Vam Nao channel, the riverbed of the Tien River is more incised than the Hau River while the Hau River is more incised than the Tien River from the Vam Nao channel to My Thuan/ Can Tho (Fig. C7.4). Fig. C7.4 also shows that riverbed incision in the upper parts: from Tan Chau to Vam Nao in the Tien River and from Chau Doc to Long Xuyen in the Hau River is faster than that in the lower parts: downstream of Vam Nao and Long Xuyen in the Tien and Hau Rivers, respectively. Additionally, riverbed incision is faster in the first five years during 2017-2022 than the later five years during 2022-2026. On average, the net mean riverbed incision of the VMD by the end of 2026 is -1.27 m in ScA, -1.48 m in ScB, and -2.04 m in ScC. Fig. 7.10 shows the annually predicted mean riverbed changes in the VMD during 2017-2026 under different scenarios of sediment supply reductions. In general, the riverbed is more dynamics in the first several years, then becomes more stable later on. In ScC, the riverbed is rapidly incised in 2020 when 84.8% of sediment supply suddenly decreases during 2019-2020. Such kind of rapid riverbed incision continues for several years later before it becomes more stable.

During the projected ten years of simulation, 2017-2026, several large-scale deep scour holes appear (Fig. 7.11 and C7.5). The most severe scour hole is at zone C with a maximum scour depth of more than 16 m in ScC. At zone A, the scour hole tends to appear on the right bank with a maximum depth of approximately 11 m. The depth and extent of the scour holes increase under reductions of the sediment supply (ScA compares to ScB and ScC). Importantly, critical riverbank erosion occurs around the locations of severe scour holes such as at zone A and zone C during 2014-2017 as analyzed above. Therefore, it is predicted that the right bank of the Tien River from Tan Chau to Vam Nao, especially at zone A, the left bank of Vam Nao channel, the left bank of zone C, right bank around the Long Xuyen station, and the left bank around the Can Tho station are more likely susceptible to critical erosion within the next ten years caused by deep scour holes. Interestingly, at the deepest location (bed level is about -46 m) at approximately 2 km upstream of the My Thuan station, the riverbed is relatively stable by the next ten years.

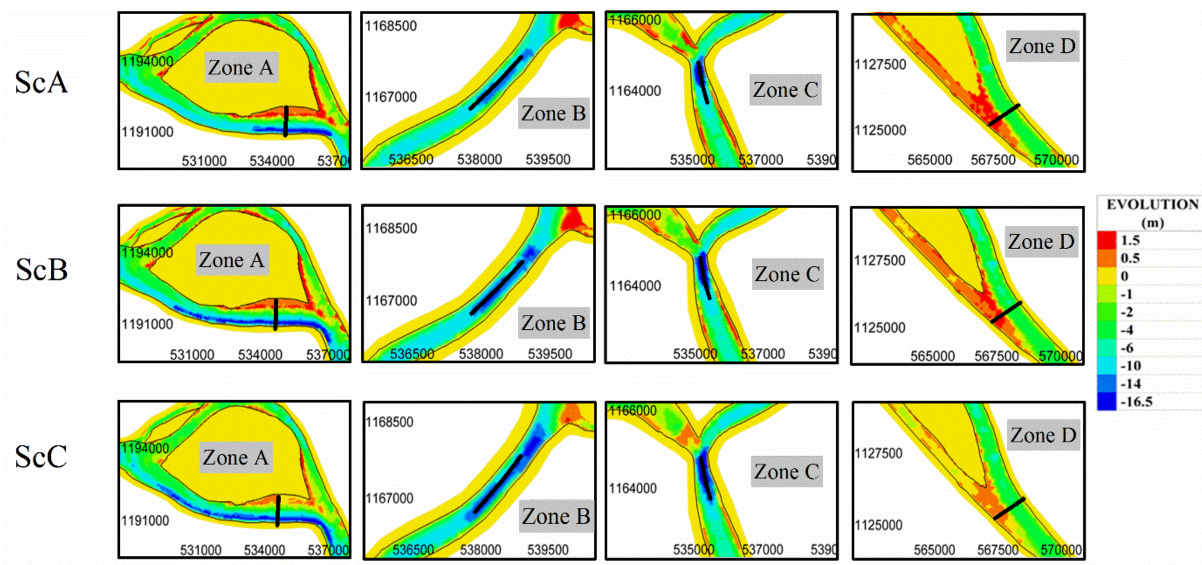

Figure 7.11 3D maps of riverbed changes among simulation scenarios at four typical zones.

7.3.6 Morphological incision effect on the possibility of obtaining intake water for irrigation

Due to rapid riverbed incision, water levels during 2017-2022 are more decreased than those during 2022-2026 (Fig. 7.12). Water level reduction rate during the former is about 2-4 times faster than during the latter. Compared to the baseline (April 2017), the water level in April 2026 significantly decreases even if the flow and sediment supply from the MR to the VMD remained unchanged during 2017-2026 (ScA) (Figs. 7.13 and 7.14). Water levels are more reduced under scenarios of reductions of sediment supply from the MR (ScB and ScC). Water levels are more reduced in the upper part than the lower part (Fig. 7.12-7.14) because of the tailwater effect from the downstream boundaries at My Thuan and Can Tho. In the upper part, water level reductions in the Tien River are more than those in the Hau River. Particularly, at around Tan Chau, the water levels in the Tien River decrease by 0.47 m, 0.54 m, and 0.68 m in ScA, ScB, and ScC, respectively, from the baseline. The corresponding numbers reduce to 0.41 m, 0.48 m, and 0.62 m in ScA, ScB, and ScC, respectively, at a location of 11 km seaward of Tan Chau. Similarly, near Chau Doc, the water levels in the Hau River decrease by 0.35 m, 0.4 m, and 0.49 m in ScA, ScB, and ScC, respectively, from the baseline. However, in the lower part, water levels in the Hau River are more reduced than those in the Tien River. For instance, water levels in the Hau River at a location of about 97 km from Chau Doc decrease by 0.13 m, 0.17 m, and 0.24 m in ScA, ScB, and ScC, respectively, from the baseline while the corresponding numbers at a location of about 96 km in the Tien River from Tan Chau are 0.08 m, 0.12 m, and 0.21 m in ScA, ScB, and ScC m, respectively.

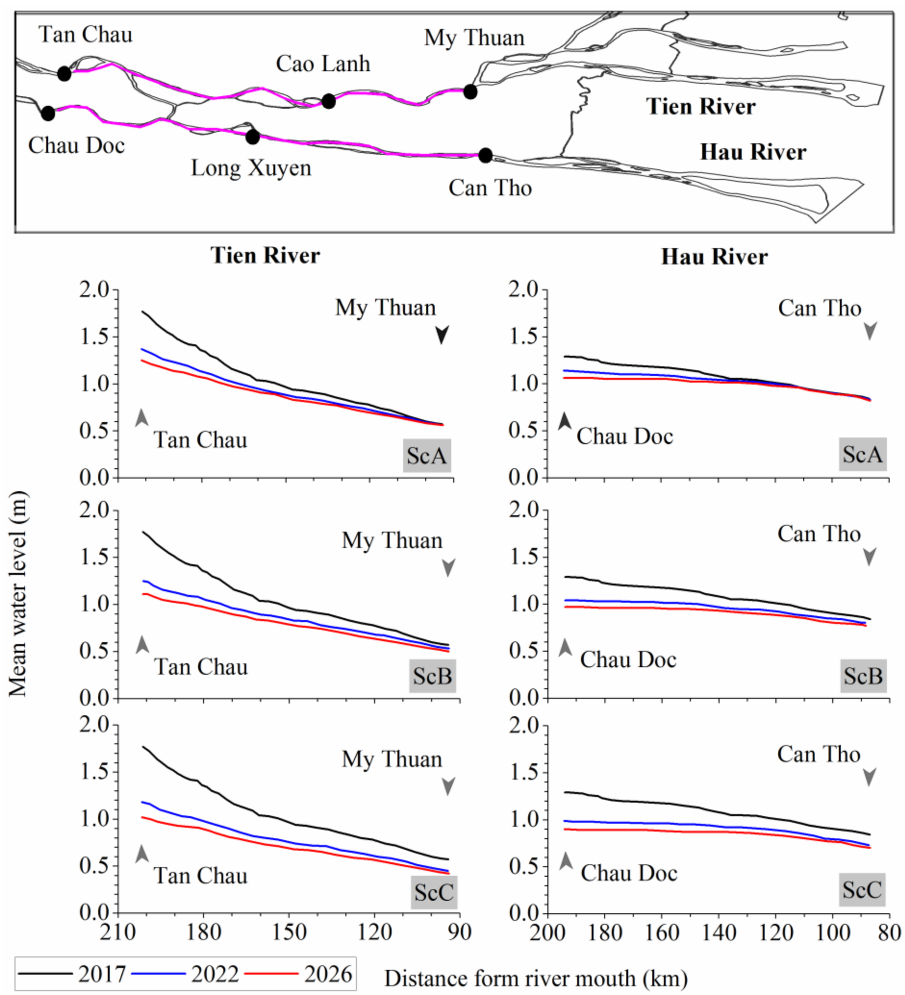

Figure 7.12 Longitudinal mean water level changes in Tien and Hau River during 2017-2026.

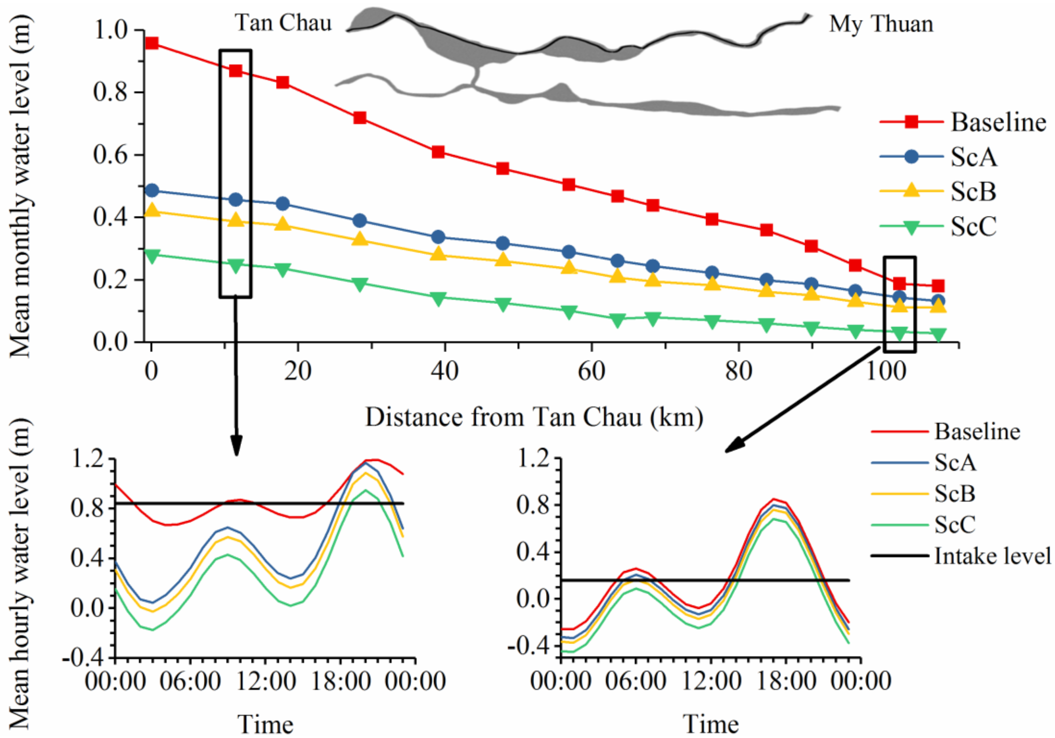

Figure 7.13 Reductions in water levels in the Tien River under effect of degraded riverbed.

Due to water level reduction induced by riverbed degradation, the duration that the farmers can obtain the water through gravitational irrigation systems decreases substantially (Figs. 7.13 and 7.14). For instance, the mean duration for operating the gravitational irrigation system in the upper part of both Tien and Hau River decreases from approximately 8 hours/day in the baseline (April 2017) to roughly 4 hours/day in ScA and 2 hours/day in ScC (April 2026 with 84.8% sediment reduction). In the lower part, the duration in operating the gravitational irrigation systems decreases from 10 hours/day in the baseline to 6 hours/day in the Tien River and 3 hours/day in the Hau River in April 2026 of ScC. Noticeably, the intake levels of irrigation channels in the VMD are not available. Therefore, the referenced intake levels shown in Figs. 7.13 and 7.14 are the results of an assumption that the intake levels are approximately 0.3-0.7 m lower than the ground levels of the floodplains based on the experience of engineers who have extensive works in designing irrigation channels in the VMD.

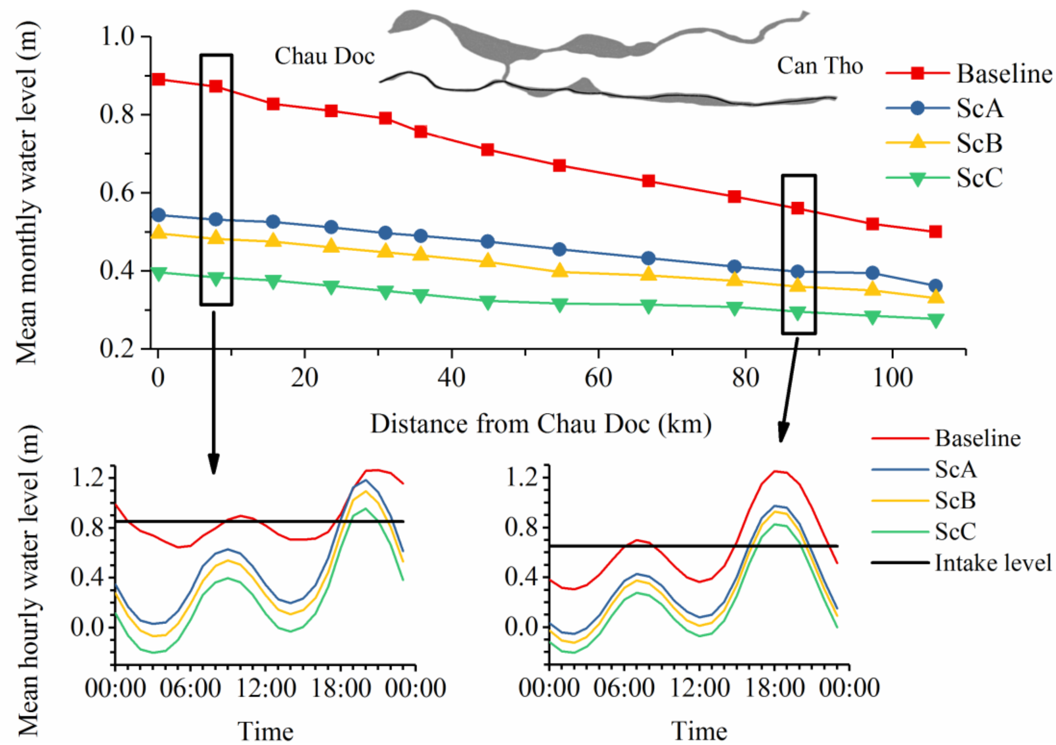

Figure 7.14 Reductions in water levels in the Hau River under the effect of degraded riverbed.

7.4 Discussions

If the current quantity and pattern of the flow and sediment of the VMD remain unchanged during 2017-2026, the riverbed will be severely incised by the end of 2026. It indicates an outweigh of the flow power to the sediment supply which is the consequence of river damming. More seriously, the riverbed will be more and more degraded if the sediment supply is more reduced due to increasing construction of hydropower dams in the MRB. Consequently, large-scale riverbed incision accompanied by several deep scour holes will be more likely to cause severe riverbank erosion in the VMD. It is predicted that the right bank of the Tien River from Tan Chau to Vam Nao, especially at zone A, the left bank of Vam Nao channel, the left bank of zone C, right bank around the Long Xuyen station, and the left bank around the Can Tho station (Fig. C7.3) are more likely susceptible to critical erosion within the next ten years.

The difference between the riverbed incision which is estimated by comparing the measured riverbed bathymetric data in 2014 and 2017 and is simulated by the coupled model is attributed to sand mining. Although overestimated, sand mining in the upper reach of the VMD is responsible for 23.1% of the riverbed incision while the remaining is due to hydropower dams in the MRB. Additionally, sand mining in the VMD is more concentrated in the areas between Tan Chau/ Chau Doc to My Thuan/ Can Tho. Therefore, sand mining is argued to contribute less than 20% of the riverbed incision in the whole VMD. Moreover, hydropower dams cause large-scale morphological degradation while sand mining is responsible for small-scale local scour holes.

By April 2026, the water levels in the VMD under different scenarios of reductions in the sediment supply from the MR significantly decrease compared to those in April 2017 in the baseline. Maximum water level reductions can reach 0.7 m and 0.5 m in the Tien and Hau Rivers, respectively, under 84.8% reduction of the sediment supply (Figs. 7.13 and 7.14). Water level reductions, in turn, reduce the duration in operating the gravitational irrigation systems to obtain the intake water. The duration in operating gravitational irrigation systems decreases from 8-10 hours/day in April 2017 to 2-6 hours/day in April 2026 in ScC. As a consequence, the farmers will be more likely to alternatively use mechanical systems such as pumping stations to obtain the water. This will lead to an increase in the farming cost, therefore, reducing their ultimate income. Therefore, solutions to maintain low-flow water levels in the VMD is of crucial importance to sustain agriculture as well as the livelihoods of the people.

Maintaining the water levels in VMD rivers in the low-flow season that warranties for rice crop's irrigation is crucial, especially under complicated impacts of upstream hydropower dams in the MR. The simulated results show that the increased flow discharge during the low-flow season by dams is helpful in obtaining intake water for irrigation in the VMD, especially under the fact that the riverbeds in the delta have been severely degraded by reservoir trapping sediment. Under a virtual low riverbed degradation (< 1.5 m), an increase of 10% of the discharge helps improve the water levels as high as initial values. Under virtual moderate (1.5 m ≤ degradation ≤ 3 m) and high (3 m < degradation ≤ 6 m) degradation scenarios, 20% and 50% increases, respectively, of the low-flow season discharges by dams are recommended (Table 7.2). While requesting for high levels of discharge releases from the upstream dams is not always warranted, the riverbed degradation in the VMD is foreseen to continue for a longer time. Consequently, the low-flow season water levels in the VMD will be more and more decreased that will cause more and more difficulty in obtaining intake water for rice crop' irrigation.

7.5 Conclusions

In the high-flow season, the SSC in the Tien River is much higher than that in the Hau River. The amount of the SSC between the Tien and Hau Rivers becomes similar in the low-flow season.

The Tien River diverts 40-50% of its suspended sediment to the Vam Nao channel annually, that combines with the resuspended sediment through riverbed incision in the Vam Nao channel contribute 60-80% of the Hau River suspended sediment budget, which is estimated at the Hau River-Vam Nao channel confluence.

The river morphology in the VMD is depended on the balance between the flow power and sediment supply from the MR. Due to river damming, the flow power already exceeded and will greatly exceed the sediment supply to the delta. If the flow and sediment budgets of 2017 remain unchanged during 2017-2026, the riverbed of the upper VMD will be, on average, incised by -1.27 m by the end of 2026. The values will reach -1.48 m, and -2.04 m under reductions of 17.5% and 84.8% of the sediment supply, respectively. Accordingly, the resulted water levels will decrease by a maximum of 0.7 m in the Tien River and 0.5 m in the Hau River by April 2026 under 84.8% sediment supply reduction.

Therefore, maintaining the low-flow water levels that warranty for rice crop's irrigation is crucial for sustainable development of the VMD. The simulated results revealed that increasing low-flow water discharges by upstream dam regulations help partly ease dams' negative impacts on water level reduction regarding riverbed incision due to sediment trapping. Under a virtual low riverbed degradation (< 1.5 m), an increase of 10% of the low-flow discharge helps improve the water levels as high as initial values. Under virtual moderate (1.5 m ≤ degradation ≤ 3 m) and high (3 m < degradation ≤ 6 m) degradation scenarios, 20% and 50% increases, respectively, of the low-flow discharges by dams are recommended.

Hydropower dams cause large-scale riverbed incision in the VMD while sand mining is responsible for small-scale local scouring. It is estimated that hydropower dams are responsible for more than 80% while sand mining is responsible for less than 20% of the riverbed incision in the VMD. However, deep scour holes at mining areas may cause riverbank collapse. Therefore, the research calls a collaborative watershed sediment management among six riparian countries in the MRB and a restriction of sand mining within the VMD as well as upstream countries.

Chapter 8 Conclusion remarks and recommendations

In this research, the impacts of existing and planned hydropower dams in the MRB on the lower MR, especially the VMD, were investigated. Long-term alterations of the flow and sediment dynamics and budget, and of the morphology in the lower MR from Chiang Saen to the VMD were analyzed. Changes in the low-flow water levels as a consequence of the morphological changes induced by sediment supply reduction were projected. Different methods were applied, including theoretical analysis, field investigation, and numerical simulations. Trend tests (Mann-Kendall, Pettitt, and Sen's slope), frequency analysis, IHA and RVA, and FQ were used to qualitatively and quantitatively evaluate the dam impacts. Five additional turbidity and salinity monitoring stations were installed and two field surveys were conducted to overcome data limitation. In terms of numerical simulation, both Mike 11 and Telemac packages were employed. Besides dam impacts, the influence of other drivers such as climate change, land use change, sand mining, and existing hydraulic structures (i.e., dikes and sluice gates) was assessed.

The findings of this study serve as a basic reference for the sound management of water conservancy, flood control, river navigation, salinity control, and agricultural development in the VMD. Following are conclusions and recommendations of this research as well as an outlook for future works based on the research outcome.

8.1 Alterations of the flow regime and budget in the lower MR and the VMD

Climate conditions controlled the flow regimes in the low-dam development period (1993-2008) while hydropower dams in the Mekong River basin intensified the impacts.

Operations of hydropower dams in the MRB were the main driver of flow regime alterations in the high-dam development period (2009-2015), and dam impacts are expected to dominate through the 2040s.

Mainstream dams manipulated the maximum and high-flow discharges while tributary dams controlled the minimum and low-flow discharges in the lower MR.

Impacts of the Lancang cascade dams up to the year 2011 (4 dams completed) on river flows at Tan Chau are not obvious. However, such impacts are significantly when all six dams in the Lancang cascade were in operation.

Impacted by all six dams, minimum discharges at Tan Chau have increased by 1.9 times, equivalent to +93.2% and the duration of the low stage decreased by 55%. However, water levels in the low-flow season generally decreased under dam' impacts because of riverbed incision as a result of the reduction in the sediment supply, leading to an increase in tidal influence into the VMD (maximum increase is 2.3 times in 2012-2015 period).

Six dams in the Lancang cascade have caused a reduction in both discharges and water levels in high-flow years in the VMD. The median discharge and the maximum water level are reduced by -13.5% and -20.2% respectively. Duration of the high stage flow decreases by 66%. These reductions, on the one hand, are helpful in mitigating losses caused by floods but, on the other hand, may have unexpectedly negative impacts on the VMD because normal floods provide important natural resources for the VMD development.

Flood peak in the VMD has shifted to happen more lately due to the upstream hydropower dams. Furthermore, these dams have created a second flood peak in August which is unusual and disadvantageous to the livelihood in the VMD.

The situation of 2016-like drought event will become more serious if eleven proposed mainstream dams in Thailand, Lao PDR, and Cambodia are constructed. It was found that the VMD will experience a maximum reduction of the flow discharge of 3.6%. More dangerously, the discharge will be reduced up to a maximum value of 14.9% while the maximum water level increase will be more than 220% under the combined effect of 47 cm sea level rise and 11 proposed mainstream dams. These allow saltwater significantly intruding into the upper parts of the VMD, even in areas having not been affected before, with higher salinity concentrations. The research also predicts that flooding in coastal regions will frequently occur if sea level continues rising.

8.2 Alterations of the sediment dynamics and budget in the lower MR and the VMD

The upper MRB was the main contributor to the sediment budget of the MR during the predam period (pre-1992). However, the contribution during the postdam periods became minor due to the completion of six mainstream dams in the Lancang cascade; instead, the Nong Khai-Pakse section became the largest sediment source.

Daily and annual discharges along the entire lower MR changed insignificantly, while daily and annual SSLs were significantly reduced during the postdam periods. Both monthly and annual suspended sediment budgets in the VMD decreased statistically since the completion of the Manwan dam in 1993.

Climate conditions controlled the flow and sediment regime of the MR during the predam period. The climate conditions, which mainly shifted the timing and intensities of tropical cyclones, still considerably contributed to the discharge variations and sediment reductions in the lower MR during 1993-2001. However, the 64 hydropower dams that were completed by 2015 were the main driver of sediment reductions in the entire MR during 2012-2015. Six mainstream dams in the Lancang cascade were the main cause of sediment reductions upstream of Nong Khai, whereas tributary dams additionally controlled sediment reductions in areas downstream of Nong Khai to the East Sea. Dams and reservoirs impacted the annual and high sediment transport months more than low sediment transport months in the VMD.

Under operations of all 64 dams in the MRB, the suspended sediment budgets at Chiang Saen, Luang Prabang, Nong Khai, and the VMD decreased by 89.5%, 77%, 80.5%, and 74.1%, respectively. Among the 74.1% sediment reduction in the VMD, from 166.7±33.3 Mt/yr during the predam period to 43.1 Mt/yr during 2012-2015, 40.2% was caused by the six mainstream dams in the Lancang cascade, and the Manwan and Dachaosan dams alone were the direct drivers of 32% of the reduction. Similarly, the annual sediment discharge to the East Sea of Vietnam from the MR has reduced by 74%, from 144 Mt/yr during the predam period to 37.7 Mt/yr during 2012-2015.

8.3 Sediment dynamics, morphological changes and the resulting influence on low-flow water level alterations in the VMD

The SSC (turbidity) in the VMD is seasonally changeable. It is very high during the high-flow season (around 1,300 g/m^3 at Tan Chau) and very low in the low-flow season (5-70 g/m^3), except for regions appearing the turbidity maximum (at around Tra Vinh) under the effect of the wind, making local resuspension, and flood tide turbidity current. In the Tien River, the SSC is high from Tan Chau to My Thuan, decreasing seaward and low from My Thuan to the river mouth, increasing seaward. In the Hau River, the SSC is relatively low from Chau Doc to the Hau River-Vam Nao channel confluence where the SSC becomes increasing due to sediment diversion from the Tien River via the Vam Nao channel. Relatively, the SSC is high from Hau River-Vam Nao channel confluence to Can Tho, decreasing seaward and low from Can Tho to the river mouth, increasing seaward.

In the high-flow season, the SSC in the Tien River is much higher than that in the Hau River. The amount of the SSC between the Tien and Hau Rivers becomes similar in the low-flow season. The Tien River diverts 40-50% of its suspended sediment to the Vam Nao channel annually, that combines with the resuspended sediment through riverbed incision in the Vam Nao channel contribute 60-80% of the Hau River suspended sediment budget.

In terms of morpho-hydro-sediment dynamics, Tien and Hau Rivers are distinguished by two reaches. The division locations are changeable in between Cao Lanh/Long Xuyen and My Thuan/Can Tho, depending on the seasons. The upper reach is dominated by the fluvial processes while the lower reach is dominated by the tide. In the upper reach, the rivers are narrow, sinuous, and deep, decreasing seaward. River cross-sections, flow velocities, and SSCs are asymmetric. SSCs are high, decreasing seaward and bed materials are fine sand with low mud content. In the lower reach, the rivers are wide, straight, and shallow, increasing seaward. River cross-sections, flow velocities, and SSCs are symmetric. SSCs are low, increasing seaward and bed materials are uniformly fine sand with high mud content. Turbidity maximum zone occurs during the low-flow season due to the saline water cycle. Mid-river islands commonly appear within the last 35 km from river mouths.

The river morphology in the VMD is depended on the balance between the flow power and sediment supply from the MR. Due to river damming, the flow power already exceeded and will greatly exceed the sediment supply to the delta. If the flow and sediment budgets of 2017 remain unchanged during 2017-2026, the riverbed of the upper VMD might be, on average, incised by -1.27 m by the end of 2026. The values may reach -1.48 m, and -2.04 m under reductions of 17.5% and 84.8% of the sediment supply, respectively. Accordingly, the resulted water levels may decrease by a maximum of 0.7 m in the Tien River and 0.5 m in the Hau River by April 2026 under 84.8% sediment supply reduction.

Therefore, maintaining the low-flow water levels that warranty for rice crop's irrigation is crucial for sustainable development of the VMD. The simulated results revealed that increasing low-flow water discharges by upstream dam regulations help partly ease dams' negative impacts on water level reduction regarding riverbed incision due to sediment trapping. Under a virtual low riverbed degradation (< 1.5 m), an increase of 10% of the low-flow discharge helps improve the water levels as high as initial values. Under virtual moderate (1.5 m ≤ degradation ≤ 3 m) and high (3 m < degradation ≤ 6 m) degradation scenarios, 20% and 50% increases, respectively, of the low-flow discharges by dams are recommended.

Hydropower dams cause large-scale riverbed incision in the VMD while sand mining is responsible for small-scale local scouring. It is estimated that hydropower dams are responsible for more than 90% while sand mining is responsible for less than 10% of the riverbed incision in the VMD. However, deep scour holes at mining areas may cause riverbank collapse. Climate change may have long-term effects on morphological changes, and hydropower dams and sand mining have short to intermediate-term influences. Therefore, the research calls a collaborative watershed sediment management among six riparian countries in the MRB and a restriction of sand mining within the VMD as well as upstream countries.

8.4 Recommendations

Resulted from reduced low-flow water levels, salinity intrusion in the VMD has increased in the magnitude and shifted to occur earlier about 1-2 months than the no-dam period. Existing salinity control sluice gates along main rivers may increase the intrusion length further into the VMD because of reduced buffering zones; therefore; the functioning of such sluice gates should be carefully revised before building more.

For flood control considering economy and ecosystem sustainability, high-dike systems should not be further built while existing high-dike systems should be permanently or periodically opened (every 3 or 5 years) during flood months to receive more nutrient-rich fine sediment to recover and enrich soil properties for rice farming and to support wetland ecosystems.

Any stakeholder's decision related to water resources issues should base on long-term flow regime alterations and results from this research is a good reference. Water resources management must be long-term investigated and implemented at a delta-scale but not provincial or local-scales.

Owing to poor temporal-spatial monitored data obtained monitoring stations under MRC framework, scientists have difficulties in understanding the realistic hydro-sediment dynamics; therefore, stakeholders have difficulties in sustainably planning and developing the VMD. Installing more monitoring stations to monitor the flow and sediment along rivers, especially near the river mouths is strongly recommended. Using modern automatic instruments with high accuracy to monitor the SSCs is necessary.

Although hydropower dams cause large-scale riverbed incision in the VMD, sand mining cause deep scour holes which may cause riverbank collapse that severely affect the properties, livelihood and human lives. Therefore, restriction of sand mining is one of the important actions for sustainable development of the VMD.

This research study calls for an integrated water and sediment resources management strategy to be adopted by all riparian countries along the MR to maximize the benefits provided by the river. Cooperating and sharing data and knowledge among countries are of particular importance. Dam owners are recommended to share operation rules of reservoirs to neighboring (especially downstream) countries to help them actively plan their water resources management strategies.

8.5 Outlook for future works

Follow up the results and limitations of this research, some research directions should be addressed in future works:

1. Expanding the developed coupled Telemac-2D and Sisyphe model to simulate the morphological changes for the whole VMD.

2. Evaluate long-term riverbank and coastal erosion to understand the past and predict for the future under the effects of hydropower dams and other drivers.

3. Quantify effects of sand mining on morphological changes in the VMD and how it affects socio-economic and human activities.

4. Quantify dam impacts on suspended sediment dynamics, budget and associated nutrients in the floodplains, thereby, quantify effects of dams on agriculture production in the VMD.

5. Evaluate impacts of sediment supply reduction and degraded river morphology to salinity intrusion in the VMD.

6. Study on water quality and ecological changes in the VMD related to sediment and salinity concentration changes.

7. Identify threshold of the SSC suitable for ecology and ecosystems in the VMD.

REFERENCES

Adamson, P. T., Rutherfurd, I. D., Peel, M.C., & Conlan, I. A., 2009. The hydrology of the Mekong River. In Cambell, I. (Ed), The Mekong, 1st edn. Biophysical Environment of an International River Basin, Elsevier, pp. 53-76.

Alcayaga, H., Belleudy, P., Jourdain, C., 2012. Morphological modeling of river perturbations due to hydroelectric structures at watershed scale, in: River Flow 2012. International Conference on Fluvial Hydraulics. Muñoz, R.M (Ed). pp. 537–544.

Allison, M.A., Dallon Weathers, H., Meselhe, E.A., 2017a. Bottom morphology in the Song Hau distributary channel, Mekong River Delta, Vietnam. Cont. Shelf Res. 147, 51–61. doi:10.1016/j.csr.2017.05.010.

Allison, M.A., Nittrouer, C.A., Ogston, A.S., Mullarney, J.C., Nguyen, T.T., 2017b. Sedimentation and survival of the Mekong Delta: A case study of decreased sediment supply and accelerating rates of relative sea level rise. Oceanography 30, 98–109. doi:10.5670/oceanog.2017.318.

Annandale, G.., 2012. A Climate Resilient Mekong: Sediment Pass-Through at Sambor Dam, in: Golder Assoc. Inc., Lakewood, CO, Nat. Heritage Inst., San Francisco, Calif.

Anthony, E.J., Brunier, G., Besset, M., Goichot, M., Dussouillez, P., Nguyen, V.L., 2015. Linking rapid erosion of the Mekong River delta to human activities. Sci. Rep. 5, 1–12. doi:10.1038/srep14745.

Arias, M.E., Cochrane, T.A., Kummu, M., Lauri, H., Holtgrieve, G.W., Koponen, J., Piman, T., 2014. Impacts of hydropower and climate change on drivers of ecological productivity of Southeast Asia's most important wetland. Ecol. Modell. 272, 252–263. doi:10.1016/j.ecolmodel.2013.10.015.

Ata, R., Goeury, C., Hervouet, J.M., 2014. Telemac Modelling System: 2D hydrodynamics user mannual, version v7p0. EDF-R&D, France, 134 pp.

Bartkes, M., Brunner, G., Fleming, M., Faber, B., Slaughter, J., 2016. HEC-SSP Statistical Software Package User's Manual Version 2.1, US Army Corps of Engineers.

Binh, D.V., Kantoush, S., Mai, N.P., Sumi, T., 2018a. Water level changes under increased regulated flows and degraded river in Vietnamese Mekong Delta. J. Japan Soc. Civ. Eng. Ser. B1 (Hydraulic Eng. 74, 871–876.

Binh, D.V., Kantoush, S., Sumi, T., Mai, N.P., 2018b. Impact of Lancang cascade dams on flow regimes of Vietnamese Mekong Delta. Annu. J. Hydraul. Eng. JSCE 62.

Bravard, J.P., Goichot, M., Gaillot, S., 2013. Geography of Sand and Gravel Mining in the Lower Mekong River: First Survey and Impact Assessment. EchoGéo 26, 1–18.

Brunier, G., Anthony, E.J., Goichot, M., Provansal, M., Dussouillez, P., 2014. Recent morphological changes in the Mekong and Bassac river channels, Mekong delta: The marked impact of river-bed mining and implications for delta destabilisation. Geomorphology 224, 177–191. doi:10.1016/j.geomorph.2014.07.009.

Chao, B.F., Wu, Y.H., Li, Y.S., 2008. Impact of artificial reservoir water impoundment on global sea level, Science. doi:10.1126/science.1154580.

Chapman, A., Darby, S., 2016. Evaluating sustainable adaptation strategies for vulnerable mega-deltas using system dynamics modelling: Rice agriculture in the Mekong Delta's An Giang Province, Vietnam. Sci. Total Environ. 559, 326–338. doi:10.1016/j.scitotenv.2016.02.162.

Dang, D.T., Cochrane, T.A., Arias, M.E., Tri, V.P.., 2018. Future hydrological alterations in the Mekong Delta under the impact of water resources development , land subsidence and sea level rise. J. Hydrol. Reg. Stud. 15, 119–133. doi:10.1016/j.ejrh.2017.12.002.

Dang, T.D., Cochrane, T.A., Arias, M.E., Van, P.D.T., Vries, T.T.D., 2016. Hydrological alterations from water infrastructure development in the Mekong floodplains. Hydrol. Process. 30, 3824–3838. doi:10.1002/hyp.10894.

Darby, S.E., Hackney, C.R., Leyland, J., Kummu, M., Lauri, H., Parsons, D.R., Best, J.L., Nicholas, A.P., Aalto, R., 2016. Fluvial sediment supply to a mega-delta reduced by shifting tropical-cyclone activity. Nature. doi:10.1038/nature19809.

Darby, S.E., Leyland, J., Kummu, M., Timo, A.R., 2013. Decoding the drivers of bank erosion on the Mekong river : The roles of the Asian monsoon , tropical storms , and snowmelt. Water Resour. Res. 49, 2146–2163. doi:10.1002/wrcr.20205.

DHI-HDR, 2015. Study on the Impacts of Mainstream Hydropower on the Mekong River. Impact Assessment Report. Volume 1-Models, Model Setup and Simulation, Ministry of Natural Resources and Environment.

DHI, 2009. Mike 11: A Modelling System for Rivers and Channels: Reference Manual.

Doyle, T.W., Day, R.H., Michot, T.C., 2010. Development of sea level rise scenarios for climate change assessments of the Mekong Delta, Vietnam. U.S. Geol. Surv. Open-File Rep. 2010-1165 110 pp.

Dugan, P.J., Barlow, C., Agostinho, A.A., Baran, E., Cada, G.F., Chen, D., Cowx, I.G., Ferguson, J.W., Jutagate, T., Mallen-Cooper, M., Marmulla, G., Nestler, J., Petrere, M., Welcomme, R.L., Winemiller, K.O., 2010. Fish migration, dams, and loss of ecosystem services in the mekong basin. Ambio 39, 344–348. doi:10.1007/s13280-010-0036-1.

Fan, H., He, D., 2015. Temperature and Precipitation Variability and Its Effects on Streamflow in the Upstream Regions of the Lancang – Mekong and Nu – Salween Rivers. J. Hydrometeorol. 2248–2263. doi:10.1175/JHM-D-14-0238.1.

Fan, H., He, D., Wang, H., 2015. Environmental consequences of damming the mainstream lancang-mekong river: A review. Earth-Science Rev. 146, 77–91. doi:10.1016/j.earscirev.2015.03.007.

Fu, K., He, D., 2007. Analysis and prediction of sediment trapping efficiencies of the reservoirs in the mainstream of the Lancang River. Chinese Sci. Bull. 52, 134–140. doi:10.1007/s11434-007-7026-0.

Fu, K.D., He, D.M., Lu, X.X., 2008. Sedimentation in the Manwan reservoir in the Upper Mekong and its downstream impacts. Quat. Int. 186, 91–99. doi:10.1016/j.quaint.2007.09.041

Fujii, H., Garsdal, H., Ward, P., Ishii, M., Morishita, K., Boivin, T., 2003. Hydrological roles of the Cambodian floodplain of the Mekong River. Int. J. River Basin Manag. 1, 1–14. doi:10.1080/15715124.2003.9635211.

García, M.H., 2008. Sedimentation Engineering: Processes, Measurement, Modeling, and Practice, American Society of Civil Engineers. American Society of Civil Engineers, Virginia.

Grumbine, R.E., Dore, J., Xu, J., 2012. Mekong hydropower: Drivers of change and governance challenges. Front. Ecol. Environ. 10, 91–98. doi:10.1890/110146.

Gugliotta, M., Saito, Y., Nguyen, V.L., Ta, T.K.O., Nakashima, R., Tamura, T., Uehara, K., Katsuki, K., Yamamoto, S., 2017. Process regime, salinity, morphological, and sedimentary trends along the fluvial to marine transition zone of the mixed-energy Mekong River delta, Vietnam. Cont. Shelf Res. 147, 7–26. doi:10.1016/j.csr.2017.03.001.

Gupta, A., Liew, S.C., 2007. The Mekong from satellite imagery: A quick look at a large river. Geomorphology 85, 259–274. doi:10.1016/j.geomorph.2006.03.036.

Gupta, H., Kao, S.J., Dai, M., 2012. The role of mega dams in reducing sediment fluxes : A case study of large Asian rivers. J. Hydrol. 464–465, 447–458. doi:10.1016/j.jhydrol.2012.07.038

Ha, D.T., Ouillon, S., Vinh, G.V., 2018. Water and Suspended Sediment Budgets in the Lower Mekong from High-Frequency Measurements (2009–2016). Water 10, 1–24. doi:10.3390/w10070846.

Hecht, J.S., Lacombe, G., Arias, M.E., Dang, T.D., 2019. Hydropower dams of the Mekong River basin : A review of their hydrological impacts. J. Hydrol. 568, 285–300. doi:10.1016/j.jhydrol.2018.10.045.

Heng, S., Suetsugi, T., 2014. Development of a regional model for catchment-scale suspended sediment yield estimation in ungauged rivers of the Lower Mekong Basin. Geoderma 235–236, 334–346. doi:10.1016/j.geoderma.2014.07.030.

Hoa, L.T.V., Nhan, N.H., Wolanski, E., Cong, T.T., Haruyama, S., 2007. The combined impact on the flooding in Vietnam's Mekong River delta of local man-made structures, sea level rise, and dams upstream in the river catchment. Estuar. Coast. Shelf Sci. 71, 110–116. doi:10.1016/j.ecss.2006.08.021.

Hoang, L.P., van Vliet, M.T.H., Kummu, M., Lauri, H., Koponen, J., Supit, I., Leemans, R., Kabat, P., Ludwig, F., 2019. The Mekong's future flows under multiple drivers: How climate change, hydropower developments and irrigation expansions drive hydrological changes. Sci. Total Environ. 649, 601–609. doi:10.1016/j.scitotenv.2018.08.160.

Hoang, P.L., Lauri, H., Kummu, M., Koponen, J., Vliet, M.T.H.V., Supit, I., Leemans, R., Kabat, P., Ludwig, F., 2016. Mekong River flow and hydrological extremes under climate change. Hydrol. Earth Syst. Sci. 20, 3027–3041. doi:10.5194/hess-20-3027-2016.

Hoanh, C.T., Jirayoot, K., Lacomne, G., Srunetr, V., 2010. Impacts of climate change and development on Mekong flow regimes First assessment – 2009, MRC Management Information Booklet Series No.4. doi:Mekong River Commission, Vientiane, Lao PDR.

Hoanh, C.T., Jirayoot, K., Lacomne, G., Srunetr, V., 2010. Impacts of climate change and development on Mekong flow regimes First assessment – 2009, MRC Technical Paper No. 29. Mekong River Commission, Vientiane, Lao PDR. doi:Mekong River Commission, Vientiane, Lao PDR.

Hortle, K.G., 2007. Consumption and the yield of fish and other aquatic animals from the Lower Mekong Basin, MRC Technical Paper No. 16. Mekong River Commission, Vientiane.

Hung, N.N., 2011. Sediment dynamics in the floodplain of the Mekong Delta, Vietnam.

Hung, N.N., Delgado, J.M., Güntner, A., Merz, B., Bárdossy, A., Apel, H., 2013a. Sedimentation in the floodplains of the Mekong Delta, Vietnam Part II: Deposition and erosion. Hydrol. Process. 28, 3145–3160. doi:10.1002/hyp.9855.

Hung, N.N., Delgado, J.M., Güntner, A., Merz, B., Bárdossy, A., Apel, H., 2013b. Sedimentation in the floodplains of the Mekong Delta, Vietnam. Part I: Suspended sediment dynamics. Hydrol. Process. 28, 3132–3144. doi:10.1002/hyp.9856.

Iida, T., Inkhamseng, S., Yoshida, K., Tanji, H., 2011. Characterization of water quality variation in the Mekong River at Vientiane by frequent observations. Hydrol. Process. 25, 3590–3601. doi:10.1002/hyp.8084.

Junk, W.J., Bayley, P.B., Sparks, R.E., 1989. The Flood Pulse Concept in River-Floodplain Systems. Can. Spec. Publ. Fish. Aquat. Sci. 106, 110–127.

Kameyama, S., Shimazaki, H., Nohara, S., Sato, T., Fujii, Y., Kudo, K., 2013. Hydrological and sediment transport simulation to assess the impact of dam construction in the Mekong River main channel. Am. J. Environ. Sci. 9, 247–258. doi:10.3844/ajessp.2013.247.258.

Kantoush, S., Binh, D.V., Sumi, T., Trung, L.V., 2017. Impact of Upstream Hydropower Dams and Climate Change on Hydrodynamics of Vietnamese Mekong Delta. J. Japan Soc. Civ. Eng. Ser. B1 (Hydraulic Eng. 73, I_109-I_114.

Kendall, A.M.G., 1938. A new measure of rank correlation. Oxford J. 30, 81–93.

Keskinen, M., Someth, P., Salmivaara, A., Kummu, M., 2015. Water-energy-food nexus in a transboundary river basin: The case of Tonle Sap Lake, Mekong River Basin. Water (Switzerland) 7, 5416–5436. doi:10.3390/w7105416.

Kingston, D.G., Thompson, J.R., Kite, G., 2011. Uncertainty in climate change projections of discharge for the Mekong River Basin. Hydrol. Earth Syst. Sci. 15, 1459–1471. doi:10.5194/hess-15-1459-2011.

Koehnken, L., 2014. Discharge sediment monitoring project (DSMP) 2009 – 2013 summary & analysis of results, Mekong River Commission, Vientiane.

Koehnken, L., 2014. Discharge sediment monitoring project (DSMP) 2009 – 2013 summary & analysis of results. Mekong River Comm. 126 pp.

Kondolf, G.M., 1997. Hungry water: Effects of dams and gravel mining on river channels. Environ. Manage. 21, 533–551. doi:10.1007/s002679900048.

Kondolf, G.M., Gao, Y., Annandale, G.W., Morris, G.L., Jiang, E., Zhang, J., Cao, Y., Carling, P., Fu, K., Guo, Q., Hotchkiss, R., Peteuil, C., Sumi, T., Wang, H.W., Wang, Z., Wei, Z., Wu, B., Wu, C., Yang, C.T., 2014. Sustainable sediment management in reservoirs and regulated rivers: Experiences from five continents. Earth's Futur. 2, 256–280. doi:10.1002/2013EF000184.

Kondolf, G.M., Rubin, Z.K., Minear, J.T., 2014. Dams on the Mekong: Cumulative sediment starvation. Water Resour. Res. 50, 5158–5169. doi:10.1002/2013WR014651.

Kondolf, G.M., Schmitt, R.J.P., Carling, P., Darby, S., Arias, M., Bizzi, S., Castelletti, A., Cochrane, T.A., Gibson, S., Kummu, M., Oeurng, C., Rubin, Z., Wild, T., 2018. Changing sediment budget of the Mekong: Cumulative threats and management strategies for a large river basin. Sci. Total Environ. 625, 114–134. doi:10.1016/j.scitotenv.2017.11.361.

Kummu, M., Lu, X.X., Rasphone, A., Sarkkula, J., Koponen, J., 2008. Riverbank changes along the Mekong River: Remote sensing detection in the Vientiane-Nong Khai area. Quat. Int. 186, 100–112. doi:10.1016/j.quaint.2007.10.015.

Kummu, M., Lu, X.X., Wang, J.J., Varis, O., 2010. Basin-wide sediment trapping efficiency of emerging reservoirs along the Mekong. Geomorphology 119, 181–197. doi:10.1016/j.geomorph.2010.03.018.

Kummu, M., Sarkkula, J., 2008. Impact of the Mekong River flow alteration on the Tonle Sap flood pulse. Ambio 37, 185–192. doi:10.1579/0044-7447(2008)37[185:IOTMRF]2.0.CO;2.

Kummu, M., Varis, O., 2007. Sediment-related impacts due to upstream reservoir trapping, the Lower Mekong River. Geomorphology 85, 275–293. doi:10.1016/j.geomorph.2006.03.024.

Lauri, H., De Moel, H., Ward, P.J., Räsänen, T.A., Keskinen, M., Kummu, M., 2012. Future changes in Mekong River hydrology: Impact of climate change and reservoir operation on discharge. Hydrol. Earth Syst. Sci. 16, 4603–4619. doi:10.5194/hess-16-4603-2012.

Letrung, T., Li, Q., Li, Y., Vukien, T., Nguyenthai, Q., 2013. Morphology Evolution of Cuadai Estuary, Mekong River, Southern Vietnam. J. Hydraul. Eng. 18, 1122–1132. doi:10.1061/(ASCE)HE.1943-5584.0000483.

Li, D., Long, D., Zhao, J., Lu, H., Hong, Y., 2017. Observed changes in flow regimes in the Mekong River basin. J. Hydrol. 551, 217–232. doi:10.1016/j.jhydrol.2017.05.061.

Li, J., Dong, S., Yang, Z., Peng, M., Liu, S., Li, X., 2012. Effects of cascade hydropower dams on the structure and distribution of riparian and upland vegetation along the middle-lower Lancang-Mekong River. For. Ecol. Manage. 284, 251–259. doi:10.1016/j.foreco.2012.07.050.

Li, S., He, D., 2008. Water level response to hydropower development in the upper Mekong River. Ambio 37, 170–177. doi:Doi 10.1579/0044-7447(2008)37[170:Wlrthd]2.0.Co;2.

Li, X., Liu, J.P., Saito, Y., Nguyen, V.L., 2017a. Recent evolution of the Mekong Delta and the impacts of dams. Earth-Science Rev. 175, 1–17. doi:10.1016/j.earscirev.2017.10.008.

Li, X., Liu, J.P., Saito, Y., Nguyen, V.L., 2017b. Recent evolution of the Mekong Delta and the impacts of dams. Earth-Science Rev. 175, 1–17. doi:10.1016/j.earscirev.2017.10.008.

Loizeau, J.L., Jüstrich, S., Wildi, W., 2010. Swiss examples of the impacts of dams on natural environments and management strategies for sediment control. NEAR Curric. Nat. Environ. Sci. Terre Environ. 88, 199–204.

Lu, X.X., Kummu, M., Oeurng, C., 2014a. Reappraisal of sediment dynamics in the Lower Mekong River, Cambodia. Earth Surf. Process. Landforms 39, 1855–1865. doi:10.1002/esp.3573.

Lu, X.X., Li, S., Kummu, M., Padawangi, R., Wang, J.J., 2014b. Observed changes in the water flow at Chiang Saen in the lower Mekong: Impacts of Chinese dams? Quat. Int. 336, 145–157. doi:10.1016/j.quaint.2014.02.006.

Lu, X.X., Oeurng, C., Le, T.P.Q., Thuy, D.T., 2015. Sediment budget as affected by construction of a sequence of dams in the lower Red River , Viet Nam. Geomorphology 248, 125–133. doi:10.1016/j.geomorph.2015.06.044.

Lu, X.X., Siew, R.Y., 2006. Water discharge and sediment flux changes over the past decades in the Lower Mekong River: possible impacts of the Chinese dams. Hydrol. Earth Syst. Sci. 10, 181–195. doi:10.5194/hess-10-181-2006.

Lyon, S.W., King, K., Polpanich, O., Lacombe, G., 2017. Assessing hydrologic changes across the Lower Mekong Basin. J. Hydrol. Reg. Stud. 12, 303–314. doi:10.1016/j.ejrh.2017.06.007.

Manh, N.V., Dung, N.V., Hung, N.N., Kummu, M., Merz, B., Apel, H., 2015. Future sediment dynamics in the Mekong Delta floodplains: Impacts of hydropower development, climate change and sea level rise. Glob. Planet. Change 127, 22–33. doi:10.1016/j.gloplacha.2015.01.001.

Manh, N. V., Dung, N. V., Hung, N.N., Merz, B., Apel, H., 2014. Large-scale suspended sediment transport and sediment deposition in the Mekong Delta. Hydrol. Earth Syst. Sci. 18, 3033–3053. doi:10.5194/hess-18-3033-2014.

Mann, H.B., 1945. Nonparametric Tests Against Trend. Econometrica 13, 245–259.

Mclachlan, R.L., Ogston, A.S., Allison, M.A., 2017. Implications of tidally-varying bed stress and intermittent estuarine strati fi cation on fi ne-sediment dynamics through the Mekong ' s tidal river to estuarine reach. Cont. Shelf Res. 147, 27–37. doi:10.1016/j.csr.2017.07.014.

Meade, R.H., 1996. Chapter 3: River-Sediment Inputs to Major Deltas. In: Sea level-rise and Coastal subsidence, U.S. Government. doi:10.1007/978-94-015-8719-8_4.

Milliman, J.D., Syvitski, J.P.M., 1992. Geomorphic/Tectonic Control of Sediment Discharge to the Ocean: The Importance of Small Mountainous Rivers. J. Geol. 100, 525–544. doi:10.1086/629606.

Minderhoud, P.S.J., Erkens, G., Pham, V.P., Bui, V.T., Erban, L., Kooi, H., Stouthamer, E., 2017. Impacts of 25 years of groundwater extraction on subsidence in the Mekong delta , Vietnam. Environ. Res. Lett. 12, 1–13. doi:10.1088/1748-9326/aa7146.

Minh, L.T.N., Josette, G., Gilles, B., Didier, O., Julien, N., Quynh, L.T.P., Thai, T.H., Anh, L.L., 2010. Hydrological regime and water budget of the Red River Delta (Northern Vietnam). J. Asian Earth Sci. 37, 219–228. doi:10.1016/j.jseaes.2009.08.004.

MRC, 2005. Annual Flood Report 2005, Mekong River Commission, Vientiane.

Mtamba, J., Velde, T.V.D., Ndomba, P., Zoltán, V., Mtalo, F., 2015. Use of Radarsat-2 and Landsat TM Images for Spatial Parameterization of Manning's Roughness Coefficient in Hydraulic Modeling. Remote Sens. 7, 836–864. doi:10.3390/rs70100836.

Ngo, L.A., Masih, I., Jiang, Y., Douven, W., 2018. Impact of reservoir operation and climate change on the hydrological regime of the Sesan and Srepok Rivers in the Lower Mekong Basin. Clim. Change 149, 107–119. doi:10.1007/s10584-016-1875-y.

Nowacki, D.J., Ogston, A.S., Nittrouer, C.A., Fricke, A.T., Van, P.D.T., 2015. Sediment dynamics in the lowerMekong River: Transition from tidal river to estuary. J. Geophys. Res. Ocean. 120, 6363–6383. doi:10.1002/2015JC010754.

Orr, S., Pittock, J., Chapagain, A., Dumaresq, D., 2012. Dams on the Mekong River: Lost fish protein and the implications for land and water resources. Glob. Environ. Chang. 22, 925–932. doi:10.1016/j.gloenvcha.2012.06.002.

Pablo, T., 2018. Sysyphe User Mannual, version v7p3, 70 pp.

Pettitt, 1979. A Non-parametric Approach to the Change-Point Problem. Appl. Stat. 28, 126–135.

Poff, N.L., Ward, J.V., 1989. Implications of streamflow variability and predictability for lotic community structure: a regional analysis of streamflow patterns. Can. J. Fish. Aquat. Sci. 46, 1805–1818.

Pokhrel, Y., Burbano, M., Roush, J., Kang, H., Sridhar, V., Hyndman, D.W., 2018. A Review of the Integrated Effects of Changing Climate, Land Use, and Dams on Mekong River Hydrology. Water 10. doi:10.3390/w10030266.

Rantz, S.E., 1982. Measurement and computation of stream flow. Volume 1: Measurement of stage and discharge; Volume 2: Computation of discharge. US Geol. Surv. water-supply Pap. 2175, 631pp. doi:10.1029/WR017i001p00131.

Räsänen, T.A., Koponen, J., Lauri, H., Kummu, M., 2012. Downstream Hydrological Impacts of Hydropower Development in the Upper Mekong Basin. Water Resour. Manag. 26, 3495–3513. doi:10.1007/s11269-012-0087-0.

Räsänen, T.A., Someth, P., Lauri, H., Koponen, J., Sarkkula, J., Kummu, M., 2017. Observed river discharge changes due to hydropower operations in the Upper Mekong Basin. J. Hydrol. 545, 28–41. doi:10.1016/j.jhydrol.2016.12.023.

REN21, 2014. Renewable Nnergy Nolicy Network for the 21th Century.

Richter, B.D., Baumgartner, J.V., Braun, D.P., Powell, J., 1998. A spatial assessment of hydrologic alteration within a river network. Regul. Rivers Res. Manag. doi:10.1002/(SICI)1099-1646(199807/08)14:4<329::AID-RRR505>3.0.CO;2-E.

Richter, B.D., Baumgartner, J.V., Powell, J., Braun, D.P., 1996. A method for assessing hydrologic alteration within ecosystem. Conserv. Biol. 10, 1163–1174.

Richter, B.D., Baumgartner, J.V., Wigington, R., Braun, D.P., 1997. How much water does a river need? Freshw. Biol. 37, 231–249.

Rubin, Z.K., Kondolf, G.M., Carling, P.A., 2015. Anticipated geomorphic impacts from Mekong basin dam construction. Int. J. River Basin Manag. 13, 105–121. doi:10.1080/15715124.2014.981193.

Schmitt, R.J.P., Bizzi, S., Castelletti, A., Kondolf, G.M., 2018. Improved trade-offs of hydropower and sand connectivity by strategic dam planning in the Mekong. Nat. Sustain. 1, 96–104. doi:10.1038/s41893-018-0022-3.

Schmitt, R.J.P., Rubin, Z., Kondolf, G.M., 2017. Losing ground - scenarios of land loss as consequence of shifting sediment budgets in the Mekong Delta. Geomorphology 294, 58–69. doi:10.1016/j.geomorph.2017.04.029.

Sen, P.K., 1968. Estimates of the regression coefficient based on Kandall’s Tau. J. Am. Stat.

Assoc. 63, 1379–1389.

Smajgl, A., Toan, T.Q., Nhan, D.K., Ward, J., Trung, N.H., Tri, L.Q., Tri, V.P.D., Vu, P.T., 2015. Responding to rising sea levels in the Mekong Delta. Nat. Clim. Chang. 5, 167–174. doi:10.1038/nclimate2469.

Stephens, J.D., Allison, M.A., Leonardo, D.R.D., Weathers III, H.D., Ogston, A.S., Mclachlan, R.L., Xing, F., Meselhe, E.A., 2017. Sand dynamics in the Mekong River channel and export to the coastal ocean. Cont. Shelf Res. 147, 38–50. doi:10.1016/j.csr.2017.08.004.

Sumi, T., Kobayashi, K., Yamaguchi, K., Tanaka, Y., 2009. Study on the applicability of the assest management for reservoir sediment management, in: International Congress on Large Dams, Q.89-R.4, Brasilia, Brazil.

Sumi, T., Okano, M., Tanaka, Y., 2004. Reservoir sedimentation management with bypass tunnels in Japan, in: Proceedings of the Ninth International Symposium on River Sedimentation, Yichang, China. pp. 1036–1043.

Ta, T.K.O., Nguyen, V.L., Tateishi, M., Kobayashi, I., Tanabe, S., Saito, Y., 2002. Holocene delta evolution and sediment discharge of the Mekong River, southern Vietnam. Quat. Sci. Rev. 21, 1807–1819. doi:10.1016/S0277-3791(02)00007-0.

Tamura, T., Saito, Y., Sieng, S., Ben, B., Kong, M., Sim, I., Choup, S., Akiba, F., 2009. Initiation of the Mekong River delta at 8 ka: evidence from the sedimentary succession in the Cambodian lowland. Quat. Sci. Rev. 28, 327–344. doi:10.1016/j.quascirev.2008.10.010.

Tena, A., Batalla, R.J., 2013. The sediment budget of a large river regulated by dams (The lower River Ebro , NE Spain). J. Soils Sediments 13, 966–980. doi:10.1007/s11368-013-0681-7.

Thanh, V.., Reyns, J., Wackerman, C., Eidam, E.F., Roelvink, D., 2017. Modelling suspended sediment dynamics on the subaqueous delta of the Mekong River. Cont. Shelf Res. 147, 213–230. doi:10.1016/j.csr.2017.07.013.

Toan, T.Q., 2014. Climate Change and Sea Level Rise in the Mekong Delta: Flood, Tidal Inundation, Salinity Intrusion, and Irrigation Adaptation Methods. In: Coastal Disasters and Climate Change in Vietnam, Elsevier. Elsevier Inc. doi:10.1016/B978-0-12-800007-6.00009-5.

Tran, D.D., Halsema, G.V., Hellegers, P.J.G.J., Ludwig, F., Seijger, C., 2018. Stakeholders ' assessment of dike-protected and fl ood-based alternatives from a sustainable livelihood perspective in An Giang Province , Mekong. Agric. Water Manag. 206, 187–199.

doi:10.1016/j.agwat.2018.04.039.

Trang, N.T.T., Shrestha, S., Shrestha, M., Datta, A., Kawasaki, A., 2017. Evaluating the impacts of climate and land-use change on the hydrology and nutrient yield in a transboundary river basin: A case study in the 3S River Basin (Sekong, Sesan, and Srepok). Sci. Total Environ. 576, 586–598. doi:10.1016/j.scitotenv.2016.10.138.

Triet, N.V.K., Dung, N.V., Fujii, H., Kummu, M., Merz, B., Apel, H., 2017. Has dyke development in the Vietnamese Mekong Delta shifted flood hazard downstream? Hydrol. Earth Syst. Sci. Discuss. Rev. 1–27. doi:10.5194/hess-2017-123.

Trung, L.D., Duc, N.A., Nguyen, L.T., Thai, T.H., Khan, A., Rautenstrauch, K., Schmidt, C., 2018. Assessing cumulative impacts of the proposed Lower Mekong Basin hydropower cascade on the Mekong River floodplains and Delta - Overview of integrated modeling methods and results. J. Hydrol. doi: 10.1016/j.jhydrol.2018.01.029.

Unverricht, D., Szczuciński, W., Stattegger, K., Jagodziński, R., Le, X.T., Kwong, L.L.W., 2013. Modern sedimentation and morphology of the subaqueous Mekong Delta, Southern Vietnam. Glob. Planet. Change 110, 223–235. doi:10.1016/j.gloplacha.2012.12.009.

USGS, 1982. Guidelines for Determining Flood Flow Frequency, U.S. Department of the Interior. Geological Survey. Office of Water Data Coordination. doi:http://dx.doi.org/10.3133/tm4–BXX/.

USGS, 1960. Flood-Frequency Analyses.

Vörösmarty, C.J., Sharma, K.P., Fekete, B.M., Copeland, A.H., Holden, J., Marble, J., Lough, J.A., 1997. The storage and aging of continental runoff in large reservoir systems of the world. Ambio 26, 210–219.

Wackerman, C., Hayden, A., Jonik, J., 2017. Deriving spatial and temporal context for point measurements of suspended- sediment concentration using remote-sensing imagery in the Mekong Delta. Cont. Shelf Res. 147, 231–245. doi:10.1016/j.csr.2017.08.007.

Walling, D.., 2008. The changing sediment load of the mekong river. Ambio 37, 150–157. doi:10.1579/0044-7447(2008)37.

Walling, D.E., 2006. Human impact on land-ocean sediment transfer by the world's rivers. Geomorphology 79, 192–216. doi:10.1016/j.geomorph.2006.06.019.

Walling, D.E., 2005. Evaluation and Analysis of Sediment Data from the Lower Mekong River. Report. Mekong River Commission. Vientiane, 61 pp.

Wang, J.J., Lu, X.X., Kummu, M., 2011. Sediment load estimates and variations in the Lower Mekong River. River Res. Appl. 27, 33–46. doi:10.1002/rra.1337.

WCD, 2000. Dams and Development: A new framework for decision-making, Earthscan.

Wolanski, E., Huan, N.N., Dao, L.T., Nhan, N.H., Thuy, N.N., 1996. Fine-sediment dynamics in the Mekong River Estuary, Viet Nam. Estuar. Coast. Shelf Sci. 43, 565–582. doi:10.1006/ecss.1996.0088.

Wolanski, E., Nhan, N.H., Spagnol, S., 1998. Sediment dynamics during low flow conditions in the Mekong River Estuary, Vietnam. J. Coast. Res. 14, 472–482.

Wu, X., Xiang, X., Chen, X., Zhang, X., Hua, W., 2018. Effects of cascade reservoir dams on the streamflow and sediment transport in the Wujiang River basin of the Yangtze River , China. Inl. Waters 8, 216–228. doi:10.1080/20442041.2018.1457850.

WUP-JICA, 2004. Vol. II: Supporting report, Paper VII: Maintenance of flows on the Mekong Mainstream. In: The study on Hydro-meteorological monitoring for water quantity rules in Mekong River Basin, Mekong River Commission.

Xing, F., Meselhe, E.A., Allison, M.A., Weathers III, H.D., 2017. Analysis and numerical modeling of the fl ow and sand dynamics in the lower Song Hau channel , Mekong Delta. Cont. Shelf Res. 147, 62–77. doi:10.1016/j.csr.2017.08.003.

Xuan, V.-T., 1975. Rice Cultivation in the Mekong Delta. South East Asian Stud. 13, 88–111.

Xue, Z., He, R., Liu, J.P., Warner, J.C., 2012. Modeling transport and deposition of the Mekong River sediment. Cont. Shelf Res. 37, 66–78. doi:10.1016/j.csr.2012.02.010.

Xue, Z., Liu, J.P., Ge, Q., 2011. Changes in hydrology and sediment delivery of the Mekong River in the last 50 years: Connection to damming, monsoon, and ENSO. Earth Surf. Process. Landforms 36, 296–308. doi:10.1002/esp.2036.

Yang, Z., Yan, Y., Liu, Q., 2012. Assessment of the flow regime alterations in the Lower Yellow River, China. Ecol. Inform. 10, 56–64. doi:10.1016/j.ecoinf.2011.10.002.

Zhang, Q., Gu, X., Singh, V.P., Chen, X., 2015. Evaluation of ecological instream flow using multiple ecological indicators with consideration of hydrological alterations. J. Hydrol. 529, 711–722. doi:10.1016/j.jhydrol.2015.08.066.

Zhang, S., Lu, X.X., 2009. Hydrological responses to precipitation variation and diverse human activities in a mountainous tributary of the lower Xijiang , China. Catena 77, 130–142. doi:10.1016/j.catena.2008.09.001.

Zhang, Z., Huang, Y., Huang, J., 2016. Hydrologic alteration associated with dam construction in a medium-sized coastal watershed of southeast China. Water 8, 1–18. doi:10.3390/w8080317.

Ziv, G., Baran, E., Nam, S., Rodríguez-Iturbe, I., Levin, S.A., 2012. Trading-offfish biodiversity, food security, and hydropower in the Mekong River Basin, in: Proceeding of the National Academy of Science of the United States of America. pp. 5609–5614. doi:10.1073/pnas.1201423109.

List of publications

Journal papers:

Kantoush, S., Binh, D.V., Sumi, T., and Trung, L.V. (2017). Impact of upstream hydropower dams and climate change on hydrodynamics of Vietnamese Mekong Delta. *Journal of Japan Society of Civil Engineering, Ser. B1 (Hydraulic Engineering),* Vol. 73, No. 4, pp. I_109-I_114.

Binh, D.V., Kantoush, S., Sumi, T., and Mai, N.P. (2018). Impact of Lancang cascade dams on flow regimes of Vietnamese Mekong Delta. *Journal of Japan Society of Civil Engineering, Ser. B1 (Hydraulic Engineering),* Vol. 74, No. 4, pp. I_487-I_492.

Binh, D.V., Kantoush, S., Mai, N.P., and Sumi, T. (2018). Water level changes under increased regulated flows and degraded river in Vietnamese Mekong Delta. *Journal of Japan Society of Civil Engineering, Ser. B1 (Hydraulic Engineering)*, Vol. 74, No. 5, pp. I_871-I_876.

Mai, N.P., Kantoush, S., Sumi, T., Thang, T.D., Trung L.V., and Binh, D.V. (2018). Assessing and adapting the impacts of dams operation and sea level rising on saltwater intrusion into the Vietnamese Mekong Delta. *Journal of Japan Society of Civil Engineering, Ser. B1 (Hydraulic Engineering),* Vol. 74, No. 5, pp. I_373-I_378.

Conference papers

Binh, D.V., Kantoush, S., Sumi, T., Mai, N.T.P., Ata, R., Kadi Abderrezzak, K.El., and Trung, L.V. (2017). Flow regime changes in Vietnamese Mekong Delta due to river-damming. In *Proceeding of 10th Symposium on River, Coastal and Estuarine Morphodynamics*, Padova, Italia, pp. 25.

La, T., Nguyen, M., Kantoush, S., Sumi, T., and Doan, B. (2017). Evaluation on the impacts of hydropower development on salinity intrusion into Vietnamese Mekong Delta. *The 3rd Symposium on JASTIP Disaster Prevention International Cooperation Research (JASTIP-WP4 Symposium).*

Binh, D.V., Kantoush, S., Sumi, T., Mai, N.P., and Trung, L.V. (2018). Changes in the sediment budget and morphodynammics of Vietnamese Mekong Delta. In *E-Proceedings of the 12th ISE 2018*, Tokyo, Japan.

Binh, D.V., Sumi, T., Kantoush, S., Mai, N.P., and Trung, L.V. (2018). Historical changes of flow and sediment budget in Vietnamese Mekong Delta due to upstream dam development. In *Proceeding of the 21st IAHR-APD Congress 2018*, Yogyakarta, Indonesia, pp. 123-131.

Mai, N.P., Kantoush, S., Sumi, T., Thang, T.D., Trung, L.V., and Binh, D.V. (2018). Impacts of cascade hydropower development on salinity intrusion into Vietnamese Mekong Delta. In *Proceeding of the 21st IAHR-APD Congress 2018*, Yogyakarta, Indonesia, pp. 503-511.

DPRI annual reports

Binh, D.V., Kantoush, S., Sumi, T., Mai, N.T.P., and Trung, L.V. (2017). Study on the impacts of river-damming and climate change on the Mekong Delta of Vietnam. *DPRI Annuals*, No. 60B, pp. 804-826.

Binh, D.V., Kantoush, S., Sumi, T., Mai, N.P., and Trung, L.V. (2018). Field investigations on river bed changes and salinity intrusion along Tien and Hau Rivers in Vietnamese Mekong Delta considering upstream dams' impacts. *DPRI Annuals*, No. 61B, pp. 770-783.

Appendix A: Methods and results of long-term flow alterations due to upstream dam development

A3.1 Mann-Kendall test

The Mann-Kendall test (Mann, 1945; Kendall, 1975) statistic S for a given time series $\{x_t: t= 1, 2, \ldots, n\}$ is calculated as follow:

$$S = \sum_{i=1}^{n-1} \sum_{j=i+1}^{n} \mathrm{sgn}(x_j - x_i) \tag{A3.1}$$

$$\mathrm{sgn}(x_j - x_i) = \begin{cases} +1 & if \;\; x_j > x_i \\ 0 & if \;\; x_j = x_i \\ -1 & if \;\; x_j < x_i \end{cases} \tag{A3.2}$$

$$Var(S) = \frac{n(n-1)(2n+5) - \sum_{i=1}^{m} t_i(t_i - 1)(2t_i + 5)}{18} \tag{A3.3}$$

In cases having the sample size $n > 10$, the standard normal test statistic Z is computed as follow:

$$Z = \begin{cases} \dfrac{S-1}{\sqrt{Var(S)}} & if \;\; S > 0 \\ 0 & if \;\; S = 0 \\ \dfrac{S+1}{\sqrt{Var(S)}} & if \;\; S < 0 \end{cases} \tag{A3.4}$$

where x_i and x_j are the data values in time series i and j ($j > i$), respectively; n is the number of data (observations); $sgn(x_j\text{-}x_i)$ is sign function; $Var(S)$ is variance of statistic S; m is the number of tie groups; t_i is the number of ties of extent i. Positive Z indicates an increasing trend while negative Z indicates a decreasing trend. The null hypothesis (no trend) is rejected when $-1.96 < Z < 1.96$ ($p < 0.05$ at the 5% significance level) and $-2.576 < Z < 2.576$ ($p < 0.01$ at the 1% significance level).

A3.2 Pettitt test

The Pettitt method (Pettitt, 1979) tests the null hypothesis that there is no changing point in the time series. The test verifies whether two samples $x_1, \ldots, x_t$ and $x_{t+1}, \ldots, x_T$ are from the same population or not. The statistic K_T is determined as follow:

$$K_T = \max\left|U_{t,T}\right| \tag{A3.5}$$

in which, the statistic $U_{t,T}$ is computed as follow:

$$U_{t,T} = \sum_{i=1}^{t}\sum_{j=i+1}^{T}\operatorname{sgn}(x_i - x_j) \tag{A3.6}$$

and the associated probability of the significant test is computed as follow:

$$p \approx 2\exp\left(\frac{-6K_T^2}{T^3 + T^2}\right) \tag{A3.7}$$

The null hypothesis is rejected if $p < 0.01$ at the 1% significance level.

A3.3 Sen's slope method

The slope (rate of change) of the trend is estimated using the non-parametric procedure, developed by Sen (1968). The estimates of the slope of N pairs of data are computed as follow:

$$Q_i = \left(\frac{x_j - x_k}{j-k}\right) \qquad for\ i = 1,\ldots,N \tag{A3.8}$$

in which x_j and x_k are date values at times j and k $(j > k)$. The N values of Q_i are ranked from the smallest to the largest and the median of the slope, that is the Sen's slope estimator, is estimated as follow:

$$Q_{med} = \begin{cases} Q_{[(N+1)/2]} & if\ \ N\ is\ odd \\ \dfrac{Q_{[N/2]} + Q_{[(N+2)/2]}}{2} & if\ \ N\ is\ even \end{cases} \tag{A3.9}$$

The Q_{med} sign reflects the time series trend and its values reveal the slope of the trend. Then, to determine whether the test is statistical significance, the confidence interval is computed as follow:

$$C_\alpha = Z_{1-\alpha/2}\sqrt{Var(S)} \tag{A3.10}$$

The Mann-Kendall, Pettitt, and Sen's slope methods are available in R programming under the "Kendall" package. The commands of these tests are mk.test(), pettitt.test(), and sens.slope(), respectively.

A3.4 Flood-frequency analysis

There are three kinds of flood-frequency analysis at a gauging station: discharge, stage (water level), and volume (USGS, 1960). Discharge-frequency curves are the most common in the hydrological analysis of river systems. The discharge-frequency analysis technique was used to investigate the changes in the magnitude and frequency of the annual extreme discharges (maximum and minimum) among different periods at various stations in the MRB. The probabilities associated with the ranked values were then estimated using Hazen equation (Bartkes et al., 2016) which has a form of $P = (m-0.5)/n$, where P: plotting position, m: rank of data (*1*: largest), and n: number of years in the data set. The predicted probabilities are then estimated using Pearson Type III distribution fitted using the method of moments as proposed by (USGS, 1982).

A3.5 Indicators of hydrologic alteration (IHA)

To assess the natural flow regime, (Richter et al., 1996) developed a set of 33 hydrologic indicators, called Indicators of hydrologic alteration (IHA). The IHA method characterizes the intra and interannual variations in the flow regime, based on daily discharges of a long-term time series. The IHA method is able to evaluate the alterations of the flow regime before and after a flow intervention, such as river damming; therefore, we can understand whether does flow intervention have the impacts on the natural flow regime or not. Because each indicator within the IHA method has its own ecological meaning (Table A.3.1), the IHA method has been widely used in determining impacts of various drivers on the natural flow regime, such as hydropower dams, in the world's large rivers (Richter et al., 1998, 1997; Yang et al., 2012; Zhang et al., 2015, 2016).

A3.6 Range of variability (RVA)

For setting river ecosystem management targets, based on the flow regime, the Range of Variability Approach (RVA) method was developed by (Richter et al., 1997). This method is associated with the timing, frequency, duration, and rates of change of the flow, normally determined by IHA method. This approach was intentionally developed for, and applied to, the conservation of native aquatic biodiversity and protection of natural ecosystem functions (Richter et al., 1997). The management strategies are controlled by ensuring the annual value of each IHA parameter falling within the selected range of natural variations that are usually classified into three categories: values ≤ 33 percentile, values in between 33^{rd} to 67^{th} percentiles, and values ≥ 67^{th} percentile (Martin, 2014). To evaluate the impact of river damming, the IHA and RVA methods divide the daily data sets into predam and postdam sub-sets, which allow estimating the hydrological alterations between the two-period flow regimes.

Table A3.1 Thirty-three IHA indicators and ecological influences. Source: (Richter et al., 1996; Zhang et al., 2015; Martin, 2014)

Group	Regime classification	Hydrologic parameters	Ecosystem influences
Group 1: Magnitude of monthly water conditions	Magnitude Timing	Mean or median value for each calendar month	➢ Habitat availability for aquatic organism ➢ Soil moisture availability for plants ➢ Availability of food/cover for fur-bearing mammals
Group 2: Magnitude and duration of annual extreme water conditions	Magnitude Duration	Annual minima 1-day means Annual minima 3-day means Annual minima 7-day means Annual minima 30-day means Annual maxima 90-day means Annual maxima 1-day means Annual maxima 3-day means Annual maxima 7-day means Annual maxima 30-day means Annual maxima 90-day means Number of zero-flow days Base flow index: 7-day minimum flow/mean flow in a year	➢ Balance of competitive, ruderal, and stress-tolerant organisms ➢ Creation of sites for plant colonization ➢ Structuring of aquatic ecosystems by abiotic vs biotic factors ➢ Structuring of river channel morphology and physical habitat conditions ➢ Soil moisture stress ill plants ➢ Dehydration in animals ➢ Anaerobic stress in plants ➢ Volume of nutrient exchanges between rivers and floodplains
Group 3: Timing of annual extreme water conditions	Timing	Julien date of each annual 1-day maximum Julien date of each annual 1-day minimum	➢ Compatibility with life cycles of organisms ➢ Predictability/availability of stress for organisms ➢ Access to special habitats during reproduction or to avoid predation
Group 4: Frequency and duration of high and low pulses	Magnitude Frequency Duration	No. of high pulses each year No. of low pulses each year Mean duration of high pulses within each year Mean duration of low pulses within each year	➢ Frequency and magnitude of soil moisture stress for plants ➢ Frequency and duration of anaerobic stress for plants ➢ Availability of floodplain habitats for aquatic organisms
Group 5: Rate and frequency of water condition changes	Frequency Rate of change	Rise rates: mean of all positive differences between consecutive daily values Fall rates: mean of all negative differences magnitude between consecutive daily values Number of hydrologic reversals	➢ Drought stress on plants (falling levels) ➢ Entrapment of organisms on islands, floodplain (rising levels) ➢ Desiccation stress on low-mobility stream edge (varial zone) organisms

A3.7 Alteration index of the hydrological regime (FQ)

In evaluating the flow alterations due to a perturbation, the alteration index of the hydrological regime (*FQ*) which was proposed by (Alcayaga et al., 2012), is adapted in this research. This index is used to assess the alterations in the frequency and duration in the high-flow, transition-flow, and low-flow seasons. The general form is as follow:

$$FQ(\%) = \frac{NQ_{post}}{NQ_{pre}} \times 100 - 100 \qquad \text{(A3.11)}$$

where $FQ(\%)$: index of frequency alteration applied to high-flow, transition-flow, and low-flow; NQ_{pre}, NQ_{post}: numbers of days (duration) exceeding the high-flow discharge or lower than the low-flow discharge or in between the low-flow and high-flow discharges (the transition-flow) of predam and postdam periods, respectively.

A3.8 Mike 11 model

The Mike 11 model is a 1-dimensional hydrodynamic model of the Mike packages. The hydrodynamic module is the core module of the Mike 11 modeling system, which forms the basis for other modules such as flood forecasting, advection-dispersion, water quality, and non-cohesive sediment transport. The Mike 11 hydrodynamic model solves the vertically integrated shallow water equations, or Saint Venant equations, including continuity and momentum equations. The numerical solution of the Mike 11 hydrodynamic module is based on an implicit finite difference scheme (Manh et al., 2014). The Mike 11 model is capable of simulating the flow in the rivers, estuaries, and irrigation systems. It can be applied to a very complex river network such as the VMD, including the interaction between the rivers and connected floodplains. It can be simulated in a quasi-two-dimensional flows. Inclusion of sluice gates, culverts, bridges, weirs, and road overtopping is possible in the Mike 11. Due to its user-friendly, Mike 11 has been widely applied in simulating the flooding in the VMD by generations of Vietnamese researchers.

Table A3.2 Trend tests of annual mean, maximum, minimum, and monthly discharges at Chiang Saen for a period of 1980-2014.

Mean discharge (m^3/s)	n (year)	Man-Kendall trend test				Sen's slope estimator	Pettitt test to find change point			
		S	Z	p	Trend	Q	K_T	t	p	Shift
Annual	35	-20	-0.270	0.787	-	-1.6	84	2008	0.766	-
Maximum	35	-94	-1.622	0.186	-	-56.3	120	2008	0.282	-
Minimum	**35**	**-94**	**-1.321**	**0.187**	**-**	**-3.1**	**172**	**1992**	**0.036**	-
January	35	93	1.307	0.191	+	+4.6	140	2007	0.139	+
February	35	41	0.568	0.570	+	+2.0	88	2007	0.697	+
March	35	93	1.307	0.191	+	+4.1	110	2007	0.386	+
April	35	113	1.591	0.112	+	+6.9	132	2006	0.187	+
May	35	111	1.562	0.118	+	+11.0	120	1999	0.282	+
June	35	-91	-1.278	0.201	-	-15.1	80	2008	0.837	-
July	35	-79	-1.108	0.268	-	-25.1	130	2008	0.201	-
August	35	-35	-0.483	0.629	-	-12.9	96	2008	0.571	-
September	35	-25	-0.341	0.733	-	-6.8	100	2008	0.513	-
October	35	-125	-1.761	0.078	-	-19.3	130	1997	0.201	-
November	35	-65	-0.909	0.363	-	-7.1	74	2001	0.949	-
December	35	40	0.554	0.580	+	+2.0	92	2006	0.632	+

Note: bold: 5 % significance level

Table A3.3 Trend tests of annual mean, maximum, minimum, and monthly discharges at Kratie for a period of 1980-2015.

Mean discharge (m^3/s)	n (year)	Man-Kendall trend test				Sen's slope estimator	Pettitt test to find change point			
		S	Z	p	Trend	Q	K_T	t	p	Shift
Annual	36	-12	-0.150	0.881	-	-4.4	82	1993	0.862	-
Maximum	*36*	-29	-0.381	0.703	-	-40.4	77	2002	0.952	-
Minimum	**36**	**292**	**3.964**	**$7.4x10^{-5}$**	**+**	**+26.1**	**269**	**1995**	**$0.2x10^{-3}$**	**+**
January	36	130	1.757	0.079	+	+16.9	143	1990	0.155	+
February	**36**	**238**	**3.228**	**0.001**	**+**	**+19.3**	**225**	**1994**	**0.004**	**+**
March	**36**	**279**	**3.787**	**$0.2x10^{-3}$**	**+**	**+26.2**	**236**	**1994**	**0.002**	**+**
April	**36**	**346**	**4.499**	**$2.6x10^{-6}$**	**+**	**+37.7**	**304**	**1995**	**$1.9x10^{-5}$**	**+**
May	**36**	**190**	**2.574**	**0.010**	**+**	**+41.1**	**238**	**1995**	**0.002**	**+**
June	36	-72	-0.967	0.334	-	-54.8	93	2004	0.678	-
July	36	-18	-0.232	0.817	-	-23.2	85	2002	0.810	-
August	*36*	30	0.395	0.693	+	+77.3	82	1993	0.862	+
September	36	-37	-0.490	0.624	-	-79.0	112	2005	0.416	-
October	36	-2	-0.014	0.989	-	-3.5	68	2011	1.121	-
November	36	-72	-0.967	0.334	-	-60.4	78	2011	0.934	-
December	36	-9	-0.109	0.913	-	-3.0	83	2002	0.845	-

Note: bold: 5 % significance level

Table A3.4 Trend tests of annual mean, maximum, minimum, and monthly discharges at Tan Chau for a period of 1980-2015.

Mean discharge (m^3/s)	n (year)	Man-Kendall trend test				Sen's slope estimator	Pettitt test to find change point			
		S	Z	p	Trend	Q	K_T	t	p	Shift
Annual	36	-4	-0.041	0.967	-	-1.0	63	1998	1.217	-
Maximum	36	44	0.586	0.558	+	+28.3	102	1993	0.544	+
Minimum	**36**	**365**	**4.959**	**$7.1x10^{-7}$**	+	**+75.2**	**312**	**1995**	**$1.0x10^{-5}$**	+
January	36	-26	-0.341	0.734	-	-6.3	69	1986	1.102	-
February	36	-10	-0.123	0.902	-	-1.4	85	1986	0.810	-
March	36	66	0.885	0.376	+	+13.0	110	1999	0.440	+
April	***36***	***188***	***2.547***	***0.011***	+	***+27.2***	***160***	***1999***	***0.081***	+
May	**36**	**156**	**2.111**	**0.035**	+	**+34.5**	**187**	**1998**	**0.025**	+
June	36	4	0.041	0.967	+	+2.0	105	1998	0.503	+
July	36	-40	-0.531	0.595	-	-21.1	71	1986	1.064	-
August	36	56	0.749	0.454	+	+31.2	88	1993	0.759	+
September	36	-50	-0.667	0.505	-	-29.2	98	2005	0.601	-
October	36	9	0.109	0.913	+	+3.9	76	1993	0.9710	+
November	36	-106	-1.430	0.153	-	-58.2	102	1985	0.544	-
December	36	-70	-0.940	0.347	-	-37.4	91	1986	0.710	-

Note: bold: 5 % significance level; bold and italic: 10 % significance level

Table A3.5 Trend tests of annual mean, maximum, minimum, and monthly discharges at Chau Doc for a period of 1980-2015.

Mean discharge (m^3/s)	n	Man-Kendall trend test				Sen's Slop estimator	Pettitt test to find change point			
		S	Z	p	Trend	Q	K_T	t	p	Shift
Annual	36	-48	-0.640	0.522	-	-3.3	107	2002	0.477	-
Maximum	36	-12	-0.150	0.881	-	-4.5	69	1984	1.102	-
Minimum	**36**	**340**	**4.620**	**$3.9x10^{-6}$**	+	**+25.8**	**320**	**1995**	**$5.5x10^{-6}$**	+
January	36	-71	-0.954	0.340	-	-5.4	121	2003	0.320	-
February	36	7	0.082	0.935	+	+0.4	80	1994	0.898	+
March	**36**	**249**	**3.379**	**$0.7x10^{-3}$**	+	**+8.1**	**231**	**1995**	**0.003**	+
April	**36**	**231**	**3.133**	**0.002**	+	**+6.0**	**195**	**1990**	**0.017**	+
May	**36**	**172**	**2.329**	**0.020**	+	**+8.1**	**208**	**1995**	**0.009**	+
June	36	-13	-0.164	0.870	-	-1.0	69	1998	1.102	-
July	36	-38	-0.504	0.613	-	-6.2	105	2002	0.503	-
August	36	74	0.994	0.320	+	+17.1	112	1993	0.4163	+
September	36	-60	-0.804	0.422	-	-12.8	91	2006	0.710	-
October	36	-1	0	1	-	-0.2	78	1993	0.934	-
November	36	-120	-1.621	0.105	-	-23.8	92	1985	0.694	-
December	36	-142	-1.921	0.055	-	-17.1	143	2002	0.155	-

Note: bold: 5 % significance level

Table A3.6 Changes of maximum discharges at Chiang Saen at different exceedance probabilities in no-dam, low-dam, and high-dam development periods.

Exceedance probability (%)	Return period (year)	No-dam Discharge (m^3/s)	Low-dam Discharge (m^3/s)	Low-dam Change (%)	High-dam Discharge (m^3/s)	High-dam Change (%)
0.2	500	20,550	31,840	+55.0	12,340	-39.9
0.5	200	19,090	28,340	+48.5	11,650	-38.9
1	100	17,940	25,700	+43.3	11,110	-38.1
2	50	16,740	23,070	+37.9	10,540	-37.0
5	20	15,040	19,600	+30.3	9,740	-35.3
10	10	13,640	16,950	+24.3	9,080	-33.4
20	5	12,070	14,250	+18.1	8,340	-30.9
50	2	9,430	10,460	+11.0	7,090	-24.8
99.99	1	2,510	6,590	+162.5	3,860	+53.9

Note: Change (%) = [High-dam (or low-dam) discharge – no-dam discharge]/no-dam discharge*100%. "+": increase and "-": decrease.

Table A3.7 Changes of maximum discharges at Kratie at different exceedance probabilities in no-dam, low-dam, and high-dam development periods.

Exceedance probability (%)	Return period (year)	No-dam Discharge (m^3/s)	Low-dam Discharge (m^3/s)	Low-dam Change (%)	High-dam Discharge (m^3/s)	High-dam Change (%)
0.2	500	69,590	73,330	+5.4	77,250	+11.0
0.5	200	66,680	70,200	+5.3	73,390	+10.1
1	100	64,330	67,690	+5.2	70,280	+9.2
2	50	61,830	65,030	+5.2	66,960	+8.3
5	20	58,170	61,170	+5.2	62,150	+6.8
10	10	55,030	57,890	+5.2	58,020	+5.4
20	5	51,350	54,100	+5.3	53,210	+3.6
50	2	44,720	47,370	+5.9	44,580	-0.3
99.99	1	21,110	25,090	+18.9	14,590	-30.9

Note: Change (%) = [High-dam (or low-dam) discharge – no-dam discharge]/no-dam discharge*100%. "+": increase and "-": decrease.

Table A3.8 Changes of maximum discharges at Tan Chau at different exceedance probabilities in no-dam, low-dam, and high-dam development periods.

Exceedance probability (%)	Return period (year)	No-dam Discharge (m^3/s)	Low-dam Discharge (m^3/s)	Low-dam Change (%)	High-dam Discharge (m^3/s)	High-dam Change (%)
0.2	500	27,360	29,870	+9.2	31,110	+13.7
0.5	200	26,570	28,850	+8.6	30,060	+13.1
1	100	25,940	28,040	+8.1	29,200	+12.6
2	50	25,270	27,190	+7.6	28,270	+11.8
5	20	24,310	25,970	+6.8	26,900	+10.6
10	10	23,490	24,960	+6.3	25,710	+9.4
20	5	22,550	23,810	+5.6	24,290	+7.7
50	2	20,880	21,840	+4.6	21,670	+3.8
99.99	1	15,450	16,160	+4.6	11,460	-25.9

Note: Change (%) = [High-dam (or low-dam) discharge – no-dam discharge]/no-dam discharge*100%. "+": increase and "-": decrease.

Table A3.9 Changes of maximum discharges at Chau Doc at different exceedance probabilities in no-dam, low-dam, and high-dam development periods.

Exceedance probability (%)	Return period (year)	No-dam Discharge (m^3/s)	Low-dam Discharge (m^3/s)	Low-dam Change (%)	High-dam Discharge (m^3/s)	High-dam Change (%)
0.2	500	9,490	9,290	-2.1	9,963	+5.0
0.5	200	9,140	8,970	-1.8	9,572	+4.8
1	100	8,850	8,710	-1.6	9,250	+4.6
2	50	8,530	8,420	-1.3	8,899	+4.3
5	20	8,060	8,010	-0.7	8,375	+3.9
10	10	7,640	7,640	+0.0	7,911	+3.5
20	5	7,140	7,220	+1.0	7,351	+2.9
50	2	6,200	6,440	+3.9	6,287	+1.5
99.99	1	2,170	3,480	+60.4	1,693	-22.0

Note: Change (%) = [High-dam (or low-dam) discharge – no-dam discharge]/no-dam discharge*100%. “+”: increase and “-”: decrease.

Table A3.10 Changes of minimum discharges at Chiang Saen at different non-exceedance probabilities in no-dam, low-dam, and high-dam development periods.

Non-exceedance probability (%)	Return period (year)	No-dam Discharge (m^3/s)	Low-dam Discharge (m^3/s)	Low-dam Change (%)	High-dam Discharge (m^3/s)	High-dam Change (%)
0.1	1000	675	210	-68.9	300	-55.4
1	100	680	295	-56.6	400	-40.6
5	20	690	380	-45.6	500	-27.5
10	10	700	420	-40.1	560	-20.7
20	5	720	480	-33.8	630	-12.9
50	2	770	590	-23.8	770	-0.1
99.99	1	1425	1,160	-18.8	1,560	+9.2

Note: Change (%) = [High-dam (or low-dam) discharge – no-dam discharge]/no-dam discharge*100%. “+”: increase and “-”: decrease.

Table A3.11 Changes of minimum discharges at Krate at different non-exceedance probabilities in no-dam, low-dam, and high-dam development periods.

Non-exceedance probability (%)	Return period (year)	No-dam Discharge (m^3/s)	Low-dam Discharge (m^3/s)	Low-dam Change (%)	High-dam Discharge (m^3/s)	High-dam Change (%)
0.1	1000	1,190	970	-18.4	840	-29.4
1	100	1,310	1,220	-7.2	1,220	-6.9
5	20	1,420	1,450	+2.2	1,560	+9.9
10	10	1,480	1,580	+7.1	1,740	+17.8
20	5	1,550	1,750	+12.8	1,960	+26.5
50	2	1,690	2,080	+23.3	2,380	+40.9
99.99	1	2,360	3,910	+65.8	4,250	+80.2

Note: Change (%) = [High-dam (or low-dam) discharge – no-dam discharge]/no-dam discharge*100%. "+": increase and "-": decrease.

Table A3.12 Changes of minimum discharges at Tan Chau at different non-exceedance probabilities in no-dam, low-dam, and high-dam development periods.

Non-exceedance probability (%)	Return period (year)	No-dam Discharge (m^3/s)	Low-dam Discharge (m^3/s)	Low-dam Change (%)	High-dam Discharge (m^3/s)	High-dam Change (%)
0.1	1000	-2,220	-730	+67.0	1,140	+151.3
1	100	-1,850	-340	+81.5	1,250	+167.5
5	20	-1,440	60	+103.9	1,400	+197.4
10	10	-1,190	290	+124.1	1,515	+227.1
20	5	-865	580	+167.5	1,680	+294.5
50	2	-140	1,210	+941	2,110	+1566
99.99	1	4,790	5,010	+4.7	6,350	+32.7

Note: Change (%) = [High-dam (or low-dam) discharge – no-dam discharge]/no-dam discharge*100%. "+": increase and "-": decrease.

Table A3.13 Changes of minimum discharges at Chau Doc at different non-exceedance probabilities in no-dam, low-dam, and high-dam development periods.

Non-exceedance probability (%)	Return period (year)	No-dam discharge (m^3/s)	Low-dam discharge (m^3/s)	Low-dam Change (%)	High-dam discharge (m^3/s)	High-dam Change (%)
0.1	1000	-1,065	-540	+49.0	220	+120.3
1	100	-895	-425	+52.5	220	+124.7
5	20	-740	-300	+59.7	240	+131.9
10	10	-655	-220	+66.3	250	+137.9
20	5	-550	-120	+78.4	270	+148.6
50	2	-350	110	+130.1	320	+192
99.99	1	590	1,640	+179.3	1,010	+71.6

Note: Change (%) = [High-dam (or low-dam) discharge – no-dam discharge]/no-dam discharge*100%. "+": increase and "-": decrease.

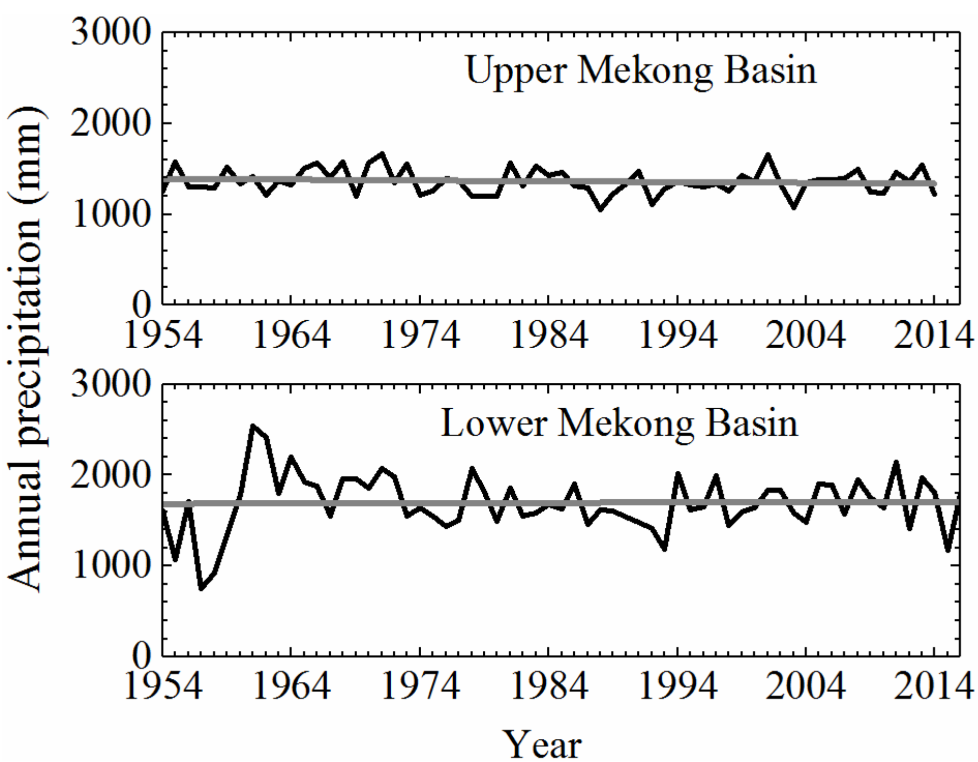

Fig. A3.1 Historical observed precipitation in the Mekong River basin

Appendix B Background of Telemac-2D and Sisyphe

B6.1 Background of Telemac-2D

B6.1.1 Governing equations

The continuity equation:

$$\frac{\partial h}{\partial t} + u\vec{\nabla}(h) + hdiv(\vec{u}) = S_h \tag{B6.1}$$

Momentum equations along x and y-directions:

$$\frac{\partial u}{\partial t} + \vec{u}\vec{\nabla}(u) = -g\frac{\partial Z}{\partial x} + S_x + \frac{1}{h}div(h\nu_t\vec{\nabla}u) \tag{B6.2}$$

$$\frac{\partial v}{\partial t} + \vec{u}\vec{\nabla}(v) = -g\frac{\partial Z}{\partial y} + S_y + \frac{1}{h}div(h\nu_t\vec{\nabla}v) \tag{B6.3}$$

Tracer conservation equation

$$\frac{\partial T}{\partial t} + \vec{u}\vec{\nabla}(T) = S_T + \frac{1}{h}div(h\nu_T\vec{\nabla}T) \tag{B6.4}$$

where *h* is water depth (m), *u* and *v* are velocities in *x* and *y*-directions (m/s), *T* is passive (non-buoyant) tracer (g/l or °C), *g* is gravitational acceleration (m/s^2), ν_t and ν_T are momentum and tracer diffusion coefficients (m^2/s), *Z* is free surface elevation (m), *t* is time (s), *x* and *y* are horizontal space coordinates (m), S_h is source or sink of fluid (m/s), S_x and S_y are source or sink terms in dynamic equations (m/s^2), S_T is source or sink of tracer (g/l/s). In these equations, *h*, *u*, *v*, and *T* are unknowns. The equations are solved in Cartesian or spherical coordinates.

B6.1.2 Inputs and outputs

The mandatory input files of the Telemac-2D are the steering file that contains the configuration of the computation, the geometry file that contains the elevation mesh, and the boundary condition file that contains the description of the type of each boundary. Additional files may be previous computation file, bottom topography file, reference file, liquid boundary file, Fortran files, friction data file, stage-discharge curve file, source file, weir file, culvert file, tube data file, and breach data file. The output files include the result file that contains the graphical results and the listing printout file.

The steering file is a text file, created by text editors. It contains sets of keywords. All keywords are defined in the dictionary file. The keyword uses the default value if no value is given. The maximum number of characters in a line is 72. The time step is specified in the steering file. The geometry file contains all the information of the mesh, including the number of nodes, number of elements, and X, Y, Z coordinates of all nodes. The mesh is first generated and incorporated with the bathymetric data to create the geometry mesh. The keyword is GEOMETRY FILE. The boundary condition file contains the type of the boundary, such as described discharge (usually at upstream boundaries), described water levels (usually at downstream boundaries), and described velocities, or free discharges, water levels, and velocities. The keyword is BOUNDARY CONDITIONS FILE.

B6.2 Background of Sisyphe

B6.2.1 Bedload transport

Bedload transport formulas are usually computed as a function of the Shields parameter θ (Pablo, 2018), having a form of:

$$\theta = \frac{\mu \tau_b}{(\rho_s - \rho) g d} \tag{B6.5}$$

and the dimensionless current-induced bedload transport rate Φ_b is as follow:

$$\Phi_b = \frac{Q_b}{\sqrt{g(s-1)d^3}} \tag{B6.6}$$

in which τ_b is bed shear stress (N/m^2), μ is correction factor for skin friction, Q_b is the bedload transport rate per unit width (m^2/s), $s = \rho_s/\rho$ is the relative density, ρ_s and ρ are density of the sediment and water (kg/m^3), d is sediment grain diameter (m), g is gravitational acceleration (m/s^2). The bedload transport rates are usually computed by using various options of empirical formulas, such as Meyer-Perter and Müller, Einstein-Brown, can Rijn’s. Other empirical formulas can be incorporated into the Sisyphe by the users.

B6.2.2 Suspended sediment transport

The suspended sediment transport is simulated by solving the two-dimensional advection-diffusion equation (Pablo, 2018):

$$\frac{\partial hC}{\partial t}+\frac{\partial hUC}{\partial x}+\frac{\partial hVC}{\partial y}=\frac{\partial}{\partial x}\left(h\varepsilon_s\frac{\partial C}{\partial x}\right)+\frac{\partial}{\partial y}\left(h\varepsilon_s\frac{\partial C}{\partial y}\right)+E-D \tag{B6.7}$$

in which $C=C(x,y,t)$ is the depth-averaged suspended sediment concentration, expressed in % volume, U and V are the depth-averaged velocities in x and y-directions, respectively, ε_s is the turbulent diffusivity of the sediment, often related to the eddy viscosity $\varepsilon_s = \nu_t/\sigma_c$, σ_c is the Schmidt number.

The erosion (E) and deposition (D) rates are computed as follow:

$$E=\omega_s C_{zref} \tag{B6.8}$$

$$D=\omega_s C_{eq} \tag{B6.9}$$

where ω_s is settling velocity (m/s), C_{zref} is the near-bed concentration, evaluated at the interface between the bedload and suspended load at $z = z_{ref}$, C_{eq} is the equilibrium near-bed concentration.

The settling velocity is computed as follow:

$$\omega_s=\begin{cases}\dfrac{(s-1)gd_{50}^2}{18\nu} & if\ \ d_{50}\le 10^{-4}\\ \dfrac{10\nu}{d_{50}}\left(\sqrt{1+0.01\dfrac{(s-1)gd_{50}^2}{18\nu^2}}-1\right) & if\ \ 10^{-4}\le d_{50}\le 10^{-3}\\ 1.1\sqrt{(s-1)gd_{50}} & otherwise\end{cases} \tag{B6.10}$$

For non-cohesive sediment, the net sediment flux E-D is calculated based on the concept of equilibrium concentration, expressed as follow:

$$(E-D)_{eq}=\omega_s\left(C_{eq}-C_{zref}\right) \tag{B6.11}$$

where the C_{eq} is determined considering the Rouse law of vertical distribution of the suspended sediment concentration, which is theoretically valid in uniform steady flow conditions:

$$C(z)=C_{zref}\left(\frac{z-h}{z}\frac{a}{a-h}\right)^R \tag{B6.12}$$

in which $R = \omega_s/(\kappa u_*)$ is the Rouse number, κ is the Karman constant, u_* is the friction velocity corresponding to the total bed shear stress, *a* is the reference elevation above the riverbed (m), *z* is the considered elevation (m). Solving the eq. 3.29 by depth-integrated:

$$C_{zref} = FC \tag{B6.13}$$

$$F^{-1} = \begin{cases} \dfrac{1}{1-Z} B^R\left(1 - B^{(1-R)}\right) & if \quad R \neq 1 \\ -B \log B & if \quad R = 1 \end{cases} \tag{B6.14}$$

$$B = z_{ref} / h \tag{B6.15}$$

The equilibrium near-bed concentration C_{eq} is computed by using various empirical formulas such as Zyserman-Fredsoe, Bijker (used when the bedload is computed), van Rijn, and Soulsby and van Rijn equations.

For cohesive sediment, the erosion flux is computed using the Partheniades formula as:

$$E = \begin{cases} M\left[\left(\dfrac{\tau_b}{\tau_{ce}}\right) - 1\right] & if \quad \tau_b > \tau_{ce} \\ 0 & otherwise \end{cases} \tag{B6.16}$$

and the deposition flux is computed as:

$$D = \omega_s C\left[1 - \left(\frac{\sqrt{\tau_b / \rho}}{u_*^{cr}}\right)^2\right] \tag{B6.17}$$

where *M* is the Krone-Partheniades erosion constant (kg/m^2/s), τ_{ce} is the critical bed shear stress (N/m^2), u_*^{cr} is the critical shear velocity for mud deposition (m/s).

B6.2.3 Bed evolution

The bed evolution formula considering both bedload and suspended load is computed as:

$$\left(1 - \lambda\right)\frac{\partial z_b}{\partial t} + \nabla.Q_b + E - D = 0 \tag{B6.18}$$

in which λ is the bed porosity, z_b is the bed level (m).

B6.2.4 Mixed sediment transport

In reality, the natural sediment consists of a sand-mud mixture, which can be simulated by Sisyphe. The sediment mixture is divided into two size classes *k* = 1, 2 for sand and mud, respectively. The depth-averaged suspended sediment transport equation for the k_{th} size class is computed as follow:

$$\frac{\partial hC_k}{\partial t}+\frac{\partial hUC_k}{\partial x}+\frac{\partial hVC_k}{\partial y}=\frac{\partial}{\partial x}\left(h\varepsilon_s\frac{\partial C_k}{\partial x}\right)+\frac{\partial}{\partial y}\left(h\varepsilon_s\frac{\partial C_k}{\partial y}\right)+E^k-D^k \tag{B6.19}$$

in which C_k is the depth-averaged concentration of the k^{th} size class, E^k and D^k are the erosion and deposition rates of the k^{th} size class.

Mean bed shear strength (critical bed shear stress)

The mean bed shear strength per layer of the sand-mud mixture is computed as a function of the mass percentage of the mud fraction, f_{2j}:

$$f_{2j}=M_{sj}^2/(M_{sj}^1+M_{sj}^2) \tag{B6.20}$$

$$M_{sj}^1=E_{sj}^1\rho_s \qquad and \quad M_{sj}^2=E_{sj}^2C_j \tag{B6.21}$$

in which E_{sj}^1, E_{sj}^2, M_{sj}^1, and M_{sj}^2 are the bed layer thickness and the mass of the sand and mud, respectively, C_j is the mass concentration per layer (kg/m^3).

- If $f_{2j} \le 30\%$ (sand dominated), $\bar{\tau}_{cej}=\tau_{ce}^1$
- If $f_{2j} \ge 50\%$ (mud dominated), $\bar{\tau}_{cej}=\tau_{cej}^2$
- If $30\% \le f_{2j} \le 50\%$, $\bar{\tau}_{cej}=\tau_{ce}^1+\frac{(f_{2j}-0.3)(\tau_{cej}^2-\tau_{ce}^1)}{(0.5-0.3)}$

where τ_{ce}^1 and τ_{cej}^2 are the critical shear stress of sand and mud, respectively.

Mean erosion flux per layer

The mean erosion rate per layer, $\overline{E}_j$ is computed depending on the mass percentage of the mud fraction:

- If $f_{2j} \le 30\%$ (sand dominated):

$$\overline{E}_j=E_j^1=\begin{cases}\omega_{s1}C_{eq}f_{1_1} & if\ \tau_b>\bar{\tau}_{cej}\\ 0 & otherwise\end{cases} \tag{B6.22}$$

- If $f_{2j} \geq 50\%$ (mud dominated):

$$\overline{E}_j = E_j^2 = \begin{cases} M\left[\left(\dfrac{\tau_b}{\overline{\tau}_{cej}}\right) - 1\right] & if\ \tau_b > \overline{\tau}_{cej} \\ 0 & otherwise \end{cases} \tag{B6.23}$$

- If $30\% \leq f_{2j} \leq 50\%$:

$$\overline{E}_j = E_j^1 + \frac{\left(f_{2j} - 0.3\right)\left(E_j^2 - E_j^1\right)}{(0.5 - 0.3)} \tag{B6.24}$$

Sand and mud deposition fluxes

The deposition fluxes for sand, D^1 and for mud, D^2 are computed as follow:

$$D^1 = \omega_{s1} T_2 \tag{B6.25}$$

$$D^2 = \omega_{s2}\left[1 - \left(\frac{T_1}{u_*^{cr}}\right)^2\right] \tag{B6.26}$$

In which T_2 is the ratio between the near-bed concentration and the mean concentration, and $T_1 = \sqrt{\tau_b / \rho}$.

Appendix C Results of the coupled Telemac-D and Sisyphe model

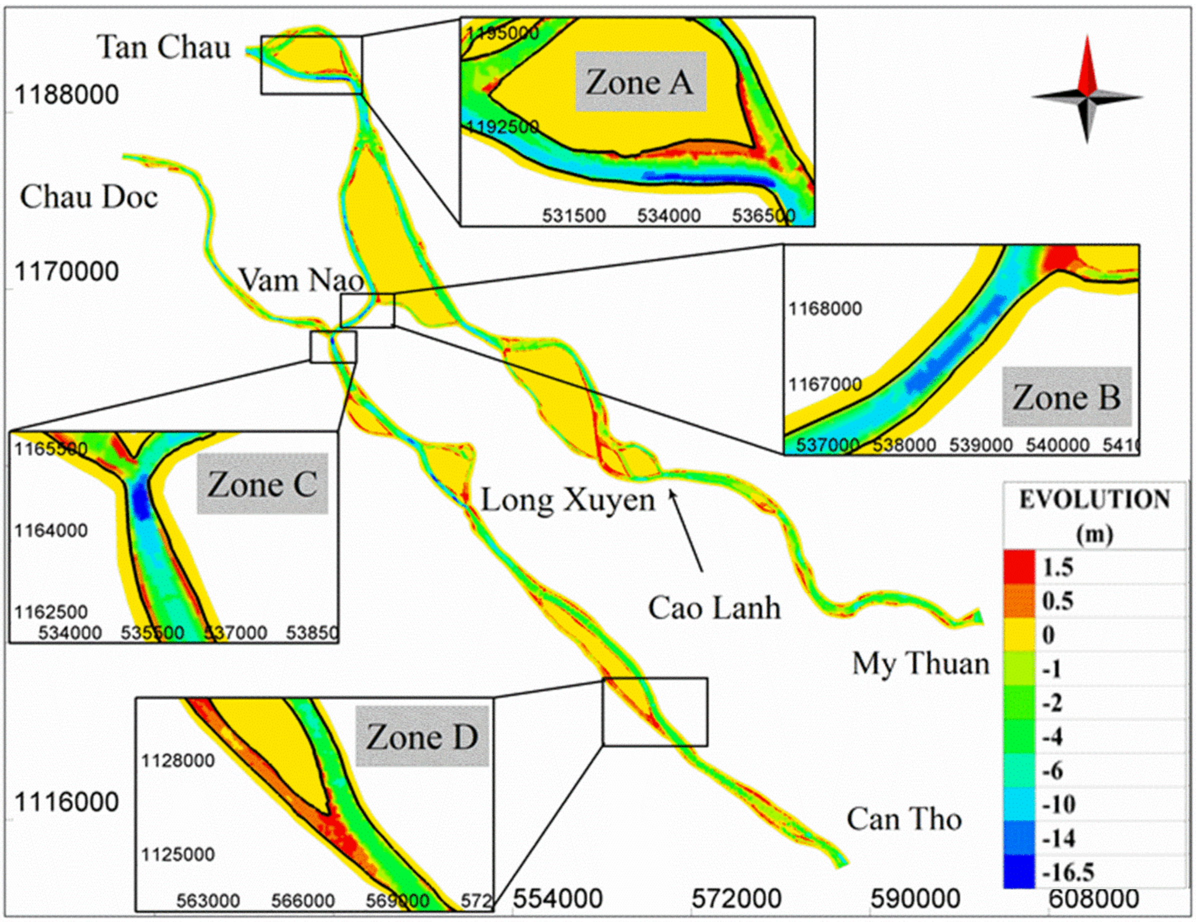

Fig. C7.1 3D map of riverbed changes between ScA in the end of 2026 and the 2017 baseline.

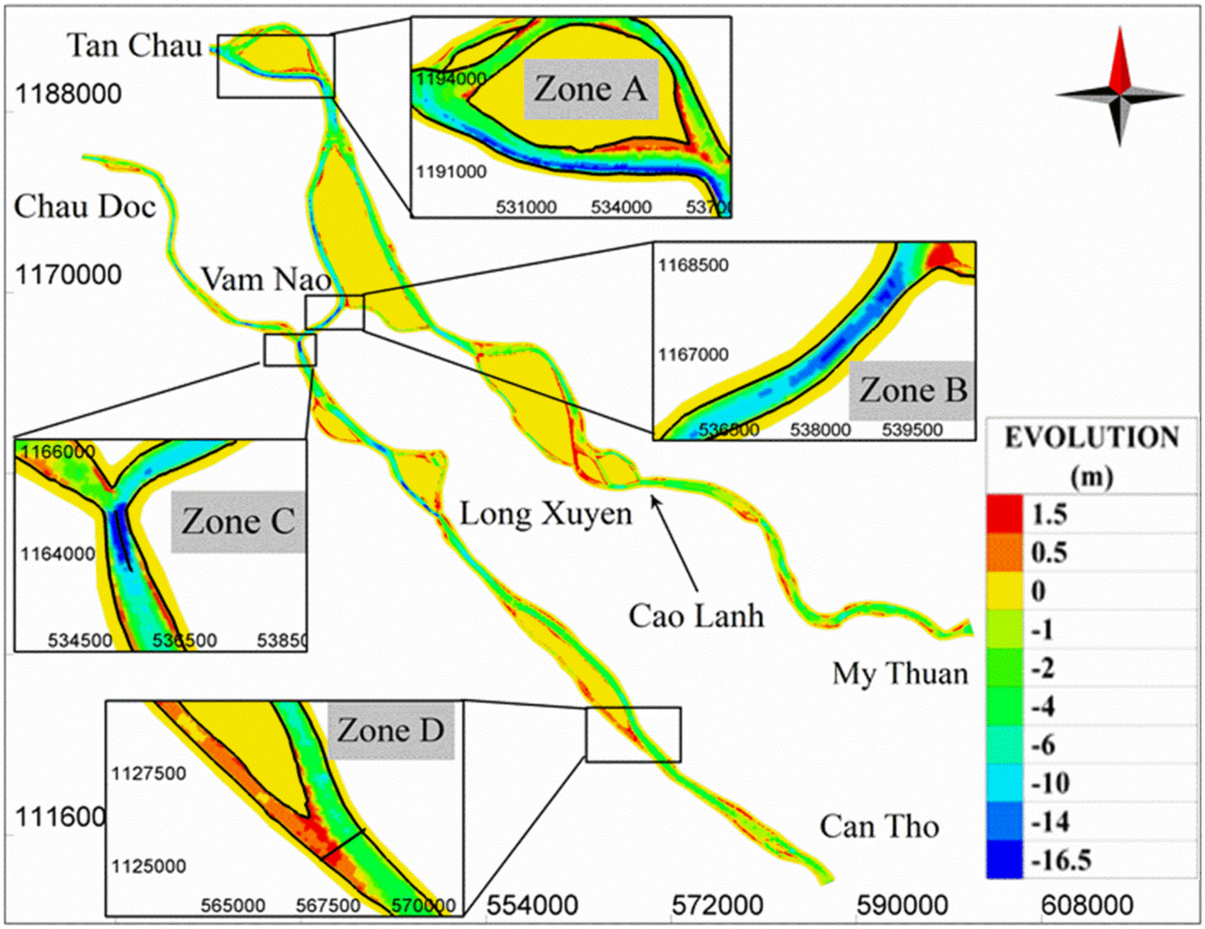

Fig. C7.2 3D map of riverbed changes between ScB in the end of 2026 and the 2017 baseline.

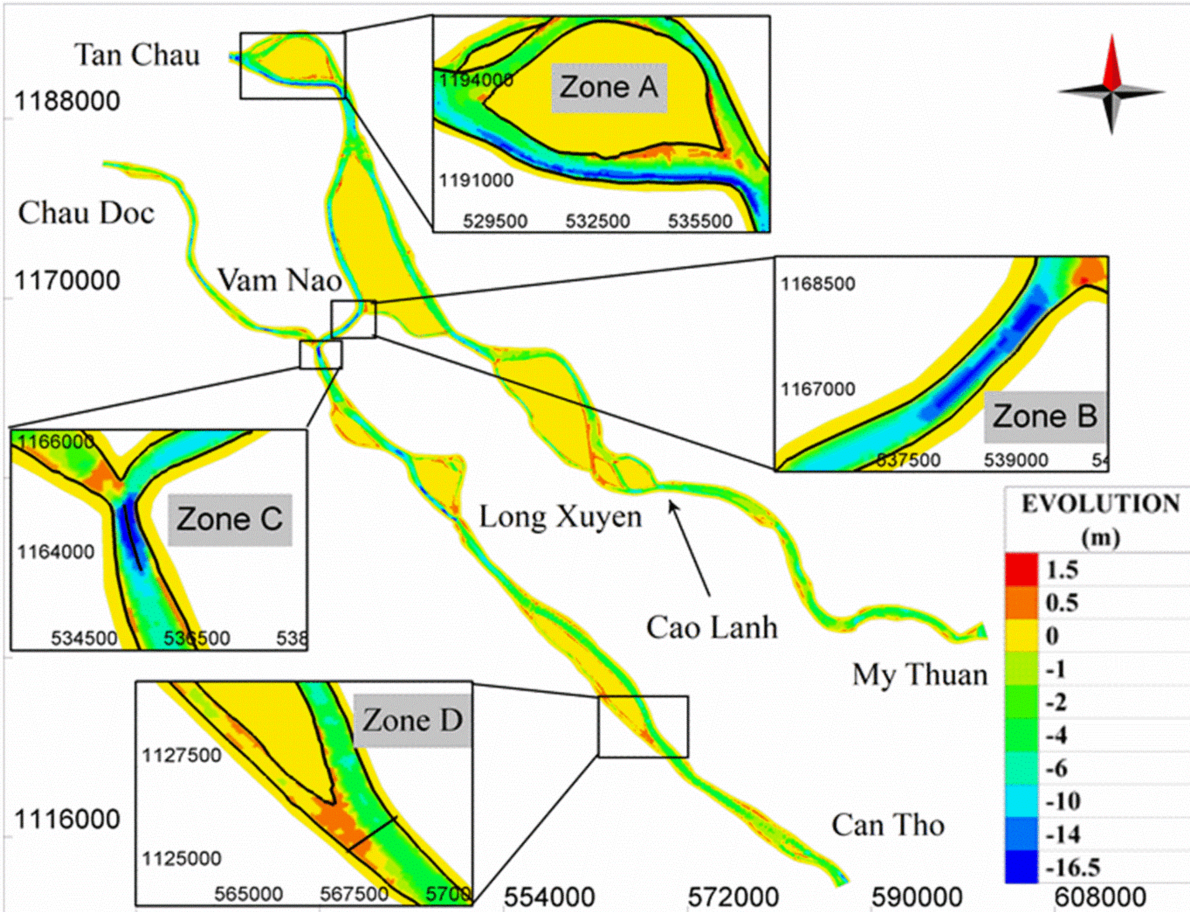

Fig. C7.3 3D maps of riverbed changes between ScC in the end of 2026 and the 2017 baseline.

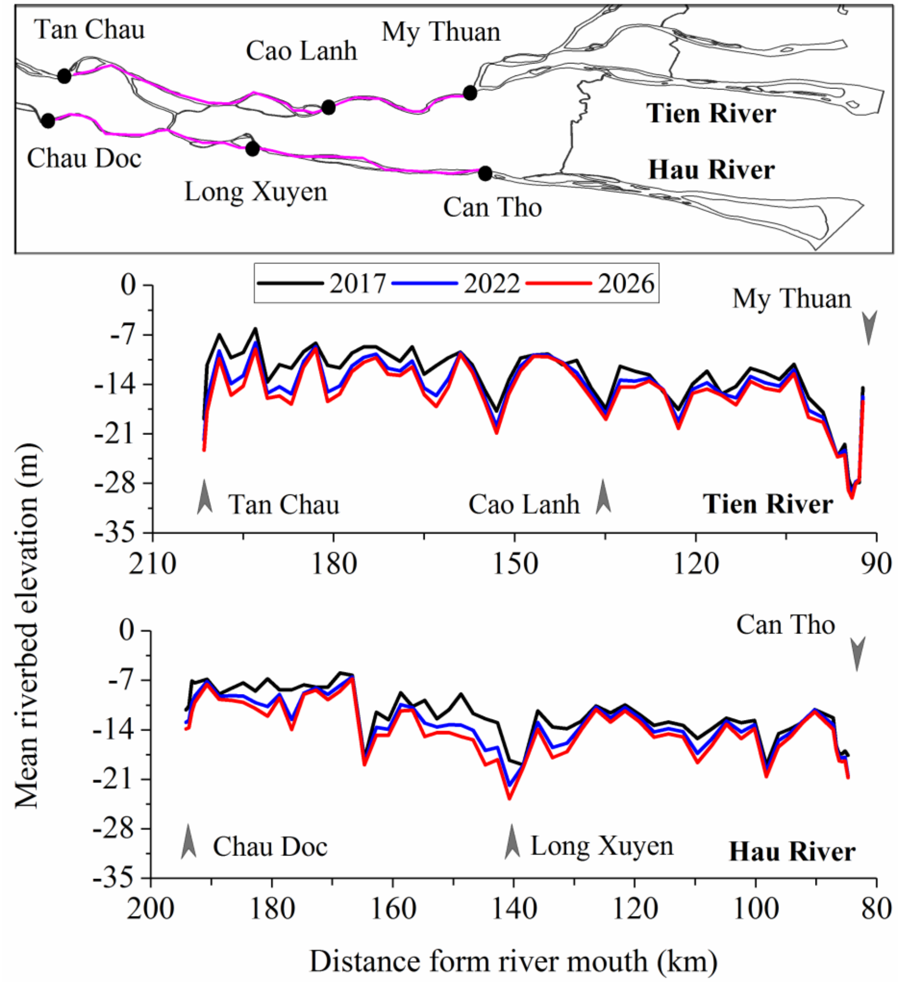

Fig. C7.4 Longitudinally mean riverbed elevation in Tien and Hau Rivers at the end of 2017, 2022, and 2026 in ScC.

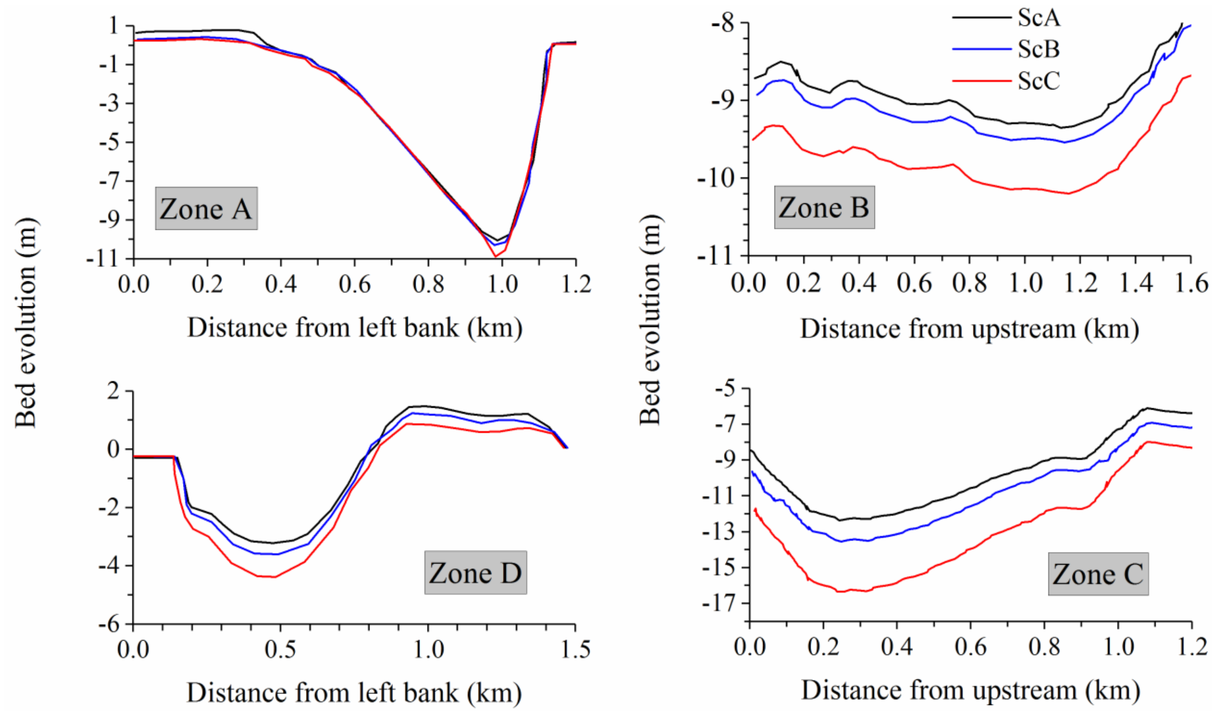

Fig. C7.5 Line graphs of riverbed changes among simulation scenarios at four typical zones.